Heating of Greenhouse Crops with Microwave Energy

Michael James Guess

School of Electronic and Electrical Engineering

University of Leeds

Submitted in accordance with the requirements for the degree of

Doctor of Philosophy

September 2011

The candidate confirms that the work submitted is his own and that appropriate credit has been given where reference has been made to the work of others.

—

—

Acknowledgements

I would like to express my appreciation for the generosity shown by Prof. Peter Urwin of the Faculty of Biological Sciences, University of Leeds, for allowing me full use of his laboratory facilities and also for the laboratory assistance provided by Fiona Moulton in setting up and maintaining my experiments.

I would like to thank Dr. Alaa Abunjaileh for allowing me access to his Aladdin's cave of books, probes, cables, tools, software, gadgets, serviettes, complimentary coffee sachets... (the list goes on) and for always being available to provide advice and encouragement.

Finally, I would like to state my sincere gratitude to Prof. Ian Hunter for providing me with both the opportunity and means to work under his expert supervision. His casual yet continual support was refreshing and encouraging and has made my post-graduate experience thoroughly enjoyable. Thanks Ian!

"To doubt is worse than to have lost; And to despair is but to antedate those miseries that must fall on us."

Philip Massinger (1583–1640)

Abstract

The greenhouse vegetable industry in Northern Europe is an extensive, high value and energy-intensive horticultural sector that is vital for food supply and security in Europe. Despite technical and legislative innovation over a period of thirty years, little improvement has been made in the reduction of absolute energy consumption for heating greenhouse growing space.

A novel free-space microwave system for heating greenhouse crops volumetrically is proposed and demonstrated. It is estimated that such a system can use one-third of the energy of a conventional heating system. This would allow for significant reductions in energy consumption, reduce environmental damage and provide financial savings of several billion Euros. Experiments on real plants demonstrate microwave heating utilising ISM band frequencies as a viable method for heating growing plants from seedling to fruition and reveal plant and fruit quality that is comparable to that attained by conventional heating.

Non-uniformity of electric-field distribution within the plants, both between and within plant components, is identified as the main limiting factor during microwave heating and can result in localised burning. This can cause catastrophic failure when occurring on stems. The necessary reduction in power and the resultant decrease in average plant temperature delays development relative to conventionally-heated plants. Poor leaf heating and development is the main source of delay in fruit formation. A novel practical technique for improving inter- and intra-object heating uniformity is thus also presented and demonstrated. This method utilises circularly polarised incident waves to allow more regular heating of plant components and greater consistency of heating between different plant components. Furthermore, this technique can be applied generally to other dielectric heating scenarios where heating non-uniformity is a problem, specifically in industrial processes.

The concept of plant sectors and sections is also defined to allow for valid comparison of the energy consumption of conventional and microwave heating systems, in a commercial setting.

Contents

List of Figures

Nomenclature

Roman Symbols

$\vec{P}_\rho$	Polarisation density
$\vec{q}$	Local heat flux
A	Area (of surface)
B	Magnetic flux density
c	Speed of light *in vacuo*
c_p	Specific heat at constant pressure
D	Electric displacement field
D_p	Power penetration depth
E	Electric field strength
E_{phot}	Photon Energy
f	Frequency
f_c	Dipole relaxation frequency
G_t	Antenna gain
H	Magnetising field
h	Planck's constant
h	Thermal boundary condition

I	Intensity of incident wave
J	Current density
J_s	Electric source current
k	Wave number
k_b	Boltzmann constant
$L_{crit.}$	Critical thickness (below which Lambert's law cannot be applied)
M_s	Magnetic source current
p_m	Moment of single dipole
P_s	Complex Power
P_v	Volumetric power dissipation
Q	Absorbed power per unit volume
q	Volumetric heat generation
Q_h	Heat
r	Range (from antenna)
S	Poynting Vector (Power flux)
T	Temperature
T_∞	Fluid temperature
T_s	Surface temperature
$tan\delta$	Dielectric loss tangent
V	Volume
Y_0	Characteristic admittance
Y_L	Load admittance

Z_0 Impedance of free space

CC Cold Control

CHP Combined Heat and Power

CO_2 Carbon Dioxide

DC Direct Current

DSP Dual-Square Patch

EM Electromagnetic

EOS Energy Research Subsidy

ETS Emission Trading Scheme

EU European Union

FDTD Finite Difference Time Domain

FEM Finite Element Method

FP7 Seventh Framework Program

GPIB General Purpose Interface Bus

HC Hot Control

HFSS High Frequency Structure Simulator

HP Hewlett Packard

IR Infra-red

ISM Industrial, Scientific & Medical

MW Microwave

NEO New Energy Research

PDE Partial Differential Equation

RF Radio-frequency

UK United Kingdom

USA United States of America

VLD Volume Loss Density

VNA Vector Network Analyser

Greek Symbols

α Attenuation factor

α_t Thermal diffusivity

$\alpha_{x\backslash y}$ Phase difference between field components

β^{-1} Power penetration depth (cm)

χ Electric susceptibility

δS Variation in S-parameter solutions

δ_p Skin depth

Γ Reflection coefficient

κ Thermal conductivity

λ Wavelength

λ_m Wavelength in material

λ_{UI} Uniformity index

μ_0 Permeability of free space

ω Angular frequency

ρ_f Free charge density

ρ Material density

ρ_b	Bound charge density
ρ_w	Volumetric energy density
σ	Conductivity
τ	Dipole relaxation time
ε_0	Permittivity of free space
ε^*	Complex permittivity
ε_∞	Optical (high frequency static) permittivity
ε_e''	Effective dielectric loss parameter
ε_r	Relative permittivity
ε_s	Static permittivity
j_r	Free current density
k_t	Rate of cooling factor

Chapter 1

Introduction

1.1 Structure of this thesis

An overview of the greenhouse vegetable industry is presented with particular emphasis on social, economic and energy themes. This is to provide context and and justify the undertaking of this research project.

A review of the state-of-the-art in the use of microwave technology in agriculture and the greenhouse industry is then presented as a foundation for the novelty of this project.

Fundamental theory relevant to experimental measurement and microwave heating in this thesis is described in Section 2.

Novel measurements of plant permittivity are presented and analysed in Section 3. The results of preliminary experiments are presented in Section 4 and novel work on achieving greater heating uniformity is presented in Section 5.

Results and analysis of novel practical experiments, that utilise the findings of Sections 3 and 5 for heating growing plants with microwaves are presented in Section 6. Extracts of this work were presented at the International Microwave Symposium, Baltimore [11]. A novel method for the calculation and comparison of the efficiency of a microwave system is then discussed in Section 7.

Technical information for equipment used is in Appendix A and some experimental simulation data is in Appendix B and Appendix C.

1.2 Commercial greenhouse horticulture

1.2.1 Size and scale

There are an estimated 1500 Ha of commercial greenhouses in the United Kingdom (UK) used for growing vegetables [12] and in Holland - by far the largest producer of greenhouse produce - this figure is over 10,000 Ha. This area has increased by an average of 400 Ha each year since 1997 [13] and in 2007 over 500 Ha of new greenhouses were constructed, as current infrastructure aged [2]. The main crops produced by both the British and Dutch growers are tomatoes, peppers and cucumbers [14] with over 80 % of Dutch produce being exported [14]. The value of the Dutch greenhouse horticultural sector as a whole was 4.6 billion Euros in 2005, with 23% of this being accounted for by the production of vegetables [14]. Total production value rose by over 50% between 1990 and 2007 [15]. Physical production has increased by 0.85% *per annum* and labour productivity by a factor of 2.5 in the decade upto 2005 [16]. In the same period, natural gas consumption and Carbon Dioxide (CO_2) emissions have declined at a rate of 2.3% *per annum* [16].

For holdings producing only vegetables, the average area of cultivation was 1.9 Ha between 2004 and 2006 [14], although over the last decade the scale of the average holding has doubled [16], and farms of 10 Ha and greater are becoming more common [14]. The construction of new greenhouses has allowed for exploitation of the latest technologies and process techniques [14]. This has resulted in increased yields and reduced energy requirements, and thus increased the profitability of high quality, year round production [2].

In order to maintain output throughout the year, every greenhouse requires heating above the outside ambient temperature; traditionally by natural-gas fired

boilers. Many growers, both in the UK and Holland, now utilise Combined Heat and Power (CHP) plants, which burn gas to produce heat and electricity. The sale of the generated electricity offsets the cost of the gas required to power the generator, and the heat and flue gas are used to warm the growing area and to provide supplementary CO_2. In the Netherlands – arguably the location of the most innovative producers – sales of electricity generated by the greenhouse horticulture sector were 2.5 billion kWh in 2006. In the same period 2.3 billion kWh was purchased by the sector [2]. By 2007, net supplies from the sector has increased to 1 billion kWh and as of 2008, the installed capacity of Dutch growers was over 2275 MW [2, 17]. Investment in CHP technology in the greenhouse horticulture sector is clearly substantial.

In some cases, growers own the CHP plants, whilst others buy the heat generated from owners of a local CHP plant. In 2007, heat was bought to supply a growing area of 1000 Ha [2] and installed CHP capacity was, in general, available to provide for a growing area of 5700 Ha. As such, around two-thirds of growers had access to alternative forms of energy other than traditional gas-fired boilers [2] and it is thus evident that the business models used by the growers are flexible towards uptake of innovative technologies.

1.2.2 Food and resource security

Food security is increasingly becoming an international concern. Specifically, but not exclusively, the effects of population growth, energy demand, land scarcity, water shortages and climate change will all impose constraints on food supply in the coming years [18]. A government commissioned report noted that *"In an environment of increasing uncertainty, the ability of global food production to meet rising demand is becoming recognised as an issue of fundamental importance. Constraints on the availability of energy, water, and land are identified as being of particular significance"* [19]. It has been stated in the Journal of the Royal Agricultural Society of England that *"It is likely that climate change, coupled with rising fuel cost and production uncertainties are the two main criteria to threaten food production* [20].

Indeed, food prices are already increasingly volatile and political disputes have been known to disrupt market behaviour [18]. Food prices are not expected to return to pre-2007 levels owing the ever-increasing demand from developing countries [19, 21] and, with world population expected to exceed 9 billion by 2050 [19], the problem is expected to worsen rapidly.

Further to this, the demands of growing populations in the developing world will be to the detriment of their food exports to the European Union (EU); further increasing pressure on current domestic supplies [20]. The necessary development and expansion of intensive domestic methods demand an increase in both productivity and sustainability [18]. Despite these threats, current trends indicate increased globalisation of the food industry, with high imports and exports and the occurrence of fewer, but larger, suppliers in order to maintain year-round supplies [22].

Oil prices have risen to record levels since 2007 and most sources indicate peak oil supply has been reached or is imminent [19, 23, 24, 25]. As such, governments worldwide have been seeking alternatives to meet the energy requirements of their populations and industries. The production and use of bio-fuels has been given much attention. In Europe, the EU had aimed to meet 5.75% of its transport fuel needs through bio-fuels by 2010 [19] and other countries such as Canada, Thailand, Japan, Columbia and two of the world's most populated and rapidly growing economies - China and India - have taken measures to increase bio-fuel production and consumption [19]. Consequently, the global demand for bio-fuels is increasing exponentially and is exacerbating demand for agricultural land [19, 21].

Over the last fifty years, food production has increased by a factor of four in the UK [20], mainly through technological advances driven by incentives and subsidies from central government. Energy costs were considerably lower however, compared to production margins, than they are now and more land was available in the middle of the twentieth-century, for agricultural use [20]. Although food production has doubled in the last 25 years, the area of agricultural land available

has increased by only 10%, and is not expected to increase substantially further [19]. It is still expected however, that it is possible to double UK food production provided the correct policy is developed and by making use of the best available technologies [21].

It has been reported that *"In order to adequately feed the world population by 2050, vegetable crop production will need to increase by 100%* [21]. However, of the several potential methods for increasing food production (increased land usage, better irrigation *etc.*), the only truly viable and sustainable (which relates the yields to environmental impacts [26]) options are to increase production by increasing yields and improving energy efficiency [21].

1.2.3 Energy consumption

As stated, greenhouses often need heating all year round, typically by the burning of fossil fuels *viz.* oil and natural gas [27]. Specific power requirements vary depending on the time and season [27] but sources, both primary (Figure 7.1) and secondary [12] indicate power requirements for heating the growing area of a commercial greenhouse in Northern Europe to be in the range of 350-800 kWh per m^2 per year. For the UK alone, sources for energy consumption in energy intensive greenhouse vegetable sector estimate power consumption of around 2750 GWh *per annum* [12]. Whilst Northern European production is energy-intensive compared to production around the Mediterranean, it does has the advantage of all year-round production and the use of 10-15 times less pesticide and water [28].

In greenhouse horticulture, energy efficiency is defined as the consumption of primary fuel per unit of product produced [13] and is measured over the area of greenhouse allocated to production. Greenhouse horticulture is by far the most energy-intensive sector of food-production and in Holland accounts for 85% of the total energy consumption in Dutch agriculture [15]. Consequently, greenhouse vegetable production is responsible for a significant proportion of CO_2 emissions, with the Dutch greenhouse horticulture sector accounting for 3% of the total national output [2].

Sustainable energy is defined as avoided primary energy usage [29]. The overall share of sustainable energy used by a grower is the total avoided primary energy divided by the sum of primary energy used and primary energy avoided [29]. In greenhouse horticulture, sustainable energy use is attained through the purchasing or sourcing of sustainable heat and electricity, as well as through the use of heat pumps, wind energy, biomass and solar energy (thermal and photo-voltaic) [2, 29]. In 2001, sustainable energy accounted for only 0.1% of all energy used within the sector and had only risen to 0.4% by 2005; nevertheless it fell far short of a government-agreed target of 4% by 2010 [13]. In 2003, the Dutch greenhouse horticulture sector was estimated to have avoided 617400 GJ of primary energy from a total primary consumption of 123.7 PJ [29].

It has long been the case that holdings purchase what would otherwise be waste heat from local power companies [13], although since the liberalisation of the energy market, holdings have moved towards using their own CHP plants to generate heat [1], CO_2 (for plant enrichment) and electricity for sale to the national grid [13, 17]. Since 2004, investment has been focussed towards improved, larger, CHP plants [14], resulting in an increase in the number of sites using such plants [1]. With more holdings now owning CHP units themselves, the energy supplied by third parties has started to decrease. Energy - typically heat - supplied from third parties was 9.8% in 2002 but already only 8.6% by 2003 [1].

It is interesting to note that electricity generated by the greenhouse horticulture sector is not always - or indeed often - used by the growers. In fact, it is estimated that only around 40% of holdings owning a wind turbine use the electricity generated [29], rather than sell it, as is the case with CHP where the sector in Holland has became a net supplier of electricity [13]. By the start of 2007, when Dutch CHP capacity was at least 1700 MW [13], it consumed around 1.8 billion cubic metres of natural gas, resulting in the production of 6.5 billion kWh of electricity and 0.9 billion natural gas equivalent units of heat [17]. Overall, however, application of this energy is very high; at more than 98% for electricity (largely to the grid) and 96% for heat used warming the greenhouses [17]. Whilst CHP is clearly very efficient in the application of the energy supplied, it has meant continued

reliance on natural gas and in 2003, 87% of energy supplied to the sector was of this form [1]. As such, the increase in the uptake and contribution of more sustainable energy options is limited [13].

Energy consumption from the use of CO_2 dosing and supplementary lighting has also been steadily increasing with the rise in their use. In particular, the intensity of lights has increased by an average of 1.2% *per annum* to around 43 W per m^2 in 2004 [1]. In the same year, assimilation lighting was used in around a quarter of all holdings [1], mainly for non-vegetable crops, although use for vegetable crops is expected to increase as demand for high-quality year-round produce increases. Around half of holdings which used supplementary lighting obtained the power from the national grid, with the remaining half generating the power themselves [1]. In 2006 an estimated 25% of total greenhouse acreage in Holland used supplementary lighting [15], which resulted in around a 12% improvement in production, at the expense of a reduction in overall efficiency [16].

The goal of better energy efficiency has been a long-standing one for the greenhouse horticulture sector. Since the high oil prices of the late 1970s, advances were sought and the early 1980s saw major improvements in energy efficiency [15]. Since then, improvements have been made steadily, but at a slower rate. Between 2000 and 2005 there was a period of significant reduction in the consumption of primary fuel per unit area of greenhouse. This was due more to a 14% improvement in yield, compared to a modest, but nonetheless significant, 7% reduction in fuel use [13]. Recent figures indicate that the energy efficiency index (EE), which is an industry-wide standard index, has improved from 40% to 56% in the period 2000 to 2006 [2], relative to 1980 levels. Also, at the end of that period, the sector used 60% less primary fuel per unit produce relative to 1980 [2, 13].

As of 2007, energy usage in the Dutch sector had increased slightly, but was again accompanied by increasing yields. This has resulted in a stabilisation of energy efficiency and an offsetting of CO_2 emissions from cultivation by the sales of generated electricity [2]. Most of this electricity was generated by CHP plants and accounted for a 6% point improvement in efficiency and a 0.7 Mt reduction

in CO_2. Purchased heat accounted for 2% points of the efficiency improvement and 0.4 Mt of the CO_2 target. Sustainable energy accounted for only 0.3% points of the efficiency savings and 0.04 Mt of CO_2 [2].

1.2.4 Climate, innovation and legislation

It has been stated for the UK that, *"the direct environmental, social and economic costs of food transport are over £9 billion each year* [22] and that it can at times be more energy efficient to grow and import Spanish tomatoes than to produce them in the UK [22]. As a result, global efforts to reduce emissions of CO_2 have led to various policy initiatives being introduced to encourage better energy efficiency. These include financial/tax incentives, levies and targets.

In order to determine the contribution of the greenhouse horticulture sector towards meeting national CO_2 reduction targets, the Dutch greenhouse horticulture sector and government agreed in 1993 to impose the obligation of a 50% improvement in energy efficiency across the sector by 2000, in relation to 1980 levels [30]. In 2003, the EE Index was 51% [1].

The EU has a directive on energy end-use efficiency which aims for a 9% improvement by 2016 compared to the period 2001 to 2005 [14]. The EU Emission Trading System (ETS) also requires the participation of all users of combustion units with a heating capacity of 20 MW (thermal) or greater [14], and in Holland the ETS applies to around 75% of growers [14]. It has been warned however, that if Dutch policy follows the EU-ETS, the production of the sector in Holland could decline by 4.8% to 8.9% [28], as the CO_2 emission per unit produce in Northern Europe is around 9-17 time larger than for production in Spain [28]. In order to increase or maintain competitiveness, the reduction in CO_2 must therefore come from a reduction in energy consumption [2].

Targets between the Dutch sector and government were since set that aimed for a 65% improvement in energy efficiency by 2010, compared to 1980 [2, 13, 14, 15]. Further to this target, the aim was also to achieve 4% of all energy needs from

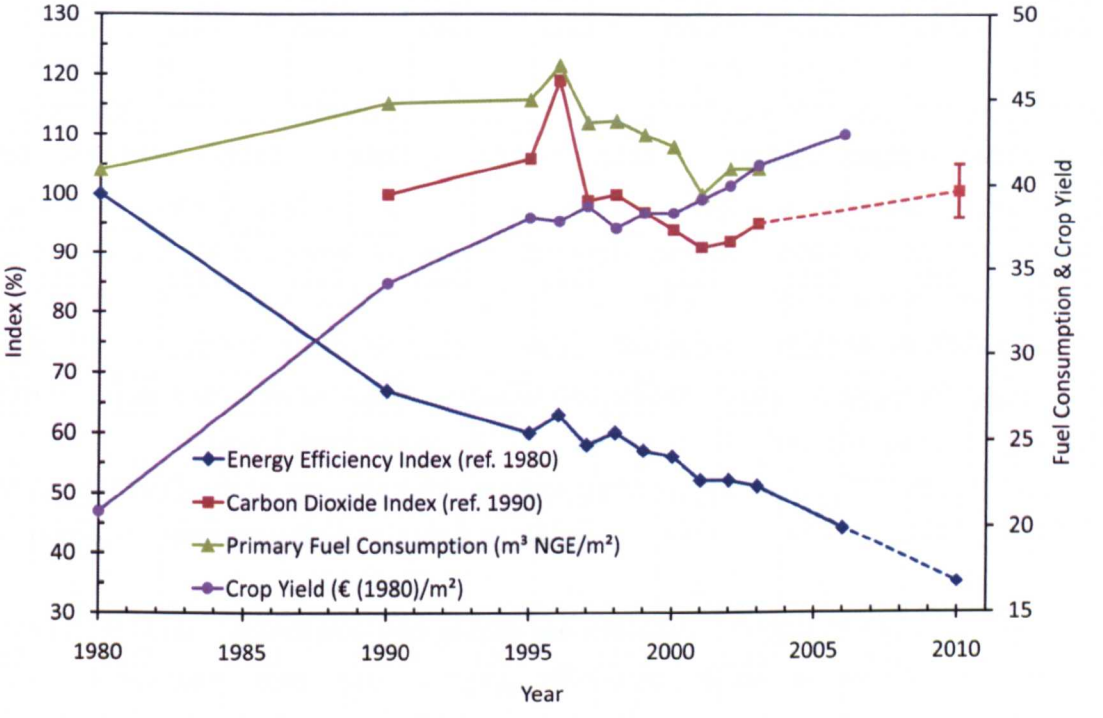

Figure 1.1: Graph of energy, carbon dioxide and yield trends in the Dutch greenhouse vegetable sector. Compiled from data in [1] and [2]. Dotted lines indicate projections towards agreed targets.

sustainable sources over the same period [29]. These targets were recorded in the Greenhouse Horticulture Decree and the Greenhouse Horticulture and Environment Covenant, signed in 2002 [14, 29].

For UK growers, emission targets were set which aimed to reduce output by 12% of 2005 levels by 2010 [12]. In Holland, specific greenhouse horticulture targets have been set for CO_2 emission: in the period of 2008 to 2012, of 6.6 Mt *per annum* for cultivation under 10500 Ha of glass, rising to 7.2 Mt should the area in increase to 11500 Ha [1, 13, 14]. The trends of energy efficiency, CO_2 emissions and yields in the Dutch sector are shown in Figure 1.1, which is a graphical compilation of available data. The dependence of efficiency improvements on increasing yields are most prominent, as is the stagnation in CO_2 reductions.

The greenhouse horticulture industry is regarded as a technologically innovative

sector [14, 16] and nearly all investments are to reduce labour and energy costs; these being the most significant costs in protected crop production [14]. This is characterised by a high rate of investment in new technologies and, in the period 2003-2005, the Dutch greenhouse horticulture sector invested considerably more than other agricultural sectors [15]. Some of the innovative, technology-based ideas for increasing production are offshore production, artificial photosynthesis and more efficient use of biomass [21]. The sector conducts numerous experiments and is investing heavily in new ideas - the most ambitious of which is the Dutch collaboration between government and industry; the *'Kas als Energiebron'* or Energy-producing Greenhouse [14, 15] (see section 1.3.5). The project aims to create a greenhouse that generates electricity with the goal of becoming energy neutral and economically profitable by 2020.

In Holland, many incentives and grants are available to support the development of new technologies that improve energy efficiency [14] and across Europe the EU Seventh Framework Program (FP7) provides financial support for international research and development for energy saving technology. The Energy Research Subsidy (EOS) is a programme aimed at creating and improving technology that improves or realises the use of sustainable energy, by providing financial support to companies and research institutes [14]. Also, New Energy Research (NEO), which is a European funding programme, offers financial support for the development of unconventional research projects that contribute to the use of sustainable energy [14].

With innovation often comes further regulation and, since 2005, the Greenhouse Horticulture Decree has required growers using artificial lighting to restrict or avoid up to 95% of horizontal and vertical light pollution at certain times of the day (and year), through the use of screens [14]. This will increase to 100% screening of light by 2014 [14].

For Dutch holdings, the most common sustainable energy technology used is the heat pump (heat storage), followed by some form of wind energy [29], although the use of moveable screens is also popular. Since 1995, the implementation of screens and heat storage has increased *per annum* by 2.7% and 3.7% respectively

[1], with a total of 79% of cultivated area employing the use of screens and 40% using heat storage as of 2004 [1]. The use of screens is expected to increase to around 90% of cultivated area and heat storage to 60%, although the use of condensers and climate-control computers is thought to have saturated [1]. The use of gas combustion condensers can result in savings of 5-10% depending on the type used [30] and in 2004, 72% of boilers had them fitted [1].

Although adding to sustainability and increasing efficiency, these technologies do not negate the use of gas boilers and CHP - although they are themselves much more efficient than traditional power stations. Despite consuming fossil fuels [13], they reduce primary fuel consumption as, although requiring more gas to operate, the costs and CO_2 emissions are offset by the sale of the electricity that they generate [2, 17]. Some energy is wasted however, owing to difficulties in harmonisation of the demand in heat and electricity with the supply [17]. This is exemplified by the fact that, although 83% of holdings employed CO_2 supplementation in a studied period, 57% of it was at times of minimal heat demand [1]. Of these holdings, 90% used heat storage tanks to recover some energy that would otherwise be wasted [1].

1.2.5 Concluding remarks

The greenhouse horticulture sector in Europe is extremely large, both in terms of its physical size, and in economic output. The market is dominated by growers in Holland but a significant number of UK growers contribute to the crucial, stable and secure supply of food within the EU. The sector is, however, very resource and energy dependent. The high energy consumption accounts for the greatest proportion of production costs and furthermore, results in significant greenhouse gas emissions.

Coordinated efforts by regulatory authorities, academia and the industry have led to a sector that is highly innovative and invests heavily in new technology, to reduce both costs and emissions. Evidence indicates that significant progress has been made in recent decades, but there is a huge requirement for further

improvement.

The most substantial gains in efficiency have thus-far came from improvements in crop yields, compared to piece-meal reductions in energy consumption. Consequently, there remains a significant need and opportunity to provide a technological solution to reduce the energy consumed in heating commercial vegetable greenhouses.

This thesis demonstrates the use of microwave energy to heat greenhouse crops as a means to substantially reduce energy consumption and so reduce greenhouse vegetable production costs and greenhouse gas emissions. The work is a combination of identifying the heating mechanisms in the plants, quantifying the plant power and heating requirements and demonstrating a feasible technical system for heating the plants. In addition, a method for calculating and comparing efficiency between microwave and conventional heating systems is presented, with an example, to substantiate the claimed benefits of such a system.

1.3 State-of-the-art in microwave heating and agriculture

1.3.1 Greenhouse plants in a microwave cavity

The use of microwaves in the growing of plants is scarcely reported in the literature. However, Teitel *et al.* investigated the heating of mature tomato and pepper crops, in a cavity within a greenhouse and using microwave radiation, with a specific emphasis on reducing the occurrence of grey mould [3]. The authors claimed that it was possible to heat the plants without visible damage and with no increase in susceptibility to grey mould [3]. They also observed that the greenhouse air did not warm up and remained at a nearly constant temperature. Heating uniformity apparent in the microwave-treated plants was said to be *"not much worse"* than for hot-air heating [3]. They also claimed that the energy required for microwave heating was 55% of that required by hot-air heating [3].

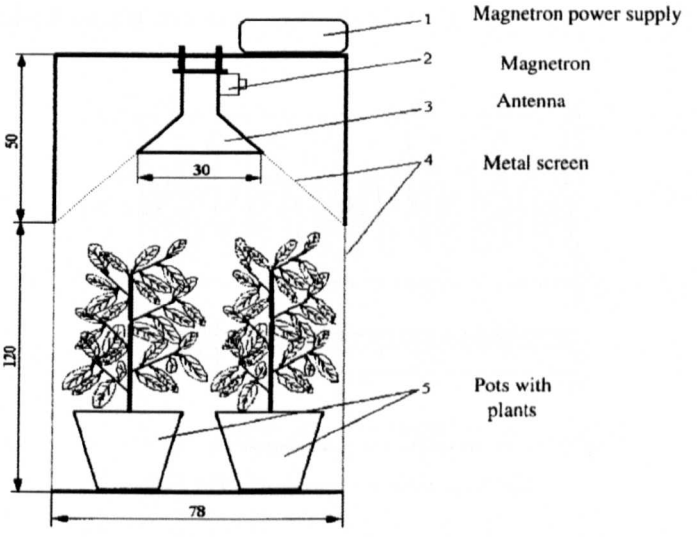

Figure 1.2: Experimental set-up of plants in microwave cavity, presented in [3].

The authors state that the experiment was conducted with mature pepper plants and lasted for two weeks in total, with plants being inspected for damage after week one and two [3]. Microwave plants were placed within a metallic cavity of 0.78 × 0.78 × 1.7 m, as shown in Figure 1.2. This cavity was place inside a polyethylene greenhouse of 2 × 2 × 2 m. Plants heated by hot air were in a similar greenhouse nearby. A microwave source of 500 W was used to heat the plants and was thermostatically controlled by a thermocouple attached to leaf 4, which resulted in a power on/off cycle of 4 per minute [3]. A similar power-control method was used for the plants heated by hot air, but resulted in a longer duty cycle [3].

Plants were deliberately infected with grey mould after or before microwave heating and placed in warm and humid conditions to encourage the onset of mould growth. The authors found that the susceptibility to grey mould was lower in the microwave plants and that the leaves of microwave plants were warmer than the air at all times [3]. The fruit was found to be cooler and nearly constant in temperature, compared to the leaves, which where the warmest components [3]. This was attributed, by the authors, to the fruit having a much larger mass of water than the leaves. It was claimed that *"exposure to microwave radiation resulted in no visible injury to leaves, flowers and fruits"* and that exposure after

two weeks *"resulted in no adverse symptoms"* [3].

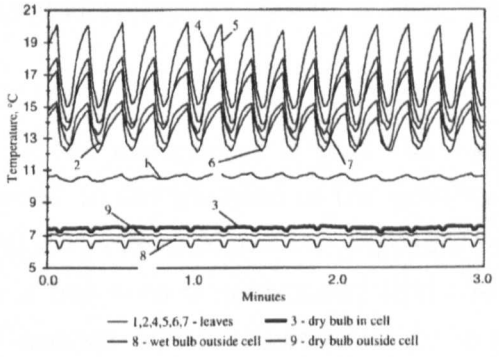

(a) MW heating – leaves and air

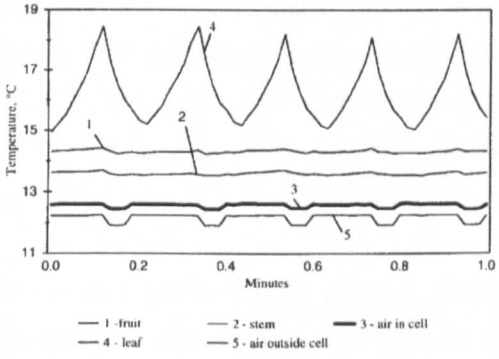

(b) MW heating – plant components

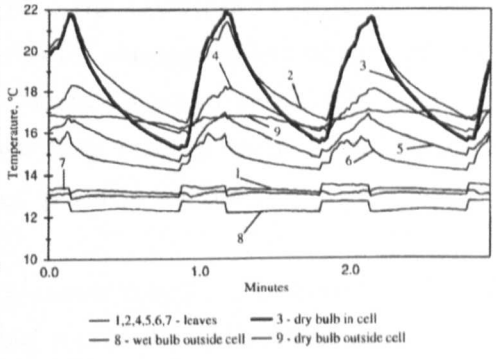

(c) Hot-air heating – leaves and air

Figure 1.3: Plant temperature *vs.* time; data presented in [3].

The leaf temperatures recorded by the authors and reproduced Figure 1.3a show a large fluctuation in temperature over a short time span. For example, leaf 5 varies between 15°C and 20°C four times every minute. Also, the average temperatures between leaves measured on the microwave plant are significantly different: 10.6°C for leaf 1, 14°C for leaf 2 and 17.5°C for leaf 5. Whilst the hot-air system also showed a range of average temperatures, for different leaves (Figure 1.3c), the range for individual leaves was generally not as large. Also, some leaves of the hot-air heated plants appeared to not be heated at all, whilst others appeared to be heated significantly. No explanation was offered for this and it is not clear to what extent this due to experimental conditions.

Figure 1.3b shows the temperatures for different plant components. It would ap-

pear that the stem and fruit do not heat up from microwave exposure, whilst the leaves heat and cool rapidly. No similar data is offered for the plants heated by hot-air. This appears to undermine the statement that uniformity between plant groups was similar.

A major shortcoming of the experiment is that the duration of the trial was very small when compared to the life-span of the growing plants. As such, it is not evident what cumulative effect microwave exposure may have on the plant. Furthermore, although it has been demonstrated that the plants can be heated, no target temperature was set and it is not clear if the range of temperatures produced in various parts of the plants are indeed adequate to grow the plants successfully over their entire life-cycle, given the duration of exposure. As such, the claim that microwaves resulted in no visible damage is premature; if the temperature is too low, cold damage would begin to occur gradually. Likewise, if higher power is required, possible damage may remain to be seen. Regardless, the ultimate fate of the microwave-treated plant is unclear.

The authors reasoned that overall, the microwave system consumed 25% of the energy used by the hot air system, but that a commercial system that burns fuel directly on-site would have an efficiency of around 85%, compared to a power station that has an efficiency of around 40-45%. They therefore adjusted the figures to find that the microwave system required around 55% of the energy used by the hot air generator. This method does not account for several important factors that will affect the efficiency of a microwave heating system. These include, but are not necessarily limited to, the size and quantity of plants, the area and volume that the plants occupy, the required plant temperature, ambient temperature and the actual power required to facilitate adequate heating of the plants. The stated calculated efficiency is, at best, a crude approximation of the relative efficiency *of that experiment only*, and can not therefore be applied or assumed generally.

1.3.2 Long-term exposure of spruce and birch trees to microwaves

The effect of long-term exposure of microwaves on spruce and beech trees has been studied and reported in the literature [4]. Four groups of trees were exposed to 2.45 GHz microwave radiation of varying power densities, as shown in Figure 1.4, for three-and-a-half years. The authors stated that the group exposed to the highest power density had an average temperature 4°C higher than the other groups [4]. Height of the plants and crown transparency – a parameter used in quantifying forest conditions – were all similar between groups, with no apparent or obvious effects on the trees from microwaves. Some calcium deficiency effects were observed in the high power density group, during the experiment, but were not present at the experiment end [4] and it is unclear to what extent the microwaves may have caused this.

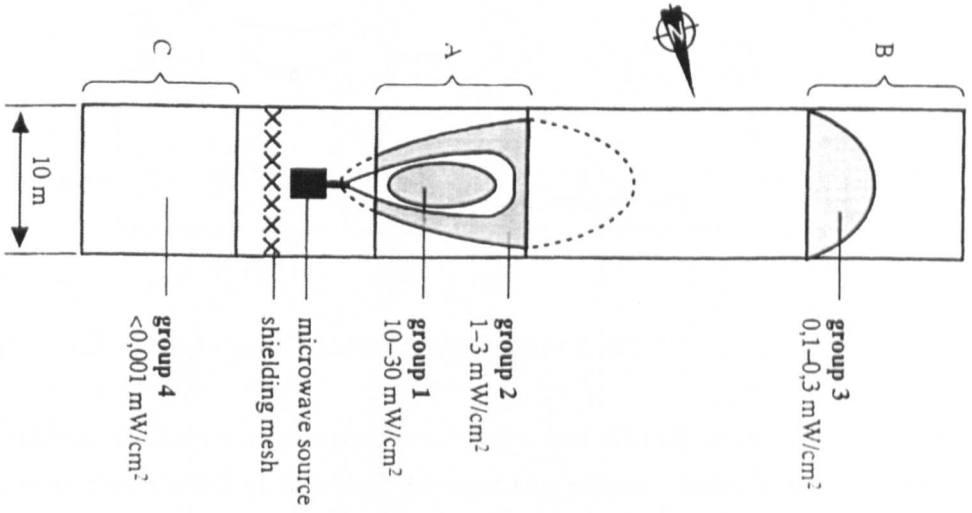

Figure 1.4: Schematic plan of tree groups exposed to microwaves, indicating incident power densities, presented in [4].

1.3.3 A patented system for greenhouse heating using microwaves

This speculative patent application calls for *"the sides and roof of a greenhouse [to be] lined with a membrane or mesh substantially transparent to optical radiation but very good at reflecting microwaves. One or more microwave generators radiate into the space so enclosed, in such a way as to set up by multiple reflections a complex pattern of standing waves filling the space. The lined greenhouse becomes in effect a very large microwave cavity, damped by a load largely created by the plants and to a smaller extent by the soil"* [5].

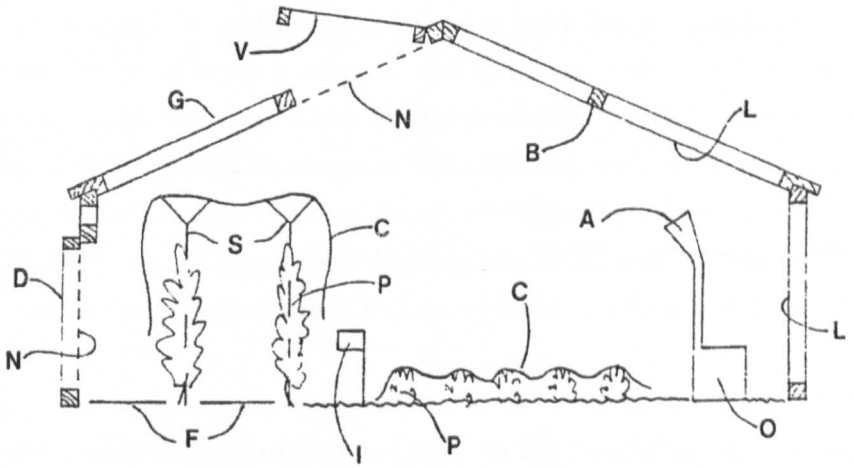

Figure 1.5: Diagram of patented equipment configuration, presented in [5].

The apparatus diagram is reproduced from the patent document in Figure 1.5. The microwave source is labelled 'O' and the patent states that microwaves are radiated from a horn antenna, 'A' towards the ceiling liner, 'L' with the intention of creating a uniform radiation density [5]. The design states that for a small greenhouse of around 20 m^2, as shown in Figure 1.5, a single magnetron of power 1 kW at around 2.45 GHz would suffice [5]. The labels 'N' and 'F' are mesh and foil shielding, respectively. Plants are labelled 'P' and are covered with polythene sheets, labelled 'C'. Plant supports are labelled 'S'.

The patent claims that by using surfaces reflective to microwaves, a substantially uniform field with low power density can be produced, and could be improved

further by using rotating mode stirrers. It is claimed that any non-uniformity in heating by microwaves would be *"levelled out due to inter-radiation and convection between the closely-spaced leaves"* [5]. The patent also claims that by shielding the inside of the greenhouse with a covering reflective to infra red would mean *"extremely uniform heating by radiation is achieved by using the two kinds of radiation"* [5]. The invention calls for microwave generators to be installed elsewhere and power transferred to where it is required by wave-guides or coaxial cable. Power is to be controlled by an infra-red sensor as part of what is essentially a closed-loop feedback system, not too dissimilar to those used currently in commercial operations.

It would seem that, for a greenhouse that is very large compared to the wavelength, it would be difficult to set up and maintain any complex standing-wave patterns or for it to act as a cavity. Radiation within the greenhouse would more likely be similar to normal free-space transmission and controlling the direction and distribution of the microwaves using reflectors would be very difficult. This would most likely result in poor electromagnetic field and heating uniformity and introduce undesired physical obstructions to light reaching the plants.

The design-idea of aiming the microwaves at the ceiling, in order to improve uniformity, would also depend almost entirely on the careful design of the reflective element; for which the patent does not specify. Such a technique would then, far from creating a uniform reflected field, only serve to attenuate the microwave signal through increased path-loss. For a 1 kW power source, used in the example greenhouse given in the patent document, and for the ideal scenario of a completely uniform field with zero losses, a power flux density of 50 Wm^{-2} would result. It is to be seen whether this power density is adequate for heating the plants – and for which plants, in what conditions. The effect on efficiency of using a remote generator and coaxial cables to distribute power is also not considered in the design specifications. The author is also perhaps over-optimistic of the effect re-radiation by infra-red would have on thermal equalisation of non-uniform resultant plant temperatures.

1.3.4 Tractor-towed microwave vegetation eliminator

A further application of microwaves on living plants has been for the destruction of weeds in agricultural fields, as an alternative to low-efficiency thermal methods [6]. It has been shown that small herbaceous species in fields can be destroyed by a tractor-towed array of high power microwave sources that irradiate the ground [6], an example of which is shown in Figure 1.6. Several patented designs that incorporate mode-stirrers into the trailer to increase field and heating uniformity have been shown in [6]. The reported power density required to eliminate plants in a field is 530 Wm^{-2} for a duration of 15 seconds [6], which would suggest that plants are surprisingly robust to microwave heating.

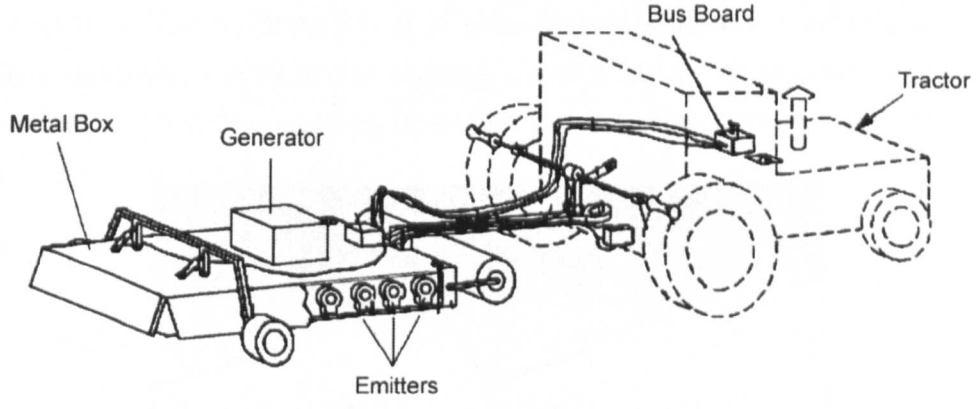

Figure 1.6: Patented design of microwave weed eliminator for use in fields, as reported in [6].

1.3.5 Energy producing greenhouse

A novel kind of greenhouse (shown in Figure 1.7) is currently being developed and is reported in the literature [7]. The design uses a specially shaped roof and reflective lining to divert near infra-red radiation towards an array of water-cooled photovoltaic cells [7].

In the summer months, this allows the collection of low grade heat, which can be stored underground at around 30°C, as well as the generation of electricity [7]. The photosynthetically active radiation is allowed to pass through the covering, enabling the plants inside the greenhouse to grow, whilst reducing overheating

[7]. This method would enable the greenhouse to be passively cooled whilst remaining sealed, allowing CO_2 dosing to be economically viable [7]. In the winter months, stored heat can be recovered using an electrically powered heat pump to supplement greenhouse heating.

The authors claim that an improved and optimised design could generate 31 $kWhm^{-2}$ of electrical energy and 270 $kWhm^{-2}$ of thermal energy, each year, although the current prototype generates 20 $kWhm^{-2}$ and 161 $kWhm^{-2}$, each year, respectively [7]. Current technological obstacles to reaching this goal are the spectral range of the reflective covering and the efficiency of the photovoltaic cells [7]. It is envisaged that the greenhouse could operate independently of fossil fuels and be in use by 2020 [7]. It is immediately apparent how an electrically-powered microwave system for heating crops could be integrated with such a greenhouse to provide complete, fossil-fuel independent, temperature regulation.

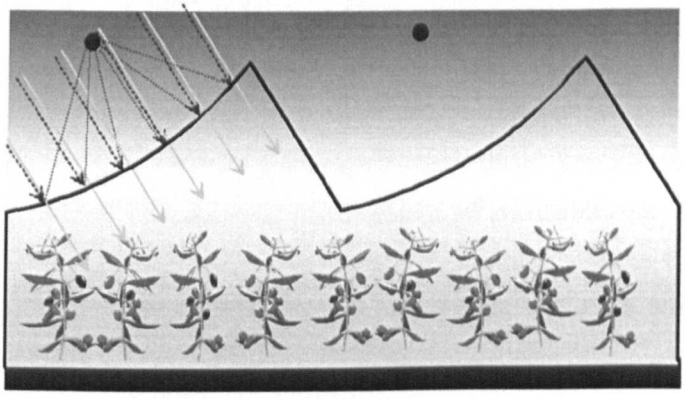

Figure 1.7: Diagram of energy-generating greenhouse concept [7].

Chapter 2

Fundamentals of Dielectric Heating

This chapter provides an overview of the means by which electromagnetic (EM) energy and power are transferred during propagation in free-space and the associated regulation of the EM spectrum. Following this, the interaction of EM radiation with matter is reviewed from the perspective of absorbed power within a dielectric medium and the intrinsic mechanisms of permittivity. In particular, a detailed model of the dipolar mechanism of permittivity is reviewed. This information is directly relevant to the study of heating effects caused by the interaction of EM radiation and matter in the context of this work and provides the basis for the work to be found in subsequent chapters.

2.1 Electromagnetic energy

EM radiation exists in a continuous spectrum which, for convenience, is subdivided into groups of similar wavelength (and by extension, similar behaviour and interactions with matter). The relationship between wavelength, frequency and (photon) energy of a wave is given by

$$f = \frac{c}{\lambda} = \frac{E_{phot}}{h} \tag{2.1}$$

where f is wave frequency, λ is wavelength, E_{phot} is the photon energy, c the

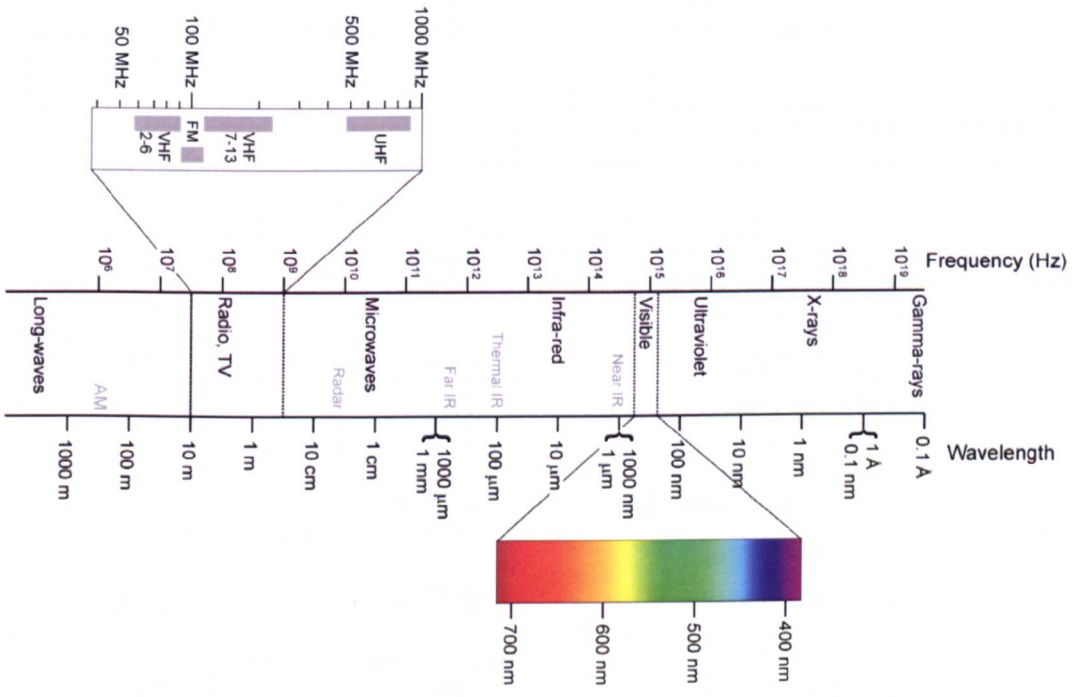

Figure 2.1: The electromagnetic spectrum. Courtesy of Louis E. Keiner, Coastal Carolina University.

speed of light in vacuum and h is Planck's constant.

It follows then, from Figure 2.1, that long-wave radio waves are the least energetic and gamma-rays the most energetic.

Wavelengths shorter than high ultra-violent are termed as non-ionising, owing to their inability to strip the electrons from atoms on which they are incident. This work concerns the use of only non-ionising radiation.

2.1.1 Regulation of the spectrum: ISM bands

Regulation of the spectrum by governments is strict and users are assigned specific bands for specific purposes [31]. The regulations state that certain frequencies are reserved for Industrial Scientific and Medical (ISM) uses and are termed ISM bands. These are shown in Table 2.1. Equipment using these bands do not

Frequency (MHz)	Bandwidth (%) or Frequency range(±)	Area of Use
13.560	7 kHz	Worldwide
27.120	163 kHz	
40.68	20 kHz	
433.92	0.2%	Austria, Netherlands, Portugal, Germany, Switzerland
896	10 MHz	United Kingdom
915	13 MHz	North and South America
2375	50 MHz	Albania, Bulgaria, Hungary, Romania, Russia
2450	50 MHz	Worldwide (except where 2375 MHz is used)
3390	0.6%	Netherlands
5800	75 MHz	Worldwide
6780	0.6%	Netherlands
24150	125 MHz	Worldwide
40680		United Kingdom

Table 2.1: Selection of radio-frequency and microwave ISM Frequency Bands [33].

require a license and must accept interference from other ISM band equipment [31]. Whilst most people are familiar with the use of 2450 MHz as the frequency used for dielectric heating in most domestic microwave ovens, commercial ovens may be designed to operate at any of the ISM frequencies [32] if they would provide improved processing times, greater efficiency, better quality *etc.*

2.1.2 Electromagnetic waves

2.1.2.1 Maxwells equations

A time-varying magnetic field will result in a spatially-varying electric field and vice-versa. This phenomenon of mutually-dependant oscillating fields is what forms an electromagnetic wave and can be described by the laws of electricity

and magnetism - collectively and commonly known as Maxwells equations [34].

$$\text{Gauss' Law: } \nabla \cdot \vec{D} = \rho_f \text{ (electric charge)} \tag{2.2}$$

$$\text{Gauss' Law: } \nabla \cdot \vec{B} = 0 \text{ (magnetic charge)} \tag{2.3}$$

$$\text{Faraday's Law: } \nabla \times \vec{E} = -\frac{\partial \vec{B}}{\partial t} \tag{2.4}$$

$$\text{Ampre-Maxwell Law: } \nabla \times \vec{H} = j_r + \frac{\partial \vec{D}}{\partial t} \tag{2.5}$$

Above, E is the electric field, B is the magnetic flux density, ρ_f is free charge density, j_r is free current density (both of which are zero in free space) and the identity,

$$\nabla = \vec{i}\frac{\partial}{\partial x} + \vec{j}\frac{\partial}{\partial y}\vec{k}\frac{\partial}{\partial z} \tag{2.6}$$

The important relationships which define the electric displacement field, magnetic field and current density, respectively, are given by

$$\vec{D} = \varepsilon_0 \vec{E} \tag{2.7}$$

$$\vec{H} = \frac{\vec{B}}{\mu_0} \tag{2.8}$$

$$\vec{J} = \sigma \vec{E} \tag{2.9}$$

Where μ_0 is the permeability of free space, ε_0 is the permittivity of free space and σ is conductivity.

2.1.2.2 Plane wave solutions

Manipulation of equations (2.2) to (2.9) allow the decoupling of Maxwells equations. Specifically, by taking the curl of Equation (2.4) (assuming free-space conditions) and by using the vector identity

$$\nabla \times \left(\nabla \times \vec{E}\right) = \nabla\left(\nabla \cdot \vec{E}\right) - \nabla^2 \vec{E} \tag{2.10}$$

the wave equation and can be found as

$$\nabla^2 \vec{E} - \frac{1}{\mu_0 \varepsilon_0} \frac{\partial^2 \vec{E}}{\partial t^2} = 0 \tag{2.11}$$

A similar result can be obtained in terms of $\vec{B}$. All field components must satisfy the wave equation with the speed of light in a vacuum given by

$$c = \sqrt{\frac{1}{\mu_0 \varepsilon_0}} \tag{2.12}$$

This generalised form of Equation (2.11) can be reduced for a plane wave travelling in the z-direction, so that

$$\frac{\partial^2 \vec{E}}{\partial z^2} - \frac{1}{\mu_0 \varepsilon_0} \frac{\partial^2 \vec{E}}{\partial t^2} = 0 \tag{2.13}$$

A solution for this wave equation can be written

$$\vec{E}(z,t) = E_0 e^{j(\omega t - kz)} \tag{2.14}$$

Where ω is the angular frequency and k is the wave-number, given by

$$k = \frac{\omega}{c} \tag{2.15}$$

Alternatively, considering only the forward wave travelling in the z-direction, the plane wave solution can be written in the form

$$\vec{E} = (E_0\hat{x} + E_0\hat{y})\, sin\,(\omega t - k\hat{z}) \tag{2.16}$$

Again, similar solutions exist for the $\vec{B}$ field. As the dot product of $\vec{E}$ and $\vec{B}$ is zero, $\vec{E}$ and $\vec{B}$ are orthogonal.

2.1.3 Power absorption in a dielectric

2.1.3.1 Energy and power in a wave

Poyntings theorem is a power balance equation that describes energy conservation for electromagnetic fields and sources. The complex power P_s delivered by sources J_s and M_s inside a closed surface enclosing a volume V, is given by [35]

$$P_s = -\frac{1}{2}\int_V \left(\vec{E}\cdot\vec{J}_s^* + \vec{H}^* + \vec{M}_s\right) dv \tag{2.17}$$

A quantity S, known as the Poynting vector, is the energy flux density in Wm^{-2} and is given by [35]

$$\vec{S} = \vec{E}\times\vec{H} \tag{2.18}$$

Expanding this and averaging over time means the complex power flow out of the closed surface can then be written in the form given by Metaxas and Meredith [34, 35],

$$P_0 = \frac{1}{2}\oint_S \vec{S}\cdot ds = \frac{1}{2}\oint_S \vec{E}\times\vec{H}^*\cdot ds \tag{2.19}$$

The real parts of P_s and P_0 represent time-average powers.

2.1.3.2 Energy and power in a dielectric

In the far-field H is proportional to E so, in a volume V of dielectric ε, Equation (2.19) becomes

$$P_{av} = -\frac{1}{2}\omega\varepsilon_0\varepsilon''\left(\int_V \vec{E}\times\vec{E}^*\right)\cdot dV \tag{2.20}$$

By then assuming that the magnitude of the complex field component is constant throughout the material (or that the material being considered is thin), the frequency-dependent power dissipated per unit volume in a dielectric can then be given by the expression [34, 36, 37]

$$P_v = \frac{1}{2}\left(\sigma(\omega) + \omega\varepsilon_0\varepsilon''(\omega)\right)|\vec{E}|^2\, Wm^{-3} \tag{2.21}$$

The total power dissipated in a volume can easily be found by integration.

$$\vec{P} = \int_V P_v dV \tag{2.22}$$

2.1.3.3 Time-domain analysis

The above equations are useful for calculating dissipated power in dielectrics, but a more detailed picture of how the energy in the wave is transferred can be seen by looking at the time-dependent fields.

The energy conversion equation in the time domain from Poyntings theorem can be written [36]

$$div\vec{\vec{S}} + \frac{\partial \rho_w}{\partial t} = -\vec{P} \tag{2.23}$$

Where $\vec{S}$ is the energy flow into a volume (Poynting Vector), and ρ_w is the volumetric energy density which, from classic Poyntings Theorem, can be written

$$\rho_w = \frac{1}{2}\left(\vec{E}\cdot\vec{D} + \vec{H}\cdot\vec{B}\right) \tag{2.24}$$

By using the identity

$$div(\vec{A}\vec{B}) = \vec{B}\cdot curl\vec{A} - \vec{A}\cdot curl\vec{B} \tag{2.25}$$

and Equation (2.4) and (2.5) with the time derivative of Equation (2.23) yields

$$div\left(\vec{E}\times\vec{H}\right)+\frac{\partial\rho_w}{\partial t}=-\frac{1}{2}\left(\vec{E}\cdot\frac{\partial\vec{D}}{\partial t}-\vec{D}\cdot\frac{\partial\vec{E}}{\partial t}\right)-\frac{1}{2}\left(\vec{H}\cdot\frac{\partial\vec{B}}{\partial t}-\vec{B}\cdot\frac{\partial\vec{H}}{\partial t}\right)-\vec{j}\cdot\vec{E} \quad (2.26)$$

The second term on the left hand side is the total losses per unit volume [36]. The right hand side of this equation thus identifies the particular means of the losses (*i.e.* the energy source) associated with a time-varying EM field; the first term on the right hand side is the instantaneous power dissipated by electrical field interaction with the dielectric, the second term being the instantaneous power dissipated by magnetic losses and the final term representing conductive losses [36]. If the fields are all time-harmonic, then by applying Equation (2.7), the original result for electromagnetic losses in a substance of a given permittivity - Equation (2.21) – is arrived at. Units are Watts per cubic metre.

2.1.4 Thermal effects

The heating effect of microwaves is volumetric [37, 38], owing to the fact the EM radiation tends to penetrate into a material as it dissipates. This is highly beneficial when striving for an efficient heating system as it can result in heat transfer from within the material interior as well as slower transfer of heat from the surface to the interior [39], compared to conventional forms of heating. This is due to the smaller thermal gradients that exist within the material. For example, during infra-red heating, all power is dissipated very close the material surface and so easily re-radiates from the heated object. This is reduced during microwave heating, where the energy remains within the material volume for longer.

When analysing microwave heating problems, the electromagnetic fields are usually solved for first, in order to calculate the power dissipated [36]. From this, the thermal consequences can be established and solved for with respect to time. Although this is convenient, the EM and thermal effects are inter-dependent and any system when EM power is constant means, of course, that EM and thermal solutions are coupled.

2.1.4.1 Temperature increase in a volume

A simple equation to describe the temperature increase with time, as caused by the power dissipated in a unit volume is given by [40]

$$\rho c_p \frac{dT}{dt} = P_v \tag{2.27}$$

The transient thermal effects can be described using Fouriers equation. This describes the local heat flux in space, with respect to time, and is given in its integral form by

$$\frac{\partial Q_h}{\partial t} = -k \oint_S \vec{\nabla} T \cdot \vec{dA} \tag{2.28}$$

Here, the left hand side is the heat transferred per unit time, in Watts, $\vec{\nabla} T$ is the temperature gradient and $\vec{dA}$ is a surface element. Integrating thus describes the heat flow rate, which leads on to the consequence of this law; the heat equation.

2.1.4.2 Temperature distribution in a volume

If u is the temperature as a function of space and time, then the rate of change of temperature at a point is given by the partial differential equation,

$$\frac{\partial u}{\partial t} - \alpha \left(\frac{\partial^2 u}{\partial x^2} + \frac{\partial^2 u}{\partial y^2} + \frac{\partial^2 u}{\partial z^2} \right) = 0 \tag{2.29}$$

Where the second partial derivatives are thermal conductions and

$$\alpha = \frac{\kappa}{c_p \rho} \tag{2.30}$$

is the thermal diffusivity - relating thermal conductivity κ, which describes the rate at which heat is transferred through a material, to specific heat, c_p, which is a measure of the ability of a material to store thermal energy [41], and mass density ρ.

A source term which accounts for the heat generation by the power absorbed in the dielectric can be introduced to give

$$\frac{\partial u}{\partial t} = \alpha\left(\frac{\partial^2 u}{\partial x^2} + \frac{\partial^2 u}{\partial y^2} + \frac{\partial^2 u}{\partial z^2}\right) + q \tag{2.31}$$

Where q is the volumetric heat generation, also a function of space and time.

Transient thermal progression in a material can therefore be described completely using Equation (2.31). Solving this equation in three dimensions, however, is very complex and involves defining specific boundary conditions and separation of the variables. It is for this reason that computer simulation software is often used, such as Ansoft ePhysics used in this study. This software divides a three-dimensional model into a finite element mesh and solves for the temperature distribution. When coupled with EM software simulators such as Ansoft HFSS, which solves for electromagnetic fields using the finite element method, complex electro-heating problems may be solved.

2.2 Permittivity of a material

It is evident that EM wave interaction in a material depends on the characteristic material properties known as the electric permittivity and the magnetic permeability - collectively known as dielectric properties. More precisely, it is these properties that determine how the electromagnetic energy in the incident wave is stored, transferred or dissipated [40, 42, 43] in a volume and so how the resultant heating effect occurs [39, 43].

Presented here is a review of the fundamentals of electric permittivity. The magnetic permeability of most non-magnetic materials (such as all of those which will be considered in this work), is identical to that of free-space and as such, is deliberately neglected here.

2.2.1 The displacement field and polarisation density

An electric field within a dielectric causes bound charges within the material to separate or re-orientate, thereby inducing a local electric dipole moment. The resultant displacement field is defined as [42]

$$\vec{D} \equiv \varepsilon_0 \vec{E} + \vec{P}_\rho \tag{2.32}$$

Where P_ρ is the polarisation density, *i.e.*, the density of the permanent and induced electric dipole moments in the material. The divergence of this polarisation vector depends on the density of the bound charges within the material.

$$\rho_b = -\nabla \cdot \vec{P}_\rho \tag{2.33}$$

Where ρ_b is the bound charge density.

By applying Gauss Law it can be seen that

$$\nabla \cdot \vec{D} = \rho - \rho_b = \rho_f \tag{2.34}$$

Where ρ_f is the free charge density.

For the case of a linear, homogeneous and isotropic dielectric, that responds instantly to variations in the electric field, the polarisation density is linearly dependent on E.

$$\vec{P}_\rho = \varepsilon_0 \chi \vec{E} \tag{2.35}$$

Where χ is a constant of proportionality known as the electric susceptibility. From (2.32) it can be deduced that the displacement in a material is given by

$$\vec{D} = \varepsilon_0 (1 + \chi) \vec{E} = \varepsilon \vec{E} \tag{2.36}$$

Where ε is the permittivity of the material and $(1+\chi) = \varepsilon_r$ is the relative permittivity of the material.

More complex, time-dependent or non-linear dielectrics are described by expressing ε, D and E as functions (of time, frequency, space *etc.*). In most real situations, this is due to the fact that a material cannot polarise instantly in response to an applied field. This time delay in polarisation can be expressed as the convolution of the electric field at a previous time with the time-dependent susceptibility:

$$\vec{P}_\rho(t) = \varepsilon_0 \int_{-\infty}^{t} \chi(t-t')\vec{E}(t')dt' \tag{2.37}$$

In the frequency domain this is simply

$$\vec{P}_\rho(\omega) = \varepsilon_0 \chi(\omega)\vec{E}(\omega) \tag{2.38}$$

Polarisation is thus causal - being in response to the applied field and can therefore be expressed as a phase delay. For this reason, permittivity is often expressed as a complex function of the angular frequency of the polarising field.

2.2.1.1 Complex permittivity

Introducing a time-dependence to Equation (2.36) and the concept of permittivity as a complex value gives,

$$D_0 e^{-j\omega t} = \varepsilon^*(\omega) E_0 e^{-j\omega t} \tag{2.39}$$

Where complex permittivity is

$$\varepsilon^*(\omega) = \varepsilon'(\omega) + j\varepsilon''(\omega) = \frac{D_0}{E_0}(cos\delta + jsin\delta) \tag{2.40}$$

The real component ε' relates to energy from the field stored within the dielectric and the imaginary component ε'' relates to energy from the field that is dissipated within the dielectric [40, 44] and δ is the phase delay between the field and

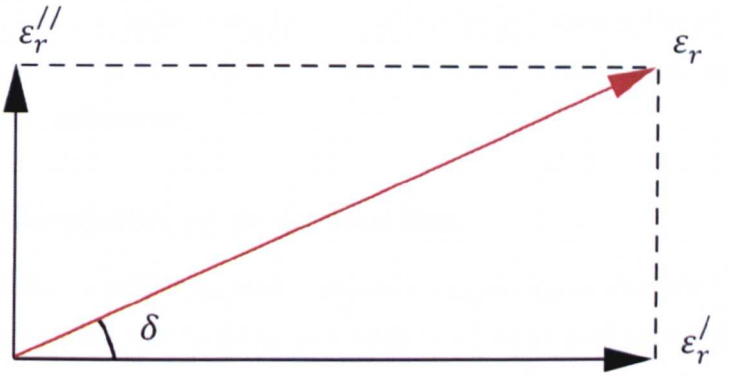

Figure 2.2: Complex permittivity phasor diagram.

polarisation.

The frequency at which the phase shift becomes noticeable or significant depends on both temperature and material properties and it can be seen that the loss factor component of permittivity is related to this phase delay. Shown on a vector diagram in Figure 2.2, where real and imaginary components are orthogonal, the relation between the phase delay and real and imaginary components is more clearly understood.

By simple trigonometry, we then have the relation

$$tan\delta = \frac{\varepsilon_r''}{\varepsilon_r'} = \frac{1}{Q} = \frac{\text{Energy dissipated per cycle}}{\text{Energy stored per cycle}} \tag{2.41}$$

For the special case of low or zero frequency, the permittivity is known as the static relative permittivity and can be expressed as

$$\varepsilon_r = \lim_{\omega \to 0} \varepsilon_r(\omega) = \frac{\varepsilon_s}{\varepsilon_0} \tag{2.42}$$

Where ε_s is the static relative permittivity, otherwise known as the dielectric constant.

At the high frequency limit complex permittivity is often referred to as ε_∞ and above a point know as the plasma frequency dielectrics behave as ideal metals with electron gas behaviour.

2.2.2 Mechanisms of polarisation

A polarisation will result from any kind of charge separation within a material. In most dielectrics this can happen in a variety of ways and on a variety of scales and each will be particularly significant over a certain frequency range. It is these different mechanisms that combine to produce the overall permittivity of a material [42].

The separation of oppositely charged particles or ions in a lattice owing to the presence of an electric field is known as ionic polarisation and is often the most significant polarisation effect at low radio frequencies because of the scale on which it operates. The polarisation in this regime is dependent on the displacement of the charges on each ion about its centre.

2.2.2.1 Ionic conductivity

Ionic conductivity is the most critical loss mechanism for most solvent-containing materials, such as water-containing foods, at low frequencies. The losses are mainly due to the electrolytic conduction of free ions (such as dissolved salts [33]), that become decreasingly mobile as frequency increases, resulting in an inversely proportional frequency dependence [42].

Whilst these conductive losses (there is no associated storage element) are technically not a polarisation that contributes directly a component of permittivity, the contribution to losses within the dielectric means it is often included when loss parameters are quoted [42, 45]. Indeed, it is often very difficult to isolate during the measurement of permittivity. This loss mechanism is therefore accounted for by the addition of a conductivity term to the dielectric loss factor to produce an effective loss parameter of the form [33, 46]

$$\varepsilon_e'' = \varepsilon'' + \frac{\sigma}{\omega\varepsilon_0} \tag{2.43}$$

2.2.2.2 Maxwell-Wagner (inter-facial) polarisation

A further low-frequency polarisation mechanism is known as Maxwell-Wagner polarisation and is from the build-up of charges at interfaces in non-homogeneous materials [42]. Losses from this mechanism tend to peak at around 100kHz [40] and are generally very small in comparison to those of other mechanisms.

2.2.2.3 Atomic (ionic) and electronic polarisation

As frequency increases still further; typically into the Infra-Red range, the polarisation effects shift to the atomic scale. This is owing to the separation and oscillation of adjacent atoms providing a separation of charge and is known as atomic polarisation.

Beyond this frequency regime, the electrons themselves become periodically displaced around the nucleus of the atom, thereby resulting in another form of charge separation. This form is known as electronic polarisation and occurs in otherwise neutral atoms when the atom's nucleus and electrons become displaced by an applied field [42]. These are very weak mechanisms, especially at lower frequencies, but are often the dominant mechanisms in dry solids at microwave frequencies [42] – where dipolar liquids are absent and there are no solvents for ionic conduction - despite resonance and peak losses occurring at much higher frequencies.

2.2.2.4 Dipole relaxation

In certain substances, such as water, there exists a permanent electric dipole owing to the structure of the water molecule and the opposite charges on the spatially separated Hydrogen and Oxygen molecules. As frequency increases, the permanent dipole interacts more significantly with the applied field by rotating in order to follow the field orientation. It is in this reorientation of the molecule

where energy is stored and dissipated within the dielectric. This occurs as the dipole relaxes back to its original state, with a peak occurring in the loss component at the relaxation frequency [42], which is in the microwave region. This mechanism is discussed in detail below.

2.2.3 Kramers-Kronig Relations and the Hilbert Transform

Over the entire EM spectrum it can be observed that there are characteristic resonant peaks in the imaginary component of permittivity representing the effect of each polarisation mechanism within each regime.

Permittivity is a complex function that is regular/analytic in the upper half of the complex -plane [47]. Complex permittivity therefore satisfies the requirements for the Kramers-Kronig relations, which allow the calculation of one part of complex permittivity from the other [48]. That is, knowing the real part would allow the imaginary part to be calculated and vice versa. Mathematically this shows that both real and imaginary parts of permittivity are interdependent owing to the causal nature of polarisation. Also, that the real part of permittivity is an even function and the imaginary part is an odd function, with respect to real angular frequency. The Kramers-Kronig relations for permittivity are given by [49]

$$\varepsilon' - 1 = \frac{2}{\pi}\mathcal{P}\int_{-\infty}^{\infty}\frac{\varepsilon''(x)}{x-\omega}dx \varepsilon'' = -\frac{2}{\pi}\mathcal{P}\int_{-\infty}^{\infty}\frac{\varepsilon'(x)-1}{x-\omega}dx \tag{2.44}$$

Where $\mathcal{P}$ denotes the Cauchy Principle Value and is used to define limits to integrals whose interval of integration is not finite [50].

As $\varepsilon''(\omega)$ is an odd function, Equation (2.44) can be written as [49]

$$\varepsilon' - 1 = \frac{2}{\pi}\mathcal{P}\int_{0}^{\infty}\frac{\chi\varepsilon''(x)}{x^2-\omega^2}dx \tag{2.45}$$

2.3 Water and the permittivity of organic substances

The dielectric properties of biological materials is dependent on their composition; in the microwave spectrum this is mainly the quantity of dipolar components (*i.e.* water) and free charge carriers (*i.e.* salts) [46] present. Indeed, most organic substances consist of a significant amount of water, with some fresh foods containing up to 98% [8]. Because of this, the dielectric properties and associated losses in organic substances such as plants and fruits are determined largely by the proportion of water they contain [33, 37, 39, 40] and also the salts dissolved within them.

Introducing salt to otherwise pure water causes the water molecules to become bound by counter-ions of the salt (A Sodium Chloride molecule binds an average of 5.5 water molecules), which results in a reduction of the dielectric constant and an increase of the loss factor from the conductive migration of the charged ions [8, 51].

The fact that the permittivity of most organic substances such as plants is governed by their water content also explains the same high dependence on frequency and temperature [32, 46]. Other factors also contribute however[39, 40, 45, 51, 52], such as the physical structure. An example of this in food can be found in the anisotropic behaviour observed in fibrous samples, such as meat and fish [32]. Other chemical constituents can also contribute [8] to the overall permittivity – particular the occurrence of sugars and fats [53].

Real permittivity can be seen to be greater in materials with increasing water content, causing the relaxation frequency to shift to higher frequencies with increasing water content [32, 45].

2.3.1 Water structure and interactions

The spatial configuration of a water molecule is widely accepted as being that of a regular tetrahedron [8]. This model, shown in Figure 2.3, assumes that hy-

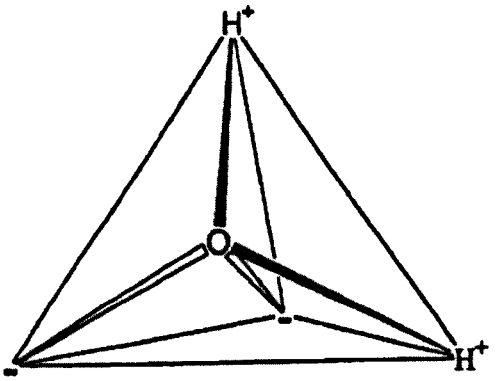

Figure 2.3: Structure of water molecule, presented in [8].

drogen atoms are in the corners of the tetrahedron with positive charge and two orbitals of paired electrons are in the opposite corners [8]. The oxygen atom is in the centre and the molecule has a van der Waals diameter of 0.282nm. It is this separation that results in the permanent dipole.

2.3.2 Permittivity of water

It has been shown using dielectric spectroscopy that water has different relaxation domains depending on its state [54]; with solid water showing relaxation in the kHz domain, bound water in the MHz domain and free water in the GHz domain [55].

Pissis performed thermally stimulated depolarisation current measurements on leaf samples in order to investigate the water in plant tissues [9]. A sample is polarised using an electric field and then cooled down to 'freeze' the polarisation. The field is then turned off and the depolarisation current measured as the sample warms up. The results suggest that there are different relaxation times of water in plant tissue, depending on the arrangement of the water in the plant.

Figure 2.4 shows the results from measurement of *C. limon* leaves; one an old leaf with 44.5% moisture content and other a young leaf with 60.5% moisture content. These results strongly suggest that relaxation times for water molecules

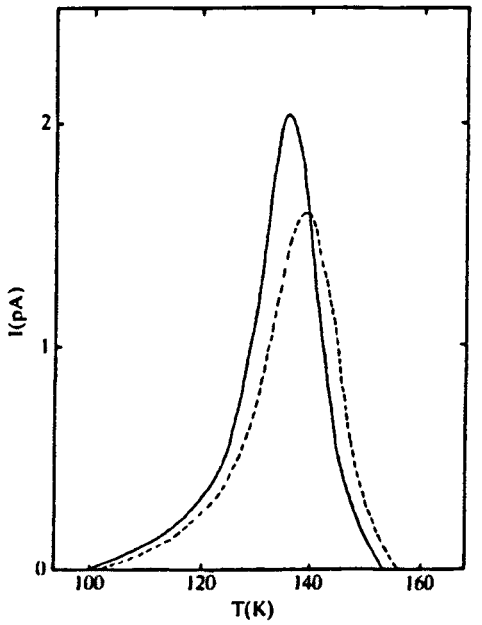

Figure 2.4: Sample temperature *vs.* depolarisation current, presented in [9].

in plants are continuously distributed and depend on the amount and extent of bound water within the plant [9]. Further evidence is presented to suggest that water within plants is organised in clusters, rather than multi-layers, and indicates strong binding of water molecules in living organisms [9]. Furthermore, characteristics differ between plants, which indicates differences in organisation of water molecules between different plant types.

When water content is low, there is less solvent for salts to dissolve in and as such the mobility of the ions is reduced [56]. There is therefore an indirect dependence on water content (which in turn is temperature-dependent) in the losses associated with ionic conduction. This effect has been observed in honey, where lowering the viscosity by the addition of water lowers the binding forces of dissolved ions and increases the contribution of ionic losses [44]. As such, in organic materials with low water content, the water is often in the bound form and it is for this reason why the dominant frequency range for dielectric heating shifts, in comparison to materials with higher water concentrations [40].

Henry *et al.* showed that dead seeds consist of mainly free water, whilst viable

seeds contain mainly bound water and that both had markedly different dielectric properties [54]. Indeed, losses in substances containing free water can be up to 10000 times those of substances containing only bound water [54] and it is this property that Henry *et al.* used to discriminate between live and dead seeds using microwaves.

A similar explanation can be given for the temperature dependence, with a high viscosity/low temperature sample restricting dipole orientation thereby resulting in a longer relaxation time (see below) [51].

Temperature increase will cause the dielectric constant to increase across the frequency range where dispersion occurs and the loss factor to increase or decrease, depending on whether the frequency of operation is above the critical frequency [45].

At constant frequency of 9 GHz, the dielectric constant of water has been shown to increase rapidly with temperature, from 40 to 65 between $0°C$ and $35°C$, from where it starts to slowly decline [57]. Dielectric losses reduce almost linearly over the same period from 40 to 15 [57].

2.3.2.1 Dipolar Polarisation and the Debye Model

There are several ways of describing the interactions of the dipoles in a polar dielectric and an applied field, including quantum mechanical descriptions of atomic and molecular interactions. The most commonly used and accepted methods however, are phenomenological models such as the Debye relaxation model [45, 58].

For polar liquids such as pure water, the dipolar mechanism is dominant over microwave frequencies and the Debye model is well suited to describing the general frequency dependent permittivity over this range [40].

It has been reported that the Debye relaxation time is a tetrahedral displacement of water molecules and has a physical significance in that it reflects the single molecule relaxation process [59]. This is a slow process, related to viscosity, and

goes some way to explain why the Debye model become less valid at very high frequencies, for example, at infra-red – where faster mechanisms become more dominant [59]. The Debye model has been shown to be accurate to at least 57 GHz however [57].

When an electric field is applied to a material consisting of polar molecules, a torque is exerted on the dipoles which cause them to rotate, in order to align with the field. Because of the presence of neighbouring molecules collisions occur which impede this rotation. The resultant frictional resistance means the molecules exponentially tend towards a state of total polarisation [42] (with respect to the applied field) with a substance-dependent time constant. This is called the relaxation time and is the time it takes for a dipole oriented by an electric field to return to 1/e of its random equilibrium value [42] after the field is removed (and *vice versa* when the field is re-applied). The inverse of this time constant defines the relaxation frequency such that [42]

$$\tau = \frac{1}{\omega_c} = \frac{1}{2\pi f_c} \tag{2.46}$$

For frequencies lower than the relaxation frequency, the dipoles are able to follow the alternating field variations. This means full polarisation can develop and the resultant losses are directly proportional to the frequency [42]. This continues as frequency increases until the dipole moment cannot keep pace with the faster changing field. As the polarisation cannot develop fully, less energy is stored in the dipole moment and this is reflected in a lower real component of permittivity, although losses continue to increase [42]. At frequencies greater than the relaxation frequency, the dipole does not have time to re-orientate [42] at all and, as such, the polarisation diminishes with a corresponding reduction in both stored energy and dissipated energy (both real and imaginary permittivity are lowered). The Debye model is used for materials that appear to exhibit a single relaxation time constant as is given by [36, 42]

$$\varepsilon(\omega) = \varepsilon_\infty + \frac{\varepsilon_s - \varepsilon_\infty}{1 + j\omega\tau} \tag{2.47}$$

With limits as defined previously,

$$\omega = 0; \quad \varepsilon(\omega) = \varepsilon_s \tag{2.48}$$

$$\omega = \infty; \quad \varepsilon(\infty) = \varepsilon_\infty \tag{2.49}$$

This equation produces characteristic curves where real permittivity is constant above and below relaxation frequency, with a transition from a high constant to a lower constant where a resonant peak appears in the imaginary permittivity.

Relaxation time and both static and infinite permittivity are also temperature dependent, although the latter is negligibly so [36].

Several models have been developed to determine a value for static permittivity [60], one of which is the Onsager model [36], which relates the moment of a single dipole to the number of dipoles present and also their density to the temperature dependent static and infinite permittivities. The equation for this is given by [36]

$$\frac{3(\varepsilon_s - \varepsilon_\infty)(2\varepsilon_s - \varepsilon_\infty)}{\varepsilon_s(\varepsilon_\infty + 2)^2} T = N \frac{p_m^2}{3\varepsilon_0 k_b} \tag{2.50}$$

Where p_m is the moment of a single dipole, N is the number of dipoles per unit volume, k_B is the Boltzmann constant and T is the temperature. The right hand side of this equation has to be estimated from measured data [36]. The dipole density is also temperature dependent and can be represented by Boltzmanns statistics such that [36]

$$N = N_0 e^{(\frac{-U}{kT})} \tag{2.51}$$

Where U is the potential energy of a dipole and N_0 is a constant. The equation now becomes

$$\frac{3(\varepsilon_s - \varepsilon_\infty)(2\varepsilon_s - \varepsilon_\infty)}{\varepsilon_s(\varepsilon_\infty + 2)^2} T = A_0 e^{(\frac{-U}{kT})} \tag{2.52}$$

With

$$A_0 = N_0 \frac{p_m^2}{3\varepsilon_0 k} \tag{2.53}$$

2.3.2.2 Alternative models and extensions

An alternative graphical depiction is the Cole-Cole plot, where real permittivity is plotted on the horizontal axis and imaginary on the vertical axis. A material with a single relaxation frequency - modelled by the Debye equation – will be a semicircle with its centre on the horizontal axis and the peak of imaginary component occurring at the relaxation frequency [42].

In practice, this symmetry is not always an accurate description and the Debye equation is modified with a correction factor α, in order to compensate [61]. This is known as the Cole-Cole model and is given by [62]

$$\varepsilon(\omega) = \varepsilon' - j\varepsilon'' = \varepsilon_\infty + \frac{\varepsilon_s - \varepsilon_\infty}{1 + (j\omega\tau)^{1-\alpha}} \tag{2.54}$$

It can be seen from these models that the intrinsic material properties that determine the actual mechanisms for dipolar polarisation, and its contribution to overall permittivity, have their roots in the chemistry and energies of the polar molecules in question.

Chapter 3

Measurements of dielectric permittivity

A solution to a microwave heating problem must first start with a thorough understanding of the dielectric properties of the medium to be heated. This section gives an overview of techniques for measuring the permittivity as a function of frequency and their previous application to the measurement of organic substances. These techniques are then applied to the measurement and analysis of the dielectric properties of water and tomato plant components. These results allow for the calculation of absorbed power within the plant at a given frequency. As such, they are important in selecting the optimum frequency of operation for a microwave heating system and essential for the accurate EM solution of computer models of plant components.

3.1 Review of reported measurements of organic materials

An extensive search of the literature found no reports of tomato plant dielectric properties. There is however, a large and growing field in the measurement of agricultural, food and biological materials' dielectric properties, which is coinciding with an increase in their applications [44].

Birla *et al.* measured the dielectric properties of the peel and pulp of some fresh fruits [63] with the intention of modifying and validating stratified computer models of the fruits. These models were designed to provide insight in the heating patterns that arise in fresh fruits so that effective heating protocols could be formed.

Fasina *et al.* measured the dielectric properties of sweet potato pure at the two ISM band frequencies commonly used in commercial heating apparatus – 915 MHz and 2450 MHz – and reported their frequency and temperature dependence [41] for optimising the dielectric heating process. Hu and Mallikarjuna used an open-ended coaxial probe to make similar measurements of oysters [64]. In both cases, dielectric losses increased with temperature whilst the storage component decreased.

Feng *et al.* measured the dielectric properties of apples as a function of moisture content and fixed temperatures of 22°C and 60°C [65]. They found that, at water content greater than 70%, free water dispersions and ionic conduction accounted for the dielectric behaviour. For water content of 23%, ionic conduction was the prominent dielectric mechanism and at low water content (4%), bound water accounted for the main dispersion mechanism [65]. Decreases in moisture resulted in a decrease in both real and imaginary components of permittivity [65]. Similar moisture and temperature dependences were found in the dielectric properties of garlic, by Sharma and Prasad [37], using the resonant cavity perturbation technique at 2450 MHz.

Sosa-Morales *et al.* investigated the dielectric properties of ripe mangoes [66] in order that microwave treatment could be used for post-harvest pest control. An open-ended coaxial probe was used to take measurements from 1-1800 MHz at a range of temperatures. It was found that real and imaginary permittivity decreased with frequency, with the loss component decreasing at a greater rate. As temperature increased, the loss factor increased but dielectric constant decreased. The effect of ionic conduction was found to be dominant at frequencies below 300 MHz [66].

Wang *et al.* used an open-ended coaxial probe to find the dielectric properties of a selection of fruits and four associated insect pests over the frequency range 1-1800 MHz [56]. The dielectric loss factor of fresh fruits and insects decreased with increasing frequency when temperature was constant, whilst loss factor increased linearly over the radio-frequency (RF) range and levelled off at microwave frequencies [56]. In another, similar, study, the dielectric properties of nuts were found to be very low compared to those of insects and fruits and showed little temperature dependence, especially at RF frequencies [67]. This is most likely due to much lower water and salt content than fruit or insects and the authors concluded that this would allow for differential heating of nuts and insects [67].

Dev *et al.* investigated the use of microwaves for the in-shell pasteurisation of eggs [68]. The authors found that the egg shell is transparent to microwave energy, whilst egg white had higher dielectric losses than the yolk, at 2450 MHz, causing the white to heat up faster during microwave heating. Both yolk and white however, displayed the general trend of water permittivity.

Heredia *et al.* found that osmotic pre-treating of tomato fruits in salt, sugar and calcium adjusted their dielectric properties such that subsequent microwave treatment resulted in superior quality drying [39]. This demonstrates the crucial effect of dissolved trace substances, as well as water content, on the dielectric properties of a biological material. Similar effects of salt on the dielectric properties of butter, in the microwave range, were reported by Ahmed *et al.* [63].

In a study of rice flour and water solutions, Ahmed *et al.* found that dielectric constant did not vary with frequency whilst losses increased with frequency [69]. Adding only 1% salt resulted in significant increases in the loss component, illustrating the significance of ionic conductivity loss-mechanisms. Both components of permittivity fitted a second order polynomial relationship with temperature. Above 70°C however, sharp changes in dielectric properties were observed and attributed to the gelatinisation of starch in the flour. Relating variations in material composition and dielectric properties allows for fast and non-intrusive sensing of food products [70, 71] in order to asses quality and condition.

Guo *et al.* measured the dielectric properties of chickpea flour up to 1800 MHz at various moisture contents and temperatures using an open-ended coaxial probe [52]. Dielectric constant and loss factor both decreased with increasing frequency at all temperatures and moisture levels and ionic conduction was found to be dominant at lower frequencies at high moisture contents. A linear correlation was found between the density of the powder samples and the dielectric constant and loss factor. Similar findings, in six different starch species, were found by Ndife at 2450 MHz [72]. Bulk density was also shown by Sokhansanj and Nelson to affect dielectric properties (or at least their measurement) of whole-grain wheat [73]. These finding show the significant effect, on measurements, of tiny air gaps that are present in a prepared sample.

Liu *et al.* compared the use of several dielectric mixture equations for the measurement of the permittivity of bread, which typically has many small air pockets dispersed throughout the dough [53]. The authors found the Lanau and the Lichtenecker equations most suitable [53], but the variation between techniques would suggest that approximating dielectric mixtures is an inexact science.

3.1.1 Summary

The above review provides precedents that determine the method by which studies into the dielectric properties in this work are undertaken. Namely, these are the careful control of temperature and measurement quality – in particular the sample density. The reported strong dependence on water content for permittivity measurements necessitate the inclusion of a control in order to observe any similarity in measurements of tomato plants. A measurement of sample water content will also provide some context for permittivity measurements.

The effect of even low concentrations of salts has been seen to be significant. A pure control sample will offer a relative comparison highlighting the presence, or otherwise, of these inclusions in the tomato plant samples. The frequency-dependent nature of these effects and the significant losses that accompany them demand that the measurement range extends such that they are included.

The application of the measurement results has been seen to be as diverse as the variety of samples measured to-date. The uses include the calculation or estimation of absorbed power for the calculation of heating rates, but also for the measurement and sensing of water and salt concentrations. In addition, the application of measurements to informing computer models has been shown to provide a valuable method for investigating and mitigating the effects of differential heating, as reported in many objects with constituent components of different dielectric properties. This has an immediate application in this work and necessitates the measurement of the different plant components.

3.2 Measurement techniques

Early dielectric measurements concerned the direct current (DC) resistance of seed grains in order to establish moisture content [32]. Sheriff described and demonstrated a complex apparatus for measuring the dielectric properties of leaves [74]. This was based on a measurement of changes in capacitance between electrodes when the leaf was both present and not present, although measurement accuracy was questionable.

Various other techniques have since been developed for measuring dielectric permittivity, each of which has certain advantages and disadvantages, with the most suitable method dependent on the desired frequency range of the measurements and the nature of the material composition. Measurement types can be broadly broken down into lumped circuit, resonator, transmission line and free-space methods, using open or closed structure [32] and all rely on extracting the dielectric properties mathematically by first measuring circuit parameters such as impedance, admittance, and reflection and transmission coefficients [32].

The transmission line technique has been shown to be most suitable for porous materials [53] although it can be difficult and time-consuming to implement as the sample must be made into precisely shaped slabs [40] and inserted within a transmission line [32]. It also requires large sample sizes at lower frequencies.

The technique involves measuring the phase and amplitude of a reflected signal from a sample placed inside a transmission line or against the end of a short circuited transmission line, such as a wave-guide a coaxial cable, with ε' and ε'' then extracted from transmission line theory [32].

Resonator techniques involve filling a resonator partly or completely with a material to be measured and comparing the results to those of a known dielectric. This allows the extraction of values for the measured sample although again, accuracy is reportedly not as good as with transmission line techniques [32]. A similar technique is the cavity perturbation method, which is often used because of its simplicity, high temperature capability, suitability for low loss dielectrics and high accuracy [32, 75, 76]. The nature of tuned cavities though, means bandwidth is severely limited [40, 75]. Permittivity is extracted from measuring the shift in resonant frequency and the change in absorption characteristics in a tuned cavity, owing to the presence of the sample material [32, 40]. This particular method is the one of the most common techniques for measuring dielectric properties of foods [37].

3.2.1 Open-ended coaxial probe technique

The use of an open-ended coaxial probe has gained particular popularity, especially for research into food properties, owing to its ease of use and large measurement bandwidth, [32, 40, 42, 53, 62, 76] which extends up to 50 GHz [75]. It is particularly useful for measuring homogeneous liquids and semi-solids [52, 76]. As essentially a modification of the transmission line technique, the permittivity is extracted from measured values of phase and amplitude of the reflected signal from the open-ended probe when immersed or pressed against a sample [32, 62]. It is however, prone to errors if care is not taken during measurements as good contact is needed between the tip of the probe and the sample [52]. Also, the method is not accurate for low-loss dielectrics [62], as there is little change in reflection coefficient for a large change in dielectric constant for large values of permittivity [42]. Accuracy is also poor at very high or very low frequencies [32].

Tomato plant matter has a high water content and is therefore likely to be high-loss. The fruits are also largely liquid and the plant must be processed (into a semi-solid paste) owing to its natural dimensions making accurate measurement difficult. Of the methods most used for measurements of organic substances, the cavity method requires a large sample and can only measure permittivity at one specific frequency of operation. For this reason, the co-axial probe offers the best compromise between accuracy and ease of measurement for the measurement of tomato plant dielectric permittivity, at low temperature.

The measurement model assumes an infinite ground plane and a semi-infinite sample depth [42, 62]. For lossy materials, these assumptions are satisfied when the material is a few centimetres deep and wider than the probe flange [75]. These conditions are easy to verify by placing an object, such as a short-circuit, behind the sample and observing any changes in measured results [42].

Calibration is performed at the measurement interface by using known dielectrics, such as air and pure water, as well as by shorting the probe tip, thus making the reflection coefficient -1 [62]. Calibration in this way is important in order to eliminate directivity, tracking and source match errors in the reflection measurement [42]. Additional errors can be introduced if air gaps become trapped in the sample, if the sample is not deep enough, or if the measurement cables are moved [42].

As noted, special effort has to be made to ensure the density of a particulate sample is of the sample density as when in its original form [52]. The effect of instrument and connection errors can also contribute to inaccurate measurements [32] and care must be taken to ensure errors and noise from cables and connectors at high frequencies are calibrated out [32]. Rigid cables were used for measurements in this section, to avoid disrupting the equipment and voiding the calibration.

The mathematical procedure for calculating complex permittivity is relatively straight-forward. First, the admittance is calculated from the reflection coefficient at the probe tip, given by

$$Y_L(\omega,\varepsilon) = Y_0\frac{1-\Gamma(\omega,\varepsilon)}{1+\Gamma(\omega,\varepsilon)} \tag{3.1}$$

Where Y_0 is the characteristic admittance of the probe and $\Gamma(\omega,\varepsilon)$ is the reflection coefficient.

Permittivity is extracted from the admittance by an iterative method and using models parameters determined in the forward process [32]. This process is given by

$$Y_L(\omega,\varepsilon) = j\omega C_i + j\omega C_0\varepsilon + j\omega^3\varepsilon^2 + B\omega^4\varepsilon^{2.5} \tag{3.2}$$

In practice, these calculations are often performed by measurement software, such as the Hewlett Packard (HP) 85070 dielectric probe kit [39] used in the experiments that follow in this section.

3.3 Measurement of permittivity of plant components

3.3.1 Probe set-up and calibration

A Vector Network Analyser (VNA) (Agilent Technologies E8358A) and a coaxial dielectric probe kit (HP 85070) were connected. A software controller was used to store calibration data and perform measurements by connecting the VNA to a computer with a General Purpose Interface Bus (GPIB) cable. The equipment was initially calibrated from a frequency of 0.2 GHz to 6 GHz, with a frequency step of 50 MHz – referred to here as the broadband sweep – followed by a narrower range of 0.8 GHz to 2.8 GHz, with a frequency step of 5 MHz – the narrowband sweep.

The broadband range was chosen to indicate the general trend of the permittivity, including any low-frequency effects. As such, the lower limit of this sweep

was chosen to be the lowest frequency for which the coaxial probe is suitable for accurate and reliable measurements. The upper limit was chosen so as to include all microwave ISM band frequencies of 896/915 MHz, 2.45 GHz and 5.8 GHz within the range of frequencies that could be reliably measured in one measurement sweep.

Improved accuracy was obtainable for the narrowband sweep owing to a smaller frequency step being used (for the same number of measurement points) and a more precise calibration being possible over a narrower range of frequencies.

Substances of know permittivity were used to provide standards, namely deionised water at a temperature of $24°C$ and air, in order to perform the calibration (Figure 3.1). In addition, as the software calculates permittivity from the direct measurement (by the probe) of the reflection coefficient, a short circuit block (Figure 3.2) was used to provide a third known standard.

Between measurements, the probe tip was dried with tissue paper. Care was taken to not move cables, which had – as reported previously and confirmed through pilot tests – been shown to disrupt measurement accuracy and repeatability. Between each reading the calibration was refreshed using the air standard.

Reflection coefficient measurements allowed the real and imaginary permittivity to be computed as a function of frequency at a fixed temperature of $24°C$. These calculations were performed automatically by the computer software using the measured data from the VNA.

3.3.2 Measurement procedure

For each measurement, the dielectric probe was fixed in position using a clamp and the sample raised towards the probe so that firm pressure was applied between probe and sample. Care was taken to ensure that contact was flush and no obvious air gaps were present. Such air-gaps, between the probe tip and sample, cause the majority of errors that results in inaccurate results for this technique.

Measurements were repeated five times and averaged. Measured results showed a high degree of repeatability – typically within 5%. Variation in the distribution of individual sample measurement points about the average was largely negligible, albeit for a few individual erroneous samples, with measurement error < 5%.

The measurements for water were taken at a constant temperature of $24°C \pm 1°C$, which is also the same temperature as the samples that were to be measured, in order to ensure a valid comparison could be made. All sample temperatures were measured with a k-type thermocouple probe before dielectric measurements were taken.

As the operating temperatures in the greenhouse are over a relatively small range (approximately $10 - 15°C$), the effect of temperature on the dielectric properties of the plant was deliberately neglected and instead, measurements were taken at the median temperature that the plants were grown at, hence the selection of $24°C$.

3.3.2.1 Sample preparation

Plant samples were taken from hot and cold greenhouses at the end of the pilot tests. These included those grown using microwave heating. This was to investigate possible effects of microwaves on dielectric properties of tomato plants and to provide a further means of showing the link between the plant temperature, the ambient temperature and the water content of the plant.

Stems and leaves from each plant group were removed and shredded to a semi-solid, homogeneous paste. To ensure the sample density was consistent with that of the original plant, the density of each plant group was measured. This was done by measuring the mass of a bunch of leaves and branches, from a similar plant, and then also their volume by immersing in liquid water (where the displacement gives the volume of the stems and leaves). The semi-solid mass of the measurement samples was then added to the measurement container (of known volume) until the mass contained in it equated to the same density as the original plant.

Figure 3.1: HP 85070 dielectric probe arrangement during calibration procedure.

The most mature ripe (red) fruits and newly developed unripe (green) fruits were picked. These were also shredded, but being essentially liquid, no particular effort was required to maintain sample density. Care was taken however, to ensure no air bubbles remained in the sample before measurement.

3.3.3 Measured permittivity of water

The permittivity of pure water was measured to provide a reference for the plant sample measurements. This is an appropriate choice as water is the main constituent of most biological material and especially tomato plant material (see Table 3.1).

From Figure 3.3, the real component of the measured permittivity of the water sample can be seen to be decreasing linearly from its static value of 80 towards 70 at 6 GHz. This decrease corresponds with an increase from almost zero of the imaginary loss component, which is also linear across the frequency range measured. These results are consistent with previous studies and it would be

Figure 3.2: Short circuit connector for use during calibration of HP 85070 dielectric probe kit (pen shown for scale).

expected that the loss component will increase towards a maximum at the point at which the water dipole becomes resonant [57, 77]. At this point, the real component has an inflexion before settling at a new 'constant' value, as described in Section 2. Most sources define this peak – known as the dipolar relaxation frequency – at around 16-20 GHz [57].

3.3.4 Measured permittivity of plant components

The broadband measured permittivity results (Figure 3.3) for the plant show a similar trend of decreasing real and increasing imaginary components, as frequency increases. The real component however, is significantly lower across the entire range. This is due to a combination of reasons. It is known that, for low water concentration, the water molecules bind to the matrix of the substrate, thereby impeding the motion of the dipolar rotation [78]. The impediment of this bound water consequently reduces the ability for energy to be stored in the dipole and this is reflected in its permittivity values. Secondly, the sample is not entirely water, so the overall measured permittivity is also that of the plant fibres, which

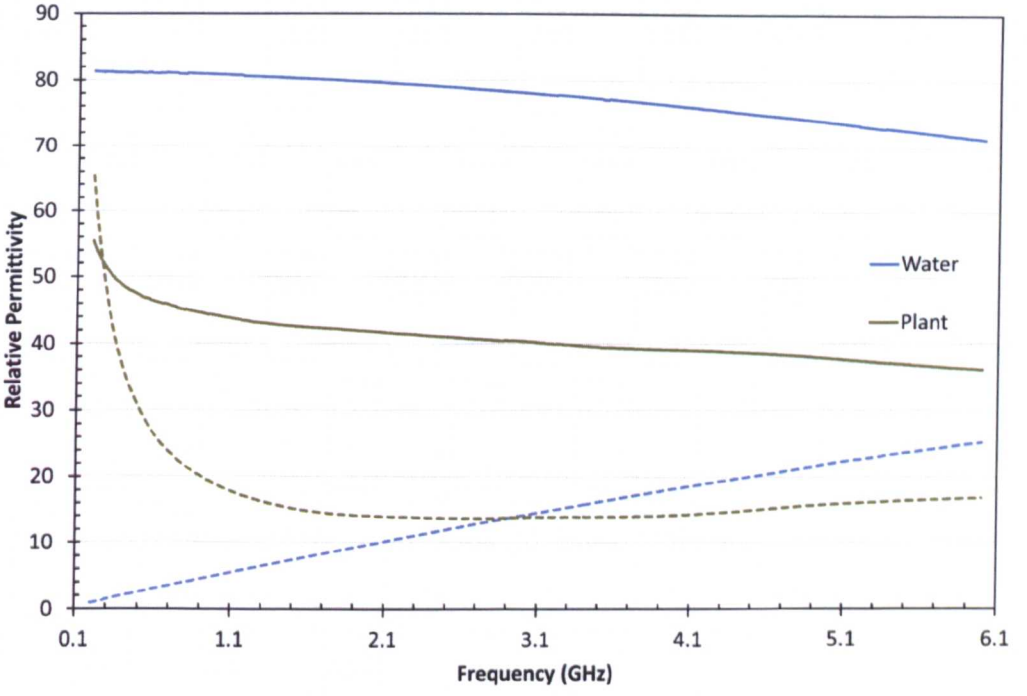

Figure 3.3: Broadband measurement results of real (solid line) and imaginary (dotted line) permittivity of plant material and fresh water.

have no intrinsic dipolar dielectric mechanisms, but serve to provide the binding matrix for the water. These reasons also explain the depression in the rate of increase in the imaginary component of permittivity. At low frequency, however, significant losses are present. As these losses appear to diminish at a rate of $1/f$, they can be attributed to the ionic conduction of dissolved electrolytes in the plant liquids. The measured results indicate a significant concentration of these substances.

3.3.4.1 Plant group sample permittivity

Narrowband measurements of the three plant groups were taken. The real component of permittivity for these groups is shown in Figure 3.4. The measurements for each group can be seen to follow the same general trend as water, with permittivity values reducing at a slightly greater rate with increasing frequency and with all values reduced substantially, for the reasons discussed above. Between

hot, cold and microwave plant material, all results show exactly the same trend, but with shifted constant values.

It is seen in Figure 3.5 that imaginary permittivity values continue to reduce, owing to the effects of ionic conduction becoming less significant as frequency increases, into the microwave regime. At the high-frequency end of the measurements, imaginary permittivity of cold control plants can be seen to be increasing, unlike for the hot and microwave samples (although some increase can be seen, it is marginal). This is indicative of the water concentration in the plant being high enough so as to behave as though it is not bound to the fibrous matrix of the plant. As such, the permittivity tends towards that of pure 'free' water, as frequency increases.

To confirm these observations and better understand the significance of the water content in the plant samples on the permittivity measurements, the dry matter content was calculated.

3.3.4.2 Dry matter content

Leaves and stems were taken from hot control plants, cold control plants and microwave plants in equal proportions (by mass) between groups. Ripe and unripe tomatoes were also collected from hot control plants to provide two further sample groups. These plant component groups were finely shredded and divided into three 50 g samples of each type (resulting in fifteen samples in total). Each sample was spread thinly (approximately 4 mm deep) in individual metal containers. The mass of the containers was measured prior to adding the samples and again after adding the samples. The subtraction of the former from the latter revealed the wet mass. Samples were then placed in an oven at $75°C$ for 6 hours, with sachets of Sodium Silicate (Na_2SiO_3) , in order to dry (*cf.* use of $CaSO_4$ in [52]). This temperature was chosen to be high enough so as to ensure evaporation of all moisture, but low enough so as not to alter the chemical composition (and therefore mass) of the sample by oxidisation.

After drying, the mass of each sample and container was measured again. The

mass of the container was assumed to have remained constant throughout the drying process and as such was subtracted to give the dry mass of the samples. The mean was calculated for the three wet and three dry measurements for each of the five sample groups. These results were then used to calculate the average percentage dry matter content for each of the plant components and are shown in Table 3.1.

Hot control plants have the highest dry matter content. This is attributable to the conditions experienced by the hot control plants, where the air being warm and humid results in greater transpiration by the plants and consequently a higher moisture loss from the plant. This therefore results in a greater percentage dry mass content.

The cold control plants were found to have the lowest dry mass content. This indicates a high water content which suggests transpiration by the cold plants was low. This is because of the cold air reducing the rate of growth of the plant.

The microwave plants, being warmer than the cold control plants, but cooler than the hot control plants, revealed a lower dry mass content. This is also indicative of a higher water content and hence lower rate of transpiration, but not to the same extent as the cold plants, indicating a non-linear dependence on temperature for plant growth.

Although the microwave equipment resulted in average plant temperature of the microwave plants being $3-5°C$ lower than the hot control plants - and this would reduce the rate of transpiration – the effect of the ambient air temperature may also be significant. Warm air has greater capability to contain moisture than the cool air, so transpiration can continue for longer before saturation, compared to in the cold air environment. This is why the hot control greenhouse results in a much more humid environment than the cold control greenhouse. These results remain ambiguous to which factor is most important in plant water content; plant temperature or air temperature.

Regardless of the cause, this has possible implications for the water requirements

Sample	% Dry matter
Cold Control Plant	16.42
Hot Control Plant	18.10
Microwave Plant	17.01
Red (ripe) Fruit	8.58
Green (unripe) Fruit	10.54

Table 3.1: Dry matter content of plant and fruit samples.

for greenhouse crops being heated by microwaves. If such a system results in a less humid environment as a result of less transpiration, it follows that the plants would require the provision of less water in order to be grown, provided that enough water is supplied to satisfy the demands of the growing plant and that comparable growth quality is indeed possible. This would further improve the environmental sustainability of greenhouse crop production and could possibly provide an additional cost saving. This observation also expands on the point made by Teitel *et al.* in the reduction of mould occurrence on microwave plants [3], owing to cold air and warm plants reducing the occurrence of condensation on the plants.

3.3.4.3 Fruit permittivity

The broadband measured results of ripe and unripe fruit permittivity are shown in Figure 3.6. Compared to pure water, the real component has a lower constant value, owing to the lower proportion of water in the sample. The losses are similar though, owing to the fact that nearly all of the water is present in a 'free' sate. In fact, the loss component of ripe fruit can be seen to converge with that of pure water at 6 GHz.

The effect of ionic particles is very evident in both ripe and unripe fruit, although is more significant in unripe fruit. This is due to a greater concentration of dissolved salts (*i.e* a lower proportion of water) in unripe fruits. This is also why the losses are lower than in ripe fruit, as frequency increases and ionic losses become less dominant, and do not converge with those of pure water.

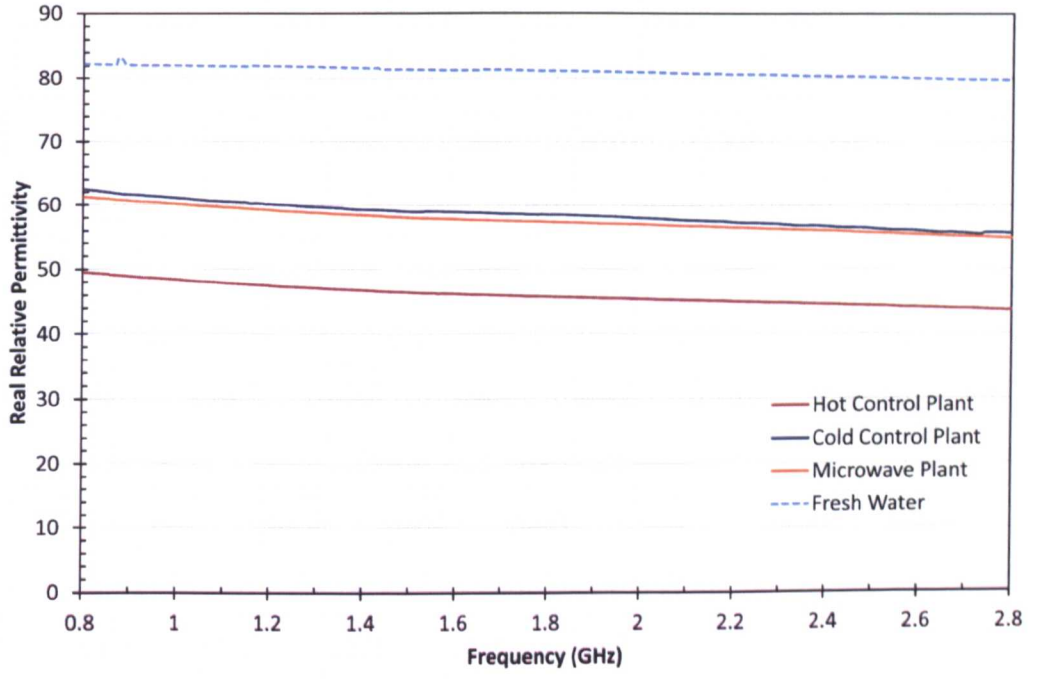

Figure 3.4: Narrowband measured results of real permittivity.

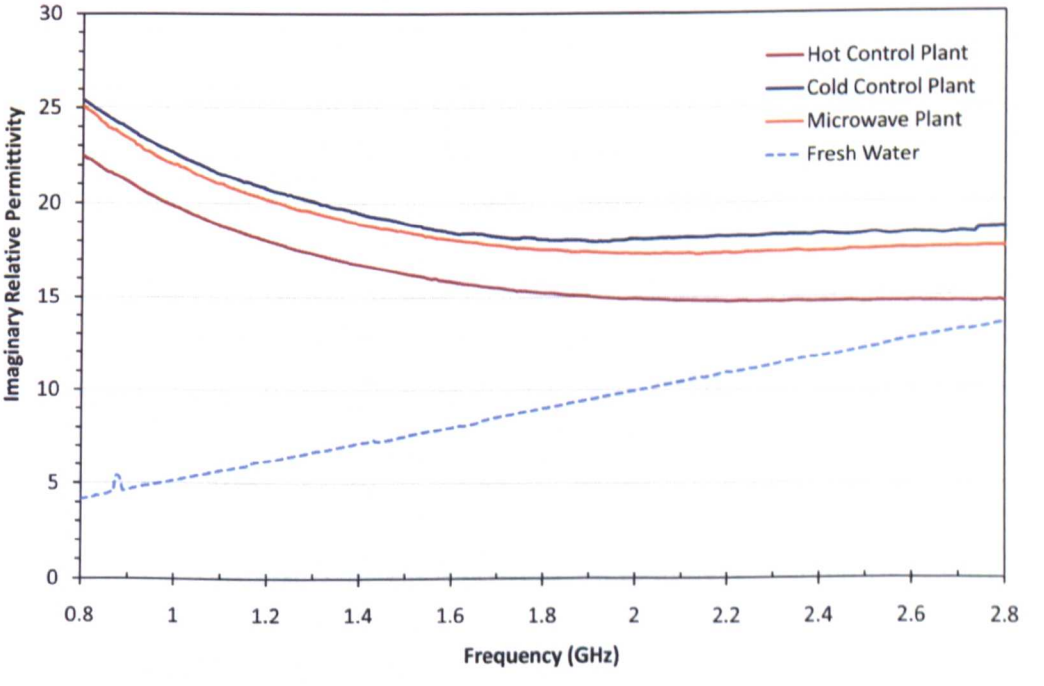

Figure 3.5: Narrowband measured results of imaginary permittivity.

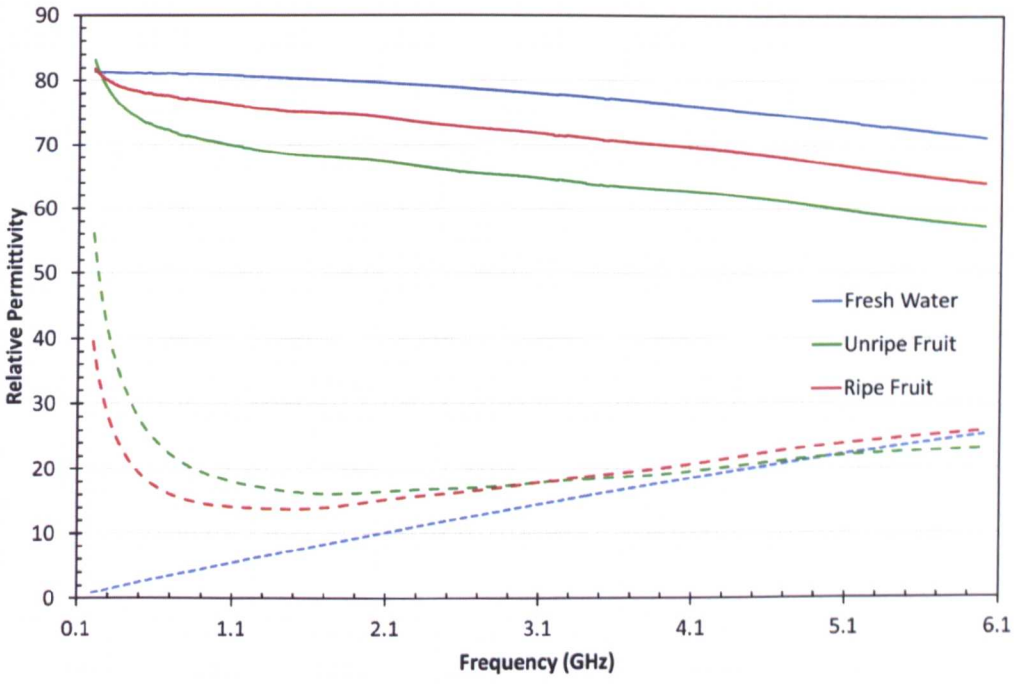

Figure 3.6: Broadband measurement of real (solid line) and imaginary (dotted line) permittivity of unripe and ripe fruit.

The narrowband measurement of real fruit permittivity, in Figure 3.7, shows a very linear response, across the entire frequency range, that is decreasing at approximately the same rate as pure water. The permittivity is higher than that of all the measured plant components owing to the higher water concentration. For this reason, there is no raised permittivity at lower frequencies as seen in the plant samples (Figure 3.4 and 3.3). This inflexion in the plant samples is possibly attributable to the effects of bound water being more dominant at lower frequencies. When total water content is higher, bound water proportion and effects are clearly lower.

Narrowband measurements of the imaginary component, shown in Figure 3.8, show the significant effects of ionic conduction on the measured dielectric losses at low frequency. Unlike in the plant samples however, the losses recover, beyond the RF regime, to similar levels as fresh water, for the reasons stated previously.

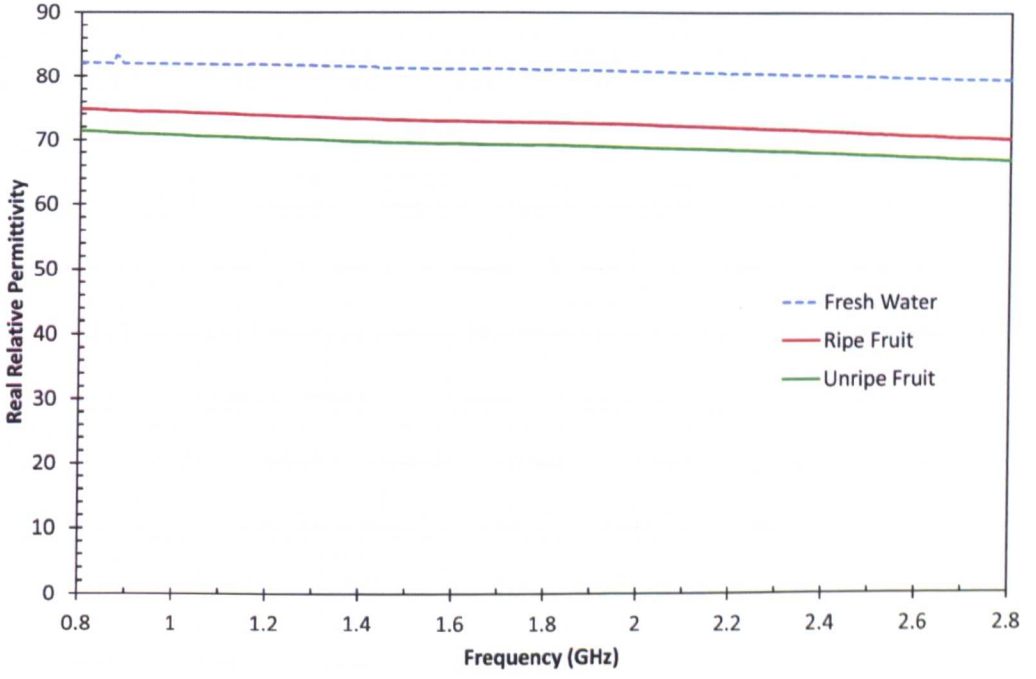

Figure 3.7: Narrowband measurement of real permittivity of unripe and ripe tomato fruit.

3.4 Selection of operating frequency

Aside from the material properties, any dielectric heating mechanism is inherently governed by the nature of the electromagnetic field in the particular medium. In the case of the plant, the fields, and subsequent heating effects, are dependent on the properties of the electromagnetic wave incident on it. The selection of a frequency of operation for optimum heating must be considered with regards to the interaction of the time-varying fields with frequency-dependent dielectric properties.

If the frequency of operation is limited to the part of the electromagnetic that does not include ionising radiation, then the available frequencies include those up to 3000 THz – or the low ultra-violet region. These are the frequencies con-

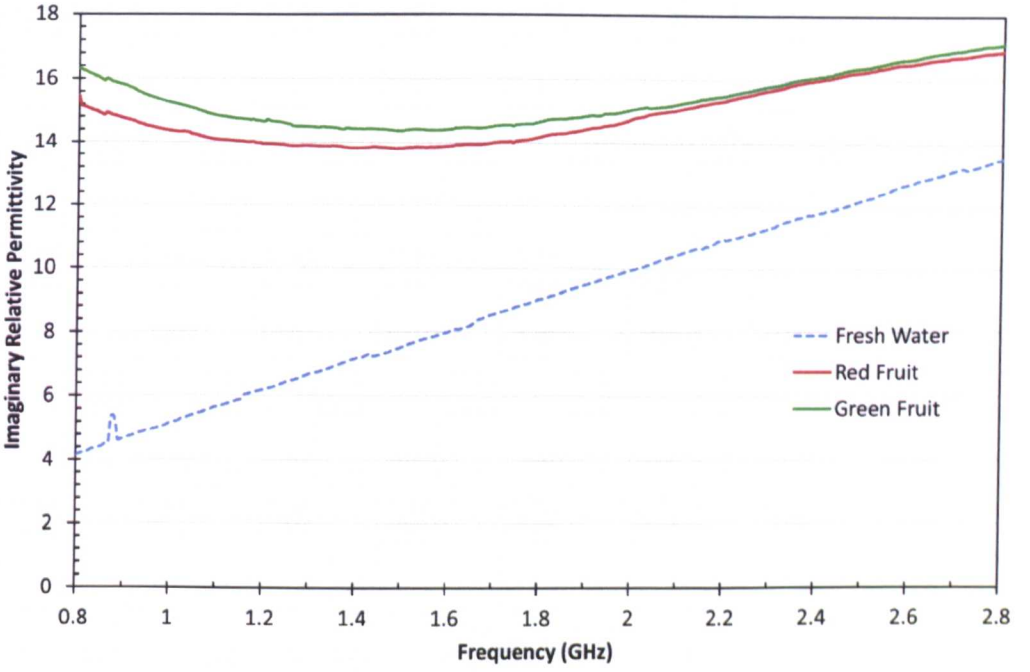

Figure 3.8: Narrowband measurement of imaginary permittivity of unripe and ripe tomato fruit.

sidered in this section.

3.4.1 Power penetration depth

As an EM wave propagates through a material it is attenuated to a degree determined by the material's effective loss factor. The inverse of this attenuation factor, α_p is defined as the skin depth, δ_p and is the depth at which the electric field has decayed to $1/e$ of its value at the material surface [33]. A more convenient term for microwave heating however, is the *power penetration* depth. As the dissipated power is proportional to the electric field, the power also decays as the field decays. For the case of a semi-infinite dielectric slab [33, 46]

$$P_v = P_0 e^{-\frac{2z}{\delta_p}} = P_0 e^{-\frac{z}{D_p}} \tag{3.3}$$

Where D_p is the power penetration depth in the direction of propagation, z, at

which the power has dropped to $1/e$ of its initial value, P_0.

Many sources give a precise solution to the above penetration depth in a semi-infinite material based on the material dielectric and wave frequency as [40, 51, 53]

$$D_p = \frac{c}{2\pi f \sqrt{2\varepsilon' \left[\sqrt{1+\left(\frac{\varepsilon''}{\varepsilon'}\right)^2} - 1\right]}} \tag{3.4}$$

Where c is the speed of light in a vacuum.

As would be expected, this depth is linked to the temperature distribution during microwave heating as materials with low power penetration depths will absorb most energy closer to the surface where the power is incident. By selecting either the frequency of operation and where possible, the dielectric properties, heating patterns may be better controlled. As an illustrative example, when the power penetration depth was similar to the radii of tomatoes being dehydrated, the absorbed power was found to be more homogeneous, which improved drying rates [39].

Figure 3.9 shows power penetration depth as a function of frequency from high RF to far infra-red (IR). In this figure, dielectric properties are assumed to be constant at all frequencies. Although this is a crude approximation of actual power penetration in a real material, it nonetheless gives an image of the relative scale of power penetration at different frequencies.

More accurate plots of power penetration depth are plotted for water and plant material, using the measured broadband permittivity data, in Figure 3.10 and 3.11. The effect of the dissolved salts on the penetration depth are immediately clear. In pure water, the power penetration depth is up to 150 mm at the lowest ISM frequency. At the same frequency in the plant material, the power penetrates only 18 mm. This is due to the conductive nature of the salts increasing the magnitude of currents nearer to the surface of the plant, resulting in greater power dissipation.

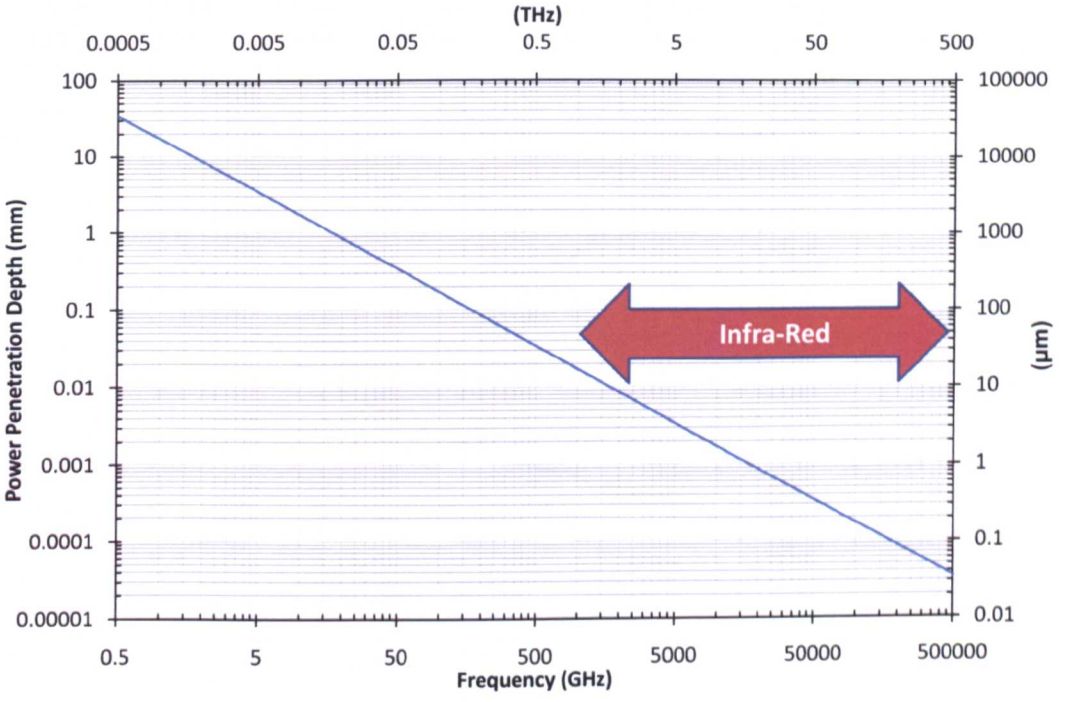

Figure 3.9: Power penetration depth as a function of frequency (for constant dielectric loss).

3.4.2 Power loss density

The power absorbed by a dielectric is given by Equation (2.20) in Section 2.1.3.2. It is clear that the losses in a dielectric increase linearly with frequency, so that a higher frequency will result in higher power loss (and thus higher temperature increase) for the same incident field strength. This power however, must be provided by the source generator. Dielectric properties are themselves frequency-dependent, though, as already shown, and water, or water-containing materials, exhibit certain peaks at particular frequencies.

The relative effect of the dielectric properties on the absorbed power can be seen for water and plant components in Figure 3.10 and 3.11, where the contribution of frequency has been removed. As for the power penetration depths, the most noticeable feature of these traces is the relative effect of dissolved salts on the power dissipated in the dielectric at low frequencies. In Figure 3.11, the trade-off between power penetration and absorbed power can be seen for the available

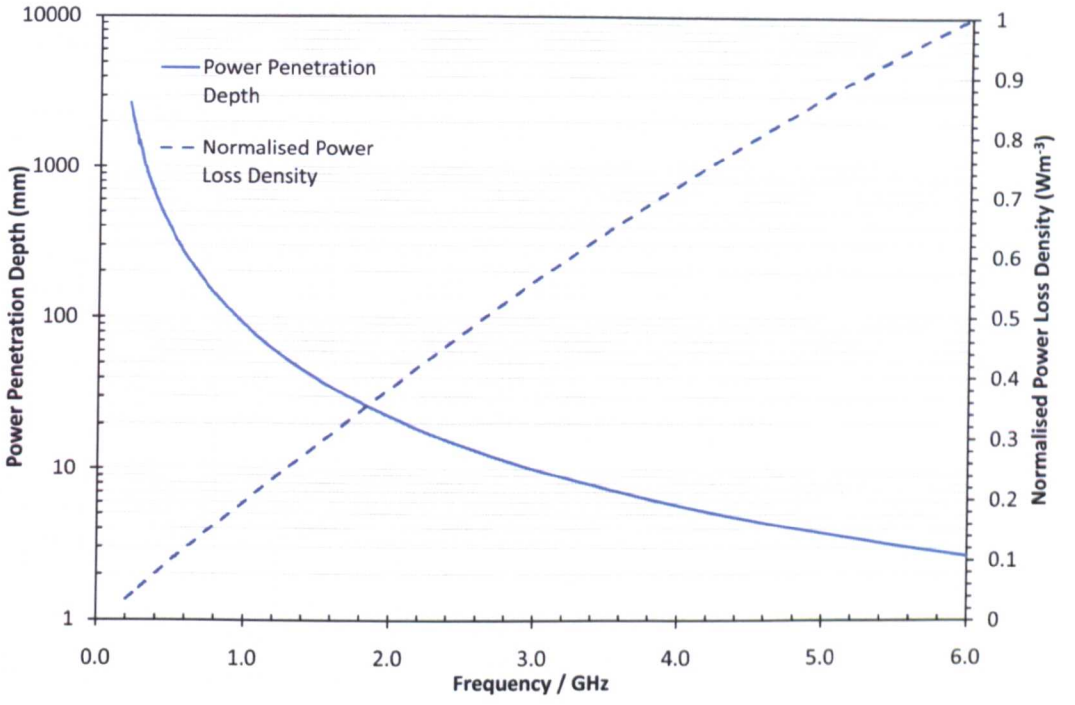

Figure 3.10: Power penetration depth and power loss density in water.

microwave ISM band frequencies, as indicated.

3.4.3 Selection from viable frequency bands

3.4.3.1 Infra-red

As frequency increases into the IR spectrum, the power penetration depth (from Figure 3.9) will be in the order of micrometres, that is; will become very shallow. It is for this reason that IR heating, although a form of dielectric heating, is classified as a surface-heating process.

Using IR radiation, heat transfer to the interior will be by conventional conduction, determined by the thermal and not electrical characteristics of the medium. For most substances – in this case plant matter – this is a slower process than the direct EM heating. During the conductive heat transfer process, heat will be lost through convection and radiation back into the surrounding atmosphere.

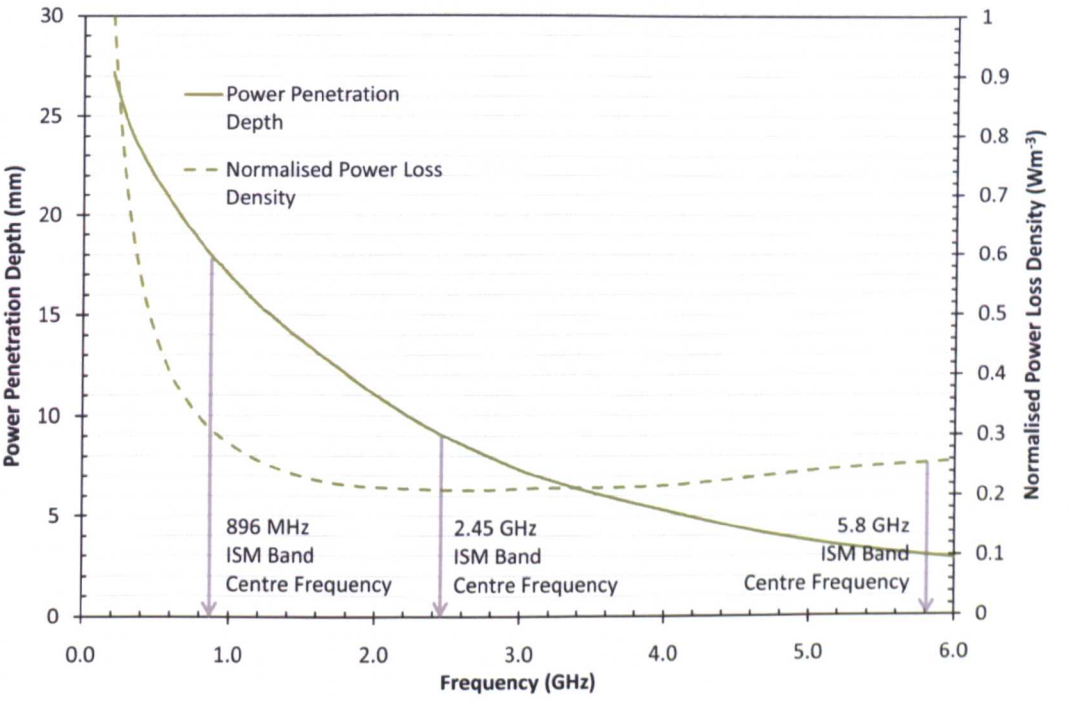

Figure 3.11: Power penetration depth and power loss density in tomato plant.

Furthermore, the high frequency nature of IR radiation results in the dominant polarisation mechanism by which power is dissipated to differ from the dipolar type found in water molecules across the MW regime, to an atomic polarisation mechanism at THz frequencies. Although there will be a resonant peak in dielectric loss within the IR spectrum, it is not as high as the strong dipolar polarisation mechanisms in water-containing materials at microwave frequencies.

This atomic polarisation mechanism will also be effective in nearly all materials that the IR radiation is incident on and, when coupled with the low power penetration depth, will result in their heating, in addition to the desired heating of the plant. This will cause the heating (and overheating) of all objects in the growing environment and particularly the casing of any heat source. This is wasted energy.

The short wavelength of IR also makes it difficult to focus the radiation effectively as, on such a small scale, creating arrays from multiple sources is not possible

and the use of lenses is impractical and inefficient.

Favourable aspects of an IR heating system are that the equipment costs would be minimal; the heating element of the source is essentially a resistive element or a solid state light source. A further advantage is the absence of any regulation governing the use and application of IR heating and the lack of any shielding requirements.

Although undoubtedly effective in its heating ability, it is apparent that an IR-based dielectric heating system would not offer the greatest efficiency.

3.4.3.2 Radio-frequency

From Figure 3.9 it can be seen that the approximate power penetration depth at RF frequencies is significantly larger than at microwave and infra-red frequencies. This would allow incident waves to penetrate deep into the plant material and, for most parts of the plant, pass through. A more precise description, at RF and MW frequencies, is shown in Figure 3.11.

Although, because of the high concentration of ionic particles dissolved in the plant liquids, the penetration is much lower than that in pure water (Figure 3.10) it is still considerable in plant material and is more than adequate to heat commercially grown plants that produce even the largest fruit.

The effect of the ionic conduction from the dissolved salts also acts to increase the losses at low frequency. Indeed, the significance of these salts on absorbed power are greater than the effect on power penetration and offer an advantage to a system where efficiency is crucial.

The costs of high power RF are greater than an IR system, but benefit from the availability of readily available 'off-the-shelf' components that are relatively cheap. These could be high power solid-state sources or very high power magnetrons as used already in many industrial processes.

An RF system would require the use of an antenna system to transmit the power to the plants. This would facilitate some control of the beam as elements could be arranged and controlled using an array. A problem with this method in a commercial greenhouse, where light levels are an important premium, could be the size of the elements. At RF frequencies antennas and arrays could be quite large, although the large wavelengths would also make any necessary shielding easier.

As described in Section 2, the RF spectrum is used heavily for communications and sensing and is heavily regulated [31]. Several ISM bands are available for use however, namely those at 13.560 MHz, 27.120 MHz, 40.68 MHz and 433.92 MHz. Because of the crowded spectrum though, bandwidth is severely limited and in some cases is as little as 0.1%. This provides a tighter design constraint on the generating equipment and applicator than for some higher frequency bands.

Whilst being capable of heating the plant material volumetrically, the large penetration depth is many times greater than the largest plant dimension and would cause power to be wasted by transmission through the plants, where it will then degrade through attenuation by the air. The benefit of having losses two-times greater than at a microwave frequency are negated if most of the radiated power passes through without dissipation.

3.4.3.3 Microwave

The power penetration depths at the high end of the microwave spectrum *i.e.* ~150 GHz, are of the order of microns. This immediately precludes their use as heating would be neither volumetric, nor have the inexpensive equipment availability or superior heating capability of infra-red. At low microwave frequencies however, power penetration depths are similar to the maximum dimensions found in the larger plant components e.g. large fruits. Indeed, between 1 and 6 GHz, power penetration depths can be seen in Figure 3.11 to be between 3 and 18 mm, which would result in nearly all microwave energy being dissipated within the interior of the plant, with little power being transmitted entirely through the plant and thus wasted.

As for RF, there are many ISM bands available which would be suitable for use [31] (see Section 2). Although the band centred on 24.15 GHz roughly corresponds with a peak in the dipolar loss mechanism of water, it can be seen from Figure 3.9 that the power penetration depths would be too small, so this frequency can be discounted. The band centred on 6.78 GHz (Netherlands only) has a very low power penetration depth and is also not universally available. It too, can be discounted for this study.

The bands 896 MHz (UK) and 915 MHz (USA) have large power penetration depths, and similar power loss densities to the ISM frequencies above. As losses here are similar to higher ISM bands, the latter must be favourable, in terms of maximising efficiency, owing to their lower power penetration depths. The two bands stated are also not universally available, particularly in Europe, where most commercial greenhouse growers operate. This then leaves 2.45 GHz and 5.8 GHz, as the intermediate band 3.39 GHz is available in the Netherlands only. This latter band is not discounted for any other practical reasons, however.

It is expected that these frequencies will offer the best efficiency through a suitable compromise between the depth at which they can penetrate the plant and the dielectric losses that result within the plant. Furthermore, the equipment required for a system at any of these frequencies would be very compact and allow for accurate control and focussing of the power. Although perhaps more expensive than other frequency options, the improved efficiency of such a system would allow for lower input power specifications, resulting in cost savings. Effective shielding would also be simple and non-obstructive.

Practical experimentation in this study will therefore be undertaken using the ISM band frequency of 2.45 GHz; the central band of the options stated above and where high power equipment is readily available. The use of 896/915 MHz and 5.8 GHz bands will be investigated, where appropriate, with the aid of computer simulations so that the results may compared to those from experimentally validated simulations at 2.45 GHz.

Chapter 4

Pilot Tests

In order to make a qualitative assessment of the response of a tomato plant when exposed to high power and high frequency EM fields, two pilot tests were performed. Specifically, the aim was to assess the feasibility of heating plants with a free-space microwave heating system and to observe for physical aberrations or other effects. Pilot test results were used to inform the design and implementation of the larger and more ambitious investigations detailed in Section 6.

4.1 Pilot test A

4.1.1 Set-up and procedure

Two similar tomato plants were selected from seedlings grown until 3-4 weeks old before being transferred to an incubation cupboard. This is a large and sealed enclosure, in which the temperature, humidity and light can be controlled. The temperature was maintained at $10°C$ and day-time light levels made sufficient for otherwise normal growth, for the duration of the test. Plants were both watered once each day.

A single square micro-strip patch antenna (as described in Appendix A) was fixed to a clamp-stand and positioned 45 cm in front of one plant, with its axis of propagation aligned with the plant main stem. The antenna was connected to a Milmega AS0825-18 power amplifier with a measured constant output power

Figure 4.1: Plant condition after microwave treatment (left) and cold control (right) at end of pilot test A.

of 15 W at the frequency of operation. The amplifier input was a sine wave of frequency 2.45 GHz and power 6 dBm, from an Agilent Technologies Signal Generator. The second plant was positioned 45 cm directly behind the antenna, so as to be exposed to minimal EM fields, and was to act as a control plant.

4.1.2 Plant performance

After four weeks of growth, the experiment was ended and the plants inspected. Figure 4.1 shows both plants at the termination of the pilot test.

From Figure 4.1, it can be seen that the microwave-treated plant resulted in a larger volume of growth (in volume occupied) than the cold control plant. Both stems and leaves also appeared generally larger on the microwave-treated plant, although both plants had begun to bear fruit, which were of similar visual quality. The strongest growth *i.e.* where there were most leaves and stems, was observed on the side nearest to the antenna – for the microwave plant – with the parts furthest away being very sparse. This is direct evidence of the encouragement of

growth from microwave radiation.

Both plants had begun to show symptoms of mild cold-shock through the slight curling and small sizes of the leaves. This was most noticeable on the cold control plant. This suggested that the visible effects described above are a result (at least in part) of the temperature-differential from exposure to microwave power and that, in this case, not enough power was being provided to all parts of the microwave plant to allow even growth. Absolute power was, however, evidently sufficient to maintain growth up-to this stage of maturity, for plant parts where power could be directed. Any non-thermal effects from the microwaves are unclear from this experiment.

4.2 Pilot test B

4.2.1 Set-up and procedure

For the second test, Minibel variety tomato seedlings were grown in ideal conditions until three-weeks old. Plants of similar size and appearance were selected from the seedlings to form a set shown in Figure 4.2, from which a further three groups of four plants were taken. These made up cold control (CC), hot control (HC) and microwave (MW) plant groups, to be used in pilot test B.

The CC and MW groups were placed in a greenhouse where the temperature was set to $15°C$ with a recorded maximum variation of $\pm 4°C$. The MW group plants were mounted on clinostats, which rotate at one revolution per minute, in order that all sides of the plants be exposed to the microwave power, given the limited number of antenna elements. A beaker of water was placed at the centre of the arrangement, to monitor the minimum temperature increase from microwaves (the centre point being the furthest from the antennas). Micro-strip patch antennas were positioned around the plants, facing towards the plants and care was taken to ensure the antennas did not point directly towards another. Dual-square patch array antennas were used – and are described in detail in Appendix A – owing to their superior efficiency and beam pattern, compared to a single patch. The

Figure 4.2: Plant group from which microwave, cold control and hot control plants were taken for pilot test B.

experimental set-up is shown in Figure 4.3. Specialist generating equipment was built and set-up as shown in Figures A.2 and A.1 in Appendix A, from which each antenna was fed with 18.2 W of power. Power was measured at the antenna input, at the resonant frequency of 2.45 GHz.

The temperature in a second greenhouse was set to $27°C$, with a recorded maximum variation of $\pm 6°C$. This greenhouse was used to grow the HC plants.

4.2.1.1 Radiated power requirements calculations

Pilot test A suggested that 15 W of radiated power was almost sufficient to maintain healthy plant growth. For pilot test B, the available power was doubled and controlled by adjusting the distance between the plants and antennas accordingly.

The field required to attain the resultant volumetric power loss (which in turn maintains a temperature differential) depends on the rate at which energy is lost from the surroundings. Calculating these accurately is complex and discussed in more detail in Section 7.

Figure 4.3: Dual square-patch array antenna configuration for pilot test B.

4.2.1.2 Failure during first run

After one week of exposure, several plants from the MW group suffered catastrophic stem damage, 2 cm above the soil line, that resulted in plant collapse. Following this, the experiment was aborted and plants from all groups were discarded. The experiment was restarted with new plants, and it is this second run that is described in this section. To avoid further damage, the distance between the plants and antennas was reduced. This damage first indicated the complex interaction of the microwaves with the plant and is discussed with regards to heating uniformity in Section 5.

4.2.2 Plant performance

After four weeks, the experiment was ended. At the specified power level, the MW plants grew to a similar standard as the HC plants, and both out-performed the CC plants in height and volume. The relative performance of MW plants compared to CC plants can be seen in Figure 4.4. This experiment confirms the findings reported by Teitel *et al.* [3], where tomato plants were grown using microwave power as the heat source for a period of four weeks, with no significant

Figure 4.4: Cold control group (left) and microwave group (right) after four weeks' exposure during pilot test B.

visual damage reported. Furthermore, Teitel *et al.* used a 500 W microwave source with a duty cycle of 50%. This experiment used six 25 W sources (18 W at antennas) to achieve the same results. This is 40% of the power used by the cavity heating method presented in [3], although no consideration of generator efficiency is made in either case.

Although Teitel *et al.* reported the temperatures of fruits and flowers when exposed to microwave heating, the experiments were performed on already-mature plants. It can be seen in Figure 4.6c that flowers formed during microwave exposure. This suggests that the microwaves do not have a detrimental effect on the formation of plant components and is an area for further investigation. Interestingly, the HC plants did not form any buds or flowers at this stage of development and CC plants had buds starting to develop, as shown in Figure 4.6a. It could be the case that flowering is forced owing to low temperatures. If so, this would further indicate under-heating in the case of the MW plants.

The leaves on the CC plants can be seen in Figure 4.6 to be very small and curled, which is typical of low-temperature growing. At this stage however, the

(a) Cold control group.

(b) Hot control group.

Figure 4.5: Plant groups at end of pilot test B.

plants do not reveal significant discolouration or further physical damage from cold. Furthmore, the leaves of the MW plants, shown in Figure 4.5c, appear to be less pert than those on the HC plants in Figure 4.5b. It then follows that if the signs of significant cold-shock do not manifest after four weeks on the CC plants, and the MW are showing *some* symptoms of possible cold shock, then it remains to be seen if damage due to under-heating would occur here or in the experiments reported by Teitel *et al.* [3]. In addition, although the absolute

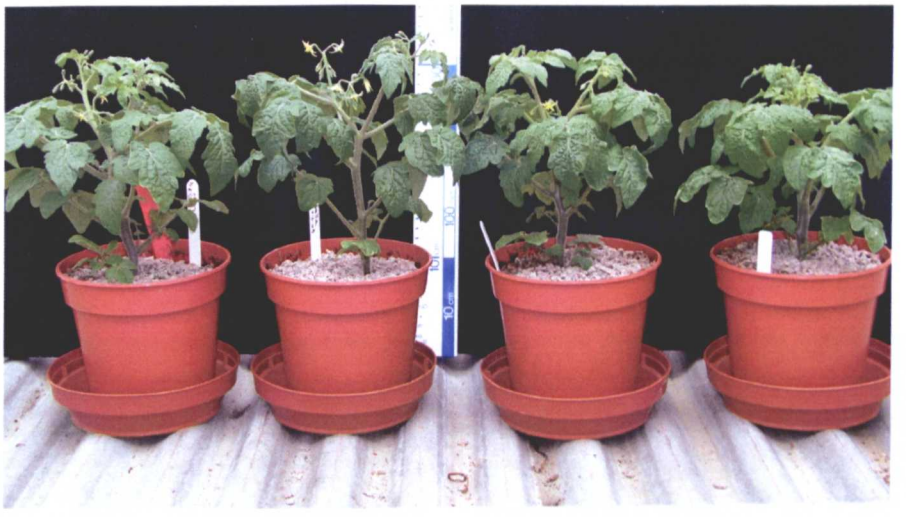

(c) Microwave group.

Figure 4.5: Plant groups at end of pilot test B.

power that is absorbed by the MW plants appears to be able to sustain healthy growth, it is not necessarily clear if this would be the limiting factor in mitigating cold-shock, as opposed to the delivery and distribution of the power. The latter case is implied by the initial stem-failures mentioned above.

4.3 Conclusions

The qualitative data collected through pilot tests confirmed that using a free-space system for heating greenhouse crops with microwaves is possible and at least as effective as the only other demonstrated method *i.e.* the cavity method demonstrated by Teitel *et al.* [3]. Preliminary findings indicate that this method has the potential to be more efficient than a cavity method (and therefore conventional heating), whilst being simple and scalable in its implementation.

Using a constant, low power, method of microwave application appears to be feasible. Evidence suggests however, that there exists significant issues regarding the uniformity of the power application. More precisely; all plant parts must be heated with the power level required to maintain the necessary temperature dif-

(a) Cold control group

(b) Hot control group

(c) Microwave group

Figure 4.6: Visual leaf quality at end of pilot test B.

ferential, without causing damage or failure. In order to assess and improve the power application, a greater insight into the mechanisms of energy distribution within the plant and the constituent plant components is needed.

The pilot tests showed that the plant was being heated sufficiently to encourage some additional growth (relative to the CC plants). However, it was not apparent whether any cold or over-heating effects would become more significant as the plant matured, owing to the apparent long time-scales of operation. This conclusion is appropriate as the CC plants had only just begun to show signs of cold damage (where it would otherwise be expected to be severe and obvious) and the possibility of cold damage on MW plants was unclear over the pilot test duration.

To assess and compare the performance and development of plant throughout an entire growing cycle, *i.e.* from seedling to ripe fruit, it is necessary to collect and compare quantitative data for analysis. In doing so, the dependencies of selected independent variables can be isolated and compared. In this way, it will be possible to ascertain, for the first time, the significance or otherwise of microwaves on the characteristics of the growing plant, from seedling to fruit.

Chapter 5

Heating Uniformity

A major problem in many applications of microwave heating is the non-uniform distribution of the absorbed power. This leads to a non-uniform temperature profile within the heated object and is well documented in the literature [67, 79, 80, 81, 82]. This has been a major obstacle to developing many large-scale industrial processes [79, 81].

Pilot tests showed that a lack of heating power impedes a plant's ability to grow. Initial greenhouse experiments with higher power levels however, revealed an uneven temperature distribution between parts of the plant. In certain locations this was extreme to the point where some parts suffered cold-shock, whilst other parts exhibited evidence of burning. It is thus apparent that the main obstacle to heating crops with microwaves is the ability to distribute the energy required to maintain a necessary plant temperature, across the entire plant, *i.e.* in a manner that results in uniform heating.

This chapter presents a brief review of the known causes and effects of heating non-uniformity and methods for improving uniformity. This is followed by investigations into the effects of the chosen frequency, the duty cycle of the applied power and the polarisation of the radiated electric fields on tomato plant components. This latter section comprises a novel piece of research and is demonstrated generally using computer simulations and practical experimentation using agar gel, before being applied to computer models of tomato plants.

5.1 Causes and effects of heating non-uniformity

5.1.1 Geometry, location and edge effects

Geometry can influence electric field and heating uniformity. For example, diffraction of microwaves at the edges of a silicon wafer that resulted in over-heating was reported in [83] and it was seen to be most prominent when the wave vector was parallel to the plate surface but perpendicular to the plate edge. Non-uniform field patterns due to sample geometry were also observed during the heating of apples and oranges [81]. Furthermore, higher power absorption from the uneven fields at edges and corners for rectangular loads, and in the centre of cylindrical or spherical loads [80] have been reported to cause the formation of localised hot and cold spots [84].

5.1.2 Resonance and wave interference phenomena

Equations for predicting steady-state temperature profiles in food slabs undergoing long-term, low-power microwave heating were developed by Fleischman [85]. In particular, the effect of wave interference and standing wave patterns on non-uniformity was studied in relation to thermal, geometric and dielectric properties. The equations are essentially solutions to the differential heat equation where the source term in derived from the solution of Maxwell's equations. As the study concerned low power heating, thermal and dielectric properties were assumed to be temperature independent. Agar gel was used to demonstrate application of the equations. Non-uniformity was reported by the range of minimum and maximum temperatures.

Temperature within the slabs was found to be a sinusoidal function of slab width and the author claims this was the first full study to apply a full solution of Maxwell's equations to the heating problem [85]. Previous studies used only Lambert's Law approximations, which had been shown in a study by Ayappa *et*

al. [86], to be inappropriate for general application and cannot be applied when the slab width is less than a critical thickness, given by[86],

$$L_{crit.} = 2.7\beta^{-1} - 0.08 \tag{5.1}$$

where β^{-1} is the power penetration depth in cm and Lambert's law is [86]

$$I(z) = I_0 e^{-2\beta z} \tag{5.2}$$

I_0 is the intensity of transmitted radiation (at the interface) and z is the distance into the material.

Basak and Ayappa [87] found that in a dielectric cylinder exposed to a uniform plane wave, heating dynamics operated on two length scales, namely D/D_p and D/λ_m where D is the sample depth, and D_p and λ_m are the penetration depth and wavelength in the sample, respectively. For D/D_p, $D/\lambda_m \ll 1$, power absorption was found to be uniform across the sample. For $D/D_p, D/\lambda_m \gg 1$, heating occurs from the face incident to the wave as power decays exponentially into the material. For $0.2 < D = D_p, D = \lambda_m < 2.0$, however, heating was found to occur from the unexposed face when the diameter was small, from both faces at intermediate diameters and from the centre and face exposed to the wave when the diameter was large. These unusual heating patterns were attributed by the authors to internal resonances within the sample.

Bhattacharya and Basak derived closed-form solutions to calculate field patterns in a material that occur when two waves are incident on opposing faces i.e. approaching from opposite sides of the material, as shown schematically in Figure 5.1. They showed that internal field effects occur over three thickness regimes: thin, $2L \ll \lambda_m/2\pi$; resonating, $\lambda_m/2\pi \not\gg 2L \not\gg D_p$; and thick, $2L \gg D_p$ [10]. It then follows that by controlling the magnitude of waves incident upon opposing faces of the material, the resonances can be controlled and the locations of hot spots controlled and/or their magnitude reduced. Figure 5.2 is taken directly from [10] and illustrates these phenomena and their control.

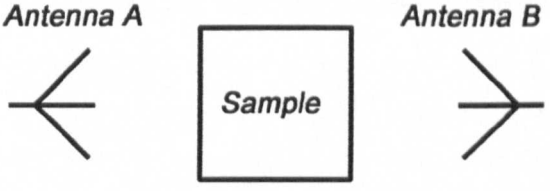

Figure 5.1: Schematic illustration of sample exposed to waves incident from two opposing directions, as in [10].

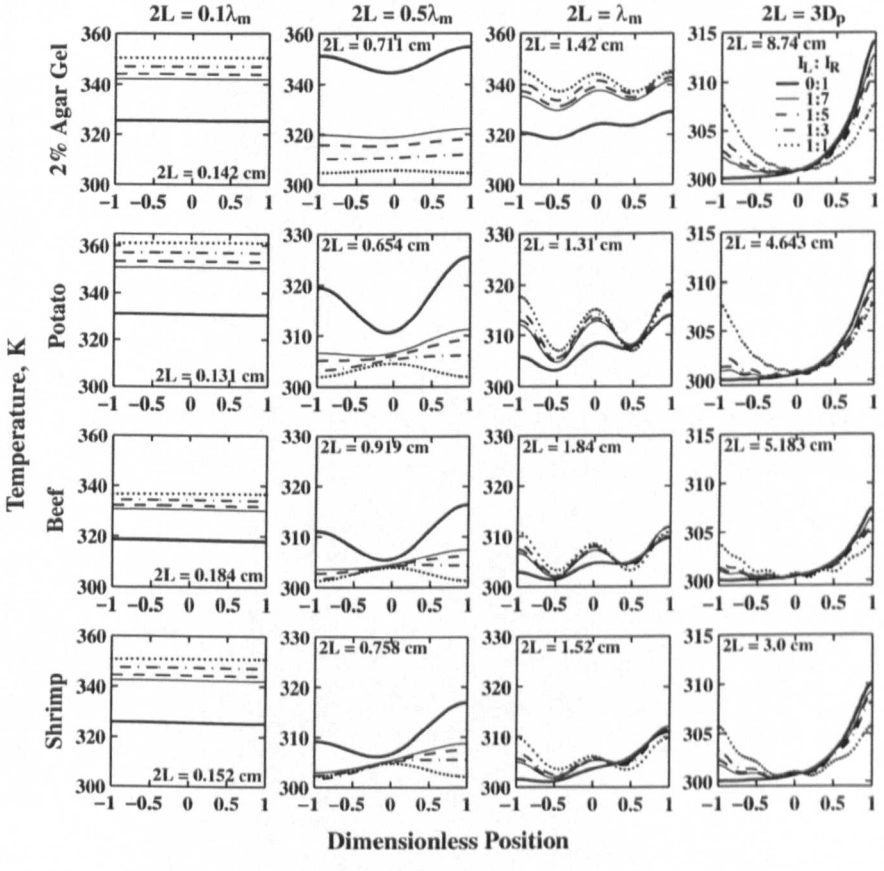

Figure 5.2: Temperature dynamics within different thickness regimes: thin first column; resonating, second and third columns; and thick, fourth column. Intensity ratios (of waves incident from left and right), 0:1, thick solid lines; 1:7, thin solid lines; 1:5, dashed lines; 1:3, dash-dotted lines; and 1:1, dotted lines. Presented in [10]

5.1.3 Dielectric and material composition

Non-homogeneous permittivity of the constituent material of a heated object also contributes to the complex internal field patterns owing to differing rates of power absorption [63]. A further complication occurs since dielectric properties are known to vary with temperature [32]. As such, non-uniform power absorption that results in overheating at one location in turn alters the dielectric properties and can result in an even greater power absorption that exacerbates the overheating. This is the well-known problem of thermal runaway.

For small, moveable objects, non-uniformity can be reduced by intermittent stirring [79]. Also, by immersing the objects to be heated in a liquid of similar dielectric properties, surface and interfacial reflections can be reduced, thereby minimising surface overheating for small objects [88]. In the case of varied dielectric composition [63], it was found that heating spherical fruits surrounded by air, in an parallel-plate RF heating system, results in uneven heating of the fruit interior, but could also be reduced by immersing the fruit in water [89]. A new problem arises however, in that the heating uniformity then became more dependent on the objects horizontal position. The authors stated that the only solution to this was the *movement and rotation* of the sphere in the water. With movement, average fruit temperatures of 49.2-52.8°C and standard deviation of temperatures in individual fruits ranging from 0.3-2.8°C were recorded. Without any movement, average fruit temperatures ranged from 48.7-60.2°C with standard deviation of temperatures within individual fruit ranging from 2.5-4.9°C [81]. These comparative results are typical of what can be considered 'good' improvement in uniformity.

Clearly, none of these methods are possible with a growing plant. As such, differences in permittivity between plant components provide constraints for the radiated power that can be used to attain the required growing temperatures. That is, if a radiated power P dissipates in a plant component of low dielectric loss and results in a desired temperature being attained, then the same power P will result in greater dissipation in an area of high loss and overheating. Radiated power must therefore be reduced in order to avoid damage, then resulting in

under-heating in the former component. This constraint is defined by the degree of difference between the permittivity of plant components and is compounded by additional, unrelated, sources of non-uniformity. It was seen in Section 3 that the greatest difference in permittivity was between the fruits and the plant. Simulation results in the following sections reveal the significance or otherwise of this difference.

5.1.4 Power application and object position

A common and effective method used in domestic microwave ovens is the use of a rotating carousel to mechanically move the heated object though the electromagnetic field. This has been shown to reduce heating uniformity in certain samples by around 40% [90]. The authors in [90] used computer software to solve Maxwell's equations by Finite Element Method (FEM) for the EM field, followed by a numerical solution of the energy equation. Transient simulations were performed by repeating simulations at discrete angular positions of the load/turntable. Simulations were validated by experimental measurement of point temperatures in real loads. Turntables are often combined with the use of a mechanical mode stirrer, which disrupts the electromagnetic field by rotation of metal blades, although this would be impractical where light and space are at a premium, as in the growing of tomato crops. Similarly, non-uniform heating in walnuts that occurred because of differences in their positions in the electromagnetic field was reduced by stirring the walnuts in the container in which they were held, whilst allowing the field to remain spatially static [79], similar to findings in the section above.

Chen (et al.) used Finite Difference Time Domain (FDTD) simulations to model the dependency of field and temperature uniformity on microwave power and object spacing, in homogeneous blocks of dielectric moving on a conveyor belt, with the goal of controlling the formation and magnitude of cold spots within the heated objects [84].

Pulsing the microwave power has been shown to result in greater depth of heat-

ing than continuous heating for the same input power when tested using 2% agar cylinders [91]. This method is useful when deep and rapid penetration of thermal energy is required but when there are also constraints on maximum temperature. Uniformity improvement is achieved through thermal transfer towards equilibrium during the 'off' phase. Gunasekaran and Yang found however, that it is the 'on' phase that is most critical when striving for optimal heating uniformity [92], as it is what defines the temperature gradient. Pulsed heating was found to be most effective for sample radii $\leq 2D_p$ and the 'off' period was found to become more significant as sample size increased [92]. This is most likely due to the flux of EM power being much faster than thermal transfer mechanisms. When trying to reach a specific temperature however, total process time increases compared to continuous operation [93].

Supplementing microwave heating with a conventional heat source such as hot air [82] or infra-red has also been shown to improve heating uniformity.

5.1.5 Summary

It is clear that heating non-uniformity is often the result of several complex and interacting factors. Control is difficult and most current solutions rely on physical disturbance of the heated object for often modest improvements in uniformity. A physical solution cannot be reliably and practically applied to a growing tomato plant and so any method for improving uniformity must be in the form of control of the applied field. Control of power and wavelength have been seen to have some effect, as has a phase delay between two interacting waves approaching from opposing sides of an object. These methods however, have only been demonstrated in simple regular geometries and their control is neither precise nor straight-forward. There are also significant regulatory constraints on the wavelengths/frequencies that can be used. The following sections investigate the heating of tomato plants with the aim of finding non-physical methods for improving heating uniformity, within the constraints given above.

5.2 Quantifying heating uniformity

5.2.1 Computer simulations

Simulation set-up and execution

Antenna models were designed for linear and circular polarisations (see Appendix A.2), with radiation boundaries at least four wavelengths from the antenna source. For power applications in this chapter, all solutions were modal with source terminals defined as wave-ports and in terms of input power. Ansoft HFSS was used to solve Maxwell's equations for the EM fields in the frequency-domain, and in particular the radiated far-fields of the antennas.

Antenna far-field solution data were used as the input parameters for excitation of the plant component models, with the same radiation boundary limits as above, in further HFSS simulations. Permittivity of each plant component was set as per the measurements in Section 3 with appropriate adjustments made according to the solution frequency. All HFSS solutions were allowed to converge to an accuracy of 5% of δS, for a minimum of four consecutive passes, where δS is the variation in the S-parameter solution from the previous pass.

The volume loss density in model components solved in HFSS was linked to Ansoft ePhysics – a thermo-mechanical solver. Thermal solutions were all transient solutions where heating was above initial object and air ambient temperature of $15°C$. For thermal solutions, a boundary condition was defined that modelled the heat loss from the surface of the model components as for free convection. This determines the rate of heat transfer q, across a surface area, A and is defined as [94],

$$q = hA(T_s - T_\infty) \tag{5.3}$$

where T_s is the surface temperature and T_∞ is the fluid temperature (in this case air). This is difficult to measure experimentally, but for air tends to range from 5-$25 Wm^{-2}K^{-1}$. For all thermal simulations presented here, $h = 10 Wm^{-2}K^{-1}$. The plant model simulation set-up and process is shown schematically in Figure 5.3.

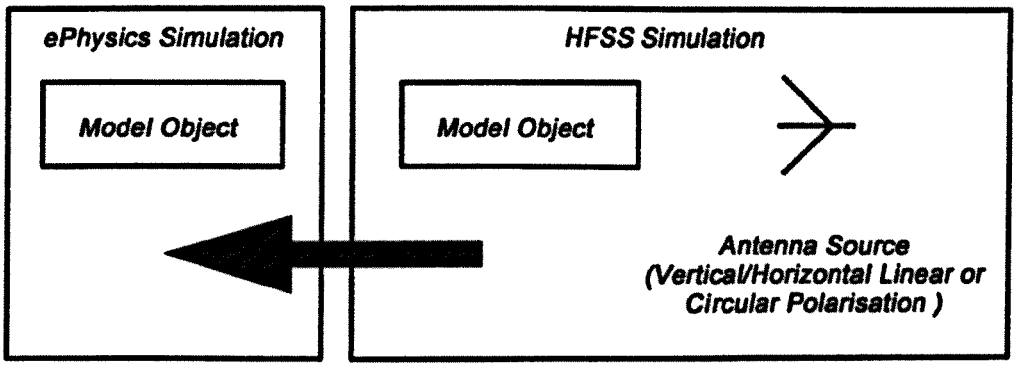

Figure 5.3: Schematic illustration of plant model simulation set-up and procedure.

Data extraction

From the EM simulations, results were in the form of the electric field per mesh cell. This enabled volume loss density (VLD) and temperature to be established at any point within, or on the surface of, the three-dimensional model from secondary thermal simulations. For more specific analysis, non-model vector lines were defined between two or more points within the models, along which data reports could be generated. These are henceforth referred to as geometry lines.

5.2.2 Data analysis techniques

Analysis of uniformity was aided by measurements of mean (VLD and temperature) and the standard deviation about the mean. Variance is useful at times where extreme variations are present, as the squared data element in calculation of variance results in greater weighting of datum further from the mean.

In addition to standard deviation, the range of temperatures is also a useful indicator of uniformity [90]. In this work, percentage difference was used to provide a clearer indication of the magnitude of a range of VLD or temperature when means were dissimilar.

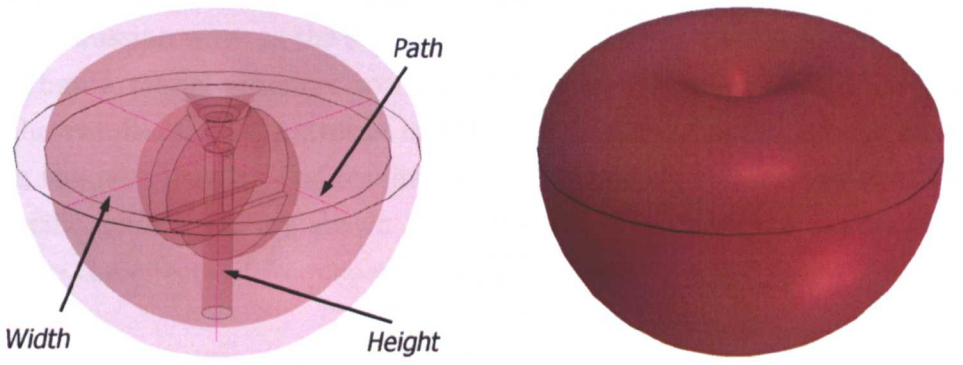

Figure 5.4: Tomato fruit simulation model, indicating geometry definitions.

A parameter used previously in describing heating uniformity is the Uniformity Index [79] which relates change in the samples mean temperature $\Delta\mu$ to the change in the standard deviation of temperatures, $\Delta\sigma$.

$$\lambda_{UI} = \frac{\Delta\sigma}{\Delta\mu} \tag{5.4}$$

Since it is expected that a rise in the standard deviation occurs at the same time as a rise in the mean temperature, the parameter above describes how much the standard deviation can be expected to rise for a given increase in mean temperature. A similar method was also used in [90]. If it is low, then a low standard deviation is expected and the object can be said to be heated more evenly than for a higher value. By normalising the standard deviation of a data set to the mean a better comparison can be made as any deviation of temperatures must clearly be considered in the context of the mean.

5.3 Frequency and heating uniformity

A tomato fruit model was created, as shown with geometry line definitions in Figure 5.4. Dielectric properties were set for each simulation frequency according to the values measured and reported in Section 3. In order to investigate any

effects of sample resonance as described above, the model was simulated with an incident Gaussian wave as the source. An incident wave was chosen for the source, rather than a model antenna, so that antenna-specific effects would be removed from the resultant field patterns in the fruit, making spatial effects dependent only on the wavelength. The results for the normalised volume loss density along the specific geometries are shown in Figure 5.5. The data was normalised so as to remove the effects of frequency-dependent losses.

In all cases, greatest power loss occurs within the sample, rather than at interfaces, and for 915 MHz and 2450 MHz, sample resonance is present in the direction of the wave propagation. Some sinusoidal dependence is visible at 5800 MHz, but it is clear that at this frequency, the sample is approaching the thick regime. Across the sample width and height, frequency-dependent effects are present at 915 MHz and 2450 MHz, but not at 5800 MHz, where power absorption is uniform. This can be atributed to the effect of spherical focussing being prominent at the two former frequencies. To illustrate this further, a simulation of the Poynting vector within the fruit at 2450 MHz is shown in Figure 5.6, where refraction and redirection of power towards the fruit centre is clear.

5.4 Duty cycle and heating uniformity

To investigate the effect of varying the duty cycle – that is, the power on and power off times – on heating uniformity in tomato plants, transient thermal simulations were performed. Initially, models were simulated to solve for the EM fields and then coupled to a thermal solver to find the steady-state average temperature in the model after a given exposure time. When steady-state temperatures were reached, source EM fields were removed and the thermal simulation allowed to continue in order to allow transient cooling. Temperature profiles along specified geometries were produced at the point where the steady-state average temperature was reached and at a later point in time, when the average model temperature had decreased to one third of the temperature increase from microwave heating.

A configuration of stems identical to that shown in Figure 5.14 was simulated as

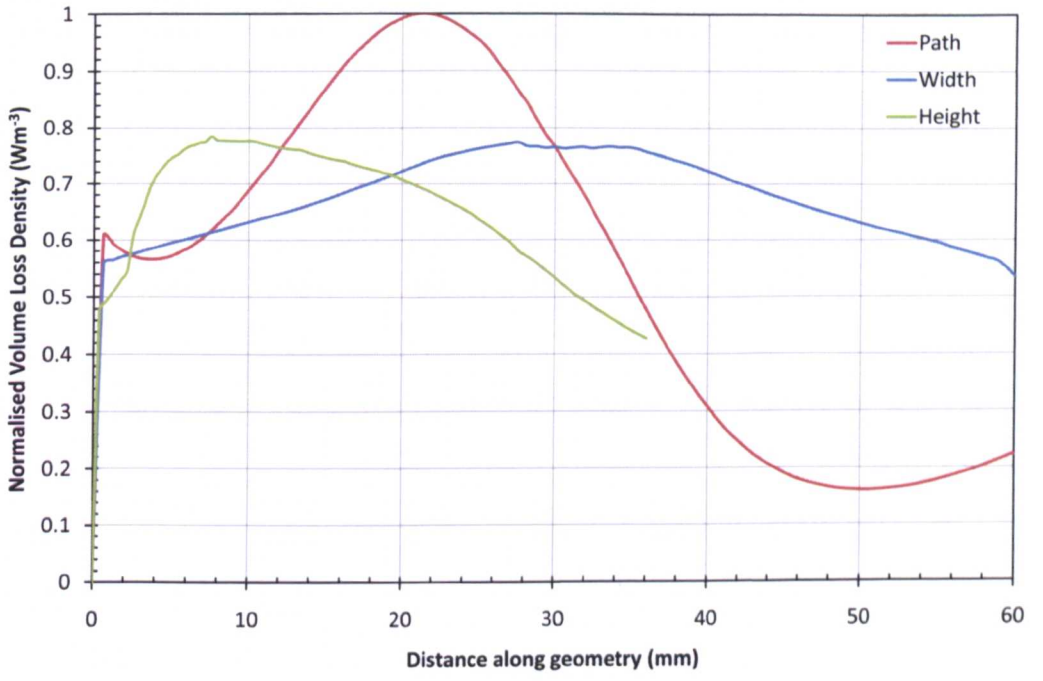

(a) 915 MHz

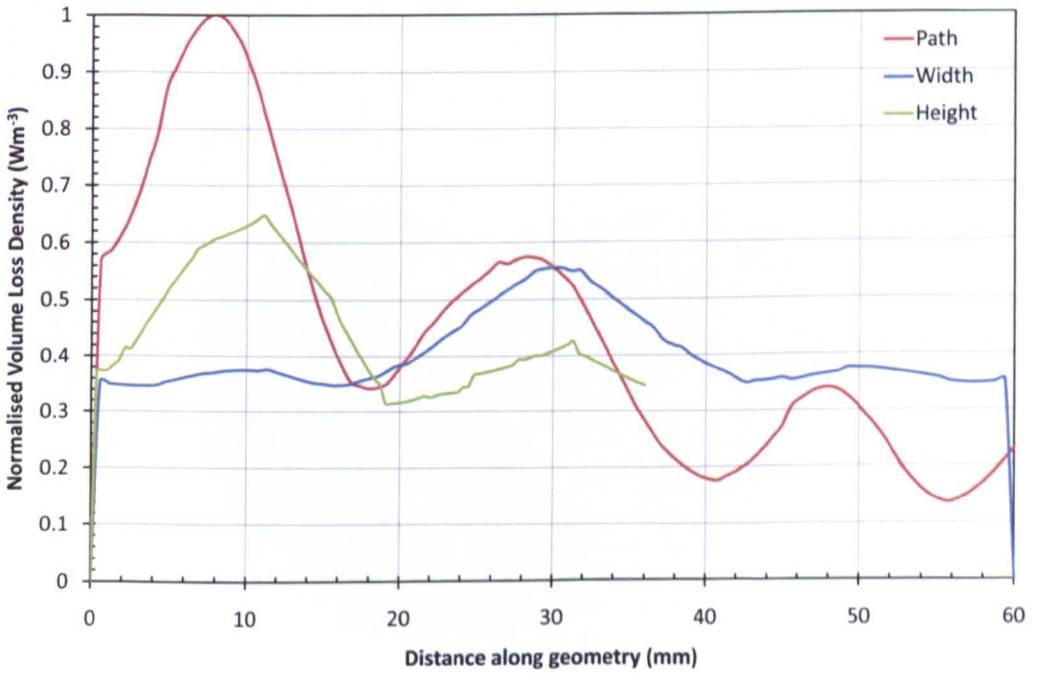

(b) 2450 MHz

Figure 5.5: Normalised volume loss density in tomato fruit geometries when exposed to simulated antenna beam.

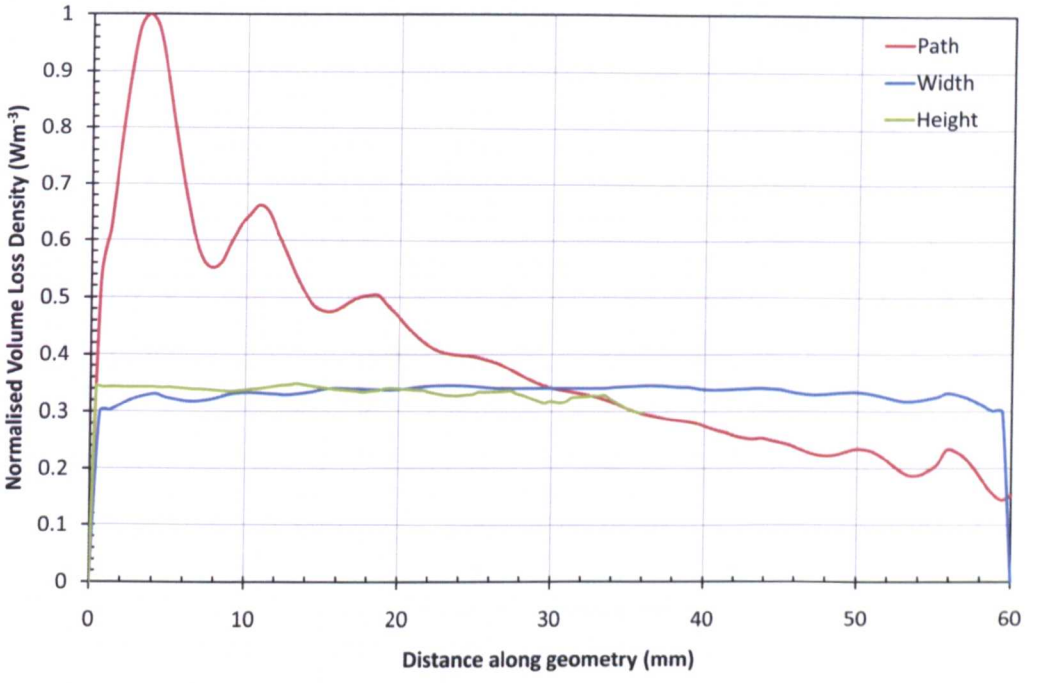

(c) 5800 MHz

Figure 5.5: Normalised volume loss density in tomato fruit geometries when exposed to simulated antenna beam.

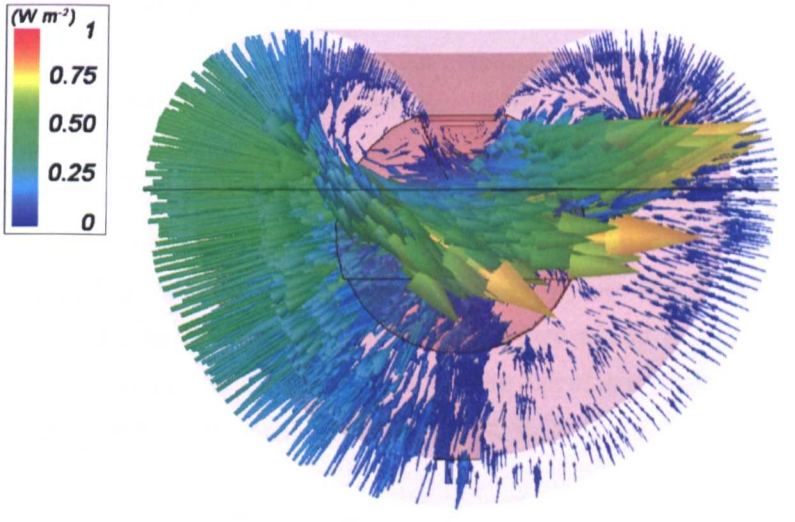

Figure 5.6: Simulated normalised Poynting vector in cross-section of tomato fruit, indicating extent of spherical focusing. Wave is incident from left.

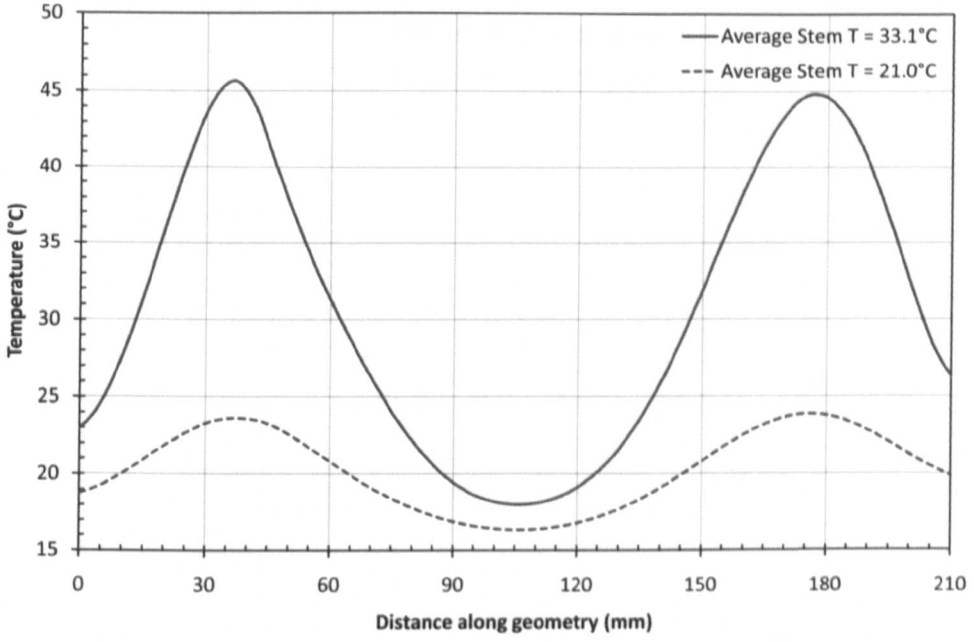

Figure 5.7: Temperature profile in stem section: cooling from steady-state to one-third of temperature increase from microwaves.

described, with the results of the temperature profile along the length of stem geometry 'Y' shown in Figure 5.7. The E-field polarisation was linear and aligned with the direction of the stem.

A similar simulation was performed using the same model for a power on time of 15 seconds, followed by a power off time of 30 seconds. In order that the average steady-state model temperature remain constant between both simulations, the power of the radiant EM field was increased by a factor of 3 for the second simulation. The total energy delivery in one cycle was therefore equal for both simulations. Figure 5.8 shows the temperature along a stem geometry after the on period and after the off period. Both temperature profiles were recorded when the average model temperature is in the steady-state.

Both of the above simulations were repeated using a leaf model, but with an adjusted duty cycle of 15 seconds power on and 45 seconds power off. Temperature profiles along a leaf geometry were recorded according to the same conditions as

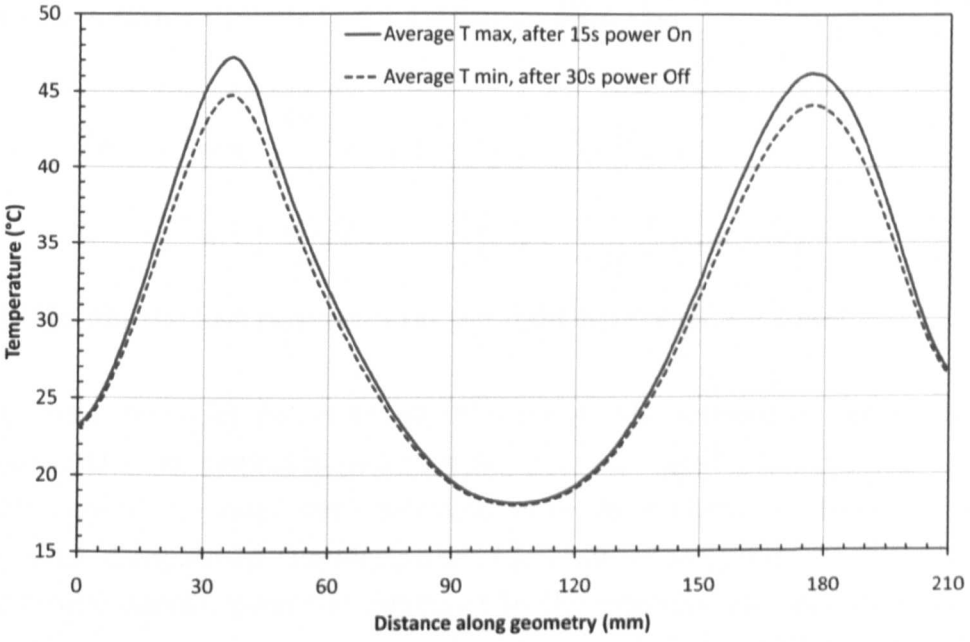

Figure 5.8: Temperature profile in stem section for duty cycle of 15 seconds power on, followed by 30 seconds power off, at steady-state average temperature.

the stem simulations and are shown in Figure 5.9 and 5.10.

If the initial condition $T_o = T_a$ (ambient), then the temperature at the end of a cycle, n is equal to

$$T_n = T_o + \Delta T_{on_n} - \Delta T_{off_n} \tag{5.5}$$

where ΔT_{on_n} is the temperature increase due to microwaves during the 'on' period and ΔT_{off_n} is the temperature decrease through cooling during the 'off' period. If, from Section 2,

$$\frac{dT_{on_n}}{dt_{on_n}} = \frac{P_V}{c_p \rho} \tag{5.6}$$

and

$$\frac{dT_{off_n}}{dt_{off_n}} = -k_t(T_{on_n} - T_o) \tag{5.7}$$

where k_t is a factor describing the rate of cooling, then

$$T_n = T_{n-1} + \frac{P_V}{c_p \rho} dT_{on_n} - k_t (T_{on_n} - T_o) dT_{off_n} \quad (5.8)$$

$$= T_{n-1} + \frac{P_V}{c_p \rho} dT_{on_n} - k_t \left[\left(T_{n-1} + \frac{P_V}{c_p \rho} dT_{on_n} \right) - T_o \right] dt_{off_n} \quad (5.9)$$

At equilibrium the last two terms on the right hand side are equal.

It is a prerequisite for power to be delivered to the interior of the heated object during the 'on' period in order for any thermal equalisation to occur during the 'off' period. If power were delivered from the surface, the tendency would be for it to dissipate to the air, rather than the object interior. For the case of plant components, power *is* delivered to the interior, but very little thermal equalisation appears to occur during the 'off' period (Figures 5.7 to 5.10). When the transient cooling is considered to operate as described by Equation 2.28, it is apparent that the thermal energy dissipated at a location within the plant is presented with a small cross-sectional area through which to dissipate to other parts of the plant and also has a relatively large distance across which thermal transfer must occur. In contrast, a large cross-sectional area (in the surface area of the leaf/stem) is presented to the thermal energy for transfer to the air, where the thermal boundary is of free or forced convention *i.e.* nearly always similar to ambient and low. Furthermore, the distance over which this transfer occurs is very small, relative to the internal transfer – at half the maximum depth of the plant leaf (or stem *etc.*). It is these differences that are responsible for the latter mechanism being 'fast' and the former being 'slow', with respect to the time period allowed for equalisation, *i.e.* the 'off' period. It is for this reason that varying the duty cycle does not result in any significant thermal equalisation within the plant, only a largely uniform reduction in temperature at all locations.

In order to maintain the same average temperature in the steady-sate, it is also necessary to increase the power radiated and absorbed during the 'on' period, which results in the occurrence of very high temperatures. This could lead to significant plant damage.

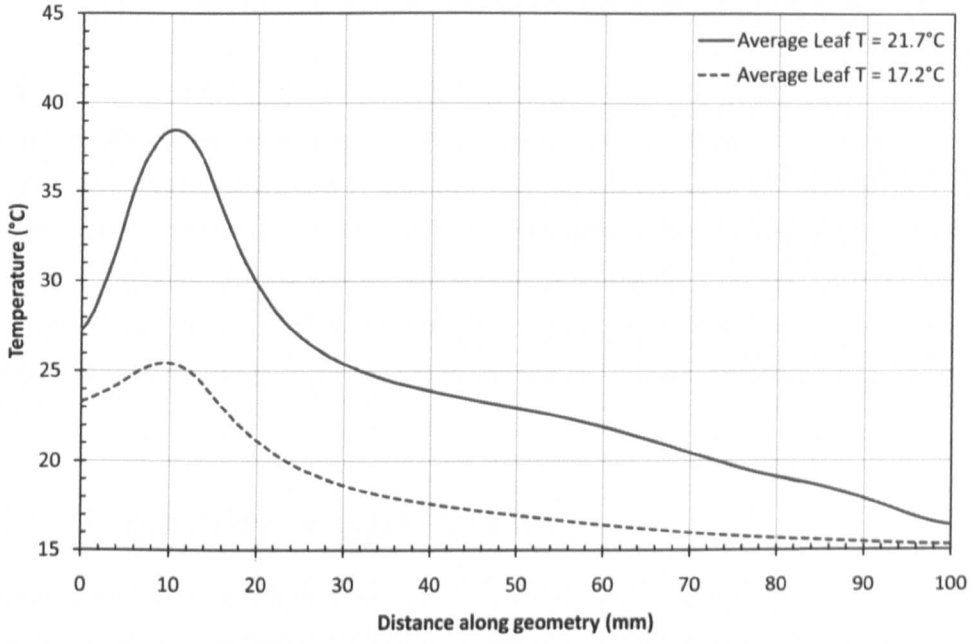

Figure 5.9: Temperature profile in leaf section: cooling from steady-state to one-third of temperature increase from microwaves.

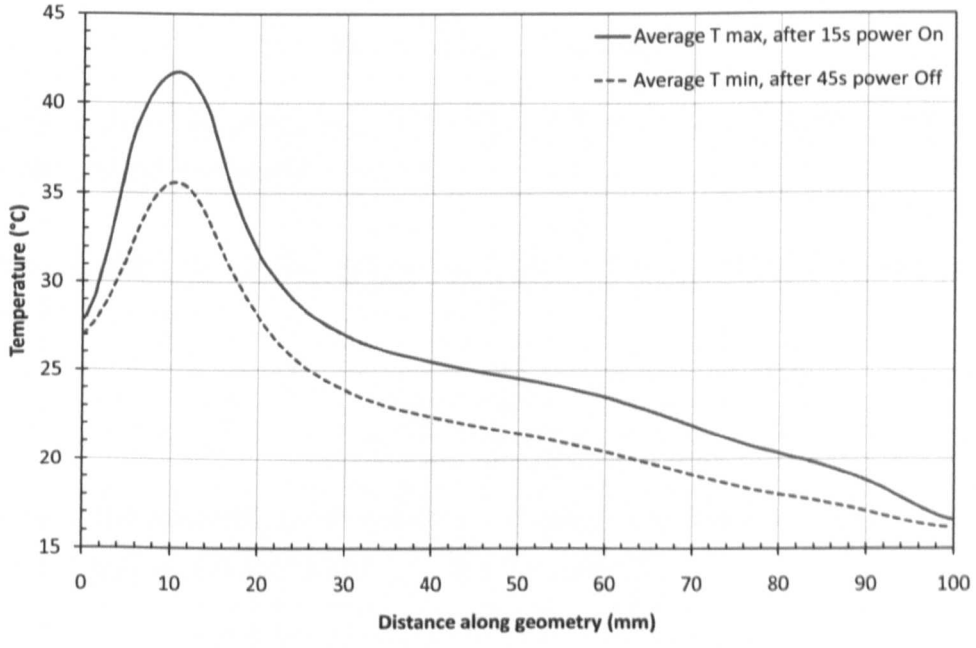

Figure 5.10: Temperature profile in leaf section for duty cycle of 15 seconds power on, followed by 45 seconds power off, at steady-state average temperature.

5.5 Polarisation and heating uniformity

A novel solution using circular polarisation to mitigate the effects of heating non-uniformity, from frequency and geometry combinations, is proposed. The method is first demonstrated in regular cuboid and cylinders, by simulation and practical experimentation using agar gel samples. The method is then applied to and demonstrated in tomato plant components, by means of simulation, in order that it can be applied to actual greenhouse experiments. This method was investigated as a primary non-physical method for improving heating uniformity.

5.5.1 Uniformity in agar blocks

The temperature increase within a sample that can be attributed to the absorbed microwave power is determined by the spatially-dependent volume loss density within the sample, given by [95].

$$Q = 2\pi f \varepsilon_0 \varepsilon'' E_{rms}^2 = \pi f \varepsilon_0 \varepsilon'' |E|^2 \tag{5.10}$$

where Q is absorbed power per unit volume (Wm^{-3}), f is frequency (Hz) and E is the electric field strength (Vm^{-1}).

The temperature rise in the sample associated with this absorbed power is given by [81, 93]

$$\rho c_p \frac{\Delta T}{\Delta t} = \frac{P}{V} = Q \tag{5.11}$$

Where ρ is the material density (kg), c_p is the specific heat at constant pressure ($Jkg^{-1}K^{-1}$), P is power (W) and V is volume (m^3).

This heating term can be added to the heat equation describing transient heat flow within the material (where k is thermal conductivity), to give an overall temperature rise in time of

$$\frac{\partial T}{\partial t} = \frac{k}{\rho c_p}\nabla^2 T + \frac{Q}{\rho c_p} \tag{5.12}$$

In order to establish the resultant heating pattern in a given object however, it is necessary to first find the electromagnetic field distribution by the solving Maxwell's equations (Equations 2.4 and 2.5), bounded by the geometry in question.

A plane wave solution to decoupled Maxwell's equations is a forward travelling wave in the z-direction:

$$E(z,t) = E_{0x}cos\left(kz - \omega t + \alpha_x\right)\hat{x} + E_{0y}cos\left(kz - \omega t + \alpha_y\right)\hat{y} \tag{5.13}$$

where the wave number $k = \omega/c$, and ω is angular frequency $(rads^{-1})$ and c is the velocity of light in a vacuum (ms^{-1}).

The wave is said to be linearly polarised when either E_{0x} or E_{0y} is equal to zero or when $\alpha_x = \alpha_y$, that is, when there is no phase difference between the field components. This will result in a field varying with time in only one dimension at any given point along z.

Circular polarisation arises when both E_{0x} and E_{0y} components are equal and the phase difference between them, $\alpha_x + \alpha_y = \pm 90°$. This arrangement will result in an electric field that varies in two dimensions with time and, at any given fixed point in z, would appear to trace a circular pattern.

It can be seen from this equation, that the electric field can have different magnitudes for different directional components. It follows that if the spatial distribution of fields (from the applied wave) present in a given geometry is also determined by its size, shape and location, then rotating the shape would result in a different configuration of the internal fields within the material. For the case of linearly polarised fields and a material that is of the same scale relative to wavelength in one direction, but very small in the other (a thin bar or slab for example), it is evident that strong standing waves could readily occur when

aligned with the field, resulting in high but non-uniform heating. A different scenario would arise however, should it be rotated by 90° (or indeed, any other angle). It should then be expected that by using circular polarisation, the field and heating pattern within the sample should be essentially independent of its orientation with respect to the source. As a result, there should be a greater consistency in heating patterns between similar samples, regardless of their position. Furthermore, for irregularly shaped objects, circular polarisation should allow for a more uniform temperature profile to arise, as the effect of standing waves and reflections cannot be maintained in one location or direction whilst the field is minimal in another, owing to the constant rotation of field alignment.

5.5.1.1 Samples, equipment and preparation

Agar gel has been used as a substrate for investigating dielectric heating in previous studies [85, 96]. Agar gel samples were made using 10 g agar flakes per 1000 ml of boiling water dissolved in a sealed container to ensure volume and density was consistent between batches. The solution was poured into moulds, which were sealed and allowed to cool before the gel was removed and cut to size. The dimensions of each sample were checked with vernier callipers to ensure a tolerance of ±1 mm. Samples were stored in individual containers and allowed to rest at room temperature for 24 hours before each experiment. Excess surface moisture was removed with paper towels before each run to minimise evaporation.

Agar dielectric properties were measured using the same technical procedure as in Section 3. The agar sample measured was moulded in a glass beaker of height 120 mm and diameter 60 mm such that it filled the container. Before each measurement the sample was allowed to rest at room temperature ($17.5 - 18.7°C$) for 24 hours and the temperature of each sample was recorded using as k-type thermocouple probe. Measurements were repeated 5 times and averaged and typical measurement error was < 5%. The results of these measurements were used to define the parameters in the HFSS simulations, and are shown in Figure B.1. For the samples used, real and imaginary components of measured permittivity at 2.45 GHz $\varepsilon_r' = 65$ and $\varepsilon_r'' = 8.5$.

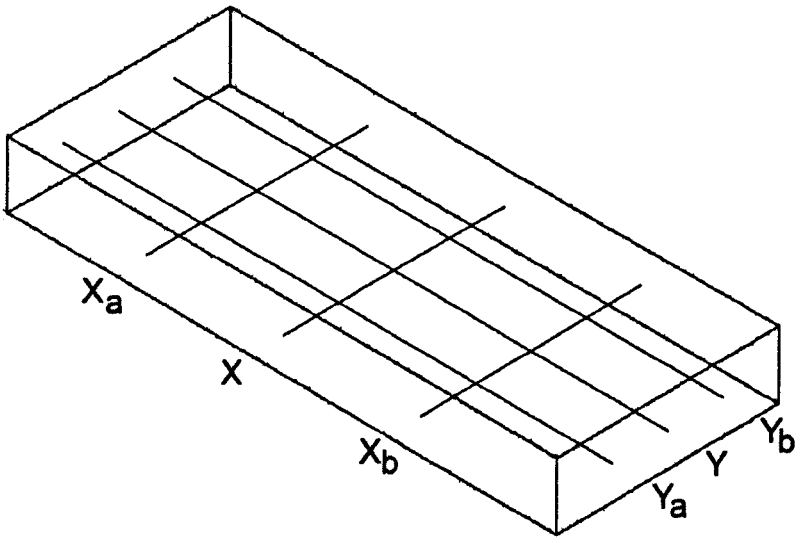

Figure 5.11: Geometry line definitions (in 125x50mm sample).

Chosen sample sizes (X and Y) were 80x80 mm cuboids, 125x50 mm cuboids and 80 mm diameter cylinders, all with thickness 15 mm. These sizes are similar to sizes used in industrial microwave processes and in other similar experiments [63]. A sample thinner than this could be a source of measurement error during probing. A thicker sample would require a higher output power for adequate heating and could result in large variations in temperature between sample depths.

Two similar probe-fed circular micro-strip patch antennas were used to obtain linearly and circularly polarised radiant fields at the frequency of 2450 MHz. These antennas are described in greater detail in Appendix A.2.

A relatively low radiated power was used to heat the samples, in order that dielectric properties of the sample would remain effectively constant, as in [85], whilst still enabling heating patterns to be observed. This allowed for a less complex experimental set-up and easier and more valid comparison to simulated data without results being obscured by other effects, such as thermal runaway. Furthermore, this reduced the significance of any mass transfer from the slab and the evaporative cooling associated with it.

Geometry lines were defined for the simulation model and were labelled according

to Figure 5.11, where X and Y lines denote the centre of the sample, and the a and b subscripts denote ±1/3 either side of the centre line. This convention was used in all sample sizes, except for cylindrical where X and Y geometries were supplemented with XY and YX geometries. These lines also defined the axes along which measurement sample points were located for heating experiments and correspond to the lines labelled in Figures B.5 to B.9, in Appendix B.

As circular polarisation cannot be defined for a specific direction, the direction of polarisation for these experiments was denoted A and B, where polarisation B has the source and sample rotated with respect to each other by 90°, relative to polarisation A. The same convention was followed for the naming of linear polarisations, where linear A refers to an electric field polarisation in the X direction, and linear B in the Y direction or, alternatively, that linear B is the result of rotating the source and sample by 90° with respect to each other, relative to linear A.

5.5.1.2 Experimental procedure

A signal generator (Agilent E8257D) with a power output of 9 dBm and an operating frequency of 2.45 GHz was connected to a solid-state power amplifier (Milmega AS0825-18) with constant output power of 15 W. An antenna was connected to the power amplifier with low-loss (1.1 dB) N-type cables. The equipment was set-up as shown in Figure 5.12, with the antenna fastened to a clamp stand and the agar gel sample positioned on a laminated cardboard holder, 25 cm below the antenna, on a wooden bench. This distance was chosen to ensure the sample was heated only by the far-field radiation from the antenna, but close enough to maximise power exposure.

Room temperature in the lab was controlled using an air conditioning unit and measured temperatures ranged from 17.5 to 18.7°C. Samples were allowed to rest in sealed containers in the room for 24 hours before each run. Each experiment was repeated six times and averaged, with temperature measurements recorded from opposite ends for each run, to mitigate possible measurement error.

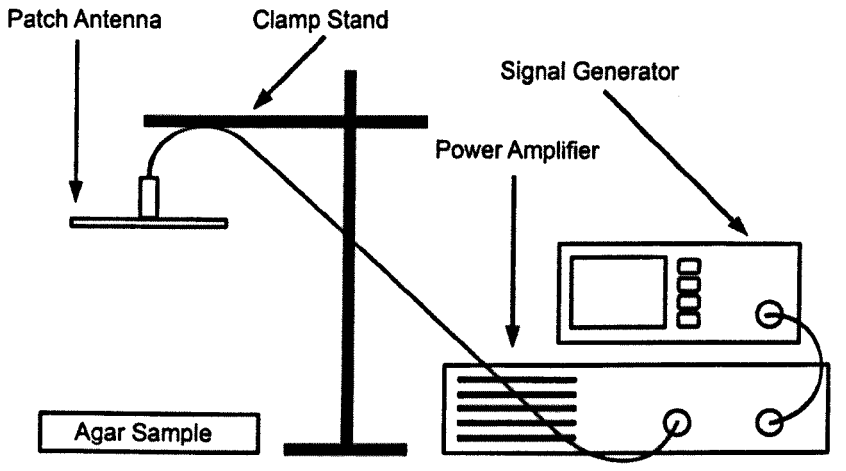

Figure 5.12: Agar gel sample and microwave heating apparatus configuration.

Temperature measurement was performed using a k-type thermocouple probe at pre-defined sample points marked on the laminated cardboard holder (Figure 5.13). The number and location of sample points was determined from simulation results with the intention of sampling data at enough locations of interest such that the temperature profile could be reconstructed. The measured data points correspond with the marker points on the graphs of measured results Figures B.5 to B.9 in Appendix B.

Simulation software was also used, with the process described in Section 5.2.1, to model the agar block being heated by the antenna elements described. Real temperature effects measured in agar blocks were therefore used to validate the simulation models, which allowed for an accurate and valid description and analysis of the field and temperature processes inside the agar samples.

5.5.1.3 Results and discussion

Real and simulated temperature data are presented graphically in Figures B.5 to B.9 of Appendix B. Reconstructed two-dimensional temperature profiles that correspond to values on these plots are shown in Figures B.3 to B.4, to illustrate resultant heating patterns.

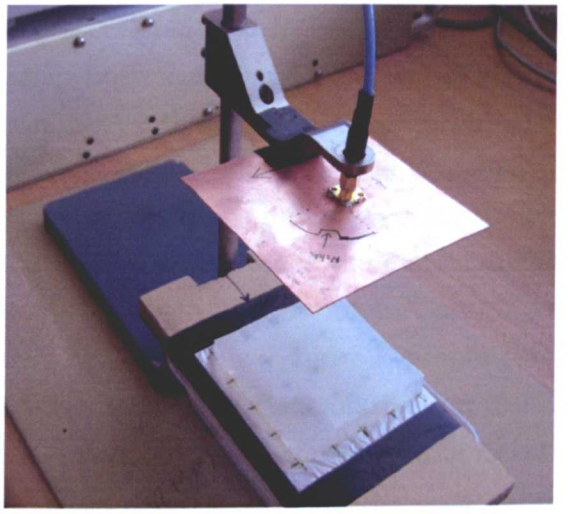

Figure 5.13: Agar gel sample and holder, showing sample location markers.

125x50 mm samples It is clear from the statistical analysis (Table 5.1) that the most uniform overall heating occurred for the Linear B polarisation. Linear A polarisation also resulted in slightly higher overall uniformity than either of the circular polarisations, although not greatly. The difference in overall uniformities between linear polarisations was, however, statistically large at 12% points (40% difference), compared to only 8% points (23% difference) between each circular polarisation. This was also the case with mean overall temperatures and temperature ranges (Table 5.1), with both circular polarisations resulting in similar means and lower ranges of temperatures, which were consistent between polarisations. Linear polarisations always resulted in a higher mean temperature and also in more significant differences between mean temperatures between polarisations or orientations. Furthermore, the results in Table 5.1 show significantly larger ranges of temperatures for linear than for either circular polarisations. If higher microwave power was to be used, it would be more likely for thermal runaway to occur using either linear polarisation, at the location of these hot spots. More importantly, for similar samples orientated differently in the same field, it is clear that heating effects will be significantly different between samples. It is evident that for circular polarisations, heating is likely to be more consistent between similar samples, regardless of their orientation in field.

A greater insight is gained from analysing uniformity along individual geometries

(Table 5.2). For circular polarisation, the results show good uniformity that is consistent and similar in both directions. Circular B shows slightly better uniformity in one dimension (Y) than the other (X), but the differences between geometries are minimal. As it would be expected that both circular polarisations produce identical results, it is perhaps indicative that the circular polarisation of the antenna was not in fact perfect, hence the discrepancies between circular A and circular B results. With differences between X and Y geometries for circular A and B of 5% points (13% difference) and 8% points (26% difference) respectively, it is clear that heating with circular polarisation results in good uniformity that is very repeatable across samples regardless of orientation.

Linear A polarisations resulted in extremely high uniformity in the X direction, but very poor uniformity in the Y direction; specifically a difference of 139%. It would be at these locations of high non-uniformity that hot-spots would occur. A slightly improved, but nonetheless similar pattern is apparent for Linear B polarisations (97% difference), albeit with the pattern of uniformity in X and Y now reversed. If a linear polarisation was used, some samples would evidently overheat whilst parts of others would remain relatively cool. To complicate matters, any hot spots that did occur would more likely than not be in different locations from one sample to the next, for randomly arranged samples.

80x80 mm samples For 80x80 mm samples, circular polarisations resulted in higher mean temperatures but also a greater range of temperatures. Figures B.3 and B.8 indicate that this is most likely because of the under-heated edge area of the sample, perpendicular to the direction of the wave polarisations for linear polarisations, rotating with the rotation of the field for circular polarisations. Regardless of this, the final result was a slightly more uniform overall temperature profile than was achieved with a linear polarisation, when the SD is viewed relative to the mean. The higher variance however, reflects the increased variation around the sample edges.

Individual geometry profiles (Figure B.8) show that, for circular polarisation, uniformity is very good for both orientations, and very consistent between ge-

ometries. This makes temperature profiles between samples very predictable, regardless of field orientation. Hence, for regularly shaped objects whose orientation in a field is nearly always the same with respect to the source (as the object is the same size in both dimensions), a higher final temperature can be achieved if consistency in uniformity *between* samples is preferable to maximum uniformity in *some* samples, but then only for one geometry direction. Linear polarisations, conversely, show good uniformity in one direction only and hence have poor consistency between geometries. This effect could however, be used to an advantage if heating uniformity is more important in one direction only and if sample orientation could be readily controlled. Results in equilateral regular samples also suggest that, in order to minimise the occurrence of thermal runaway, linear polarisation should be used as it will result in a lower range of temperatures.

The effect of linear polarisation when the sample is aligned diagonally to the incident field was not considered, but it can be expected that in this case uniformity will be consistent with the observed results only when circular polarisation is used. Linear polarisation will result in perhaps greater non-uniformity from multiple internal reflections, or at least uniformity that vaires with the rotation/orientation of the sample.

As is also the case for 125x50 mm samples, differences between the two circular polarisations can be attributed to the handedness and imperfections in the circular polarisation obtained from the antenna. This can be observed in measured heating patterns in Figures B.3 to B.4, that appear to show the handedness of the polarisation in the direction of the skew in heating pattern.

80 mm cylindrical samples As for other sample shapes, circular polarisation resulted in a more uniform temperature profile compared to linear and a significantly lower range of temperatures in cylindrical samples (Table 5.1). Linear polarisation resulted in significantly higher mean temperatures in this experiment than those achieved using circular polarisation. It is not immediately clear why this is the case, as simulation results and measured results do not appear to correlate well for linear polarisation, but the very large range of temperatures present

could perhaps indicate a resonance or standing wave pattern, that could not be maintained for circular polarisation, but that was perhaps caused by imperfections in the production of the cylindrical sample. Regardless of the cause, this could be an issue if the heated object is sensitive to large temperature variations or susceptible to thermal runaway.

5.5.1.4 Comparison of simulated and measured results

Measured and simulated results appeared to fit well for most data points, with the exception of results near to sample edges. These regions were expected to be cooler than other parts of the sample as the greater surface area would provide greater opportunity for cooling and also appeared to be areas of lower field intensity. The below-expected heating however, is most likely due to cooling by evaporation being greater near to sample edges where again, the surface area is larger. Whilst efforts were made to minimise this by ensuring samples were as dry as could be before each run, some evaporation inevitably occurred. The simulations did not account for this change in enthalpy and all models were assumed to be fixed masses. This simplification did not, however, significantly affect the analysis as all edge anomalies where consistent across all samples and polarisations. The exception to these anomalies were for linear A polarisation in the X direction, where cooling at the edges appears to have been offset by a very uniform field and heating pattern.

Not all detail anticipated by simulated results was apparent from the measured results. This is an effect of the measurement sampling, which was of too low a resolution to detect all features shown in simulated results, most likely combined with an inaccurate value for the thermal conductivity of the simulated sample. For simulated models it was assumed to be the same as water, but without the consideration of the effects of free convection within the sample, hence why simulated results appear to show less transient equalisation of temperature.

Sample	Polarisation	Mean (°C)	S.D.	Variance	Range $\Delta T(°C)$	Uniformity Index
125x50mm	Circular A	20.77	1.08	1.17	3.3	0.39
	Circular B	21.28	1.01	1.02	3.4	0.31
	Linear A	21.34	1.19	1.42	4	0.36
	Linear B	22.05	0.96	0.92	3.6	0.24
80x80mm	Circular	24.3	1.90	3.63	6.3	0.30
	Linear	23.02	1.70	2.88	5.5	0.34
80mm	Circular	20.72	0.98	0.96	3.1	0.21
Cylindrical	Linear	25.88	2.64	6.95	7.5	0.34

Table 5.1: Overall temperature uniformity statistics for agar samples and polarisations.

Sample and Polarisation	Geometry	Mean (°C)	Variance	Uniformity Index λ_{UI}	% Difference $\lambda_{UI(x-y)}$
Circular A	X	21.12	1.59	0.40	
125x50mm	Y	21.19	1.23	0.35	13%
Circular B	X	21.47	1.35	0.33	
125x50mm	Y	21.66	0.87	0.25	26%
Linear A	X	22.03	0.08	0.07	
125x50mm	Y	21.29	1.63	0.39	139%
Linear B	X	21.26	0.73	0.26	
125x50mm	Y	22.97	0.23	0.09	97%
Circular	X	25.73	2.59	0.21	
80x80mm	Y	25.79	2.47	0.20	5%
Linear	X	24.67	1.44	0.18	
80x80mm	Y	23.88	2.69	0.28	43%

Table 5.2: Geometry specific temperature uniformity statistics for agar samples and polarisations.

5.5.1.5 Conclusions

It is evident from this work that while in some cases a linear polarisation can result in greater uniformity or higher mean temperature in an individual sample, more often circular polarisation offers not only greater uniformity in individual samples but has the important and useful characteristic of ensuring consistency between samples. The processing of irregularly shaped objects becomes more straightforward using circular polarisation as the field and object orientation become essentially decoupled owing to the constant rotation of the field. Correct alignment with the field is then no longer an issue. This property would find many useful applications in continuous industrial processes such as heating or cooking of objects on a conveyor belt and allow many irregularly shaped objects, that would otherwise be difficult to heat, to be processed with microwaves.

Linear polarisation can usually be used to provide a higher mean temperature when the alignment of the object and field can be controlled and when temperature ranges or thermal runaway in the heated object is not a significant issue. However, for most applications, the greatest overall heating uniformity, lowest range of temperatures and repeatable and predictable results can be attained without consideration of the objects position, by the use of circular polarisation.

5.5.2 Uniformity in plants

The application of circularly polarised radiant fields, for improving heating uniformity in tomato plant components, is now considered.

5.5.2.1 Stems

A major problem encountered during pilot tests was the collapse of the main growing stem, from cauterisation above the soil level, resulting in plant failure. In addition, in the first greenhouse trial it was observed that some plant parts experience severe cold shock, whilst other parts suffered burning along parts of branches and leaf stems. The burning appeared nodal in nature and was effective

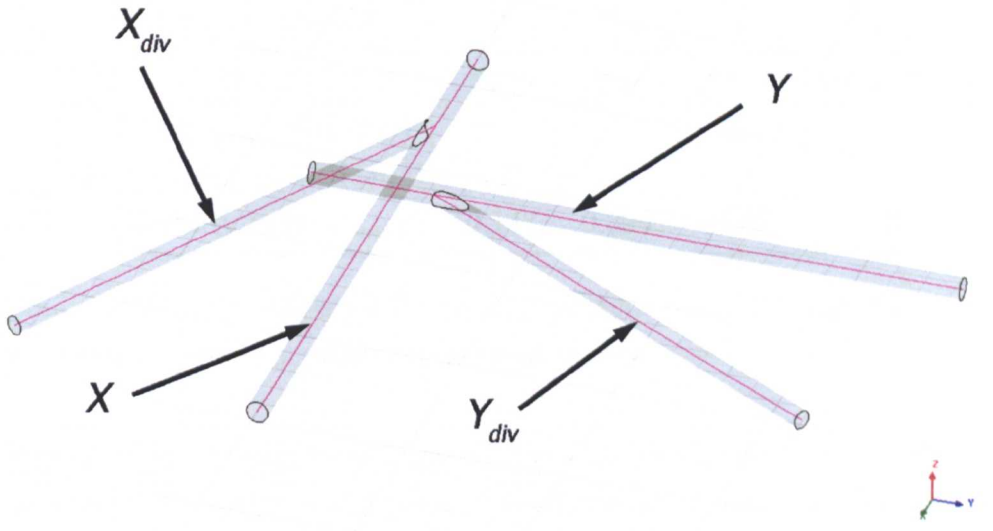

Figure 5.14: Stem model configuration for polarisation investigations. Simulated antenna waves incident from negative z direction.

over a short distance; approximately 1 cm. Increasing output power to compensate for cold areas would prove ineffective and increase incidents of stem burning. Simulations of stem configurations were performed to investigate the effects of incident wave polarisation on the absorbed power, as a potential solution to this issue.

The stem model was set-up as shown in Figure 5.14 and dielectric properties were defined as for those measured in Section 3. One simulation used a linearly polarised antenna wave with the frequency and radiated power used in the actual greenhouse experiments, *viz.* 2.45 GHz and 60 W. The linear polarisation was in the Y-direction. A second simulation used a circularly polarised antenna wave. Circular polarisation was right-handed, from the source. Models were solved for the EM field distribution and data was reported in the form of the volume power loss density, along the geometry lines defined in Figure 5.14. VLD was used as it is directly proportional to the increase in temperature, *i.e.* the temperature profile will follow the VLD profile. Simulation results are shown in Figure 5.15.

Geometry direction	Linear X	X_{div}	Y	Y_{div}
S.D.	3726	23342	157720	203057
$Mean_{geometry}$ (kWm^{-3})	26.1		263	
$Mean_{polarisation}$ (kWm^{-3})	144			
Uniformity $Index_{geometry}$	0.143	0.894	0.600	0.773

Table 5.3: Uniformity statistics for simulated stem temperatures, along specific geometries, using linearly polarised incident waves.

It is immediately obvious from Figure 5.15a that the linear wave results in significant power absorption along parts of the branches Y and Y_{div}. The results of statistical analysis of this data are shown in Table 5.3 and indicate the difference between minima and maxima along these stems is approximately a factor of 10. This situation will clearly result in significant over and under-heating at various points along the same stem and explains how them observed stem burn in the greenhouse experiments occurs. In contrast to this, branches X and X_{div} show relatively little variation between maxima and minima - around a factor of 2 for X_{div}. This is reflected in the uniformity indices shown in Table 5.3, although the mean is only one-tenth that for the Y-group, so consistency between the two groups is poor. That is, the relative magnitude of absorbed power in branches X and X_{div} are significantly lower than for the Y-branches and branch X shows very little absolute power absorption at all. This explains the process behind the plant parts that appeared to suffer severe cold shock despite being adjacent to areas that suffered burning.

Figure 5.15b shows a more complex situation for the case of circular polarised waves. Results of statistical analysis of this data is shown in Table 5.4. In the Y and Y_{div} branches, there is still a significant range of absorbed power density, although the absolute maximum is lower than for the linear polarisation case and in the case of Y_{div} at least, the minima have increased, resulting in a less extreme range. This would have the effect of reducing the likelihood of burning occurring at a point along the stem whilst increasing the overall average power absorbed

Geometry direction	Circular X	X_{div}	Y	Y_{div}
S.D.	83825	76175	128661	130836
$Mean_{geometry}$ (kWm^{-3})	141		221	
$Mean_{polarisation}$ (kWm^{-3})	181			
Uniformity $Index_{geometry}$	0.596	0.541	0.583	0.593

Table 5.4: Uniformity statistics for simulated stem temperatures, along specific geometries, using circularly polarised incident waves.

by that stem, for the same radiated power. Unlike for the linear polarisation, the branches X and X_{div} now show a level of power absorption approaching that of the Y branches, *i.e* the mean VLD of the X-group and Y-group are not as significantly different as in the case of linear polarisation (see Table 5.3). The maxima of X and X_{div} are roughly the average of the entire branch group and the minima are similar to the minima of the Y branches. Although from Table 5.4, uniformity of the X branch is seen to have decreased compared to the linear case, this needs to be viewed in context of the substantially higher mean VLD. Furthermore, the consistency in uniformity between X and X_{div} has improved greatly (and similarly for Y and Y_{div}), and the variation between uniformity between X and Y groups has reduced, compared to the linear case, in Table 5.3.

It can be inferred that the X-branches will now experience average heating, albeit with some cold spots, where before they would not be heated at all. Likewise, the results suggest that, whilst the Y branches will experience some hot-spots and perhaps burning, it will be to a lesser extent than for linear polarisation and all temperatures would be closer to the average. This point is confirmed by observing the the average temperatures in each two-section stem group. Here the EM field distribution was linked to a thermal solver and the resultant average temperatures found. The results are shown in Figure 5.16, where stems are heated from an ambient temperature of $15°C$ until a steady-state is reached. A statistical review of these results is presented in Table 5.5. The mean temperature of both stem groups is similar, at 27 and $30°C$ for linear and circular polarisation,

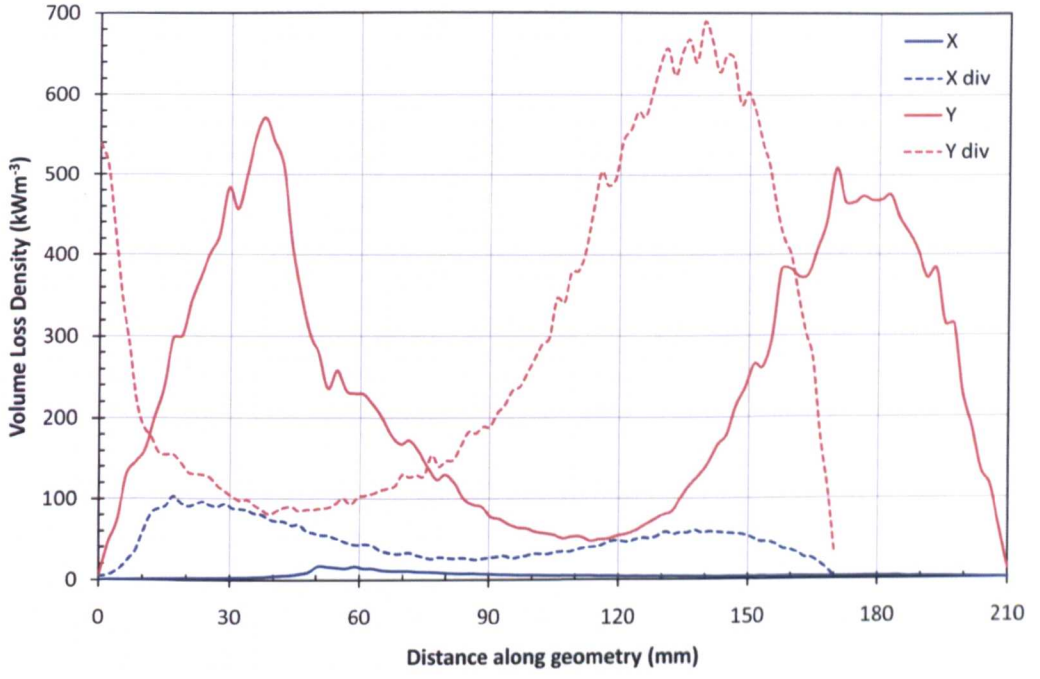

(a) VLD for linear polarisation.

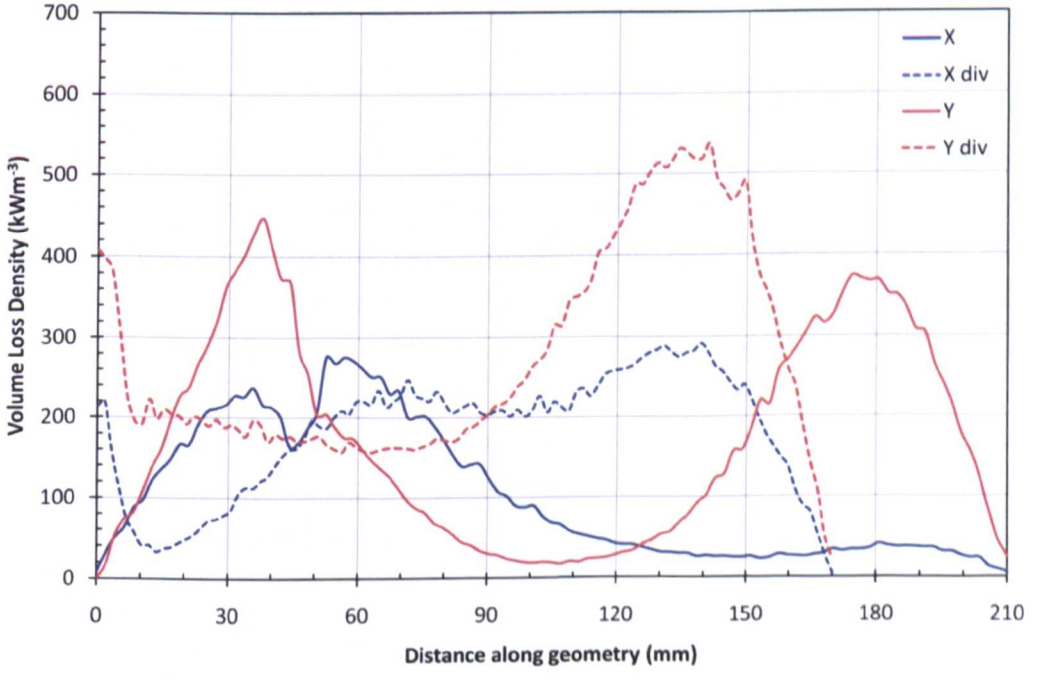

(b) VLD for circular polarisation.

Figure 5.15: Simulated volume loss density along geometry lines in stems for linearly and circularly polarised incident waves.

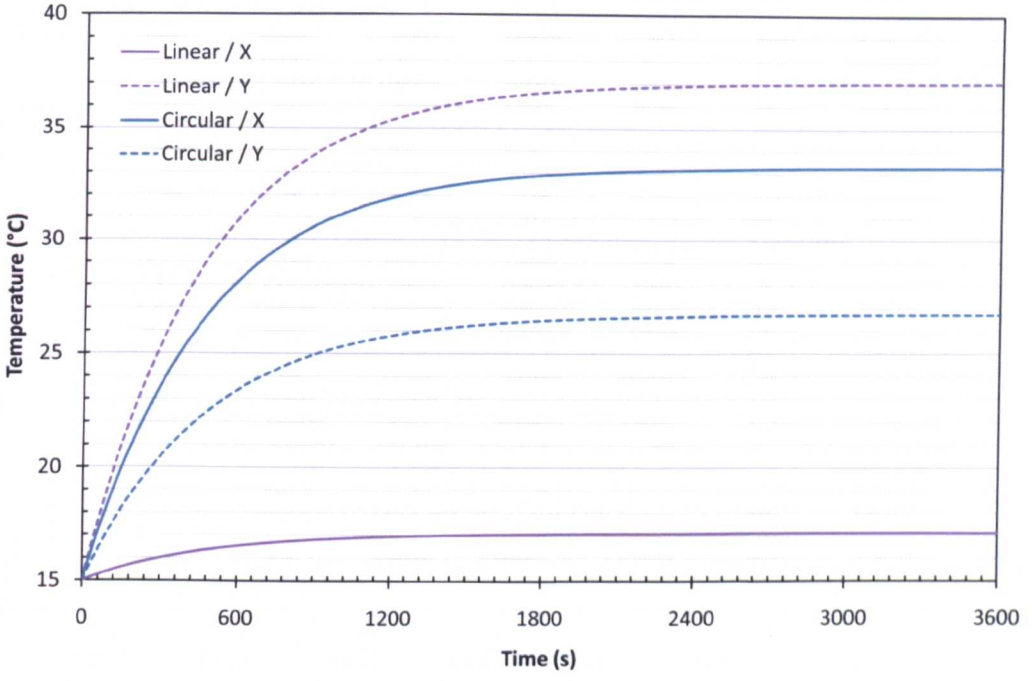

Figure 5.16: Simulated stem temperature increase above ambient, in X and Y stem geometries, for linearly and circularly polarised incident fields.

respectively. For linear polarisations, the range of average temperatures between each stem group is $19.9°C$, which is consistent with the results observed in the greenhouse. Using circularly polarised fields reduces this range to $6.6°C$. Linear polarisation results in a range of temperature increase from microwave heating that is over one-third of the mean temperature, compared to a one-tenth variation for circular polarisation.

The results and analysis presented here make the case for using circular polarisation, in order to improve heating uniformity and consistency of uniformity in the plants stems, compelling.

5.5.2.2 Leaves

A leaf model was created using the same characteristics as for the stems models and is shown in Figure 5.17 with definitions for geometry lines indicated. Six

Geometry direction	Linear		Circular	
	X_{group}	Y_{group}	X_{group}	Y_{group}
$T_{steady-state}$ ($°C$)	17.12	37.05	33.30	26.72
Range (between X and X) ($°C$)	19.94		6.58	
$Mean_{group}$ ($°C$)	27.08		30.00	
% Difference to mean	±36.82		±10.97	

Table 5.5: Uniformity statistics for simulated average stem temperatures using linearly and circularly polarised incident waves.

model combinations were created where the the wave is incident from a different direction in each case. These are described in Table 5.6. All six model combinations were simulated for linearly and circularly polarised antenna waves. After solving for EM fields a linked thermal solution was found which described the transient increase in average leaf temperature to the steady-state. These results are shown in Figure 5.18. The results of a statistical analysis for each model simulation are shown in Table 5.7 for linear polarisation and Table 5.8 for circular polarisation.

It can be seen that the range of resultant temperatures across all models (I-VI) is similar for linear and circular polarisation, at $3°C$ and $3.2°C$ respectively. However, the mean temperature of the circular polarisation group was higher in all cases except one, from the same radiated power. The range of temperatures when expressed relative to the mean increase in temperature above ambient reveals that the circularly polarised wave results in greater consistency of average leaf temperature, regardless of the angle of incidence of the radiated field. It can therefore be said that a closer grouping of temperatures would occur between different leaves on a plant when circular polarisation is used, than for linear. Indeed, the mean temperatures for orientation I and III in Table 5.7, which is effectively demonstrating the effect of orthogonal linear polarisations, are $2°C$ apart. In contrast, the same orientations for circular polarisations shown in Table 5.8 indicate a range of only $1°C$, despite the average temperature for each orientation being higher than for the linear case. This is general trend is reflected by the average

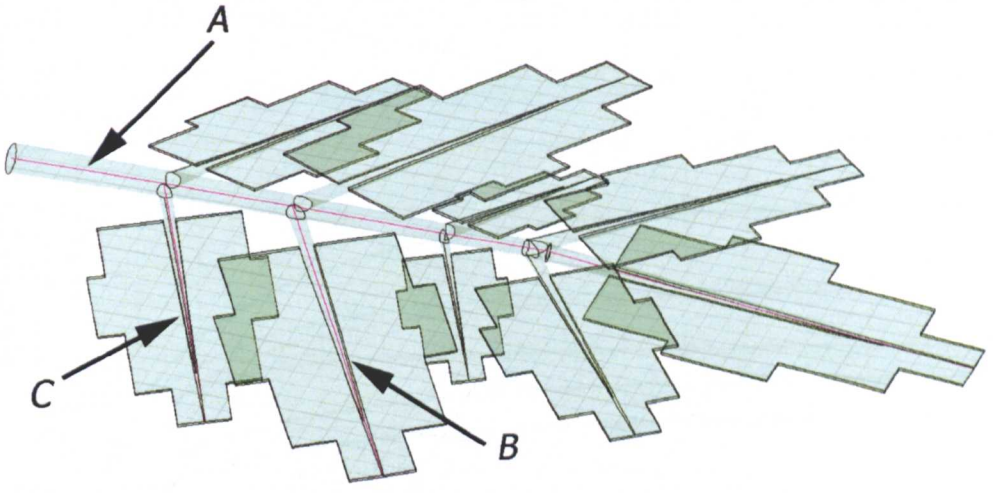

Figure 5.17: Geometry line definitions for leaf model simulations.

	Incidence Direction
I	Wave is incident perpendicular to face of leaf.
II	As I, but with leaf rotated by 45° about its centre.
III	As I, but with leaf rotated by 90° about its centre.
IV	Wave is incident on surface of leaf at an angle of 45°.
V	Wave is incident on surface of leaf at an angle of 67°.
VI	As V, but with leaf rotated by 45° about its centre.

Table 5.6: Definitions of incident wave directions for leaf model simulations.

UI for both polarisation regimes, although the difference is not as marked as for the stems; this most likely being due to the less regular shape of the leaves.

Although revealing, by definition, the average temperatures of the leaves do not describe the whole heating patterns within the leaves. In order to reveal such processes, temperature was plotted throughout the three-dimensional structure of the leaf for orientations I-IV and both polarisations. These are shown in Figure 5.19 and Figure 5.20 for linear and circular polarisation, respectively.

Areas of overheating can be seen clearly on the stem-sections of leaves for both

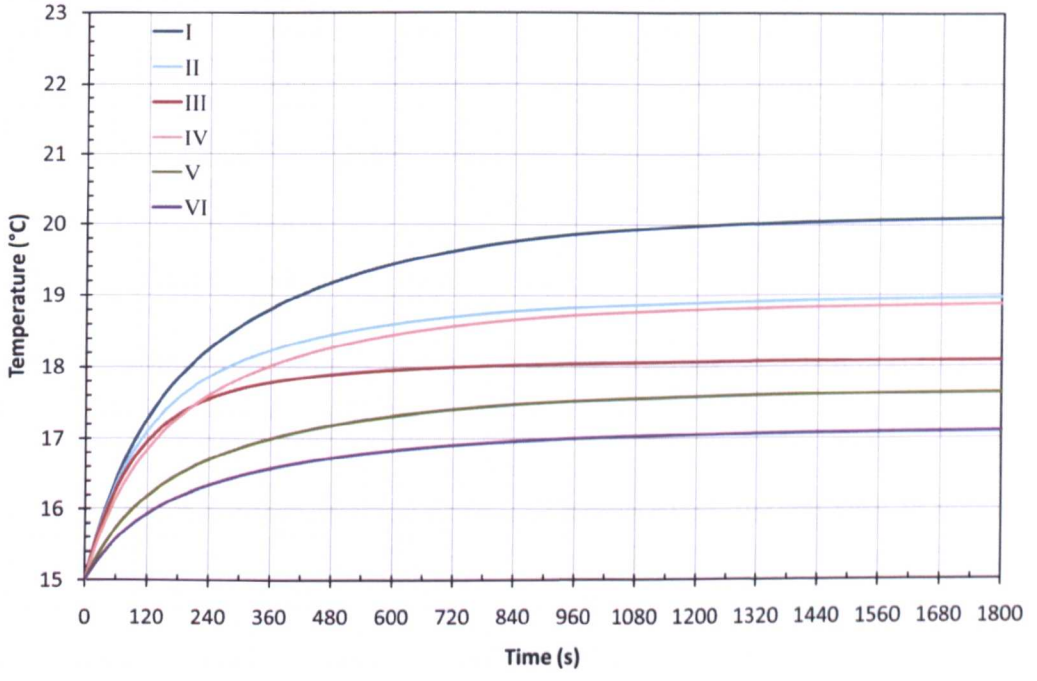

(a) Average leaf temperatures from using linear polarisation.

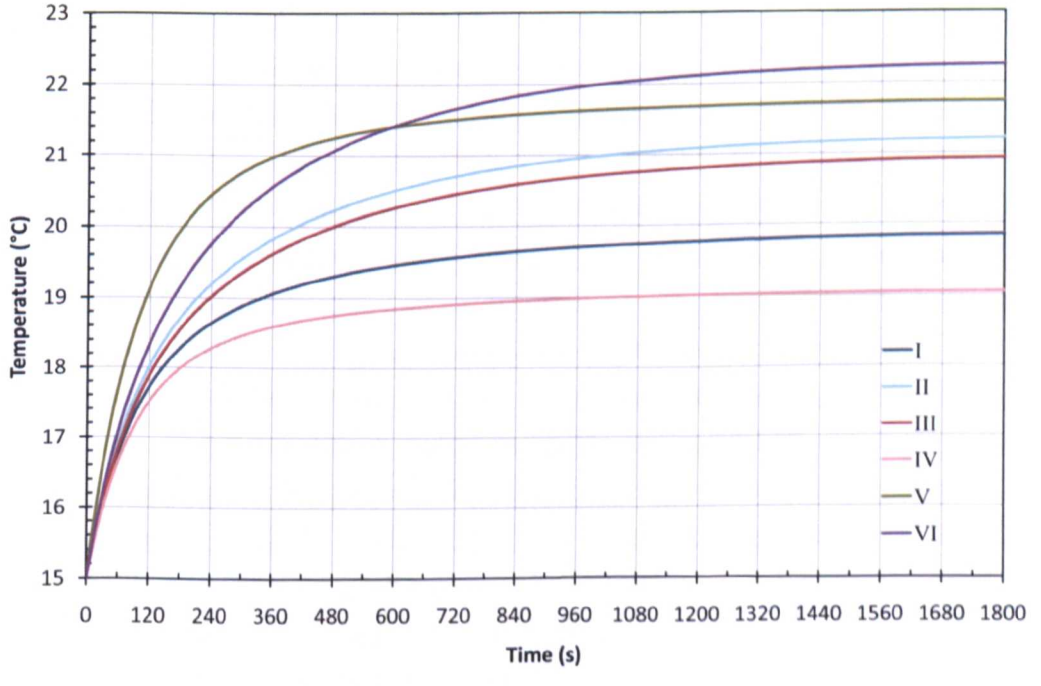

(b) Average leaf temperatures from using circular polarisation.

Figure 5.18: Simulated average leaf temperature for different angles of wave incidence/leaf orientation, using linear and circular polarisation of equivalent radiated power.

Orientation	I	II	III	IV	V	VI
$T_{steady-state}$ ($°C$)	20.09	18.95	18.09	18.86	17.63	17.09
% Difference (to local mean)	8.9	2.7	-2.0	2.2	-4.5	-7.4
Local Mean ($°C$)	18.5					
Range (as % of ΔT_{av})	87					
Uniformity Index	0.311					

Table 5.7: Uniformity statistics for simulated average leaf temperatures using linearly polarised incident waves.

polarisations but a more general uniform temperature distribution is visible for all models where circular polarisation is used. The selective nature of linear polarisation is most apparent in models I and III in Figure 5.19, where heating is mainly in the direction of the polarisation (model III is model I rotated 90° with respect to polarisation), with other sections remaining cold.

To further investigate the significance of the over-heating that was visible is Figures 5.19 and 5.20, temperature profiles were plotted for individual geometries, as defined in Figure 5.17. These results are shown in Appendix C. The statistical analysis of this data is shown in Table C.1 and Table C.2. It is informative to compare the UI of the results presented in these tables, as the significance of the mean temperature is removed when comparing the standard deviations for each combination of geometry and leaf orientation. In the case of linear polarisation (Table C.1), the UI for individual geometries can be seen to vary greatly along the same geometry for different orientations of the leaf with respect to the on-coming wave. Considering geometry A, for linear polarisation, values range from 0.48 to 1.05 – a percentage difference of 75%. For the case of circular polarisation and the same geometry (Table C.2), the percentage difference is 46%. This shows a much more consistent uniformity along the specified geometry is attained using circular polarisation. The variance of UIs of the aggregated data in both tables describes this consistency, with the overall variance of the linear mean temperatures in all geometries being three times that of the equivalent geometries when using circular polarisation. Variance is a useful indication of the consistency of

Orientation	I	II	III	IV	V	VI
$T_{steady-state}$ ($°C$)	19.84	21.21	20.92	19.04	21.73	22.25
% Difference (to local mean)	-4.8	1.8	0.4	-8.6	4.3	6.8
Local Mean ($°C$)	20.8					
Range (as % of ΔT_{av})	55					
Uniformity Index	0.205					

Table 5.8: Uniformity statistics for simulated average leaf temperatures using circularly polarised incident waves.

uniformity, as extreme data values are given more emphasis in its calculation.

Despite strong evidence for circular polarisation resulting in heating of leaf sections that would otherwise remain cold, the simulation results also indicate that burning is still possible and this was in fact observed in the second and third greenhouse experiments. Photographs of damage to leaf stems shown in Figure 5.21 correspond almost exactly with that indicated by the simulation models shown in Figure 5.20. It is important to note however, that the leaves that were damaged in Figure 5.21 continued to grow, whilst damage caused by burning from linear polarisation nearly always resulted in total stem/leaf cauterisation. This could be owing the fact that linear polarisation results in smaller, more concentrated, areas of high power absorption, as suggested in Figure 5.19d. This in turn may be due to the formation of standing-waves within plant sections that results in specific nodal burning. These standing-waves do not have the same opportunity to be maintained when circular polarisation is used, as the node is effectively moved as the phase changes, thus allowing the power to be spread over a greater area thereby saving the plant section from complete destruction.

5.5.2.3 Fruits

The effect of geometry/wavelength on resonances and reflections inside fruit was shown in Section 5.3. The effect of circular polarisation on heating patterns within a spherical object, such as tomato fruits, is perhaps less intuitive. The

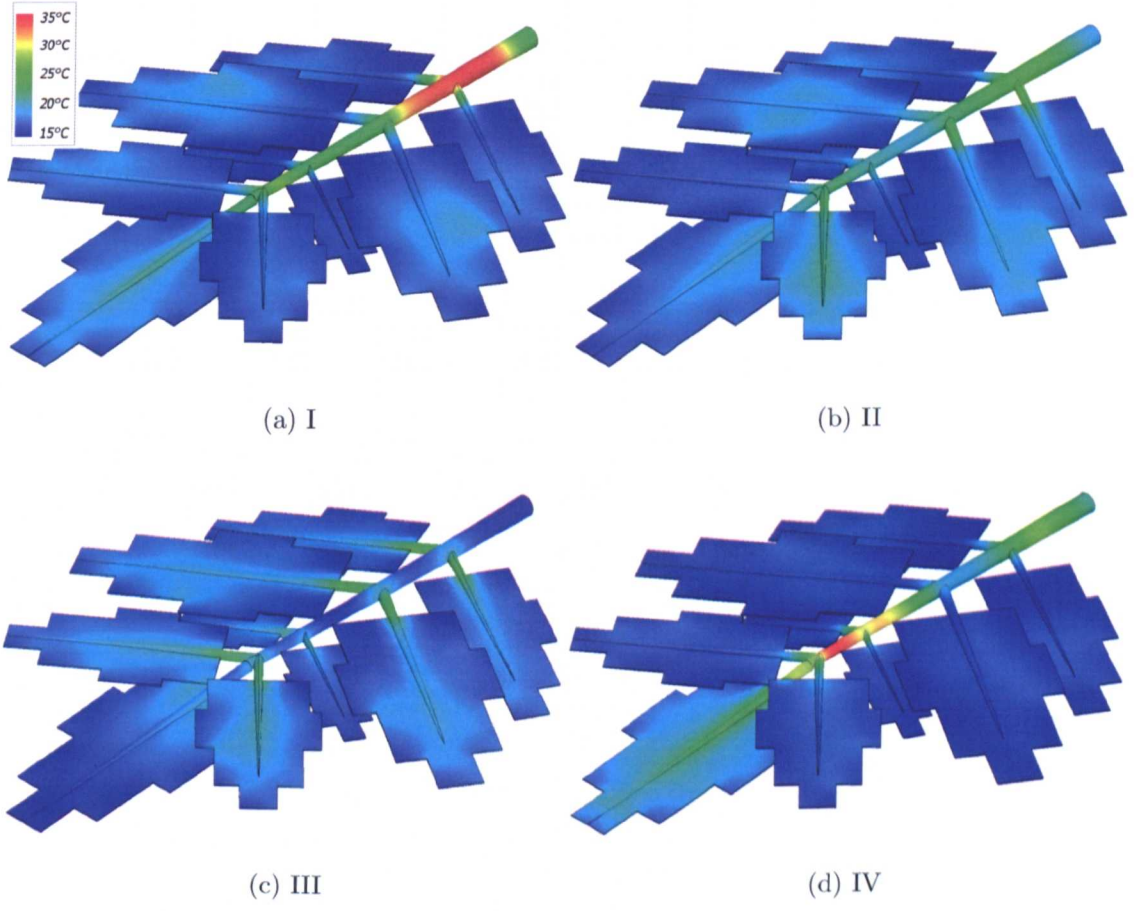

(a) I (b) II

(c) III (d) IV

Figure 5.19: Simulated temperature distribution in leaf, from linearly polarised incident waves.

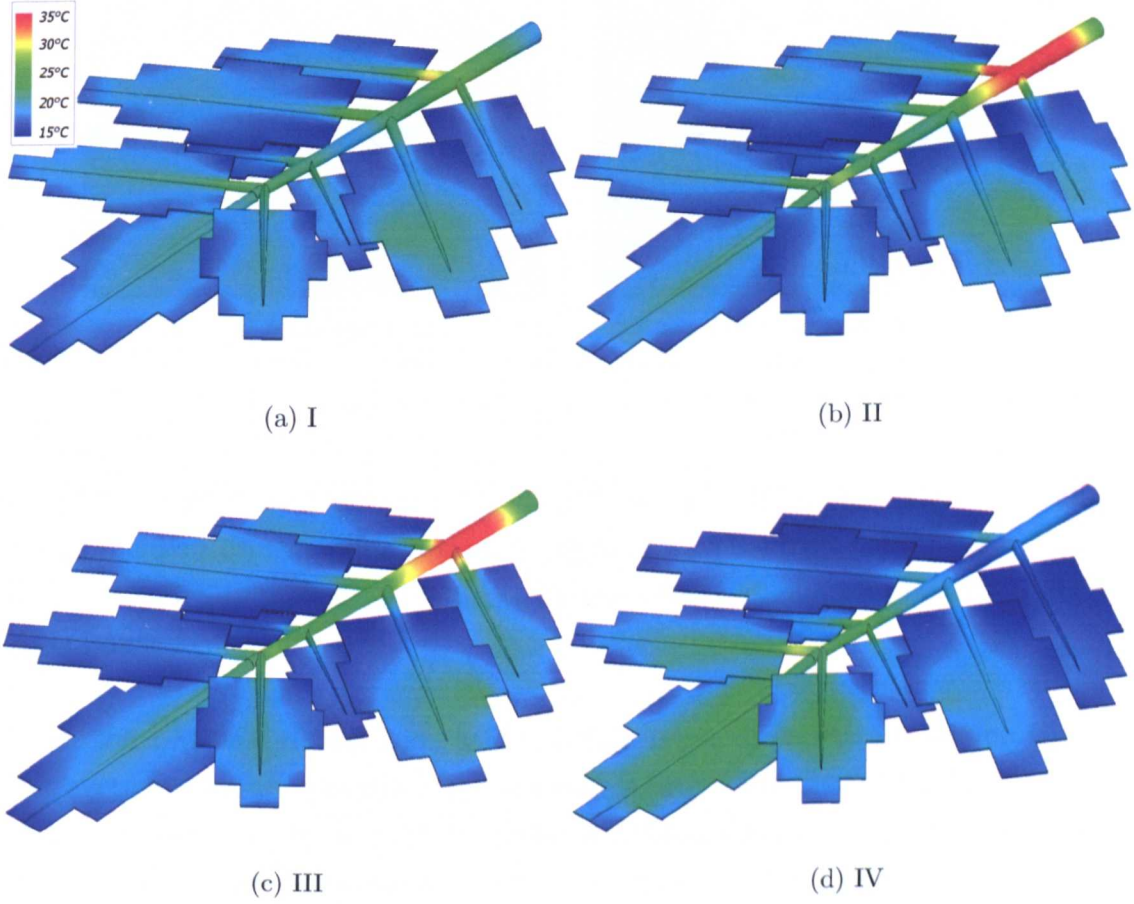

(a) I (b) II

(c) III (d) IV

Figure 5.20: Simulated temperature distribution in leaf, from circularly polarised incident waves.

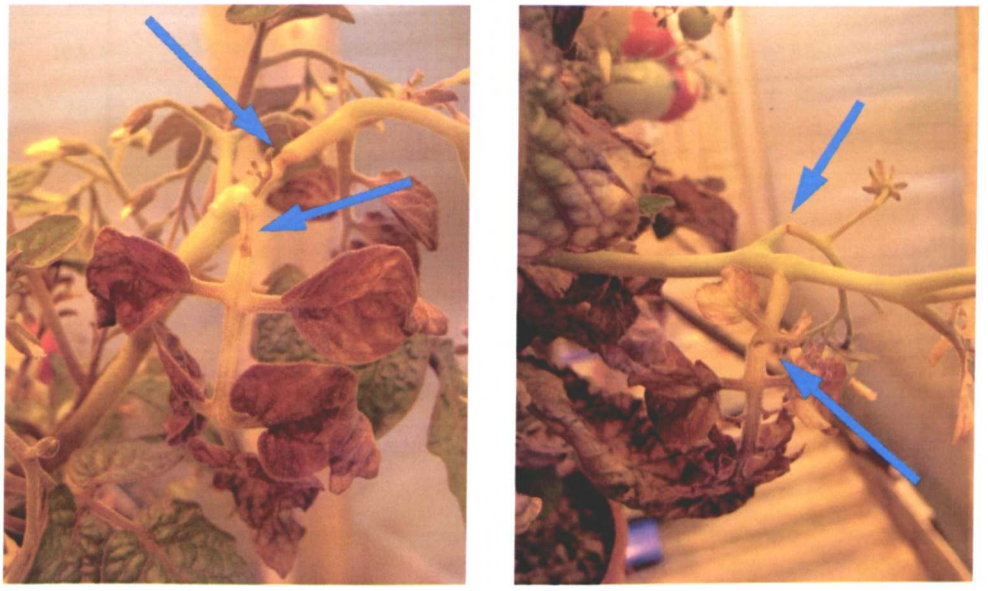

(a) Example A.

(b) Example B.

Figure 5.21: Typical damage on plant exposed to circularly polarised microwaves.

EM fields inside the fruit were found for linear and circularly polarised antenna waves incident on the model shown in Figure 5.4. This fruit model has a 30 mm radius – which is typical of the fruits on the variety of tomato plant used in the greenhouse experiments.

From the EM field distribution a linked thermal solution was performed to find the average fruit temperature in the steady-state. The results of these simulations are shown in Figure 5.22. It can be seen from these results that the average temperature is less dependent on the orientation of the fruit, with respect to the incident field for circular polarisation than linear polarisation. Specifically, a lower range of average temperatures results from using circular polarisation, despite higher mean temperatures. This difference is highlighted by the heating statistics shown in Table 5.9: the standard deviation about the mean is much lower between the two circular cases, as is the percentage difference in the range between both polarisation regimes. Removing the influence of the mean by using the UI reinforces this point. Nevertheless, it is also evident that both polarisation regimes result in good consistency of average fruit temperatures when compared

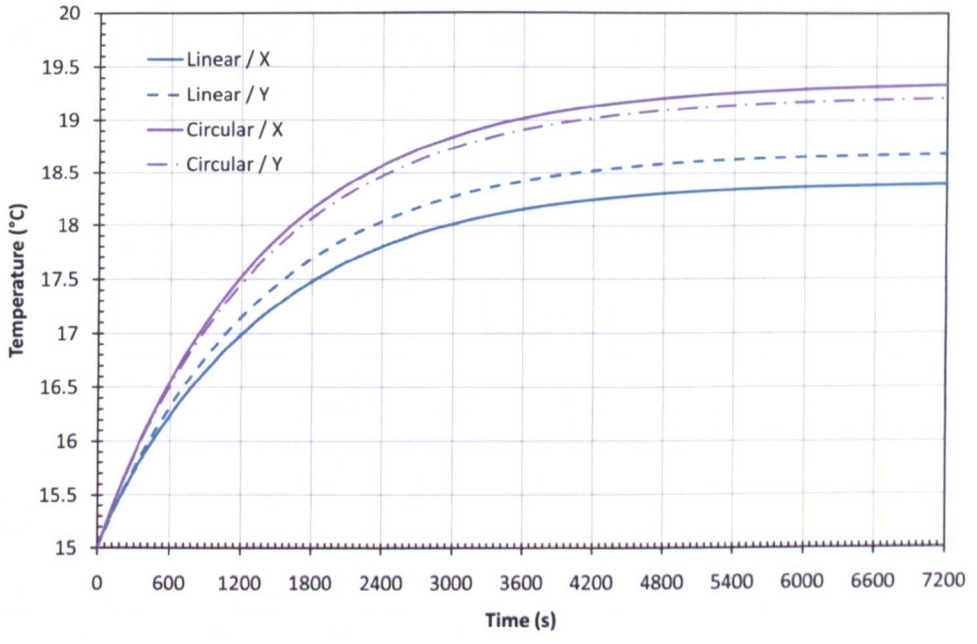

Figure 5.22: Simulated fruit temperature increase for linearly and circularly polarised incident fields.

to that of leaf and stem components. That is, several fruits on a plant are unlikely to experience significantly different average temperatures owing to there orientation in the incident field. The results in Table 5.9 suggest instead that the low mean temperatures observed in fruits could be a significant obstacle to heating the entire plant as increasing the radiated power to obtain a higher mean temperature in the fruits will evidently result in burning in leaves and stems, as demonstrated through simulations described above. A solution to this may be to grow the plant using a particular radiated power until such a stage is reached where fruit is beginning to set. From here on, power could be increased to encourage fruit growth, at the expense of possible leaf damage. A similar technique used in commercial greenhouses and reported by growers is the addition of electrolytes to the plant liquid supply. This has the effect of controlling fruit quality but to the detriment of the plant leaves.

It has already been shown in Section 5.3 that the dimensions of the fruit, relative to the wavelength of the incident wave, can result in certain resonances and spher-

	Linear		Circular	
Geometry direction	X	Y	X	Y
$T_{steady-state}$ ($^{\circ}C$)	18.40	18.69	19.33	19.21
Mean ($^{\circ}C$)	18.54		19.27	
SD	0.204		0.082	
% Difference of T_X and Y_Y	1.56		0.62	
UI	0.011		0.004	

Table 5.9: Uniformity statistics for simulated average fruit temperatures using linearly and circularly polarised incident waves.

ical focusing of the field within the fruit. In order to gain greater insight into how this phenomenon operates with using different polarisations, temperature profiles were plotted along the geometry lines specified in Figure 5.4, at a time when the average fruit temperature was in the steady-state. These temperature profiles are shown in Figure 5.23. For the case of uniformity in the direction of wave propagation, the statistics in Table 5.10 actually show greater, or at least similar, uniformity is obtained for either orientation of the fruit with respect to the field when linear polarisation is used and also have a lower standard deviation of mean temperatures. The mean temperatures and UI for both circular polarisations however, indicate a greater consistency between orientations (*i.e.* they are both very similar in value) as was shown in the analysis of average fruit temperature above. Similar results were observed in regular samples in Section 5.5.1.

The temperature profiles through the width of the fruit reveal the effect the spherical focusing (Figure 5.23b). It is evident from the profiles that uniform focusing towards the centre of the fruit is only obtained when the field is polarised along the direction of the fruit that is uniform (the cross-section is circular in one plane only and irregular in the others). Consequently, an orthogonal linear polarisation results in non-uniform refraction as the distance perpendicular to the tangent at the air/fruit interface is not identical at all points along the interface. The constant rotation of the E-field alignment when using circular polarisation goes some way to eliminate this, as can be seen by the lower range of UI for circular

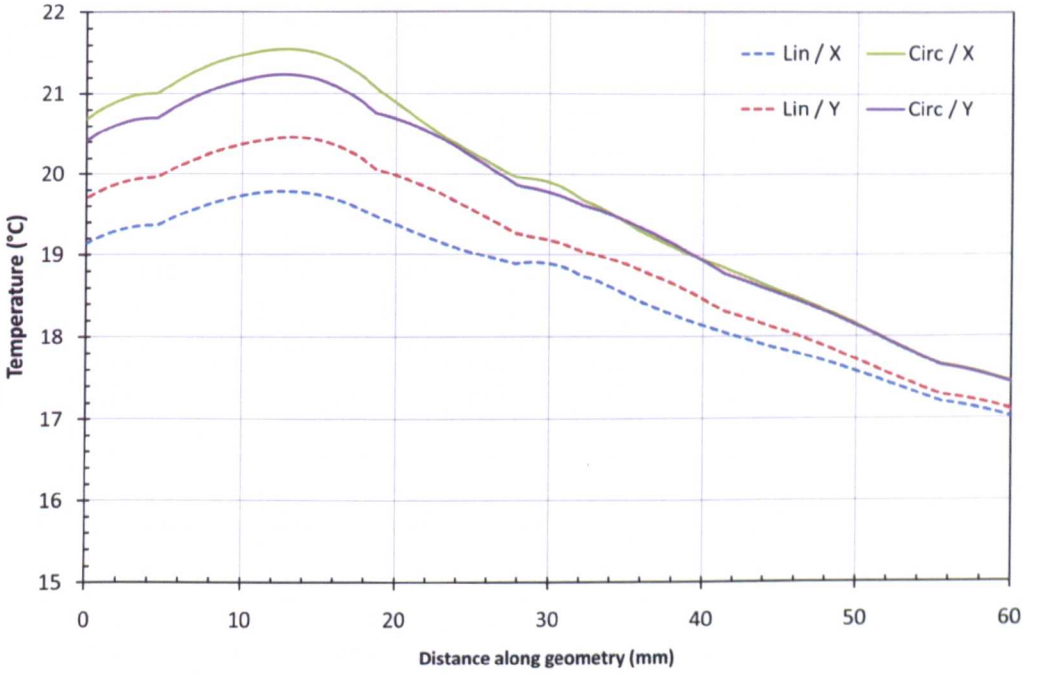

(a) Geometry in direction of wave (path) through fruit.

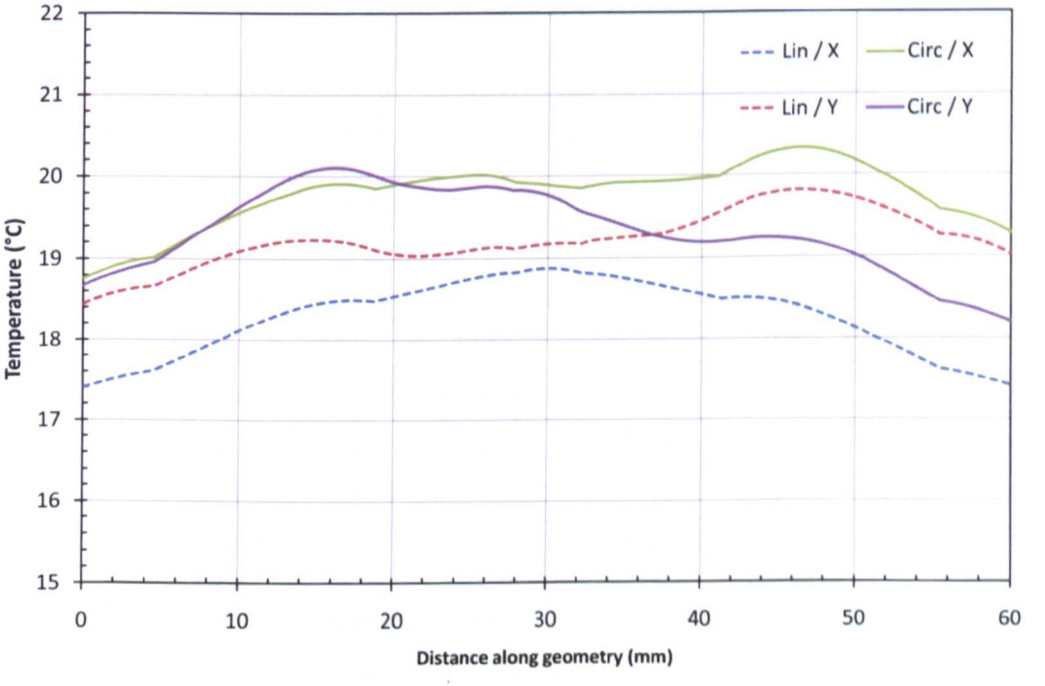

(b) Geometry through width of fruit in plane of wave.

Figure 5.23: Simulated fruit temperature profiles along geometry lines.

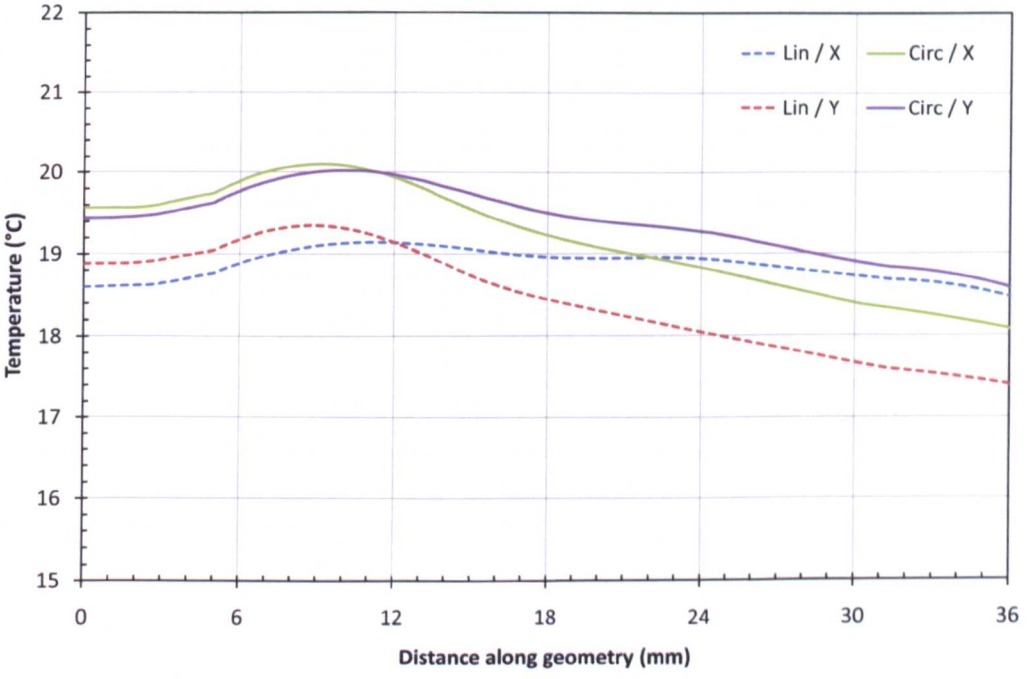

(c) Geometry through height of fruit in plane of wave.

Figure 5.23: Simulated fruit temperature profiles along geometry lines.

	Lin /X	Lin / Y	Circ / X	Circ / Y
Mean	18.6	19.0	19.7	19.6
SD	0.87	1.07	1.34	1.23
Variance	0.76	1.16	1.79	1.50
Range	2.76	3.35	4.11	3.81
UI	0.241	0.267	0.282	0.266

Table 5.10: Uniformity statistics for simulated fruit temperature profiles along path geometry using linearly and circularly polarised incident waves.

	Lin /X	Lin / Y	Circ / X	Circ / Y
Mean	18.9	18.4	19.2	19.4
SD	0.18	0.63	0.64	0.41
Variance	0.03	0.40	0.40	0.17
Range	0.68	1.95	2.03	1.44
UI	0.047	0.183	0.152	0.092

Table 5.11: Uniformity statistics for simulated fruit temperature profiles along height geometry using linearly and circularly polarised incident waves.

	Lin / X	Lin / Y	Circ / X	Circ / Y
Mean	18.3	19.2	19.8	19.3
SD	0.46	0.32	0.37	0.51
Variance	0.21	0.10	0.14	0.26
Range	1.48	1.36	1.58	1.91
UI	0.139	0.075	0.077	0.117

Table 5.12: Uniformity statistics for simulated fruit temperature profiles along width geometry using linearly and circularly polarised incident waves.

polarisation in Table 5.12. The discrepancy between UI for X and Y orientations when using circular polarisation can perhaps be attributed to the imperfection and handedness of the circular polarisation, as mentioned for similar effects in stem simulations (Section 5.5.2.1.

A similar analysis can be applied for the temperature profile along the height geometry line, shown in Figure 5.23c and analysed in Table 5.11.

Although it has been seen that linear polarisation can, at times, offer greatest uniformity within individual fruit, the results presented show that using circular polarisation offers greatest consistency between fruits with similar levels of intra-fruit heating uniformity. The main issue when heating the fruit, aside from that of overall average temperature mentioned above, would appear to be the

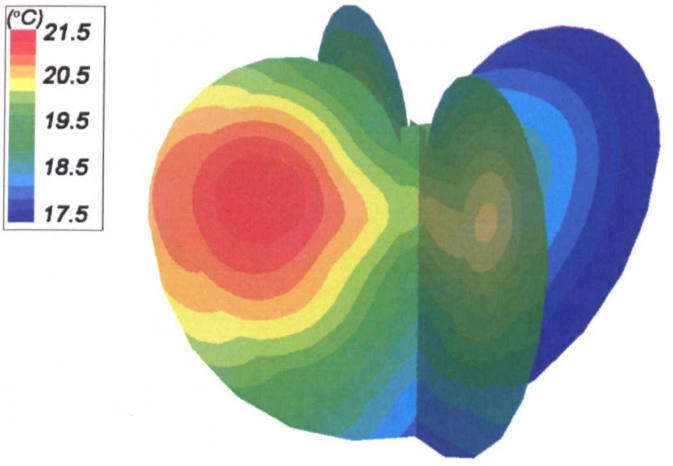

Figure 5.24: Simulated steady-state temperature distribution in fruit model cross-sections, from circularly polarised incident fields.

differential between the 'front' and 'rear' of the fruit, where the 'front' is the side where the radiant field is first incident. This problem is common to both polarisations at the frequency used here (2450 MHz) and it's consequences on fruit formation remain to be observed in greenhouse experiments. Fruit damage from over-heating would at least not appear possible, however. To illustrate this, a graphic visualisation of the simulated temperature distribution in two orthogonal planes of the tomato fruit model is shown in Figure 5.24.

Chapter 6

Main Experiments

6.1 Methodology

The successful experiments in this section apply the findings of the dielectric measurements, pilot tests and computer simulations to the growing of tomato plants from seedlings to fruition. This is the first time such an experiment has been reported and, as such, the emphasis is on the relative plant performance – between microwave-treated and conventionally heated plants – rather than the optimisation of a microwave process. With regards to microwave-treated plants specifically, a particular emphasis is also placed on the relative performance of plants heated with linearly and circularly polarised electric fields (as a means for providing effective heating), in order to validate the findings of Section 5.

By this approach, the mechanisms by which a growing plant can be heated with microwaves will be better understood. These findings can then be used to directly inform the design and application of a microwave heating system for commercially grown greenhouse crops. This will, in turn, allow efficiency improvements to be calculated and implemented in the context of relative plant performance.

6.1.1 Data collection

It was seen in the work by Tietel *et al.* [3] that the temperature of plant components vary between fruit, flowers and leaves *etc.* Furthermore, the work in Section 5 showed that the same plant components can reach different temper-

atures for different orientations in the applied field. It was thus decided that, for the purposes of consistency of measurement, that all temperature measurements were to be taken in two locations in the plant compost. Measurements were performed at the side nearest to the antennas and the opposite side, using a k-type thermocouple probe. Similar measurements, at opposite sides, were taken for HC and CC plants. Ideally, temperature would be monitored using infra-red imaging to reveal spatial variation of temperatures in detail. This technique was not available, however.

In addition to recording plant temperatures, the height of each plant was recorded periodically, as was the number of flowers, green fruit and red fruit. Furthermore, the occurrence of the first buds, flowers and fruits was tracked. Collecting this data allowed for the graphical reconstruction of the plants' performance with time and also temperature. This provides a useful and informative way of quantitatively comparing the relative performance for given control variables *viz.* ambient temperature, microwave power and polarisation of incident fields.

When facilities were available, the humidity of the two growing areas was also recorded.

Qualitative indicators of plant performance and health were recorded photographically. The shape, size and colour of plant components provide useful indicators of the plants' response to their environment, particularly when exposed to severe cold or overheating.

The greenhouse trials described in this section are, to the best knowledge of the author, the first of their kind to attempt to grow and investigate the performance of live tomato plants over their entire life cycle of approximately 14 weeks.

6.1.2 Calculation of power and range

The microwave power required to maintain a temperature differential is dependent on many factors: the thermal and dielectric properties of the plant, the

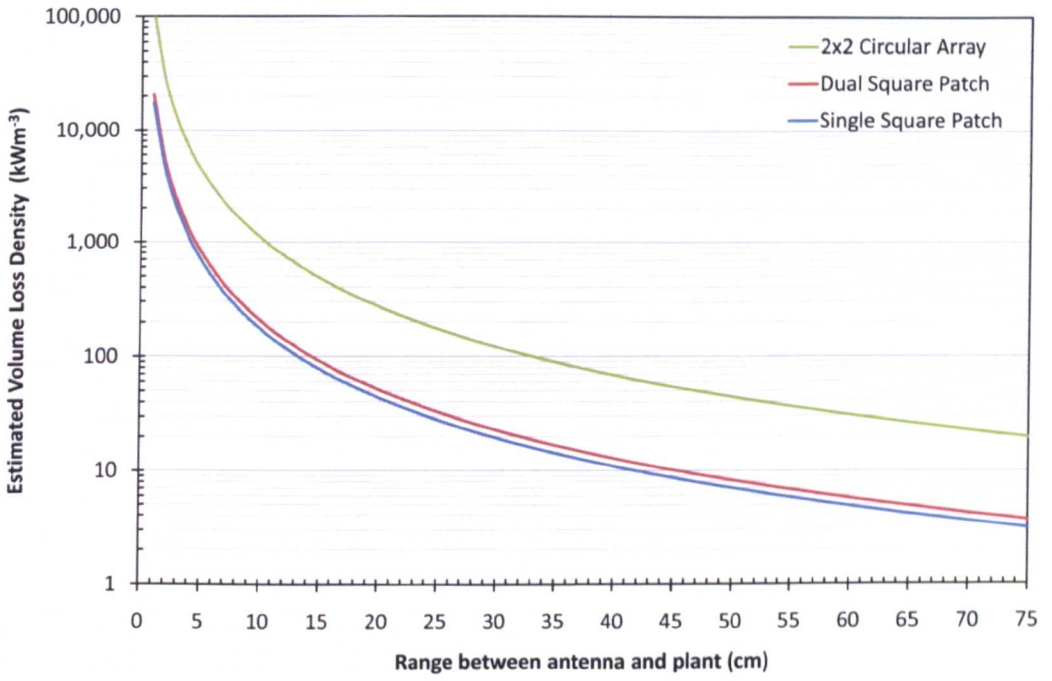

Figure 6.1: Estimated volumetric power loss density in plant at a given range, for different antenna elements.

physical size and shape of the plant, the ambient air temperature and also the fluid properties of the air.

The results of several computer simulations (of which Figure 5.15 in Section 5 is typical) show that a power dissipation of 100-200 kWm^{-3} is required to maintain a minimum of $10°C$ temperature difference in the plants. By then using the antenna characteristics described in Appendix A.2 and the dielectric properties measured in Section 3, the range required (for a fixed gain and radiated power) to achieve the necessary electric field that results in this desired volume loss density was calculated. This is shown graphically in Figure 6.1.

As the estimated VLD in Figure 6.1 is assumed to be uniform within the plant, the range shown in Figure 6.1 can be considered, at best, the minimum safe range for the desired temperature rise. This is because it has been shown that there will also be areas in the plant that will have significantly higher VLD (and similarly

areas significantly lower) for any given range. As such, the range may need to be increased if localised burning occurs. Despite these limitations, this method provides a useful starting point for obtaining adequate heating, without destroying the plant, in the absence of a suitable automated closed-loop feedback system for power regulation.

A temperature increase of $\Delta 10°C$ was chosen as it is approximately the average increase above the UK mean temperature required to grow tomatoes and was judged to be attainable with the available equipment.

6.2 First greenhouse trial

6.2.1 Set-up and procedure

'Minibel' variety tomato seedlings were propagated and similar plants chosen to create the set shown in Figure 6.2. From this set, three groups were selected to form the hot control (HC), cold control (CC) and microwave (MW) groups. As in pilot test B, the MW and CC plant groups were grown in the same greenhouse with a low ambient temperature ($15°C$) and the HC plant group was grown in a separate greenhouse with optimum ambient temperature ($27°C$). Plant numbers correspond to plants from the initial planting group and are not consecutively numbered for each group.

Pilot test results suggested that plants were being under-heated. Increasing available power (*i.e.* moving the antennas closer) resulted in burning, however. As the findings of Section 5 indicated more uniform heating is possible when the incident fields are circularly polarised, an antenna element was designed to facilitate this. The technical design and characteristics of this antenna are described in Appendix A.2. In order to provide more available power form one antenna source, the antenna was designed to accept four inputs from the generating equipment and thus had a maximum radiated power of 72 W. The antenna and clamp stand arrangement for circularly polarised fields is shown in Figure 6.3. Plants were arranged such that one, mounted on a clinostat, was in the direct path of the

Figure 6.2: Experiment I: Plant groups at start of first main experiment.

antenna array for circular polarisation. A further plant, on a static mount, was positioned at the angle of 3 dB power, about the antenna centre. This is referred to hereupon as the offset plant and was to compare the plant performance when heat is provided to only one side of the plant and when heat is provided to all sides (through rotation of the plant). Secondly, being positioned off-axis, as specified, will result in the static plant receiving approximately half of the power of the rotating plant. The purpose of this was to enable comparison of plant performance when heating rates (and therefore temperature) differed.

In addition to the circularly-polarised antenna element, a single linearly vertical polarised (LVP) dual-square patch (DSP) antenna, as used in the pilot tests, was positioned in front of a third plant mounted on a clinostat (Figure 6.4). This antenna had a maximum radiated power of 18 W. The purpose was to compare the heating rates and plant performance to those receiving circularly-polarised microwaves. With this arrangement, it was expected that the effect of average plant temperature and localised plant temperature could be distinguished and the effects of polarisation and power compared to the plants receiving circularly polarised fields.

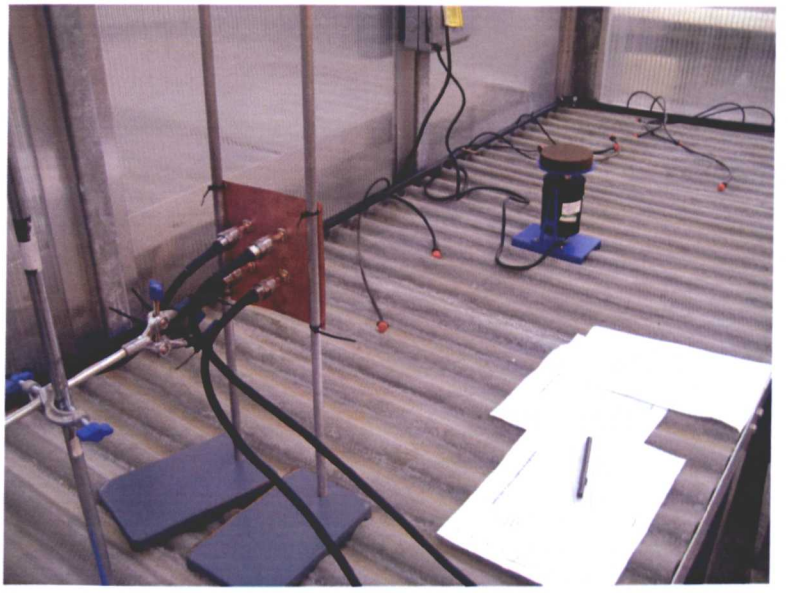

Figure 6.3: Experiment I: Four-element circular patch antenna with notches configuration, for two plants positioned on a static mount and a clinostat.

6.2.2 Experiment progress

At the start of the experiment, all plants were 13 cm high, measured from the surface of the soil, vertically to the level of the highest point of the plant.

A link-budget analysis of equipment power is given in Appendix A. To maintain the required field where the plants were positioned, the antenna distances were initially set at 35 cm for plant 13 (with the DSP antenna) and 55 cm for the circular array plants 6 and 7. This results in an estimated average field strength of approximately 200-300 Vm^{-1}, which corresponds to a VLD of 15-35 kWm^{-3} and was deliberately cautious to avoid damaging the plants early in the trial.

After one week, the growth of plant 7 obstructed the rotation of plant 6 and the leaf edges appeared burnt. Plant 7 was rotated by 180° to remove this obstruction. More generally, parts of leaves of plant 6 appeared to be be drying when inspected closely and slight damage was visible on a leaf on plant 7. Antennas were moved to 65 cm for plant 6 and to 50 cm for plant 7. The antenna for plant 13 was moved 5 cm closer, to 30 cm. This was a precautionary measure as soil

temperatures did not indicate over-heating.

After four weeks, significant cold damage was visible on plants 3, 4 and 12 of the cold control group. This is shown in Figure 6.5a. The CC plants were however, also producing flowers.

The MW plants were also showing signs of under-heating with the leaves becoming curled and dark and, although the condition was superior to the CC plants, the MW plants were visibly inferior to the HC plants – a typical example of which is shown in Figure 6.5b. The performance and quality of the MW plants can be seen in Figures 6.6 to 6.8.

At this point, fruit had begun to set on trusses on the HC plants. Leaves were generally larger and paler than on the CC and MW plants, but with lower plant leaves suffering from significant discolouration and drying. This is a natural consequence of the plant development as it produces fruit and indicates that not all discolouration and drying of the microwave plants is a consequence of microwave treatment.

At this stage, the height position of the circular array antenna was raised 15 cm to match the growth of plant; ensuring the beam centre remained approximately directed at the plant centre.

After approximately two months of microwave exposure, yellow and purple marks were clearly visible on the leaves of plants 6 and 7, with some on plant 13 (Figures 6.9b, 6.10b and 6.11b). These would appear to be the development of the cold damage detected in the previous weeks and an indication of insufficient power being absorbed by the plants. Similar mottled purple patterns were present on the CC plants – 3, 4 and 12 – although with slightly less yellowing. This suggests that the yellowing is not a consequence of burning, but a chemical response by the plant at the boundary between areas of cold damage and areas of adequate heating. That the microwave plants have more areas of adequate heating, as revealed through simulations, would then explain why this effect is more prevalent on the MW plants. The general condition of the plants is shown in Figures 6.9a,

6.10a and 6.11a.

The leaves on plant 13 (Figure 6.9b) were very dark and showed severe curling as a result of exposure to cold air. However, there were still areas of plant 13 that showed burn damage from the microwaves, despite the apparent general under-heating of the plant and the lower radiated power from the DSP antenna. In fact, plant 13 was observed to have approximately four times the number of brown patches on leaves that were attributed to areas of over-heating, than plant 6 and 7. This corroborates the results of the simulations in the previous section, which indicated that little average heating would occur when using a linearly polarised antenna beam, but that localised burning and damage would still occur. Plant bud and fruit development was continuing, however.

Plant 6 was moved laterally into the path of the main antenna by 10 cm. No obstruction to plant 7 was caused. The range of all antennas was also reduced by 5 cm because of evidence of insufficient heating and an apparent lack of damage. As fruit was starting to set and the plants matured, ensuring the high quality of the leaves was not as critical and higher absorbed power (and temperature) would encourage fruit development.

6.2.3 Plant condition at end of experiment I

Figure 6.13 shows MW plant 6 at the end of the experiment. It can be seen that the plant has grown into a larger volume than the CC plants in Figure 6.22. Many leaves however, such as those shown in Figure 6.14, are of only marginally better quality (in terms of size, shape and texture) than the leaves on CC plants (Figure 6.25), although MW leaves are not as severely cold-shocked. It would appear that the microwaves coupled readily to the stems, as suggested by simulations, allowing healthy growth where burning does not occur. As expected, it appears that leaves do not absorb as much microwave power, nor retain thermal energy as readily, hence their apparent lower growth performance relative to stems.

The visual quality of plant 7 can be seen in Figure 6.19 to be similar to plant 6,

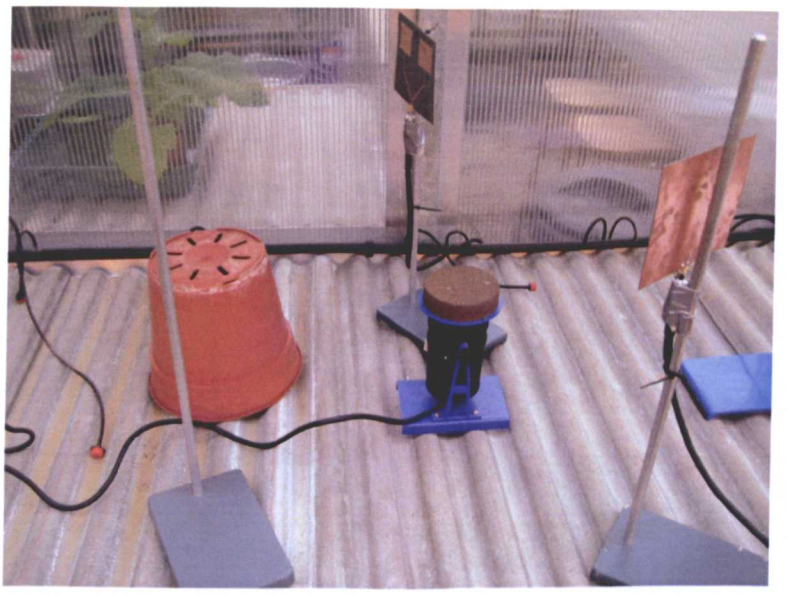

Figure 6.4: Experiment I: Dual-square patch antenna configuration for a plant positioned on a clinostat.

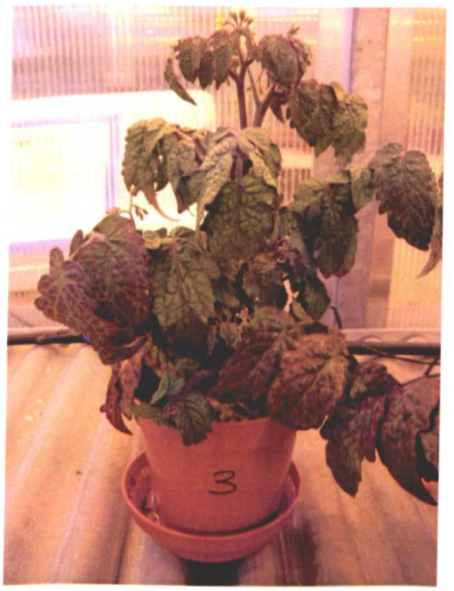

(a) Leaf discolouration typical of cold control plants.

(b) Strong growth typical of hot control plants (some leaf discolouration).

Figure 6.5: Experiment I: Hot and Cold control group plants after 1 month.

(a) Growth performance. (b) Leaf damage and discolouration.

Figure 6.6: Experiment I: Plant 6 (MW/CP) after 1 month exposure.

(a) Growth performance. (b) Leaf damage and discolouration.

Figure 6.7: Experiment I: Plant 7 (MW/CP/offset) group after 1 month exposure.

(a) Growth performance. (b) Leaf damage and discolouration.

Figure 6.8: Experiment I: Plant 13 (MW/LVP) after one month exposure.

(a) Growth performance. (b) Leaf damage and discolouration.

Figure 6.9: Experiment I: Plant 6 (MW/CP) after two months exposure.

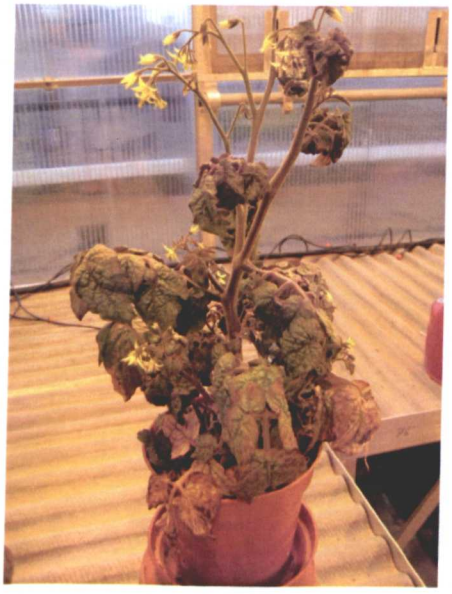

(a) Growth performance.

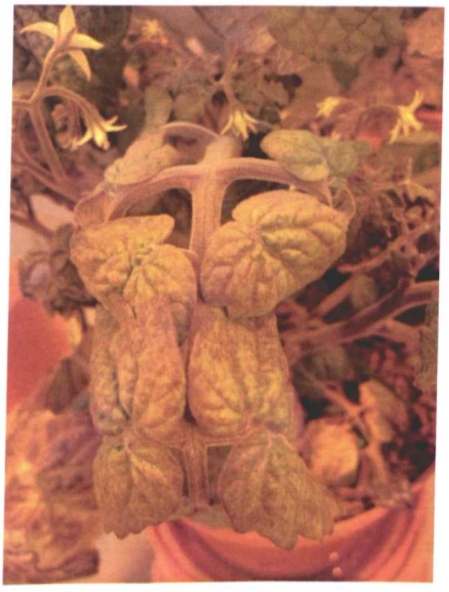

(b) Leaf damage and discolouration.

Figure 6.10: Experiment I: Plant 7 (MW/CP/offset) after two months exposure.

(a) Growth performance.

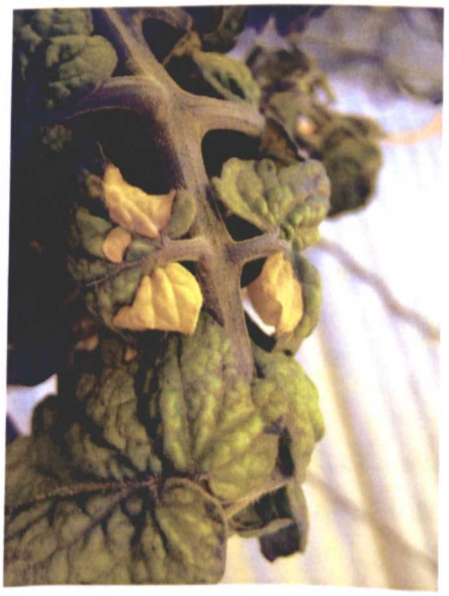

(b) Leaf damage and discolouration.

Figure 6.11: Experiment I: Plant 13 (MW/LVP) after two months exposure.

(a) Growth performance. (b) Leaf quality.

Figure 6.12: Experiment I: Typical plant from hot control group after two months.

despite receiving a lower incident power flux density owing to its off-axis position. Nonetheless, growth was also vigorous compared to CC group plants (Figure 6.22) and fruit had set on several trusses, as shown in Figure 6.17. The consistency of fruit setting was poor, however, with some trusses having two or three ripe fruits amongst undeveloped flowers and other trusses having several smaller, unripe, fruit. The leaf and flower quality shown in Figure 6.18 was similar to plant 6 and superior to all CC group plants – where flowers had begun to dry and leaves were small and dark purple in colour. Fruit set on CC group plants was also minimal (Figure 6.24a) and sporadic. Where fruit did set, the size was typically very small (< 1 cm diameter), as shown in Figure 6.24b.

Figure 6.19 shows plant 13 at the experiment end. Despite receiving an even lower incident power flux density that either plant 6 or 7, the plant still grew into a similar volume to the other MW plants. This could be owing to the vertical alignment of stems with the polarisation of the incident field and provides an explanation for tall, healthy stem growth, despite poor leaf performance. Indeed, many leaves showed signs of cold shock, as on plants 6 and 7, but also had many instances

(a) Front. (b) Reverse Angle.

Figure 6.13: Experiment I: Plant 6 (MW/CP) at end of experiment.

of leaf burn; a typical example of which is shown in Figure 6.21b. Flower condition, as shown in Figure 6.21a appeared to be identical to those on plants 6 and 7.

(a) Full truss of unripe fruit.

(b) Ripe fruit.

Figure 6.14: Experiment I: Fruit on plant 6 (MW/CP) at end of experiment.

(a) Flower quality.

(b) Leaf quality example.

Figure 6.15: Experiment I: Leaf and flower on plant 6 (MW/CP) at end of experiment.

(a) Front.

(b) Reverse Angle.

Figure 6.16: Experiment I: Plant 7 (MW/CP/offset) at end of experiment.

(a) Ripe fruit.

(b) Unripe fruit.

Figure 6.17: Experiment I: Fruit on plant 7 (MW/CP/offset) at end of experiment.

(a) Flower quality.

(b) Leaf quality example.

Figure 6.18: Experiment I: Leaf and flower on plant 7 (MW/CP/offset) at end of experiment.

(a) Front.

(b) Reverse Angle.

Figure 6.19: Experiment I: Plant 13 (MW/LVP) at end of experiment.

(a) Full truss of unripe fruit.

(b) Full truss of unripe fruit.

Figure 6.20: Experiment I: Fruit on plant 13 (MW/LVP) at end of experiment.

(a) Flower quality. (b) Leaf quality example.

Figure 6.21: Experiment I: Leaf and flower on plant 13 (MW/LVP) at end of experiment.

Figure 6.22: Experiment I: Cold control group at end of experiment.

Figure 6.23: Experiment I: Hot control group at end of experiment.

(a) Flowers on plant 3.

(b) Flower and fruit on plant 4.

Figure 6.24: Experiment I: Flowers on cold control group plants at end of experiment.

As was expected and suggested by simulation results, stem burning occurred on all plants, regardless of the field polarisation used. Incidences of stem burning were, however, more frequent on plant 13 – that had been exposed to linearly polarised microwaves – than on plants 6 and 7, that had been exposed to circularly polarised microwaves. Furthermore, the severity of burning was often more severe on plant 13, with many stems failing completely or having their growth checked shortly after development. Figures 6.27 and 6.28 show examples of damage after stem burning that match closely to the scale and locations predicted through simulations. Interestingly, not all damage results in stem failure, as is seen by subsequent fruit development on the stem in Figure 6.27a. This suggests that, although stem damage appears to occur rapidly (in 1-2 days), if the branch or stem is growing quickly it can often withstand the damage. This is due to the increasing length of a growing stem altering the geometry-dependent field patterns in the stem, as shown in Section 5. This results in the position of the hot-spot moving slowly along the stem as it grows, reducing the concentration of power and therefore minimising damage. This effect is most evident in Figures 6.27a and 6.28b, where the area of damage is large and the plant stem has recovered.

(a) Leaf on plant 3.

(b) Leaf on plant 4.

(c) Leaf on plant 12.

Figure 6.25: Experiment I: Leaves on cold control group plants at end of experiment.

(a) Cold control. (b) Microwave-treated. (c) Hot control.

Figure 6.26: Experiment I: Comparison of leaves from three plant groups.

(a) (b)

Figure 6.27: Experiment I: Examples of stem burning, using linear polarisation, at end of experiment.

(a)

(b)

(c)

Figure 6.28: Experiment I: Examples of stem burning, using circular polarisation, at end of experiment.

Plant leaves from each group are shown for relative comparison (of appearance) in Figure 6.26. Leaves from CC group plants appear generally smaller than MW plant leaves, which in turn appear smaller than HC plant leaves. The small sample sizes makes this observation difficult to validate statistically though.

The most striking difference between leaves from each group is the colour and texture. Those shown in Figure 6.33a are purple and brown through prolonged exposure to cold air. The MW group leaves (Figure 6.33b) are generally healthier looking with localised areas of possible cold-shock together with areas of possible over-heating, as anticipated from computer simulations.

Leaves from HC plants (Figure 6.26c) are a much paler green colour and smoother in texture. This is due to the more uniformly warmer growing environment and higher absolute temperature. The paleness is also attributable in part to the later stage of development of HC plants, where most plant resources would be utilised in fruit development (with a detrimental effect on the leaves). It is of note that many HC plant leaves were also brown, crisp or otherwise discoloured and curled, although most usually on older leaves on lower branches. This is clearly a result of a natural process but also indicative that not all leaf abnormalities are a consequence of microwave treatment or low ambient temperature.

6.2.4 Analysis

Experiment I showed that the leaf, bud and flower quality of tomato plants heated with microwaves was superior to that of cold control plants, but also underperformed when compared to conventionally heated plants (grown at the optimum temperature). Figure 6.29 shows the progress of plant height over the duration of the experiment. It can be seen that progress between groups is initially similar. At the experiment end, the average height of the MW plant group is much greater than the CC plants, which grew poorly, but still slightly outperformed by the HC plants. These results show that, by heating the plants with microwaves, the main plant stem and branch structure can be formed to a very similar standard as that achieved by conventional heating.

When key indicators of plant progress are plotted however, as in Figure 6.30, the subsequent performance of the microwave (and CC) plants is revealed to be delayed, when compared to the progress of HC plants. That is, the development of flower and fruit *etc.* occurs later for MW plants than on HC plants. The delay also increases for each subsequent event owing to the cumulative effect of each delay. Despite this, the MW plants again significantly outperform the CC plants. The reasons for the delay in the key events shown in Figure 6.30 can be attributed to the temperatures of the plant components. This is because, although it has been shown above that the plant stem structure can form readily under microwave heating, poor leaf development occurs owing to the lower average temperature in the leaves, compared to the stems. Failure for the leaves to develop fully therefore slows plant progress and results in a lack of plant resources for subsequent fruition.

The lower heating of the leaves is not a symptom of the inability for microwave heating to heat the leaves, *per se* however, but rather due to the limitation on increasing the available microwave power imposed by the ease at which the stems burn.

During experiment I, the incident power density on the MW plants was only one-fifth of the estimated requirements. The resultant heating was therefore significantly lower than anticipated. The effects of this temperature on plant performance are shown in Figure 6.31. The height is revealed to be clearly and linearly dependent on the temperature of the plant, as was shown above. A greater dependence on temperature is revealed by fruit formation however. This is further evidence that the low leaf temperatures lead directly to reduced fruit formation.

In experiment I, the use of a clinostat appeared to not have any appreciable effect on plant performance, with any relative superiority being entirely attributable to a higher power and temperature.

Although linear polarisation resulted in more plant damage, the effect on fruit formation appeared negligible. This is most likely due to the regular shape and

(relatively) large size of the fruit.

Experiment I was deliberately cautious in its execution, which resulted in significant under-heating. Regardless, fruit-bearing plants were successfully grown and an understanding of the heating mechanisms and limitations gained.

6.2.4.1 Note on polarisation quality

An important consideration when analysing the results of experiment I is the quality of the circular polarisation achieved. Owing to a workshop error, the phase rotation achieved was, in fact, not perfect. The result of this imperfection was to make the vertical component of the electric-field effectively 50% greater in magnitude than the horizontal, making the resultant polarisation elliptical and aligned in the vertical direction.

Experiment I was continued using this imperfect antenna, with a new antenna to be constructed for experiment II. This was to gain further insight into the effects of polarisation on plant performance and to allow an initial assessment of the plant sensitivity to polarisation to be made.

Further implications of this are discussed, in context of the results, in the analysis of experiment II.

6.3 Second greenhouse trial

6.3.1 Set-up and procedure

As per the first experiment, 'Minibel' variety tomato seedlings were propagated at 27°C for three weeks before being potted on to 6 inch diameter plant pots and transferred to a holding greenhouse, where the ambient temperature was 20°C. Slow release fertiliser and water-retention gel was added in equal measure to the compost of each plant, in order to ensure sufficient nutrition as the plants grow.

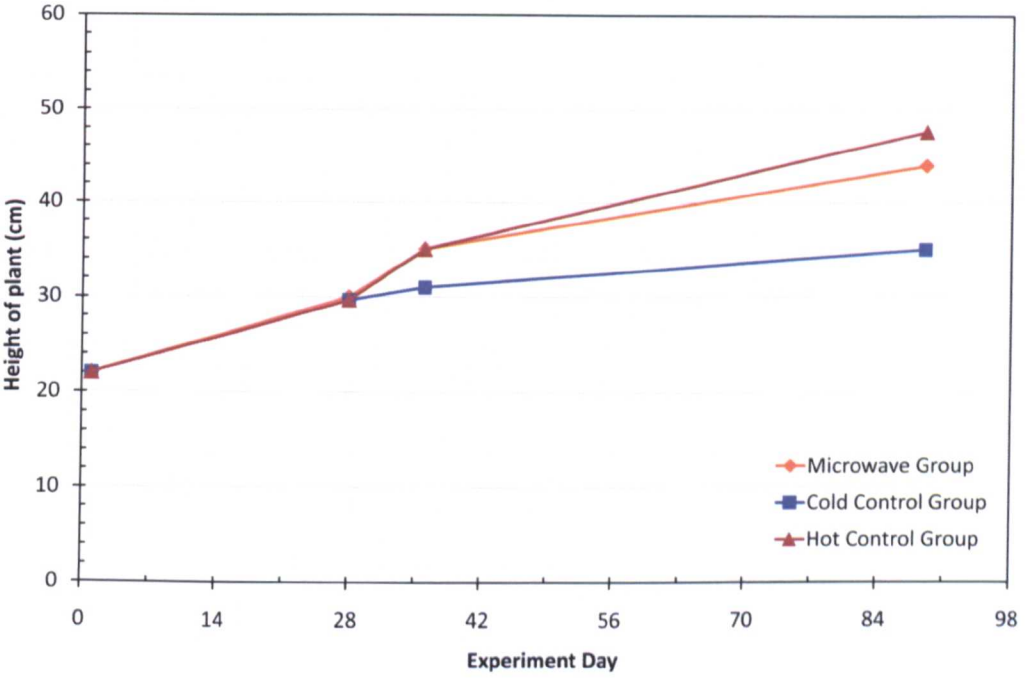

Figure 6.29: Experiment I: Plant height as function of time.

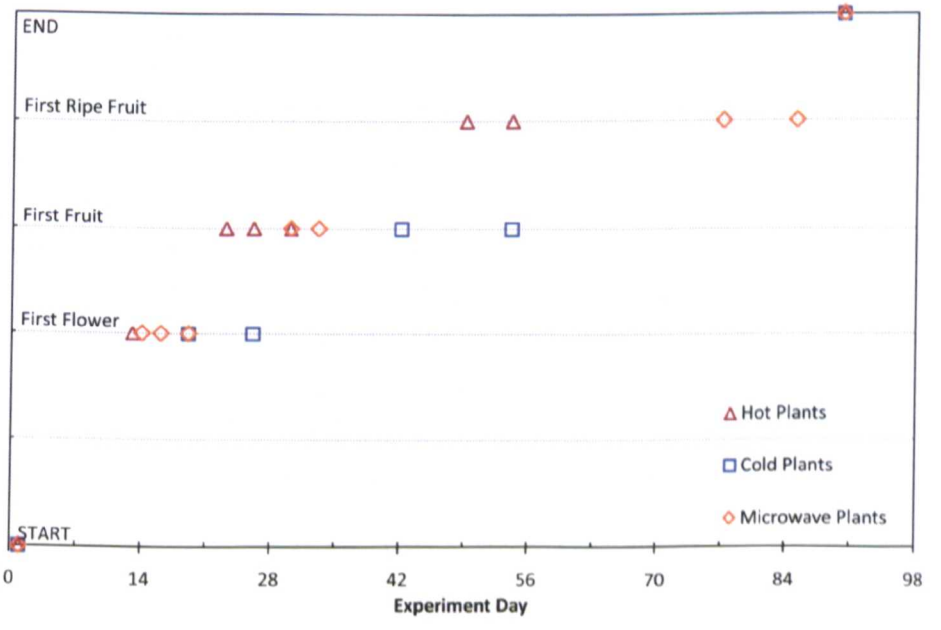

Figure 6.30: Experiment I: Plant performance as function of time.

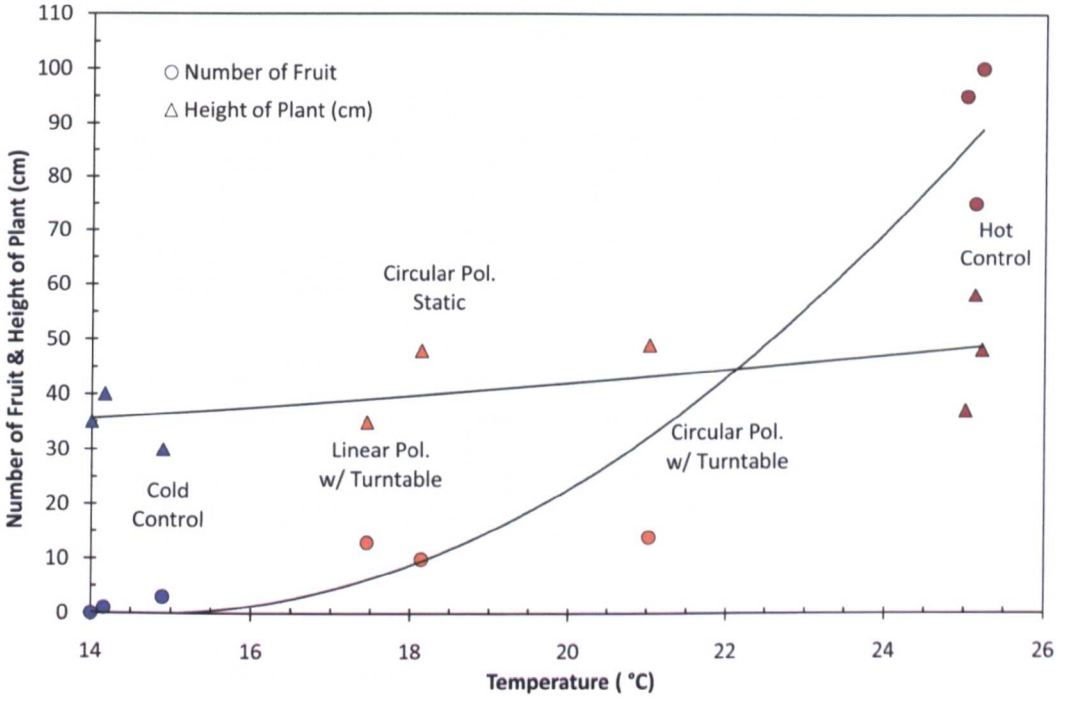

Figure 6.31: Experiment I: Plant performance as function of temperature.

This was to avoid mistaking nutrient deficiencies for microwaves effects.

After a further two days, the plants were divided into subgroups: plants 1, 7 and 12 constituting the MW group; plants 2, 4 and 6 constituting the HC group; and plants 5, 8 and 12 as the CC group. These are shown at the experiment start in Figure 6.34 The HC group was transferred to the hot greenhouses, where the temperature was set at 27°C and the MW and CC groups transferred to a cold greenhouse, where the ambient air temperature was set at 15°C. The purpose of the intermediate greenhouse was to reduce the possible shock of a sudden change of temperature resulting in damage or effects to the plant that could be mistaken for microwave effects. The ambient day and night temperatures for both greenhouses are shown for the experiment duration in Figure 6.33.

6.3.2 Experiment progress

At the start of the trial, the generating equipment and radiated power was as for the first trial and antennas and plants arranged as in experiment I and shown in Figure 6.32. The range between plant and antenna was 30 cm for plant 1, which was positioned on a clinostat in front a the circularly polarised array; 42 cm for plant 7, that was statically positioned and offset from the circularly polarised array; and 28 cm for plant 12, which was positioned on a clinostat in front a the horizontally/linearly polarised antenna. This was closer than the first trial in order to improve overall heating, although still a cautious starting range – with VLD ranging from 25-55kWm^{-3}. The linearly polarised antenna element (plant 12) was rotated 90° about the axis of propagation so that the linear polarisation was in the horizontal direction (LHP), rather than the vertical direction used in experiment I.

The purpose of the second trial was to verify the findings of the first trial and to improve upon the plant performance results by increasing the incident power flux density. In addition, the second trial was to further highlight previously unknown effects that occur when heating plants with microwaves, so that a better understanding of the heating mechanisms within the plant could be achieved.

After two weeks the range of the antenna to plant 1 was increased to 35 cm after damage was observed on a leaf stem that had begun to burn. Very slight damage to the edge of a leaf was observed on plant 7, but the antenna range was maintained. Plant 12 was starting to shown signs of cold damage – with leaves beginning to curl – and buds were beginning to form.

After one month, with the plants still young, relative humidity was 31% in the cold greenhouse and 29.3% in the hot greenhouse. Although the readings were similar, it can be inferred that the air in the hot greenhouse was more moist than in the cold, owing to the greater saturation point of warmer air, *i.e.* the warm air can consist of a greater proportion of water vapour than cold air. This suggests a greater rate of transpiration by the HC plants, which in turn is indicative of their more vigorous growth. Towards the experiment end, the relative humidity

Figure 6.32: Antenna and plant configuration for experiment I and II.

of the HC greenhouse had increased to 56%.

After a month and a half, the flowers on the CC plant appeared to be drying up, with only a few beginning to develop into very small tomatoes, the largest of which were 6 mm in diameter. The fruit on the microwave plant measured approximately 30 mm in diameter for the largest fruits, with similar sizes and larger quantities on the HC plants. The flowers on the MW plants were in good condition and many had begun to set fruit. On HC plants, fruit had already developed, mostly fully-ripened and begun to fall. The leaf condition of the HC plants had started to deteriorate as the plants reached the end of their life-cycle.

6.3.3 Plant condition at end of experiment II

Growth of MW plant 1 – which was positioned on a clinostat in the direct path of the radiated power and exposed to circularly polarised fields – can be seen in Figure 6.35 to have been strong. The plant occupied a large volume and leaf coverage was dense. The quality of the leaves can be seen in Figure 6.36 to be much improved over the first trial, with little discolouration from cold-shock. This is

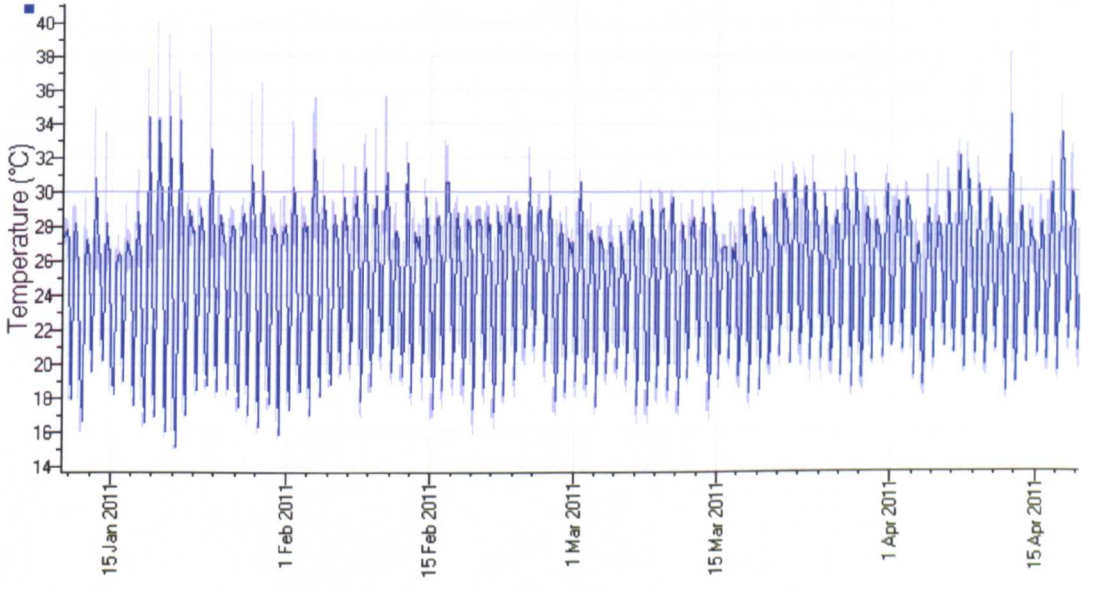

(a) Hot greenhouse.

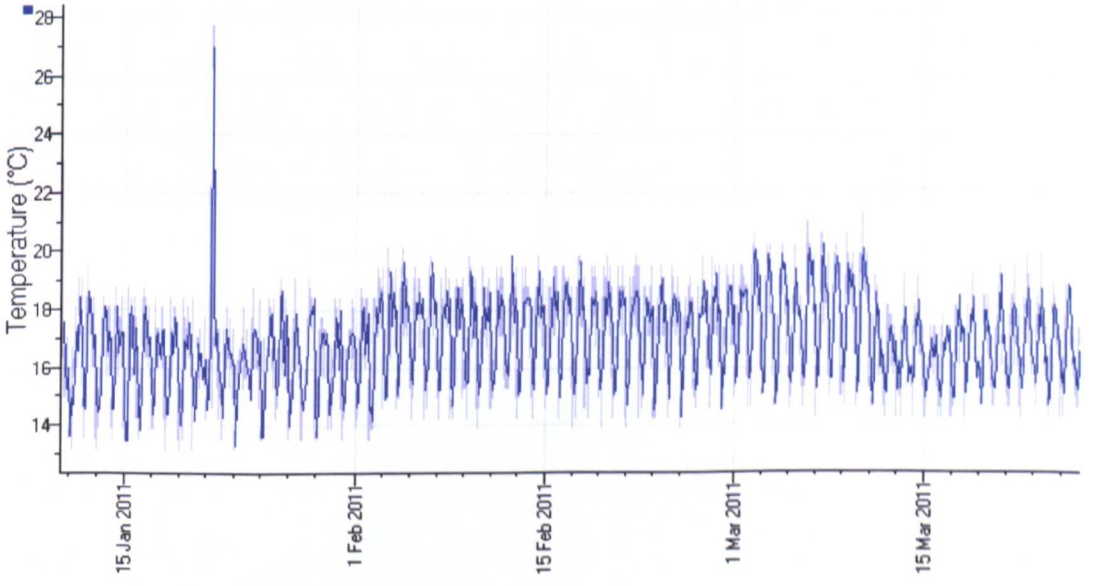

(b) Cold greenhouse.

Figure 6.33: Greenhouse temperatures during experiment II.

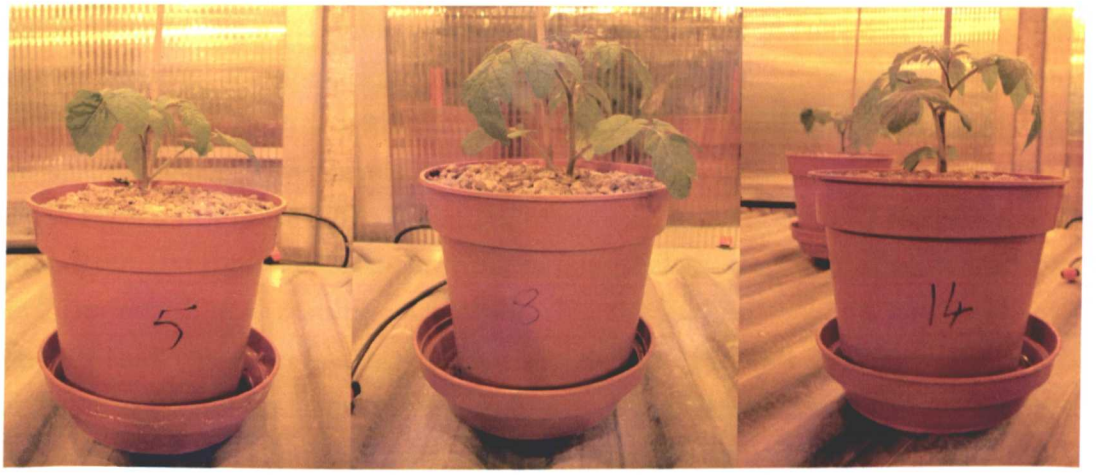

(a) Cold control group .

(b) Hot control group.

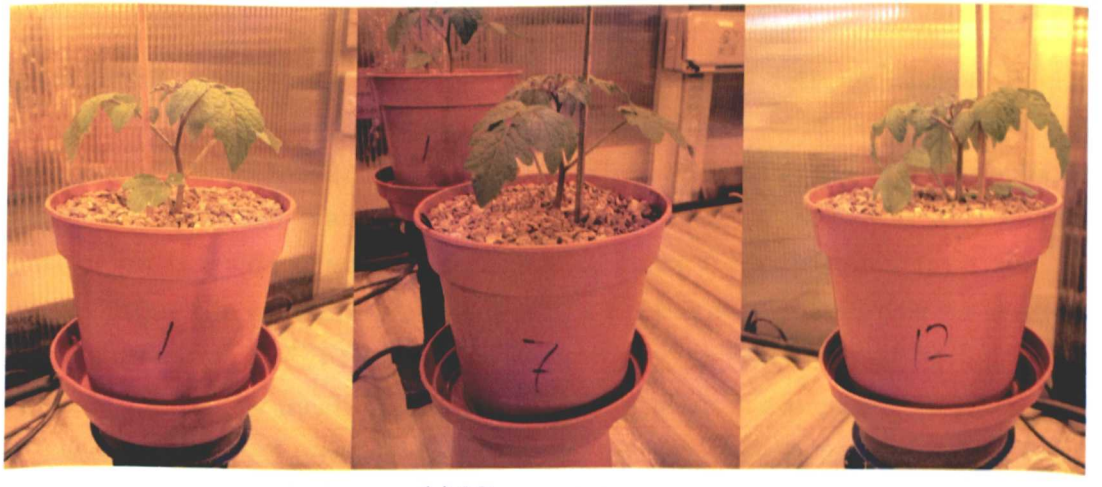

(c) Microwave group.

Figure 6.34: Experiment II: Plant groups at experiment start.

due to the increased incident power flux density compared to the first trial. There is still, however, significant curling of the leaves as in the first experiment, which suggests heating is still inadequate for growth comparable to HC plants (Figure 6.52). At the power levels used though, stem damage was beginning to occur and is shown in Figure 6.37. Although many stems in Figure 6.37 recovered somewhat from the damage, stem burning is nonetheless detrimental to overall plant performance. These results – achieved using the highest incident power density – confirm that the stem heating mechanism defines the limit in microwave heating for tomato plants and, although apparently adequate for strong growth, is such that simultaneous adequate heating of the leaves is difficult and improbable with the set-up described here.

Fruit-set on plant 1 was very good. Figure 6.38a shows a full truss of fruit developed after approximately 70 days. The same fruit, once ripened, can be seen in Figure 6.38. The fruit is large and uniform in shape, with no apparent external or internal damage or defects. Other parts of the plant had fruit set, as shown in Figure 6.39, although this was smaller, more sporadic in location and unripe. Although not full trusses, a clear improvement is seen compared to MW plants in experiment I. That more power was available during the second experiment and that fuller trusses were lower on the plant (and thus nearer to the antenna and higher power density) suggests a pure temperature dependence on fruit development, although again, the effect of microwaves or field polarisation cannot be ascertained or discounted statistically with such a small sample size.

Plant 7 grew to a similar standard as plant 1 and can seen in Figure 6.40. Although, because of its position, plant 7 was exposed to lower incident power density, it grew to occupy approximately the same volume as plant 1. In addition, and although plant 7 was mounted statically, growth was only slightly stronger on the side nearest the antenna (Figure 6.40a) compared to the side furthest from the antenna (Figure 6.40b). This is most likely due to the relatively 'thin' nature of the plant and shows that the issue of heating uniformity is mainly limited by localised heating effects in plant components, provided that the average delivered power is generally enough for healthy growth. That is, the variation of temperature in the direction of propagation is significantly lower than

(a) Front Angle.

(b) Reverse angle.

Figure 6.35: Experiment II: Plant 1 (MW/CP) at experiment end.

(a) Front Angle.

(b) Reverse angle.

Figure 6.36: Experiment II: Plant 1 (MW/CP) leaf quality at experiment end.

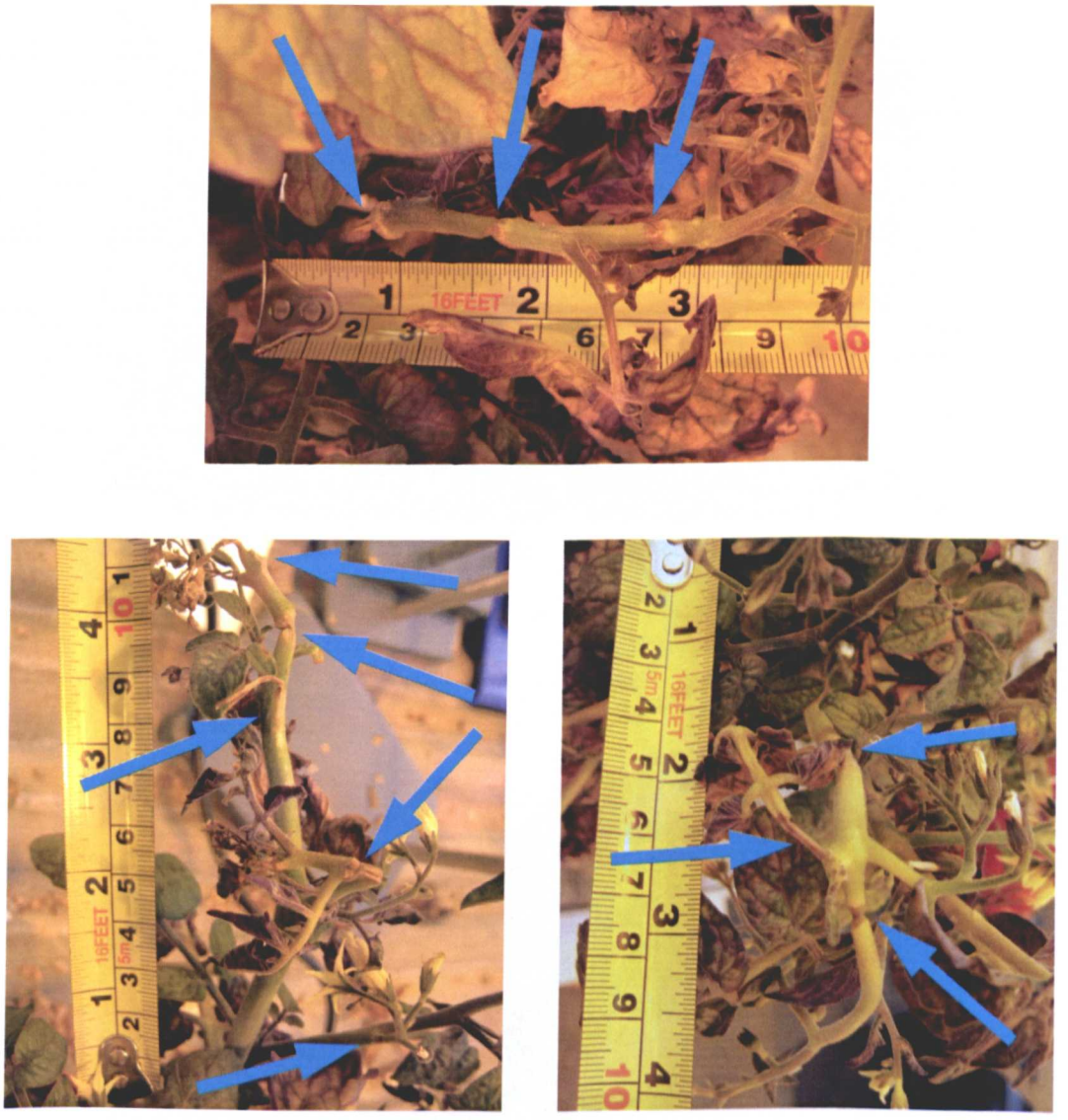

Figure 6.37: Experiment II: Examples of stem burning on plant 1 (MW/CP) at experiment end.

(a) Full truss of unripe fruit, after 70 days.

(b) Fruit at experiment end, after ripening.

Figure 6.38: Experiment II: Full truss of fruit on plant 1 (MW/CP).

Figure 6.39: Experiment II: Unripe fruit on plant 1 (MW/CP) at experiment end.

the variations along certain geometries (and also reduce at a constant rate) and are thus less significant with respect to heating uniformity.

Leaf quality on plant 7 was slightly poorer than on plant 1, with many discoloured or small and curled leaves as shown in Figure 6.41.

As would be expected, the fruit on plant 7, shown in Figure 6.42 were smaller and fewer in number than on plant 1. Trusses were mostly filled with fruit however, which would suggest that circular polarisation does not adversely affect the distribution of fruit on the plant and trusses and any such effects on plant 1 are due to natural variation.

Plant 12 was positioned on a clinostat and was subjected to linearly polarised microwave fields of approximately the same power as plant 7. Growth was vigorous on all sides of the plant and is shown at the end of the experiment in Figure 6.43. The axis of polarisation was however, rotated by 90° for the second experiment so that fields were horizontally aligned. The stem simulations in Section 5 indicated that a stem aligned perpendicular to the axis of polarisation would receive

(a) Front angle.

(b) Reverse angle.

Figure 6.40: Experiment II: Plant 7 (MW/CP/offset) at experiment end.

(a) Typical leaf showing some cold damage.

(b) Small and curled leaves from cold shock.

Figure 6.41: Experiment II: Leaves on plant 7 (MW/CP/offset) at experiment end.

(a) Full truss of unripe fruit.

(b) Several trusses amongst plant.

Figure 6.42: Experiment II: Fruit on plant 7 (MW/CP/offset) at experiment end.

negligible heating, whilst those perpendicular to field polarisation would receive significant heating with potentially damaging hot-spots. It is seen in CC plants, both in the first experiment and the second, that under-heating stunts growth and results in reduced plant height. It is therefore apparent in plant 12 that little heating of the central stem occurred and as such, its height is significantly shorter than either of the other microwave plants (see Figure 6.47 for comparison) and is actually similar to the CC plants in Figurte 6.48. Furthermore, the height is also significantly shorter than the equivalent plant that received vertically polarised fields in experiment I. Interestingly, side-stems and branches on plant 12 performed well and it can be seen in Figure 6.47 that the horizontal growth of the plant was greater than either of the other MW plants.

Fruit formation on plant 12 was very good, perhaps owing to the nature of the alignment of the fruit trusses, *i.e.* they are generally horizontally aligned, and thus with the electric field polarisation. Trusses were generally fully populated although there was a significant range in fruit sizes. Both of these points are illustrated by Figure 6.45. No fruit was damaged, although no fruit had fully developed and ripened either. Both could be attributed to the lower incident power density however, fruit did ripen on plant 7, which received a similar power but circularly polarised fields. As the sample size is small, it is difficult to ascertain whether the circularly polarised fields that result in marginally greater fruit penetration encourages faster ripening, or whether this is due to purely natural variation or indeed, purely lower absolute power. Many flowers had failed to begin to develop fruit at all, as shown in Figure 6.45a, although they were healthy in appearance. Leaves in the vicinity of flowers/undeveloped fruit were also small and slightly curled, compared to the larger leaves around fruit trusses such as those shown in Figure 6.45b. This suggests development stagnation is a result of inadequate power distribution.

Microwave group plants 1 and 7 had leaves that were generally all of intermediate quality. Plant 12 however, generally had leaves of distinct poor quality and also higher quality. Leaf damage typically occurred in places suggested by leaf simulations and can be seen in Figure 6.46 to be similar to that observed for plants 1 and 7.

(a) Front Angle.

(b) Reverse angle.

Figure 6.43: Experiment II: Plant 12 (MW/LHP) at experiment end.

Cold control group plants (Figure 6.48) grew significantly shorter than HC and MW plants and leaves were of vastly inferior quality. Many were curled and rough in texture, with brown patches common. This confirms that similar effects found on MW group plants are a result of exposure to cold air, rather than any microwave effect. Some leaves, such as that in Figure 6.51c had effects similar to burning, but are now evidently revealed to be a natural defect. Plant development was generally sporadic, with flowers being slow to develop and extremely small, unripe, fruit occurring infrequently and often in isolation. This is common across all CC plants and is shown in Figure 6.49 for plant 5, Figure 6.50 for plant 8 and Figure 6.51a for plant 14. Further fruit development on CC plants was also unlikely as many flowers, such as those shown in Figure 6.50c, had begun to dry up.

The growth of MW plants appears chaotic. However, when the results are considered relative to the growth patterns of HC plants, shown in Figure 6.52, the

(a) Full truss of unripe fruit.

(b) Full truss of unripe fruit.

Figure 6.44: Experiment II: Fruit on plant 12 (MW/LHP) at experiment end.

(a) Buds and flowers on plant.

(b) Trusses of fruit amongst leaves.

Figure 6.45: Experiment II: Fruit trusses and flowers on plant 12 (MW/LHP) at experiment end.

Figure 6.46: Experiment II: Typical leaf quality on plant 12 (MW/LHP) at experiment end.

Figure 6.47: Experiment II: Microwave group plants at experiment end.

Figure 6.48: Experiment II: Cold control group plants 5, 8 and 14, at experiment end.

(a) Fruit size.

(b) Fruit quality.

(c) Quality and quantity of flowers.

Figure 6.49: Experiment II: Plant 5 (CC) components at experiment end.

(a) Fruit and leaf size.

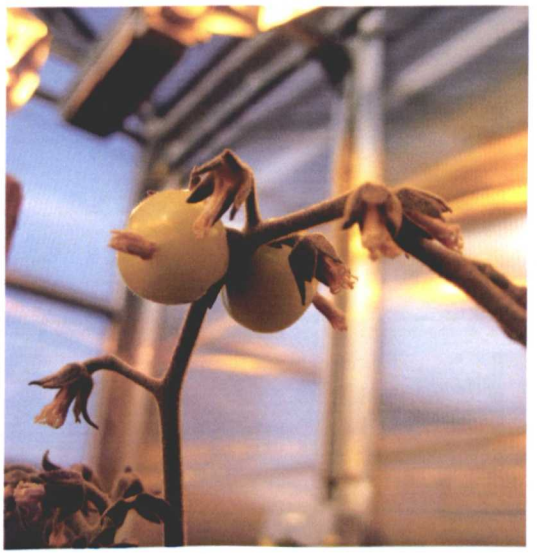

(b) Fruit and flower quality.

(c) Quality and quantity of flowers.

Figure 6.50: Experiment II: Plant 8 (CC) components at experiment end.

(a) Fruit size.

(b) Fruit quality.

(c) Quality and quantity of flowers.

Figure 6.51: Experiment II: Plant 14 (CC) components at experiment end.

Figure 6.52: Experiment II: Hot control group plants 2, 4 and 6, at experiment end.

random nature of the plant growth can be observed to be typical of this variety of tomato plant. The superior performance of HC plants is almost entirely attributable to the higher ambient air temperate. Leaves were of pale green colour, flat/thin in shape and smoother in texture (Figure 6.53b), compared to both CC and MW plants. The superior development of the leaves clearly hastens the onset off fruit formation and the high ambient temperature encourages ripening. Furthermore, the even distribution of temperature allows for consistent and regular fruit formation across the plant (Figure 6.53), and most fruit can be seen to develop simultaneously (Figure 6.53a); as is typical for a healthy plant of this (determinate) type.

6.3.4 Analysis

From Figure 6.54 the performance, in terms of height, of HC plants can be seen to be superior to that of MW and CC plants and increases at a similar rate for most of the experiment duration. These results are consistent with the first experiment. Performance of MW plants are still superior to CC plants though, where performance plateaus after around two-months' growth.

The rate of growth for microwave plants appears to increase when incident power

(a) Fruit quality and size.

(b) Leaf quality.

(c) Fruit truss distribution.

Figure 6.53: Experiment II: Hold control group plant components at experiment end.

density is increased and decreases when power density is decreased (*i.e.* growth rate changes correspond to antenna range changes), again indicating the temperature dependent nature of the plant performance.

The key indicators of plant progress, shown in Figure 6.55, show that, as in experiment I, the growth of MW plants lags that of the HC plants. More specifically, MW plants do not form fruit until three weeks after the first fruit on a HC plant, although it is a further three weeks before fruit begins to form on a CC plant – that never ripen.

Although, as in the first experiment, the delay between each event appears to increase with each subsequent event, ripening of the fruit occurs quite rapidly on the MW plants, once it has formed. This is further evidence to suggest that it is the inferior leaf temperature that initially delays the fruit formation but, once fruit are formed, are adequately heated so that ripening can occur. The problem is therefore not one of available power levels, but of differing power absorption and requirements between plant components.

As before, the execution of experiment II was cautious, although with incident power density greater than that used in experiment I; being only one-third to one-half of the estimated requirements. The plants nonetheless performed well and there was seen a significant improvement in terms of plant quality and fruit yield compared to experiment I. Microwave plants produced a quarter of the fruit that the HC plants produced, during the same period, in experiment II. This is compared to only one-eighth over the same period in experiment I.

The strong linear temperature dependence on plant height is again observed in experiment II and shown in Figure 6.56. The temperature dependence of fruit formation is again apparent, although is more linear than before, despite the lower recorded temperatures. This is most likely due to superior leaf heating, through using circular polarisation, providing a more extensive and robust plant and leaf structure to maintain the fruit.

The effect of the horizontal linear polarisation on plant height and fruit formation

is clear and more remarkable when compared to the other MW plants. As stated previously, it is possible that this is due to superior heating in the horizontal fruit trusses (providing improved fruit formation) and inferior heating in the vertical stem (resulting in shorter main stem growth). The importance of localised temperature variations on the general performance of plant components is therefore clear.

In contrast, as previously stated, the effect of clinostats is negligible in comparison owing to the relatively lower rate of decay in the direction of propagation through the 'thin' plant.

As mentioned in the analysis of experiment I, the polarisation obtained from the antenna in experiment I was actually more elliptical in the vertical direction than circular. The polarisation obtained from the antenna used in experiment II was high-quality. As has been described, a purely vertical polarisation would cause more heating in the main stem. As experiment I had a greater vertical field component, this explains why the average recorded temperature was slightly higher despite the lower incident power density. More importantly though, is the effect of the polarisation on fruit formation.

When pure circular polarisation was used, resultant fruit formation was almost double that of when elliptical polarisation was used, although the mechanism of this improvement was indirect. As mentioned above, this is because of the higher temperature of the leaves facilitating greater fruit formation but this, in turn, was only possible because of the superior heating uniformity achievable using circular polarisation. That is, increasing the power flux density to allow greater heating of the plants (and specifically the leaves) was only possible – without significant damage – through the use of circularly polarised fields. This was shown using computer simulations and is confirmed by the results presented here. In particular, through the results of experiment II, where power was increased from the levels of experiment I with little (or even reduced) burning and superior growth performance.

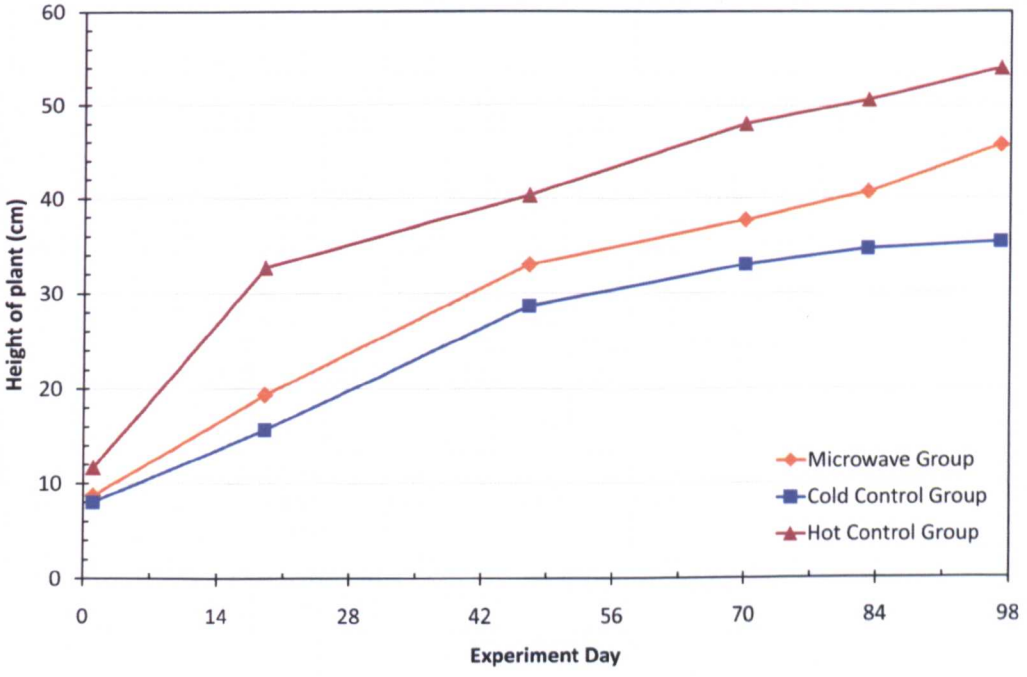

Figure 6.54: Experiment II: Plant height as function of time.

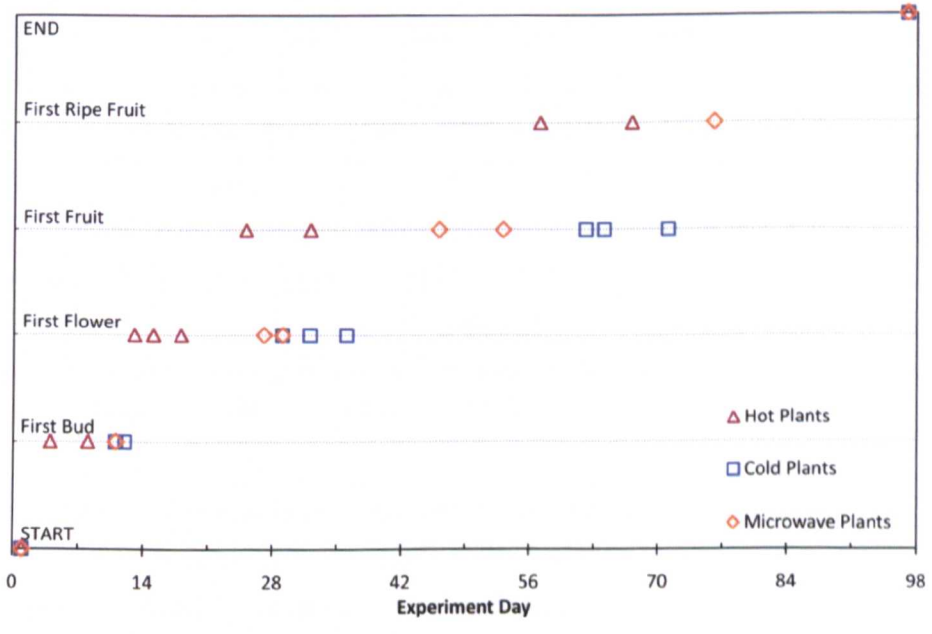

Figure 6.55: Experiment II: Plant performance as function of time.

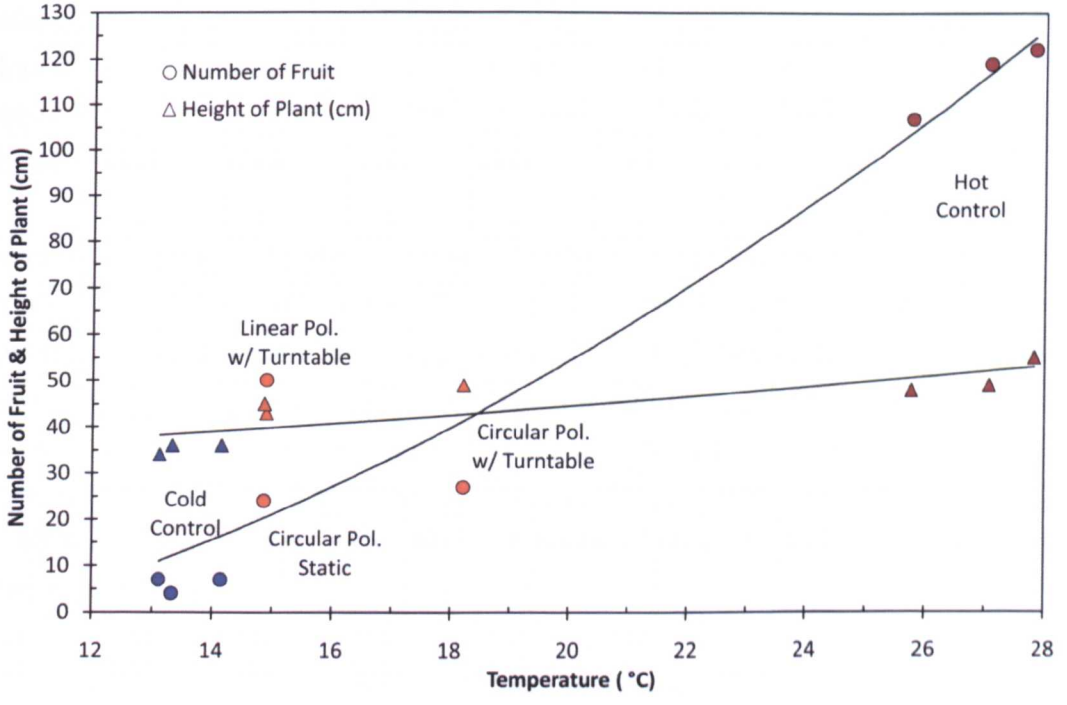

Figure 6.56: Experiment II: Plant performance as function of temperature.

6.4 Conclusions

The experiments in this section have revealed the mechanisms by which microwaves heat a growing tomato plant and also how such heating affects the growing characteristics of the plant. The simulation results in Section 5 have been confirmed. Furthermore, the practicality of heating all parts of the plant to similar levels has been revealed to be non-trivial. Indeed, the difference in heating rates between leaves and stems revealed the limitation on heating power levels, as defined by the threshold at which damage occurs on the stems. In contrast, the resultant under-heating of the leaves has been shown to be the limiting factor on the formation of fruit.

Despite the practical obstacles, microwave heating has been shown, for the first time, to be a viable and effective method for heating tomato plants from seedling to fruition. Importantly, fruit quality has been shown to be of the same standard as achieved through conventional heating.

Aside from localised over-heating, no non-thermal effects of microwaves have been identified from these experiments. All available evidence suggests that any difference between plants is entirely attributable to the overall temperature of the plants and their constituent components.

Several stages of plant development have been identified as having differing microwave heating requirements. Namely, these are stem formation, leave development, fruit formation and fruit ripening. Furthermore, the effect of incident power density and the polarisation of the incident field has been shown to be crucial and different for each stage. The use of circularly polarised incident fields has been shown to be most effective compromise in providing the necessary heating to all plant components to allow for stem and leaf growth, fruit formation and fruit ripening.

Linear polarisation has be seen to cause damage and limit the growth, in directions perpendicular to the polarisation, owing to a lack of power absorption and thus heating. Initial indications presented here also suggest however, that horizontal linear polarisation may offer some advantages for setting fruit, when the fruit trusses are also horizontally aligned.

The significance of field strength and uniformity in the plane and direction of propagation has also been discussed; the former being the most significant with regards to heating uniformity. The later has been seen, through use or otherwise of a clinostat, to have negligible effects. This is, of course, provided the average field across the 'depth' of the plant is sufficient for good heating.

The main limitation to the microwave system used here is the increased development time and fruit quantity produced when heating with microwaves, although the correlation between fruit produced, time taken and estimated volume loss density in the plant is clear enough to suggest that this could be mitigated, provided the power could be increased. Indeed, progress between the two experiments described is already substantial.

Possible methods by which this process could be developed and improved are

discussed in Section 8.

Chapter 7

Efficiency

The work detailed thus far has been concerned purely with the relative and absolute efficacy of a microwave system for heating greenhouse crops. An estimation of the efficiency of such a system, relative to a conventional heating system, is now required. The mechanisms by which each of these systems operate is very different however, and this makes an accurate comparison of the power consumption difficult.

The method presented here requires certain assumptions of the problem to be made, along with delimitations of the processes, to account for the unique variety of variables between growers and situations (see below). This is in order that the two heating processes can be considered directly comparable, or at least such that significant differences between processes can be defined as distinct variables in the efficiency calculations.

Given these assumptions, the power consumption of a real conventional system is described, followed by a method for calculating the power consumption of a microwave system. This is based on the principles used for the heating experiments in this work. Finally, a relative comparison of each is made with a discussion of sources of error and variation to validate the findings.

The method is simple, but nonetheless new to the application of microwave heating as free-space heating techniques are not common, nor typically practical for

most applications. The technique is described so as to be easily applicable and scalable to other, similar, heating scenarios.

The assumptions and definitions made for both systems are:

- The external air temperature is constant and equal to the internal air temperature prior to any heating.
- The internal air is not replenished *i.e.* no forced convection.
- For conventional heating, plant and internal air temperature are equal.
- Conventional heating is uniform within the entire volume of the greenhouse.
- Microwave heating is uniform and effective only within the plants.

7.1 Power consumption (conventional system)

It is first necessary to identify the power dynamics of the system. In the case of conventional heating, power is used in heating a fixed volume *i.e.* the greenhouse space. Power is dissipated by the thermal transfer of energy through the surface area of the greenhouse covering.

In the steady-state, the energy input into the greenhouse is equal to the energy transferred through the covering. The power consumption of a conventional system is therefore determined by

i The volume of the greenhouse.

ii The surface area of the greenhouse covering.

iii The thermal properties of the covering.

iv The (specified) internal air temperature.

v The external air temperature.

Given these dependencies, it is evident that many of the variables will be unique for each greenhouse and location, resulting in a variety of power requirements. For the estimates given in this chapter, the external air temperature is assumed to be the approximate UK mean of $10°C$ [97] and the required internal air temperature is $25°C$. Primary data was collected from a commercial grower in the UK that is respected within the industry as being one of the most efficient and productive in the UK and, as such, can be assumed to operate using the latest technology and processes.

The average weekly power consumption for this grower (using a conventional system) is shown in Figure 7.1 to be at least $500000\,kWh$ per week, although further sources indicate typical power consumptions of $600000\,kWh$ and up to $800000\,kWh$ per week [12]. For the initial case, the grower has an approximate growing area of $3.2\,Ha$, or $32000\,m^2$.

Energy use per square metre is therefore: $500000\,kWh/32000\,m^2 = 15.625\,kWh\,m^{-2}$

Averaging over the 168 hours in one week gives an instantaneous power consumption per unit area of growing space (which is the industry standard figure of merit) of $93\,Wm^{-2}$.

This is the steady-state power consumption, per square metre of growing area, required to maintain the temperature differential described above within the entire greenhouse.

7.2 Power consumption (microwave system)

Where in a conventional heating system the power dynamics are characterised by thermal conduction through object surfaces and into their interior, microwave heating is more specific and volumetric in nature. This makes the thermal processes more complicated than the conventional system.

Unlike in the conventional system, where the greenhouse volume is known and

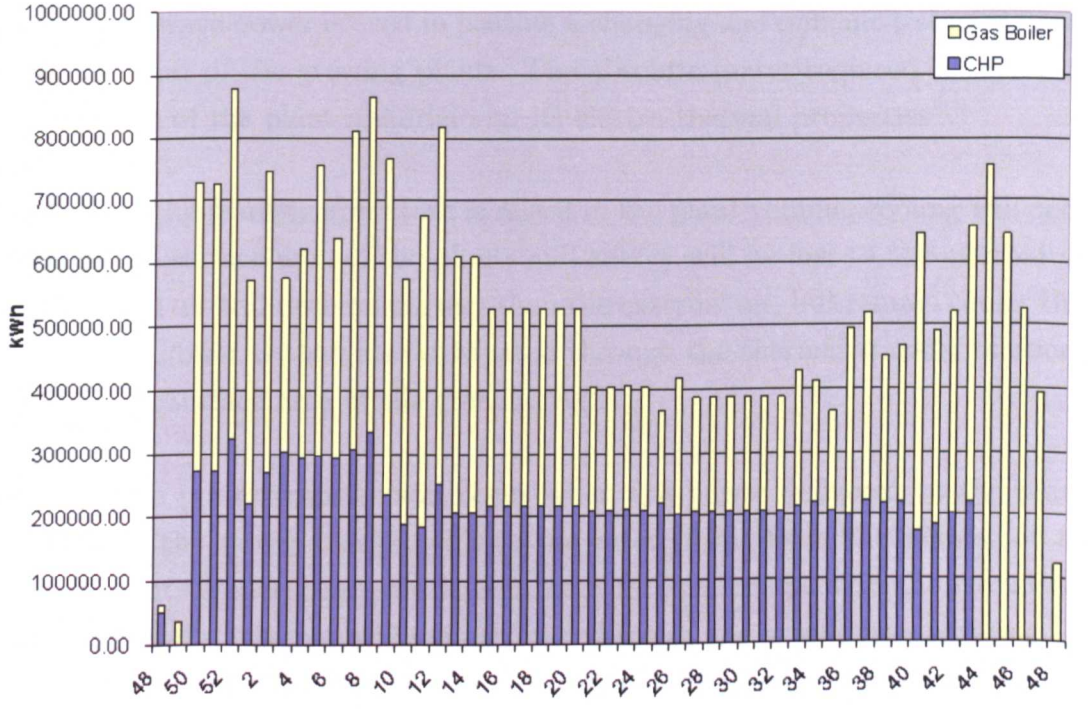

(a) Year One.

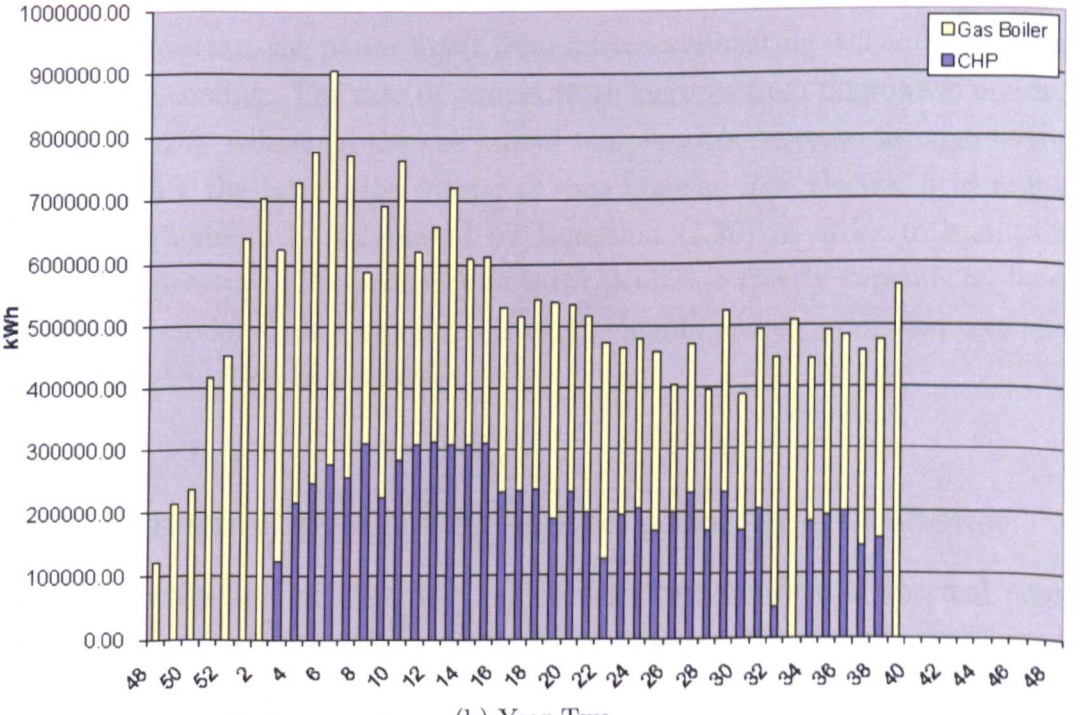

(b) Year Two.

Figure 7.1: Weekly energy consumption of commercial Tomato grower, in North-West England, over a two-year period.

fixed, microwave power is used in heating a changing and difficult-to-quantify volume, *i.e.* that of the growing plants. The absolute power required is dependent on the mass of the plant material and its electro-thermal properties.

Given that the plant temperature is raised in the plant volume, cooling will occur through the surface area of the plants and energy will be lost to the internal air. The internal air will become warmer than the external air, but remain cooler than the plants. Power is then also dissipated through the thermal transfer of energy through the surface area of the greenhouse.

Steady-state power transfer will occur when the power delivered to the plants is equal to the power dissipated into the internal air from the plants, at the desired plant temperature, which is in turn in equilibrium with the transfer of energy from the internal and external air through the greenhouse covering. In large greenhouses with modern glass coverings, the internal air is estimated to rise around 1°C.

In the steady-state, the power input from microwave heating will equal the power lost through cooling. The rate of temperature increase from microwave power, in Equation (7.20), will equal the the rate of temperature decrease through cooling. By calculating the latter, the former is thus known. The electric field requirements can therefore be stipulated by Equation (7.20) in order to maintain a specific temperature. The accuracy of this calculation clearly depends on having an accurate model of the power loss from the plants and so a detailed consideration of its calculation is warranted.

7.2.1 Thermal process of heated plant in greenhouse

The well known unit of heat flux, which describes the flow of thermal energy between a temperature gradient, in time and space is given by.

$$\vec{q} = -\kappa \nabla T \tag{7.1}$$

where $\vec{q}$ is the local heat flux in $W\,m^{-2}$ and κ is thermal conductivity in $W\,m^{-1}\,K^{-1}$

Fourier's law states that the heat flux across a surface, S is proportional to the negative gradient in temperature, T and to the area perpendicular to the gradient. Given in integral form,

$$\mathcal{F} = -\kappa \int_S \vec{\nabla} T \cdot d\vec{A} \tag{7.2}$$

where the left hand side is the heat transferred per unit time and $d\vec{A}$ is an orientated surface element.

From this and other principles, a full heat equation can be derived as in [98]. This is a partial differential equation (PDE) for $T = T(x, y, z, t)$. Following the assumptions made in [98], the total heat, $\mathcal{H}$ inside a subregion B at time t can be given by the volume integral

$$\mathcal{H} = \int_B c_p \rho T \, dV \tag{7.3}$$

A heat source/sink term is also defined as a function of time and space [98]

$$\mathcal{E} = \int_B f \, dV \tag{7.4}$$

where f is the density function on the internal heat source/sink. This term is positive during microwave heating and zero during conventional heating and thermally describes the difference between the two mechanisms.

Now, for a subregion B bounded by the surface S it is stated that: *"At each instant in time, the heat content inside B is $\mathcal{H}$ and the increase in this heat content in going over to the next instant in time should be due to heat gained due to flux inwards across the bounding surface S plus the heat added by sources inside B."*[98] *i.e.*

$$\frac{d\mathcal{H}}{dt} = -\mathcal{F} + \mathcal{E} \tag{7.5}$$

Therefore,

$$\begin{aligned} \frac{d}{dt}\int_B c_p \rho T \, dV &= \int_S \kappa(\nabla T)\, d\vec{A} + \int_B f \, dV \\ &= \int_B div(\kappa \nabla T)\, dV + \int_B f \, dV \end{aligned} \tag{7.6}$$

Here, Gauss's divergence theorem has been used to convert the surface integral to the volume integral in Equation (7.6). Rewriting Equation (7.6) and given that B is an arbitrary volume of a subregion,

$$\lim_{B \to 0} \quad \frac{\partial}{\partial t} c_p \rho T = \nabla(\kappa \nabla T) + f \tag{7.7}$$

There are many solutions to this PDE. All require specific boundary conditions to be defined and an initial value specified. In the case of the tomato plant, the boundary is non-homogeneous and difficult to model. Furthermore, it will change depending on the conditions present.

7.2.1.1 Newton's cooling law

Computer-aided modelling can be used to solve Equation (7.7) accurately, as used to great effect in previous sections of this work. However, for accurately calculating specific power consumption requirements, detailed knowledge of thermal and geometry properties are required for all plant components. Further data is required for the the air *e.g.* flow rates, temperature, humidity *etc.* Collecting this data is non-trivial and the resultant simulation required very large and resource-dependent.

A simplification is to model the boundary such that the average rate of temperature lost by the plant when cooling can be used in its calculation. Although basic in its generality, the use of Newton's cooling equations provides a means to describe the boundary conditions of the plant to a degree of accuracy that is known. This can be achieved by simply measuring the average rate of cooling from the plant to the air, through a series of temperature measurements. Where

the facilities exist to enable a more accurate boundary to be defined with confidence, this method can be improved.

If the boundary conditions conform to Newton's cooling then

$$-\kappa \nabla T = h(T - T_a) \tag{7.8}$$

where T_a is a function specifying the temperature of the external environment in time and space. When assigned to Equation (7.7), the solution to the PDE simplifies to that of Newton's cooling law. A full derivation is available in [98]. The heat flux per unit area at any boundary point is proportional to the area and h is the heat exchange coefficient.

If a function of time is defined that relates an object temperature and the surrounding temperature as

$$y(t) = T(t) - T_a \tag{7.9}$$

with the initial conditions

$$y_0 = T(0) - T_a = T_0 - T_a \tag{7.10}$$

then taking the derivative of y(t) yields

$$\begin{aligned} \frac{dy}{dt} &= \frac{d}{dt}(T(t) - T_a) \\ &= \frac{dT}{dt} - \frac{dT_a}{dt} \end{aligned} \tag{7.11}$$

Now, from assumptions already stated, T_a is constant and $y = (T - T_a)$ so (7.11)

$$\begin{aligned} \frac{dy}{dt} &= \frac{dT}{dt} \\ &= -h(T - T_a) = -hy \end{aligned} \tag{7.12}$$

A solution to this is

$$y(t) = y_0 e^{-ht} \tag{7.13}$$

By inserting Equation (7.10) and a value for y at some other time into this equation, a complete solution becomes

$$T(t) = T_a + (T_0 - T_a)e^{-ht} \tag{7.14}$$

Empirical values of h can now be calculated that characterise the rate of cooling for a given internal air temperature. This can be done easily by measuring the temperature of a plant of known and uniform initial temperature, cooling in a volume of air of lower uniform temperature. By measuring at several points within the plant and averaging gives a crude but general value for h that can be used, in this case to model the boundary of the whole plant, for the purposes of estimating the microwave power required for heating.

The graph of values from which h was calculated and used in the following estimations is shown in Figure 7.3 for two separate ambient temperatures (and initial starting temperatures), to indicate the typical variation that can be expected.

7.2.2 Rate of change of temperature due to microwaves

The temperature in the plants is described in space and time by the heat conduction equation (see section 7.2.1) as given by.

$$\rho c_p \frac{dT}{dt} = \nabla \cdot (\kappa \nabla T) + Q \tag{7.15}$$

where c_p is the specific heat capacity, ρ is the density, κ is the thermal conductivity and Q is the source term for volumetric heat generation by the microwaves.

Now, as described in Section 2, Poynting's vector gives the average power dissipated in a volume of dielectric as

$$P_{av} = \frac{1}{2}\omega\varepsilon_0\varepsilon'' \int_V (E \cdot E^*)\, dV \tag{7.16}$$

$$= \frac{1}{2}\omega\varepsilon_0\varepsilon'' E^2 V \tag{7.17}$$

It is the last term in Equation (7.15) that entirely defines the temperature rise in the plants during microwave heating (assuming no other heat sources), and is to be specified to achieve and maintain a required temperature difference.

It then follows that by setting the initial conditions in Equation (7.15) so that $\nabla T = 0$ (*i.e.* initial temperature is uniform) gives

$$\rho c_p \frac{dT}{dt} = Q(t) \tag{7.18}$$

which combining with (7.17) yields

$$Q(t) = \frac{P_{av}}{V} = \frac{1}{2}\omega\varepsilon_0\varepsilon'' E^2 \tag{7.19}$$

Rearranging terms, the power dissipated per unit volume and corresponding temperature rise is then

$$\frac{dT}{dt} = \frac{P_{av}}{V} \cdot \frac{1}{\rho c_p}$$

$$= \frac{1}{2} \cdot \frac{1}{\rho c_p}\omega\varepsilon_0\varepsilon'' E^2 \tag{7.20}$$

It is apparent that a certain field strength E in a dielectric ε'' results in a power dissipation per unit volume P_V. Assuming that a volumetric power density can be maintained, the required radiated power can be calculated independent of the size and surface area of the plant, assuming that the radiated power density is uniform across the plant.

By equating this rate of temperature increase to the rate of temperature decrease through cooling from the specified temperature, value of the power and field requirements can be ascertained.

Experimental work has shown that, at the ISM frequency used throughout this work, the plants can be considered to be thin. That is, the field in the direction of propagation through the plants is assumed to be constant and result in uniform power dissipation at every depth into the plants.

For a free-space system, the problem is now the two-dimensional case of illumination by a beam area with an associated incident power flux density, that results in a volumetric power dissipation in a dielectric in order to maintain the specified rate of temperature increase in the plants.

Such a system will be therefore be maximally efficient when the incident beam area is equal to the plant area that is to be heated. The total power is then the sum of the transmitted power from all antenna elements required to heat a given area.

7.2.2.1 Power in a transmitted wave

It is now necessary to calculate the required transmit power to achieve the fields specified in Equation (7.20).

Assuming that the wave incident on the plants is plane, the power flux density is

$$S = E \times H \tag{7.21}$$

The impedance of free space is

$$Z_0 = \frac{E}{H}$$

and for a plane wave

$$E \approx H$$

so

$$E = \sqrt{S \times Z_0} \tag{7.22}$$

The power flux density at a distance, r from an antenna with gain, G_t is

$$S = \frac{P_t G_t}{4\pi r^2} \tag{7.23}$$

It then follows that, for a desired rate of temperature increase, the required electric field strength E can be found using Equation (7.20). Secondly, by using Equations (7.22) and (7.23), the transmission power P_t required to satisfy the field demands for a specified gain can be ascertained.

7.2.3 Power calculation using experimental data

A solution to Equation (7.14) was found from the data in Figure 7.3, where the temperature differential is $10°C$.

Calculating the mean value of h_{plant} = 0.004882 and then using (7.12) gives the rate of cooling as

$$\frac{dT}{dt} = h_{plant}(T - T_a) = -0.04882 \tag{7.24}$$

At equilibrium, the rate of temperature decrease through cooling will be equal to the temperature increase from the microwaves, that is the above equation will be equal to Equation (7.20):

$$0.04882 = \frac{1}{2} \cdot \frac{1}{\rho c_p} \omega \varepsilon_0 \varepsilon'' E^2 \tag{7.25}$$

Now, if $c_p = 4000\, J\, kg^{-1}\, K^{-1}$, $\rho = 1000\, kg\, m^{-3}$, $\varepsilon'' = 16$, and frequency $\omega = 2\pi f$ where $f = 2.45\, GHz$, then the field requirements at the plant/air interface are,

$$E = 423\, Vm^{-1} \tag{7.26}$$

Consequently, from Equation (7.22), the required radiated power flux density to maintain the prescribed temperature differential through microwave heating is

$$S = 475\,Wm^{-2} \tag{7.27}$$

Data for h was unavailable for when the temperature differential is $15°C$, as was assumed for the case of conventional heating, but if it is assumed to be similar to when the differential is $10°C$, then electric field and power flux density would become $E = 518 : Vm^{-1}$ and $S = 713 : Wm^{-2}$, respectively.

7.3 Efficiency comparison

Power requirements for both conventional and microwave systems have been calculated. It is now that the fundamental differences between each method become apparent. Although the microwave system appears to require a greater power per unit area than a conventional system, the actual total microwave power used depends on the sector area that is heated, as shown in Figure 7.2. It is this possibility to focus the microwaves only on the plants to be heated that offers the potential to improve efficiency compared to the conventional system, where the entire growing area is heated.

To make an accurate comparison, information about the area of the plane in which the plant grows (see Figure 7.2) and the spacing between rows is required (see Figure 7.4). This situation assumes that the variety grown is a vine type, as used by all commercial greenhouse growers.

It was stated in section 7.1 that the power consumption of a conventional system is $93\,Wm^{-2}$ where the area refers to the floor area.

It was found in section 7.2.3 that a power flux density of $S = 713\,Wm^{-2}$ is required to maintain the same plant temperature using a microwave system, where here the area is as described in Figure 7.2. The energy to satisfy this required power flux density must of course be provided by an antenna. Maximum efficiency is

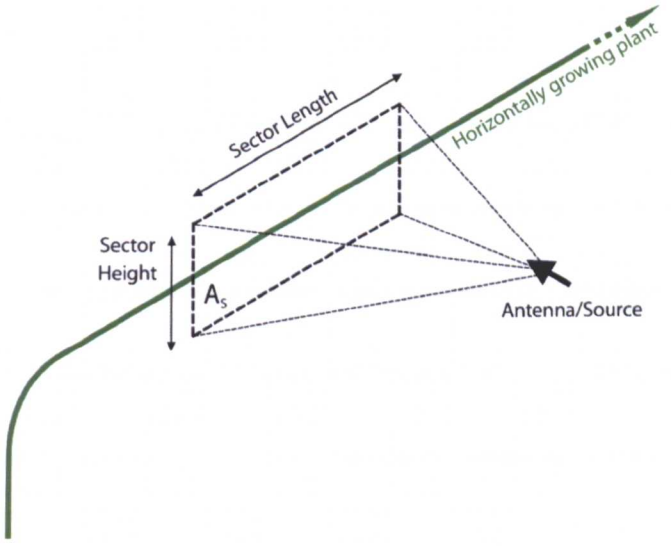

Figure 7.2: Illustration for definition of plant sector and plant sector area.

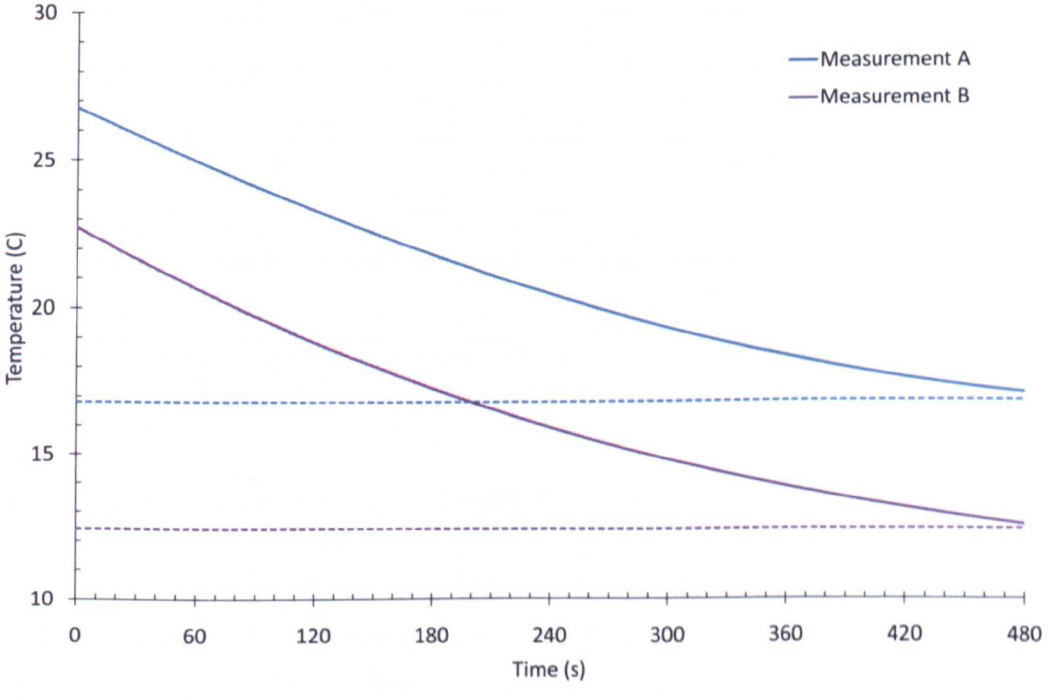

Figure 7.3: Measured temperature profiles of tomato plants during cooling, for calculation of values for h.

achieved when the beam width of the antenna is ideally focused on only the sector area (or the plant within) and when gain is high. With gain and beam width being

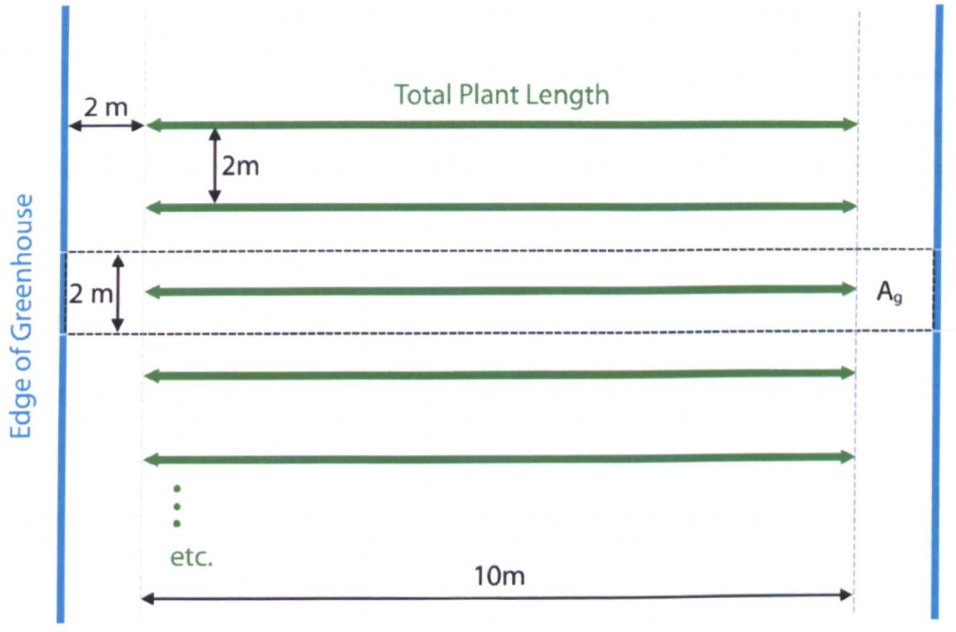

Figure 7.4: Top down view of greenhouse growing area, illustrating the relative area occupied by a plant section

largely inter-dependent, careful antenna design is crucial to maximising efficiency.

For the realistic case of an antenna with gain of 16 dB that is capable of illuminating an entire plant section (*i.e.* a 1 m (horizontal) by 0.3 m (vertical) plant section) at a range of approximately 60 cm: using Equation (7.23) reveals a required input power to the antenna of 86.5 W and thus $86.5\,W^{-section}$.

To accurately compare this to the power used in a conventional system it is useful to also find the power consumption of a conventional system in terms of plant 'sections'. For example, if the same one metre horizontal plant section mentioned above continues in the greenhouse for a total of $10\,m$ and is repeated with spacings between rows of $2m$, with a spacing at each end of each row of a further $2m$, then the plant section density is $10\ sections \div 28\,m^2 = 0.357\ sections\,m^{-2}$ for each area of floor space.

In this case, the relative power consumption per plant section for the conventional system is $93\,Wm^{-2} \div 0.357\ sections\,m^{-2} = 260.5\,W^{-section}$

This useful conversion allows for both power consumptions to be stated in the same units. A direct and valid comparison of efficiency can now be made. In this case (with the figures above) the *microwave system uses 33% of the energy used by the conventional system.*

These efficiency calculations clearly depend on

- The growing area of the irradiated plant section, i.e the *height and length* of the plant section in x and z;
- The floor area occupied by a plant section, i.e. *spacing density* in x and y;
- Careful design of antenna elements;

These calculations are sensitive to small variations in parameter values. Figure 7.5 shows the sensitivity of S, E to variations in the empirical value of h. The power P is also included and refers to the practical experiments described in Section 6.1.2. For h calculated above, the graph indicates a value of required E consistent with that specified for the heating simulations in Section 5 and practical experiments in Section 6.

7.4 Summary notes

The calculations for the microwave system here consider only the radiated power. The assumption that antennas and generating equipment are 100% efficient is clearly not valid. Losses up to and including the radiating elements can be included in the figure as an adjusting factor for the microwave power, when known.

The microwave power calculations above are valid for a very specific set of conditions, and so cannot be considered general, although the technique itself is generally applicable to other conditions. An important assumption made is that the power flux density radiated across one sector results in an even distribution of power within the plant such that normal growth can occur. Previous chapters

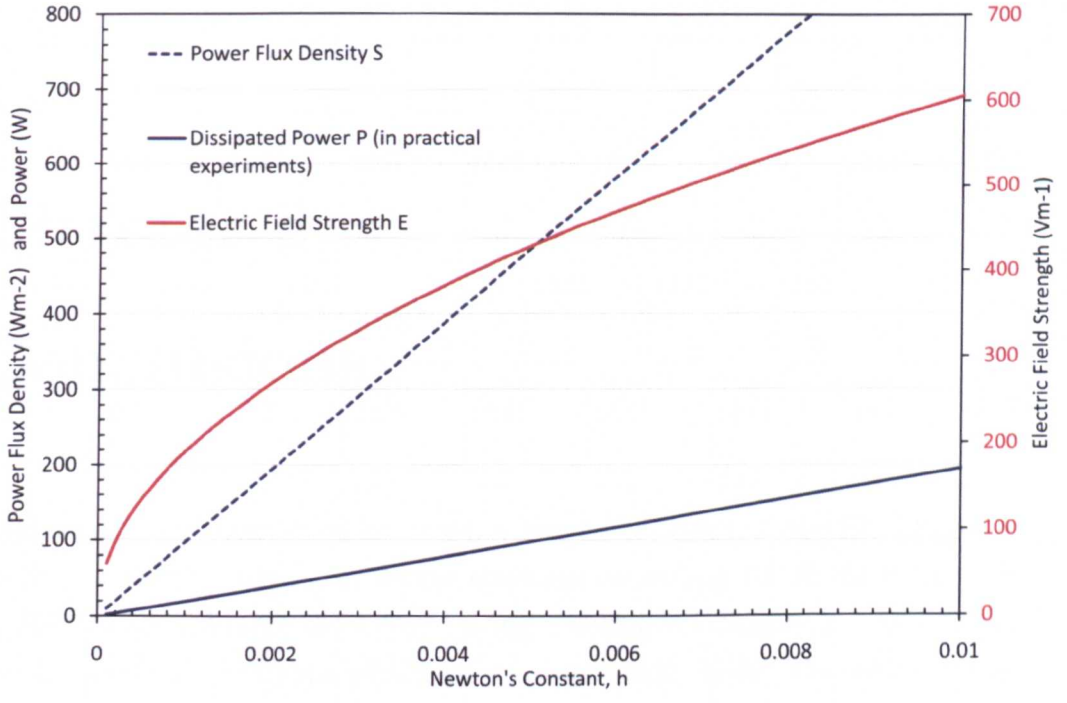

Figure 7.5: The effect of the constant, h on the required electric field and power flux density.

have detailed the various issues that can arise when this is not the case and the effect they have on plant growth and performance. Furthermore, the wave front is in reality not plane and more likely to have a spherical wave-front at distances relatively close to the antenna, as in the case of heating greenhouse crops. This has not been considered and its significance is unknown.

Although estimates in this chapter indicate a heating power requirement of only a third of that for conventional heating, assumptions made suggest that this figure most likely represents an upper limit. Even if required microwave power was doubled however *i.e.* a 100% margin of error exists in the calculations, a saving of 33% would still be achieved over conventional heating.

Chapter 8

Conclusions

Analysis of the commercial greenhouse vegetable sector in the EU reveals an extensive industry – with greenhouse coverage exceeding 10000 Ha in the UK and Netherlands combined; the latter having a commercial value in excess of 4.6 billion Euros in 2006. Crops produced are specifically high value salad crops such as cucumbers, peppers and tomatoes.

The industry is revealed to be growing in size and scale, year-on-year, not least because of the high yields attainable from greenhouse crops and the security offered by localised food production. This enables the demand for fresh produce, from increasing populations, to be satisfied. In addition to high yields, the order of magnitude lower use of resources during greenhouse production (water, pesticide *etc.*) makes for a very efficient production system when compared to field-based methods.

Despite the many apparent benefits of greenhouse production however, energy consumption is shown to be very substantial. Indeed, energy accounts for 50% of all production costs for tomatoes, with nearly all of this energy being used for heating the growing space. In the UK, energy consumption by the greenhouse vegetable sector is estimated to be 2750 GWh per annum and to be many times greater in the Netherlands. Aside from the obvious financial implications, the CO_2 emissions associated with this power generation are huge; accounting for 3% of the entire national emissions in the Netherlands.

Owing to cost and emission issues, growers and governments are found to be very progressive, flexible and innovative in both technology and target-led legislation. This has led to significant improvements in energy efficiency within the greenhouse vegetable sector, although most gains have been through increased yields, rather than reduced energy consumption.

This work has shown the viability of a microwave system for heating greenhouse crops in order to reduce the energy consumption, due to heating, in commercial greenhouses. Given that there exists few precedents for such a system, practical experimentation supported by computer modelling was used to analyse and demonstrate the efficacy of such a system. Having established a viable concept, an estimation of the efficiency of a viable theoretical commercial implementation is made, relative to the current state-of-the-art conventional heating systems.

Measurement of dielectric properties show the dominance of water content on the permittivity of tomato plants. Small but noticeable differences exist between plants that have been exposed to microwaves and plants that have been in controlled hot and cold temperatures. The distribution of the differences correlate with the average temperature of the plants, which indicates a dependence purely on the temperature of the plant itself. That is, the water content (and dielectric properties) of the plant, are apparently not affected *directly* by microwave exposure.

The dielectric properties reveal significant loss components at low frequencies that are attributable to dissolved ionic particles. Losses are highest at low RF frequencies but reduce rapidly into the low microwave regime. They then increase almost linearly as frequency increases further. A compromise for the operating frequency of the system is found between optimum power loss density and optimum power penetration depth. Frequency selection is constrained, however, by the availability of ISM bands and also the effect of wavelength on the uniformity of field patterns within the plant. ISM frequencies of 915 MHz, 2450 MHz and 5800 MHz are conveniently found to offer the best compromise, and also where equipment can be easily designed at low expense.

Pilot tests indicate that the use of a high power, free-space microwave system can mitigate the effects of cold growing temperatures by heating tomato plants volumetrically. Growth performance is far in excess of comparable plants grown at the same ambient temperature, but without microwave heating. Over short experiment durations, no significant adverse effects are noticeable on microwave plants, as has been reported previously [3].

Problems do occur however, when plants are allowed to grow for their entire life-cycle. Significant issues of burning and areas of under- and over-heating occur across all parts of growing plants. When this occurs on branches, cauterisation can occur. Catastrophic failure results when this occurs on main stems. The source of this damage is revealed by computer simulations to be from poor electric field uniformity and, when occurring within leaves, results in poor leaf formation. This inhibits plant development which, although not critical, delays fruit formation. Heating within developed fruit is good, however, and ripening during microwave heating is as effective and timely as in conventionally heated plants. This latter point is evidence that isolates the non-uniformity of the fields within the plant as the cause of poor leaf development, rather than it being a direct consequence of microwave exposure. Thermal equalisation through IR re-radiation did not result in an adequately uniform temperature distribution, as suggested in [5], and heating was entirely characterised by applied microwave power.

Power requirements of the growing plants are higher than might be expected owing to the large surface area and relatively thin geometries of the various plant components. This results in rapid dissipation of thermal energy to the cold ambient air. It is clear that the plants are very sensitive to variations in temperature (*i.e.* cold), yet increasing the radiated power can often result in the damage described above. The non-uniformity of the electric field is therefore identified as the main limiting factor in the heating of plants with microwaves. The required power density for heating plants, as suggested by simulations and experimentation, was in the range of 200-300Wm^{-2}. Damage was observed at power densities as low as 50Wm^{-2} however. Given that it is known that power densities of around 500Wm^{-2} quickly result in plant death [6], the tolerance of plant to heating by

microwaves can be said to be low.

Varying the on-off duty cycle of applied power does little to improve heating uniformity. Likewise, nor does rotation of the plants. By using circularly polarised incident fields, uniformity is significantly increased. This effect can be demonstrated in regular geometries as an improvement in the intra-object uniformity and also in greater inter-object uniformity, *i.e.* heating becomes consistent between different objects, as well as within the objects themselves. When this novel technique is applied to growing plants, power can be increased without further damage to that which occurs when a lower power linear polarisation is used. In doing so, plant performance is improved relative to cold control plants and other microwave plants (subject to linearly polarised fields). This improvement can be observed in the development time of the plant height, flower formation, fruit formation and fruit ripening. This technique also has obvious potential benefits for the continuous microwave processing of irregular objects in other industrial scenarios.

Use of horizontal linear polarisation appears to improve fruit formation on similarly aligned trusses, although at the expense of limiting growth in the vertical direction. The use of polarisation therefore also offers a mechanism for the control of plant growth and development.

A theoretical commercial implementation is described as a free-space system of antenna arrays, each radiating within discrete plant 'sectors'. By defining a plant 'section' as being within each sector, energy consumption can be calculated and compared for conventionally heated and microwave heated systems. Estimates indicate a carefully designed microwave system requires a third to two-thirds the energy for heating of a conventional system.

In addition, the electrical power required by a microwave system could be provided with little financial or environmental cost by integration with the next generation 'energy-producing greenhouses' that are currently being developed [7].

8.1 Future Work

The experiments in this work and the power and efficiency calculations presented assume that a constant temperature must be maintained at all times. In practice, the night-time temperature in the greenhouse can often be lower than during the day and is often necessary to encourage fruit ripening. This was not performed in the experiments presented here.

The applied power from a microwave system could, however, be easily and rapidly adjusted to accommodate the lower required plant temperature with little loss of energy (other than the heat allowed to dissipate from the cooling plant during the transition). Performing this using a conventional system would result in either the loss of energy in the air (by allowing it to escape the greenhouse) or require the application of low-grade thermal storage, with associated inefficiencies of its own.

Reheating of the plants the following day could be performed easily, efficiently and at a controlled rate using a microwave system. The conventional system would require the entire volume to be reheated. This transient process would, in particular, be the greatest source of inefficiency, relative to the microwave system. Research into the technical and economic aspects of this technique would reveal the benefits or otherwise of such a process.

The variety of tomato plant used in this work was a determinate variety. This bush-like plant grows until fruit sets on the end of a truss. This then encourages the rest of the flowers to set, usually within four weeks. The plant grows in a dense and compact manner. The varieties grown commercially are indeterminate types. These grow in long vines and continue to grow until the growing tip is removed. Fruit sets successively in trusses along the vine, which has a lower and more regular leaf density. Although the former variety was used in this work, owing to convenience in laboratory experiments, further experiments are required using vine varieties. It is anticipated that heating of this variety will be more straight-forward, owing to its regular growth and arrangement.

Using the vine-variety plants, further work would involve a large-scale laboratory trial, prior to commercial trials. The purpose of such experiments would be to optimise the process and system for use by commercial growers.

The first aspect of such development would be to specify and design equipment and application processes, using the knowledge gained from this work, so that power can be applied as optimally as possible to the crops. This would involve designing antenna elements to match a specified sector area (which would of course differ between plant varieties), and specifying and designing a heating regime for such a system with appropriate control equipment; an example of which could be the use of sector-scanning system with a passive infra-red temperature feedback. Secondly, given a sound prototype equipment design, the collection of detailed statistical measurements are necessary, such that an accurate and detailed comparison can be made between plants and processes *i.e.* comparison to conventionally grown plants.

Given a greater sample size, it would also be possible to describe the consistency in the setting of fruit and reveal any correlations between the heating conditions and fruit formation. For example, by recording the conditions, location and progress of how trusses develop, including whether full trusses set or if only isolated fruit set, for given polarisations and/or power levels, any microwave heating-induced effects will become apparent.

Whilst this study has expanded the field of heating plants with microwaves, progress has been limited to electro-thermal and mechanical effects. Although RF and microwave bands are all non-ionising and, as such, cannot damage the molecular structure of the plants directly, no part of this study considered the effects of the radiation on the chemical processes within the plant that may affect growth rates and/or chemical composition. For example, the effect or otherwise of microwave heating on the formation and action of chlorophyll is not known and could therefore be an influencing factor in a microwave-treated plant's growth performance. As such, a study of the biology of a microwave-treated plant is needed in order to fully understand any pertinent effects.

The differing moisture contents between plant groups, observed during practical experimentation, was attributed to differing rates of transpiration that was in turn due to differing plant temperatures. How or if this process is caused or effected by microwaves was not established however, and further investigation is required.

The use of a varying duty cycle as a means of controlling the average power applied to the plants (to control the resultant average temperature) requires further investigation. For this method to be implemented successfully, it is first important to further and more specifically quantify the robustness of the plant in terms of how much power it can be exposed to and for how long, before damage begins to occur. From simulations using a continuous power application, it was observed that small areas of high power absorption quickly resulted in higher temperatures, but the time-scale over which damage occurred on real plants was not obvious, nor always clearly describable as 'burning'.

The use of circular polarisation has been shown to offer the best compromise between heating uniformity and plant growth. However, as described in Section 6, the use of linear polarisation can, at times, offer some advantages in terms of controlling the extent of the plant growth, at the expense of the heating uniformity. Furthermore, some results suggest that a horizontal polarisation may offer superior fruit setting along similarly aligned trusses. It is therefore clearly of value to further investigate the use of multiple linear polarisations, either concurrently or consecutively as the plant develops, as a means of improving or controlling performance and development.

Simulations of heating patterns along the length of a stem model indicated peaks and troughs in the two-dimensional power/temperature distribution. The location and number of peaks and troughs were very clearly frequency dependent. If, at one frequency, a peak results in overheating and a trough under-heating, then power may be reduced such that the peak now results in optimal heating at that location. By using a different, higher, frequency that results in peaks at other locations, the cold area from the lower frequency can be heated. This can be continued for any number of available frequency bands. Initial exper-

imental simulations suggest that this method offers great potential in further increasing uniformity. It is however, difficult to control without some form of temperature feedback and possible beam control, given the strong dependence on the orientation of plant elements and direction of wave incidence on the heating patters within the plant. Further work is required on the application of this multi-frequency technique, which could potentially combine infra-red temperature measurement as a feedback system. Feedback would control the power and direction of a beam from an amplitude (or duty-cycle – see above) and phase-controllable antenna array.

Use of a steerable beam would allow for a reduction in the number of antenna/array elements required to heat a given number of sectors, or for further improvements in heating uniformity. For example, if an array N_0 has a beam angle perpendicular to the direction of plant growth, then the sector on which the beam is incident is S_0. By scanning this beam by a fixed angle, sectors S_{-1} and S_{+1}, either side of S_0, can be heated by the beam from array N_0. Likewise, the next array element along the length of the plant, N_1 would scan similarly, resulting in a further heating of the sector S_{+1}, but from a different direction. By this means, every sector will be subjected to waves incident from at least three directions, improving the resultant heating uniformity. This technique could also be incorporated with multi-frequency applications as described above. Furthermore, depending on the design of the antennas, beams could scan several sectors thereby reducing the number of antenna units required to heat a given number of plant sections. The relative radiation efficiency and beam-width would decrease as the scanning angle increased however, and this would need to be considered against the savings obtained from using fewer antenna elements.

The array elements in this work were all micro-strip patch antennas. Whilst convenient and suitable for demonstrating the concept of heating crops with microwaves, greater efficiency could be obtained by using another form of antenna, such as a wire antenna. A common dipole antenna could be used, but would require the use of a balun, which would introduce further losses into the system. Although circular polarisation could be easily obtained by using crossed-dipoles, the antenna complexity would increase. One possible alternative antenna solu-

tion would be an array of helical wire antennas, operated in end-fire mode. The would allow the beam to be constrained in the vertical and horizontal directions by array factor design, whilst radiating circularly polarised waves in the direction of propagation. The elements are basic and non-obstructive. Matching to the power source would also be straightforward.

Whilst this study has used *Lycopersicon esculentum, var.* 'Minibel' as the subject crop, the heating effects and techniques described could easily be transferred to other crops. Indeed, tomato plants show great variety in the dimension and composition of their constituent components. As such, heating less complex crops is likely to prove more straightforward than for tomato crops. It would be interesting to assess the viability of microwave heating for other greenhouse food crops, in particular salad crops such as lettuce leaves, cucumbers *etc.* In addition to greenhouse food crops, this technique could be utilised in non-food crops and indeed, crops that are traditionally non-greenhouse crops. For example, government agencies and drug companies could utilise a microwave heating system in order to grow medicinal marijuana or opiates in easily controllable and secure environments, whilst keeping energy and production costs low.

8.2 Final remarks

This thesis has been demonstrated, in a suitable and valid context, to provide a novel, effective and efficient means of heating growing crops. If implemented across the entire greenhouse sector in Northern Europe, this would result in energy savings in the order of thousands of GWh per annum and immediately half the current CO_2 output of the greenhouse vegetable industry. In Holland, this would equate to a reduction of 2% of national CO_2 emissions. This would also result in an energy efficiency improvement equal to that which has been achieved in the thirty years to-date. A reduction in primary fuel and CO_2 emissions on this scale is unprecedented in the greenhouse vegetable sector.

Appendix A

Antennas and Equipment

A.1 Power generating equipment

Microwave power generating equipment, used for practical experiments in Section 4 and Section 6, was designed as shown in Figure A.1 and with component specifications as shown in Table A.1. The constructed apparatus (Figure A.2) was then sealed in an IP65-rated enclosure for protection against dust and water.

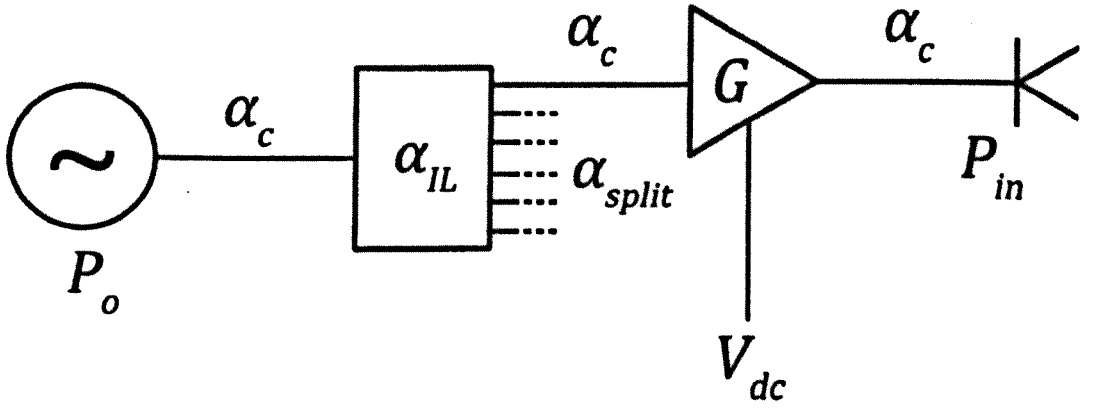

Figure A.1: Microwave equipment system diagram

Label	Value (@ $f = 2.45GHz$)
P_o	7 dBm
G	50.85 dB
P_{1db}	43.7 dBm
α_c	-1.1 dB
α_{IL}	-1.1 dB
α_{split}	-7.78 dB
V_{dc}	28 (6.3 A)

Table A.1: Parameter values for experimental set-up, as shown in Figure A.1.

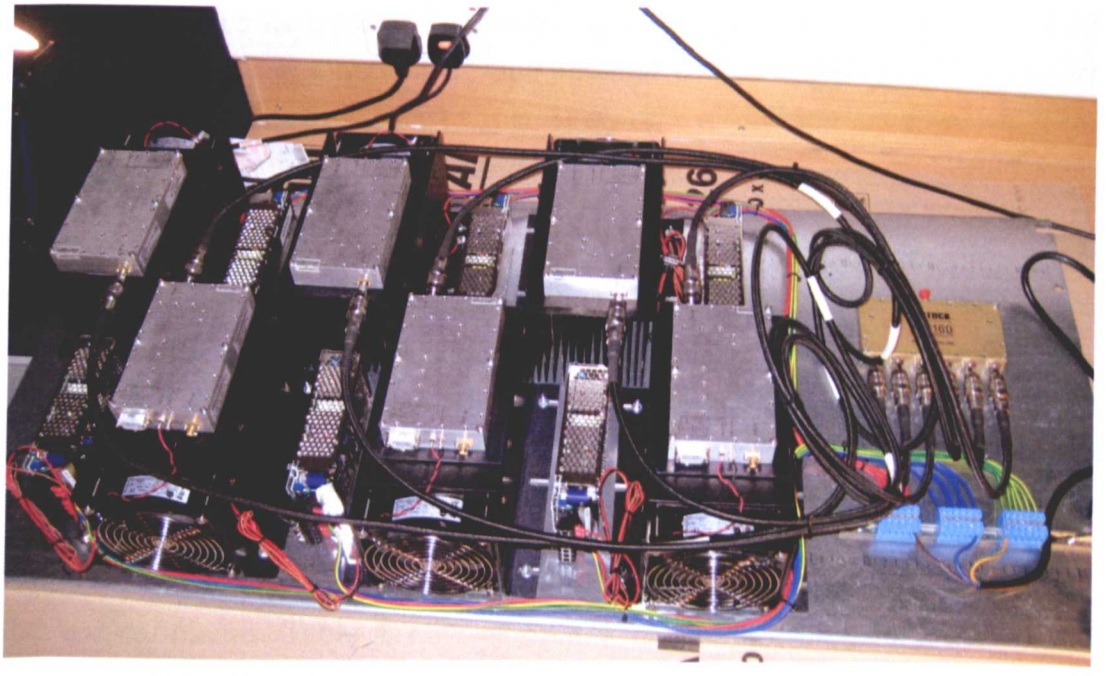

Figure A.2: Microwave power equipment.

Link budget analysis between signal generator and antenna input

Output from each of six amplifiers is given by

$$P_o - \alpha_c - \alpha_{IL} - \alpha_{split} = -2.98dBm \; -2.98 + G > P_{1db}$$

The specified amplifier input power results in operation at saturation. Output from each amplifier is therefore P_{1db}. This is then attenuated by α_c cable loss to the antenna. The maximum power at each antenna input is thus 18.2 W.

A.2 Antennas

A.2.1 Single circular microstrip patch and circular patch with notch

Antenna elements used for heating uniformity experiments in Section 5 were circular micro-strip patch antennas. One antenna was designed to radiate linearly polarised fields at the frequency of operation and a second was designed to radiate circularly polarised fields.

The radius and probe locations for each design was specified according to the procedure described in [99]. Circular polarisation was obtained from the second antenna by the inclusion of a notch in the antenna circumference, as described in [100]. This allowed two resonant modes, at different frequencies and with 90° phase difference, to operate. Designing the antenna such that the frequency of operation was between the two modes allows for circularly polarised radiant fields.

Figure A.3 shows the simulated gain patterns for both antennas in the horizontal and vertical planes. Table A.2 shows simulated antenna characteristics for both antennas. Measured return loss at resonant frequencies of 2.445 GHz were -10 dB and -17 dB, for circular and circular with notch, respectively. Operating the circular patch with notch at the lower frequency linear mode of 2.41 GHz resulted

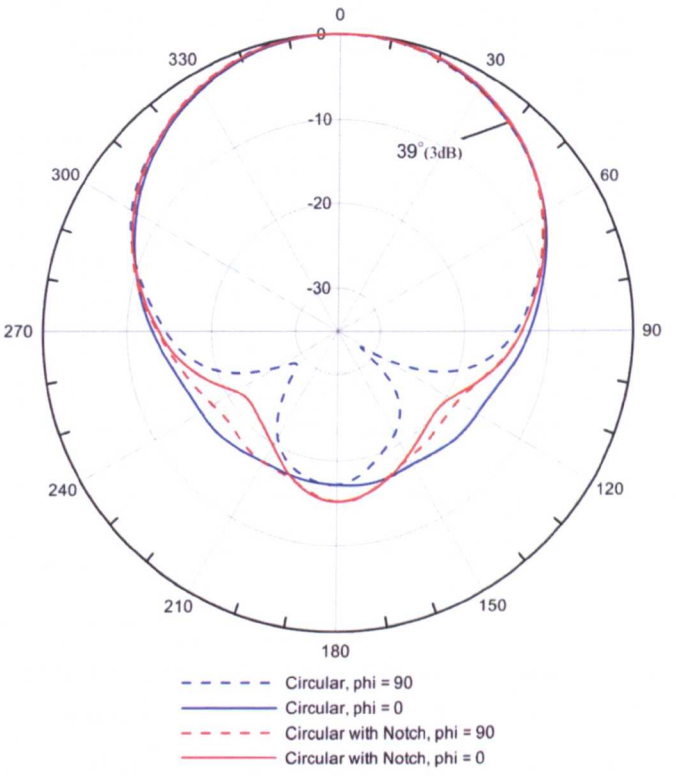

Figure A.3: Simulated gain of circular patch and circular patch with notch antennas.

in a return loss of -12 dB.

A.2.2 Single and Dual square micro strip patch

Heating experiments in Section 4 and Section 6 used two forms of square element patch antennas. The first consisted of a single element, with the design specified by the procedure in [99]. The second was an array of two of the former elements, with the array factor specified as in [101]. The array feed was a basic divider as described in [35]. A HFSS model of this array is shown in Figure A.4 and an illustration of the polarisation obtained is shown, by means of the Poynting vector, in Figure A.5.

Quantity	Circular	Circular with Notch
Peak Directivity (dB)	7.94	7.90
Peak Gain (dB)	7.34	7.31
Peak Realized Gain (dB)	6.94	7.2
Radiation Efficiency	0.87	0.87
Front to Back Ratio	41.0	35.1

Table A.2: Simulated antenna parameters for circular patch and circular patch with notch antennas.

Simulated gain patterns are shown, for two orthogonal planes, in Figure A.6. Simulated antenna properties are also shown for both antennas in Table A.3. Measured return loss at resonant frequencies of 2.46 GHz and 2.47 GHz was -26 dB and -28 dB, respectively.

	Single-Element	DSP Array
Peak Directivity (dB)	10.4	10.5
Peak Gain	10.3	9.9
Peak Realized Gain	10.3	9.9
Radiation Efficiency	0.73	0.89
Front to Back Ratio	368.6	169.0
-3dB Beam width (ϕ = 0\90°)	23°\52.3°	20°\49.4°

Table A.3: Simulated antenna parameters for single-element and DSP array antennas.

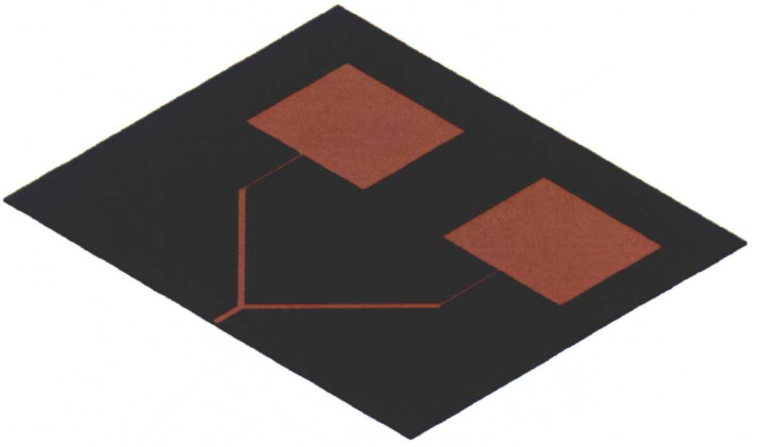

Figure A.4: HFSS model of dual-square patch antenna array.

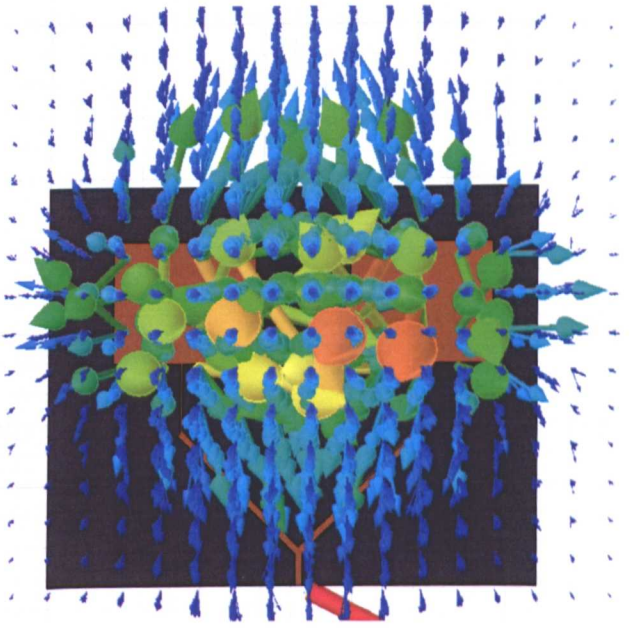

Figure A.5: HFSS simulationn of Poynting vector – illustrating the effect of linearly polarised radiant fields from DSP array antenna.

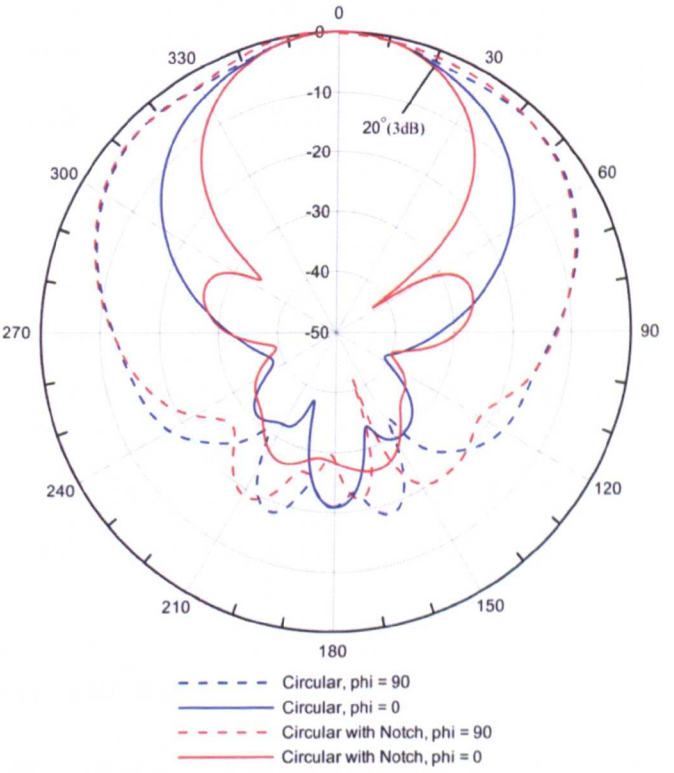

Figure A.6: Simulated gain of single and dual square patch antennas.

A.2.3 Four-element circular micro-strip patch array

A.2.3.1 Antenna Array Theory

The far-field radiation pattern of an array of identical antenna elements can be approximated by multiplying the far-field pattern of a single element by an array factor [99, 101]. The array factor is a function of the array geometry and the amplitude and phase excitation of each element. For N uniformly spaced and excited elements, the general form of the array factor is given by [99, 101]

$$AF = \sum_{n=1}^{N} e^{j(n-1)(kdcos\theta+\beta)} = \sum_{n=1}^{N} e^{j(n-1)\psi} \tag{A.1}$$

where

$$\psi = kdcos\theta + \beta \tag{A.2}$$

and d is the spacing between elements and β is the phase difference between element excitation. By choosing the above parameters accordingly, the shape and direction (location of minima and maxima) of the far-field pattern can be controlled.

A.2.3.2 Constructed Array

An array was created using $N = 4$ circular patch elements, with notches for circular polarisation (Figure A.7). Each element was spaced 50 mm apart. Amplitude and phase excitation was uniform for each element in order to preserve the circular polarisation of the radiant field, which is graphically illustrated in Figure A.8. These parameters were chosen to create one narrow (relative to a single element) circularly polarised main beam with no side-lobes. This allows for all available power to be focused over a smaller area, where it can be used to heat the plants. Furthermore, by exciting each element with separate outputs from the power amplifiers, the radiated power from one source could be increased without the possibility of interference from using multiple antennas.

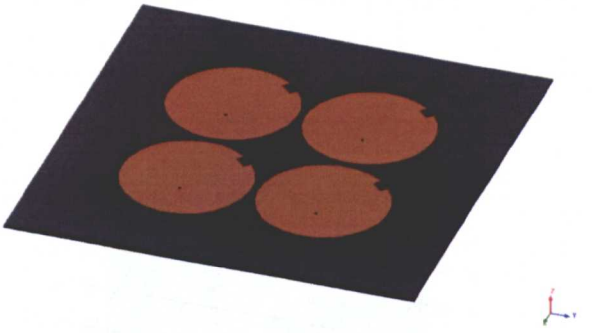

Figure A.7: HFSS model of 2x2 circular patch antenna array.

The measured return loss of the constructed array is shown in Figure A.9. The operating frequency was selected to be 2.411 GHz in order to obtain circular polarisation. Maximum return loss at this frequency was -9.2 dB. The simulated gain and radiation properties are shown in Figure A.10 and Table A.4 respectively. Simulated antenna properties are shown in Table A.4.

	2 x 2 Array
Peak Directivity (dB)	10.9
Peak Gain (dB)	10.8
Peak Realized Gain (dB)	10.8
Radiation Efficiency	0.97
Front to Back Ratio	289.1

Table A.4: Simulated antenna parameters for 2x2 array of circular patches (with notches).

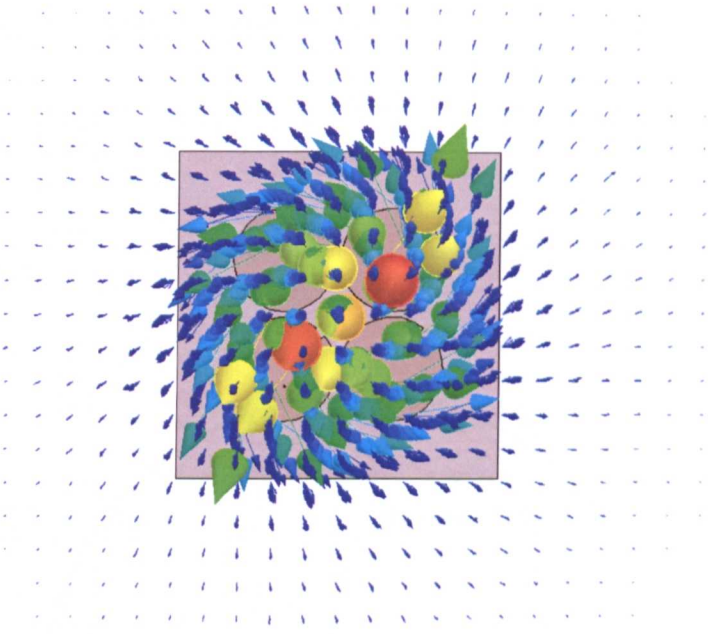

Figure A.8: Graphic representation of Poynting vector illustrating the effect of circularly polarised radiant fields from circular patch array.

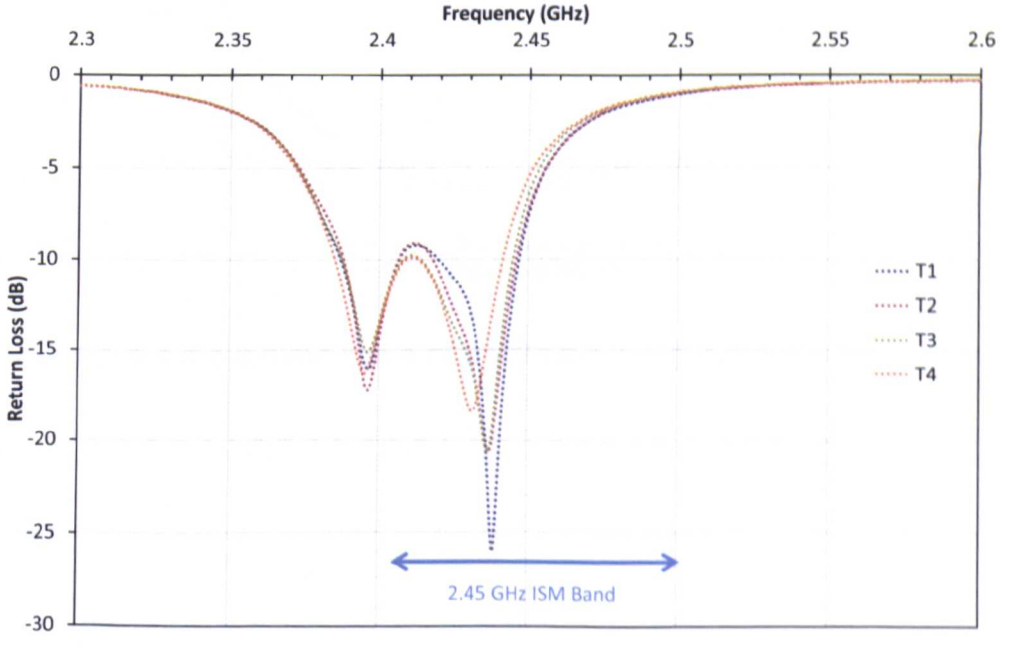

Figure A.9: Measured return loss of 2x2 array antenna.

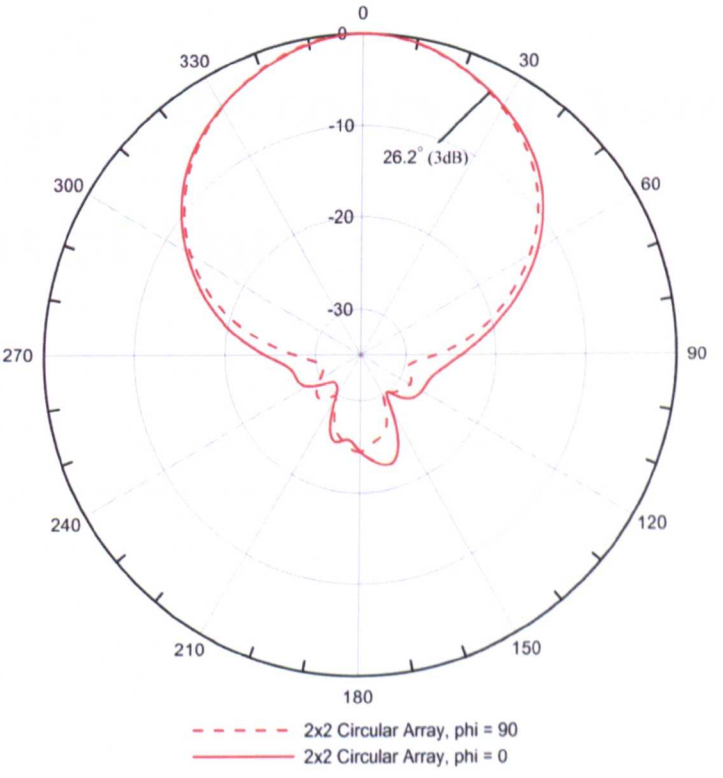

Figure A.10: Simulated gain of 2 x 2 circular patch with notch array.

Appendix B

Heating Uniformity in Agar - Graphs of Data

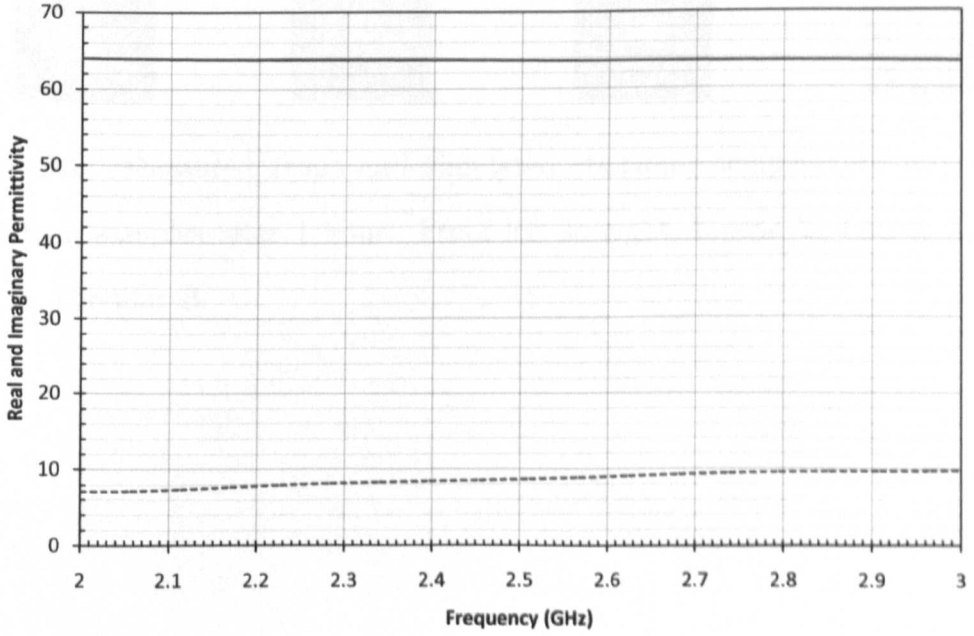

Figure B.1: Measured permittivity of agar (real, solid; imaginary, dotted).

B.1 Cross-sectional plots of temperature in Agar

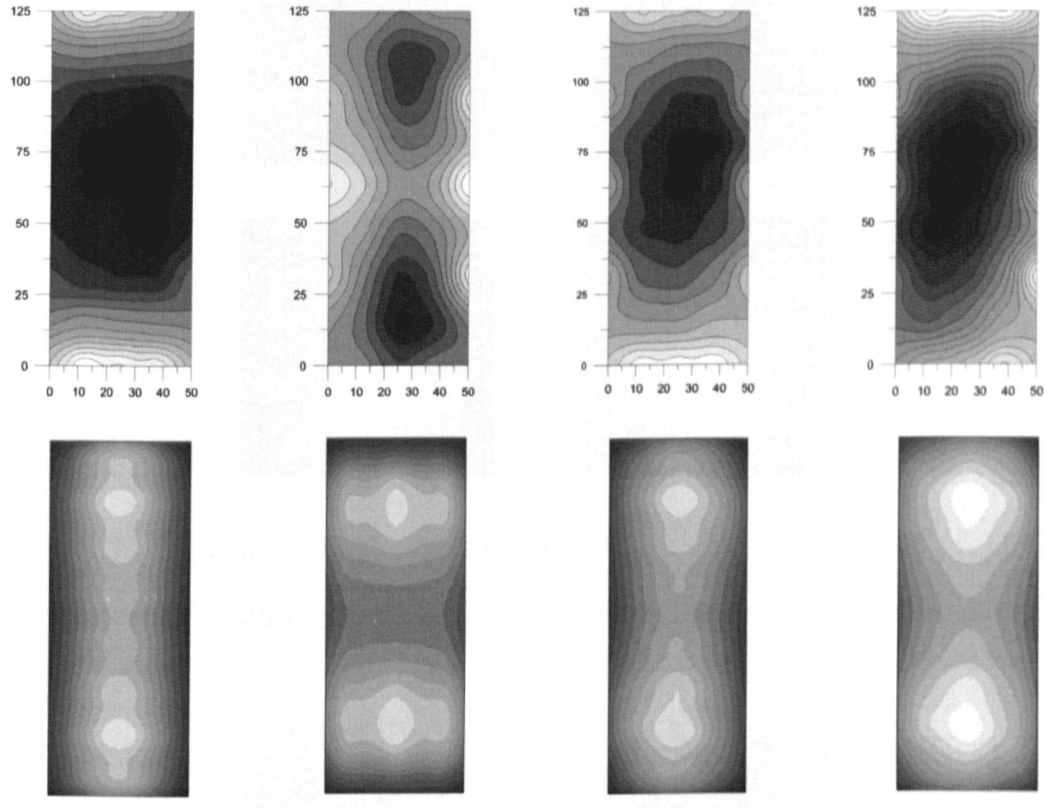

Figure B.2: Measured (top) and simulated (bottom) temperature profiles in 125x50mm samples after 1 hour. From left to right, Linear Y, Linear X, Circular A, Circular B.

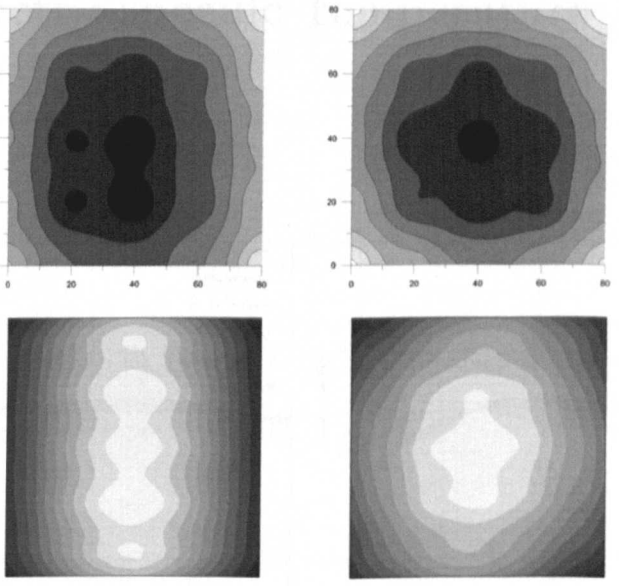

Figure B.3: Measured (top) and simulated (bottom) temperature profiles in 80x80mm samples after 1 hour. Linear (left) and Circular (right) polarisation.

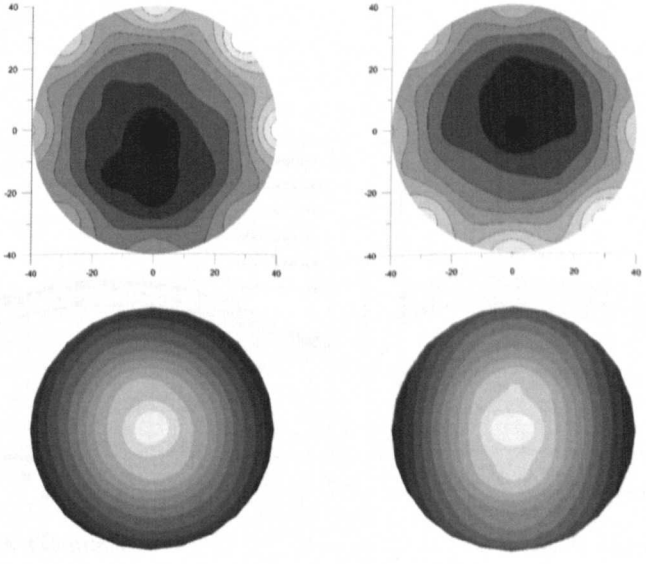

Figure B.4: Measured (top) and simulated (bottom) temperature profiles in 80mm cylindrical samples after 1 hour. Linear (left) and Circular (right) polarisation.

B.2 Geometry-specific temperature profiles in Agar

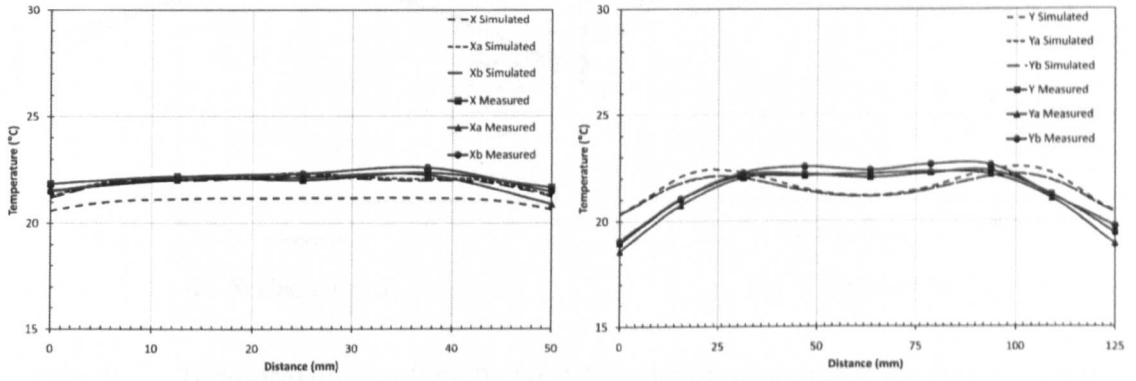

(a) X Geometries (b) Y Geometries

Figure B.5: Temperature profiles in 125 x 50 mm agar samples for linear A polarisation.

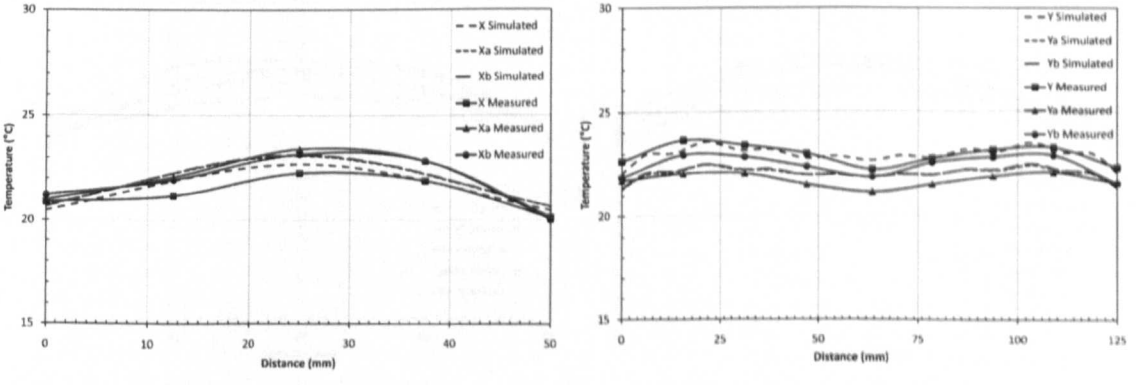

(a) X Geometries (b) Y Geometries

Figure B.6: Temperature profiles in 125 x 50 mm agar samples for linear B polarisation.

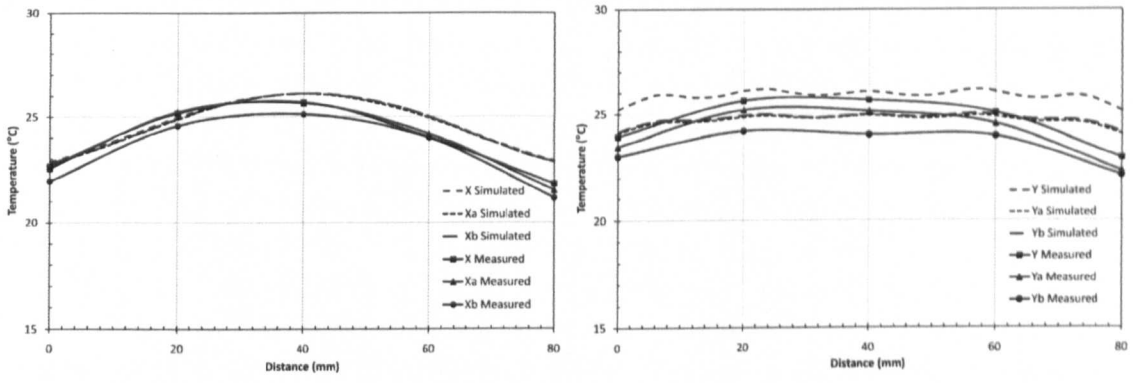

(a) X Geometries (b) Y Geometries

Figure B.7: Temperature profiles in 80 x 80 mm agar samples for linear polarisation.

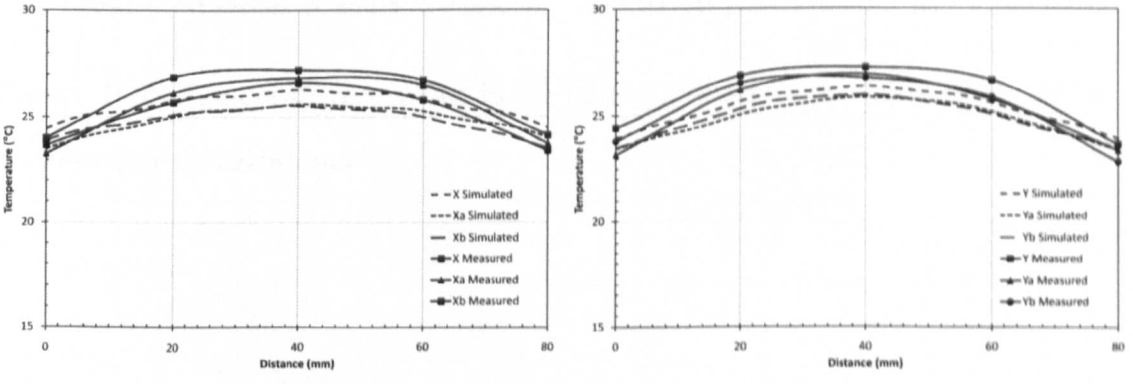

(a) X Geometries (b) Y Geometries

Figure B.8: Temperature profiles in 80 x 80 mm agar samples for circular polarisation.

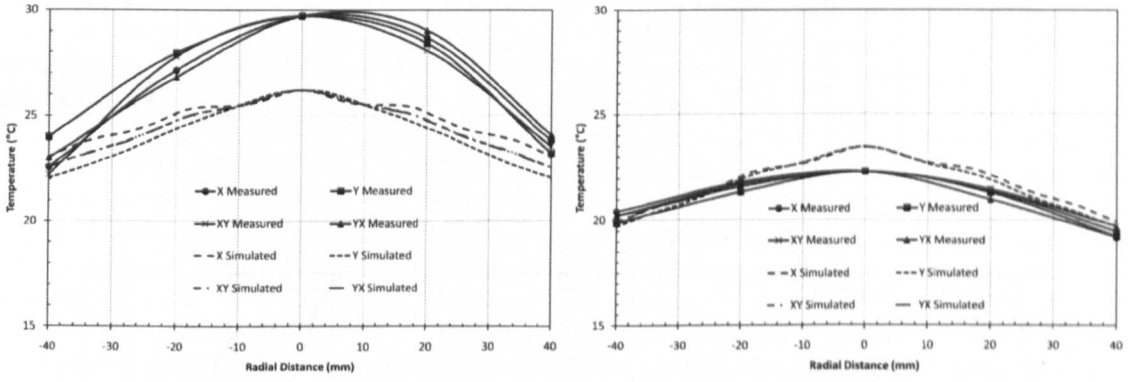

(a) Linear polarisation: X and Y Geometries (b) Circular polarisation: X and Y Geometries

Figure B.9: Temperature profiles in 80 mm cylindrical agar samples for linear and circular polarisations.

Appendix C

Heating Uniformity in Leaves - Data

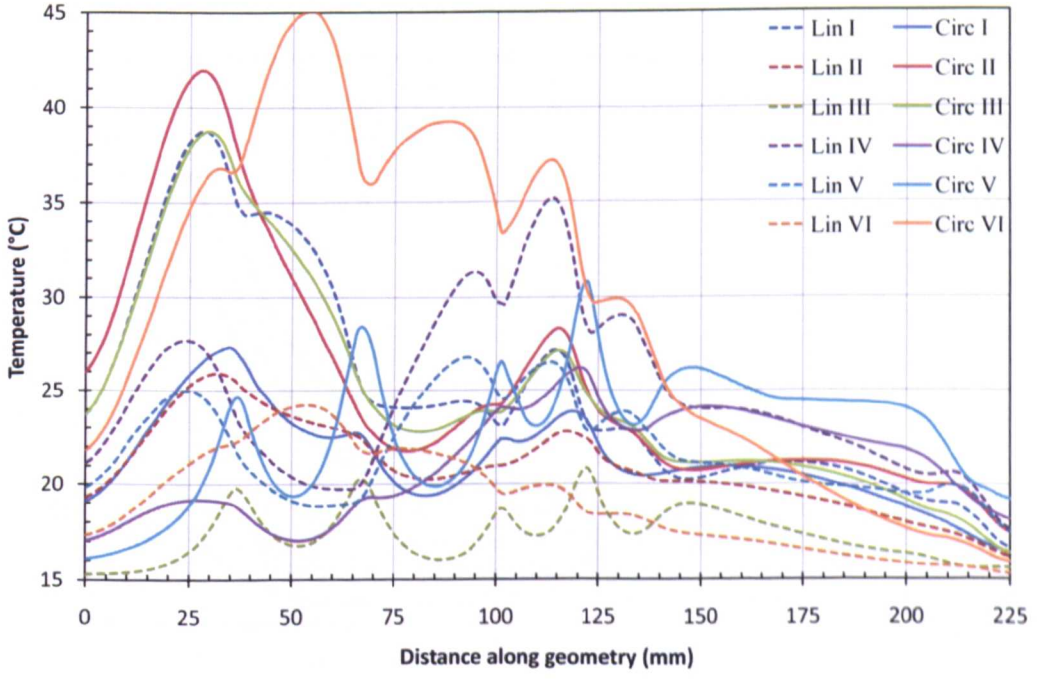

Figure C.1: Simulated temperature profile along geometry A (in leaf model).

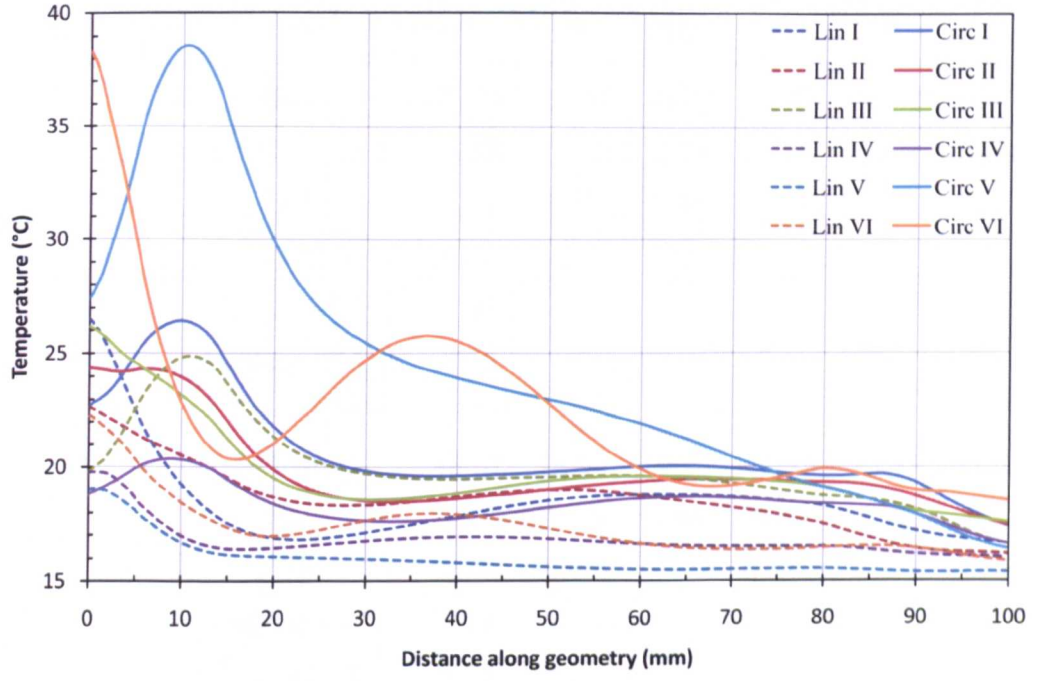

Figure C.2: Simulated temperature profile along geometry B (in leaf model).

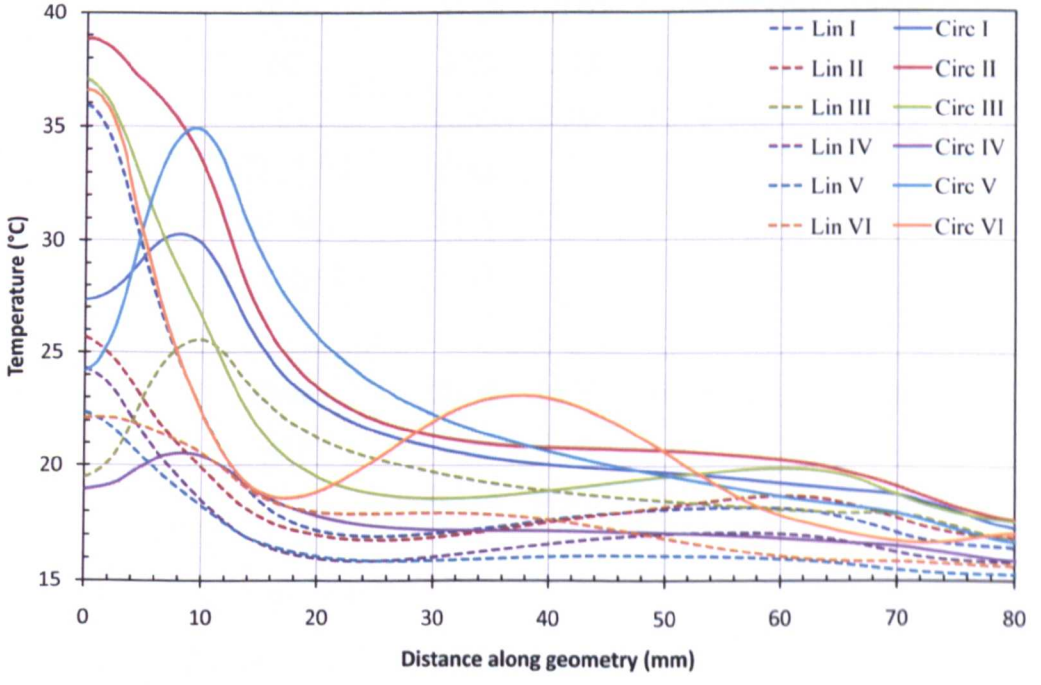

Figure C.3: Simulated temperature profile along geometry C (in leaf model).

Geometry		I	II	III	IV	V	VI
A	Mean	19.14	18.34	19.72	17.12	16.52	17.68
	SD	4.33	1.97	2.28	1.85	1.60	1.84
	UI	1.05	0.59	0.48	0.87	1.05	0.69
	SD of UI	0.24					
	Var. of UI	0.06					
	Average of UI	0.79					
B	Mean	18.37	18.54	19.93	16.75	15.91	17.29
	SD	1.78	1.40	1.84	0.73	0.79	1.25
	UI	0.530	0.396	0.372	0.416	0.871	0.545
	SD of UI	0.19					
	Var. of UI	0.03					
	Average of UI	0.52					
X	Mean	25.10	20.92	17.33	24.70	21.88	19.12
	SD	5.76	2.31	1.32	4.13	2.48	2.64
	UI	0.571	0.390	0.567	0.426	0.361	0.642
	SD of UI	0.12					
	Var. of UI	0.01					
	Average UI	0.49					
Aggregate	Mean	20.87	19.27	18.99	19.52	18.10	18.03
	SD	3.96	1.89	1.81	2.24	1.63	1.91
	UI	0.715	0.458	0.474	0.571	0.761	0.624
	Av. SD of UI	0.18					
	Av. Var. of UI	0.03					
	Av. Average UI	0.601					

Table C.1: Statistics for simulated temperature profiles along leaf geometries for linear polarisation.

Geometry		I	II	III	IV	V	VI
A	Mean	21.63	23.30	21.03	17.53	22.46	20.94
	SD	3.67	5.79	4.62	1.22	5.06	4.37
	UI	0.55	0.70	0.77	0.48	0.68	0.73
	SD of UI	0.11					
	Var. of UI	0.01					
	Average of UI	0.65					
B	Mean	20.68	19.78	19.75	18.39	24.28	22.24
	SD	2.15	1.84	1.91	0.81	5.93	3.83
	UI	0.378	0.385	0.403	0.238	0.638	0.528
	SD of UI	0.14					
	Var. of UI	0.02					
	Average of UI	0.43					
X	Mean	21.35	25.44	24.93	21.16	22.80	29.43
	SD	2.39	6.26	5.73	2.60	3.16	8.86
	UI	0.376	0.600	0.577	0.422	0.406	0.614
	SD of UI	0.11					
	Var. of UI	0.01					
	Average UI	0.50					
Aggregate	Mean	21.22	22.84	21.90	19.03	23.18	24.20
	SD	2.73	4.63	4.09	1.54	4.72	5.68
	UI	0.436	0.561	0.582	0.380	0.574	0.626
	Av. SD of UI	0.12					
	Av. Var. of UI	0.01					
	Av. Average UI	0.526					

Table C.2: Statistics for simulated temperature profiles along leaf geometries for circular polarisation.

References

[1] A. van der Knijff, J. Benninga, C. Reijnders, and J. K. Nienhuis, "Energy in the dutch greenhouse horticulture sector; developments in the sector and at holdings to the end of 2004," *The Hague, LEI*, 2006. Report 3.06.02. x, 6, 7, 8, 9, 11

[2] N. J. A. van der Velden and P. X. Smit, "Energy monitor for the dutch greenhouse sector, 2007," *The Hague, LEI*, 2008. Report 2008-084. x, 2, 3, 5, 6, 7, 8, 9, 11

[3] M. Teitel, A. Shklyar, V. Dikhtyar, E. Jerby, and Y. Elad, "Development of a microwave system for greenhouse heating," *Proceedings of the International Conference and British-Israeli Workshop on Greenhouse Techniques Towards the 3rd Millennium*, pp. 189–195, 2000. x, 12, 13, 14, 59, 75, 76, 77, 78, 129, 206

[4] P. Schmutz, J. Siegenthaler, C. Stger, D. Tarjan, and J. B. Bucher, "Long-term exposure of young spruce and beech trees to 2450-mhz microwave radiation," *Science of The Total Environment*, vol. 180, no. 1, pp. 43-48, 1996. x, 16

[5] M. F. Huber, "A method of heating for horticulture," 1983. x, 17, 18, 206

[6] B. Velzquez-Mart, C. Gracia-Lpez, and R. de la Puerta, "Work conditions for microwave applicators designed to eliminate undesired vegetation in a field," *Biosystems Engineering*, vol. 100, no. 1, pp. 31–37, 2008. x, 19, 206

[7] P. J. Sonneveld, G. L. A. M. Swinkels, J. Campen, B. A. J. van Tuijl, H. J. J. Janssen, and G. P. A. Bot, "Performance results of a solar green-

house combing electrical and thermal energy production," *Biosystems Engineering*, vol. 106, pp. 48–57, 2010. x, 19, 20, 207

[8] P. P. Lewicki, "Water as the determinant of food engineering properties. a review," *Journal of Food Engineering*, vol. 61, no. 4, pp. 483–495, 2004. x, 37, 38

[9] P. Pissis, "The dielectric relaxation of water in plant tissue," *Journal of Experimental Botany*, vol. 41, no. 6, pp. 677–684, 1990. x, 38, 39

[10] M. Bhattacharya and T. Basak, "On the analysis of microwave power and heating characteristics for food processing: Asymptotes and resonances," *Food Research International*, vol. 39, no. 10, pp. 1046–1057, 2006. xi, 83, 84

[11] M. J. Guess and I. C. Hunter, "Improving energy efficiency by heating greenhouse crops with microwaves," *IEEE MTT-S International Microwave Symposium, Baltimore*, 2011. 1

[12] C. Plackett, "Uk greenhouse horticulture," *FCRN Meeting*, 2005. 2, 5, 9, 189

[13] N. J. A. van der Velden and P. X. Smit, "Energy monitor of the dutch greenhouse horticulture sector 2000-2006," *The Hague, LEI*, 2007. Report 2.07.15. 2, 5, 6, 7, 8, 9, 11

[14] A. Breukers, O. Hietbrink, and M. Ruijs, "The power of dutch greenhouse vegetable horticulture: An analysis of the private sector and its institutional framework," *The Hague, LEI*, 2008. Report 2008-049. 2, 6, 8, 9, 10

[15] K. Boone, C. de Bont, K. J. van Calker, A. van der Knijff, and H. Leneman, "A view of sustainable agriculture in 2007; people, planet and profit results of dutch agriculture and horticulture," *The Hague, LEI*, 2007. Report 2.07.09. 2, 5, 7, 8, 10

[16] M. N. A. Ruijs, C. E. Reijnders, M. G. M. Raaphorst, J. B. Campen, J. C. J. Ammerlaan, and J. O. Voogt, "The tomato case, farm concepts for a low-emission greenhouse 2010-2015," *The Hague, LEI*, 2009. Report 2009-007. 2, 7, 10

[17] P. X. Smit and N. J. A. van der Velden, "Energy application. combined heat and power in dutch horticulture," *The Hague, LEI*, 2008. Report 2008-019. 3, 6, 11

[18] S. Ambler-Edwards *et al.*, "Food futures: Rethinking uk strategy," *Chatham House (Royal Institute of International Affairs)*, 2009. 3, 4

[19] S. Ambler-Edwards *et al.*, "Uk food supply, storm clouds on the horizon?," *Chatham House (Royal Institute of International Affairs)*. 3, 4, 5

[20] B. Marshall and G. McKelvey, "Food supply - can we meet the demand?," *Royal Agricultural Society of England*, vol. 168, 2007. 3, 4

[21] P. Berkhout, "Food security: A three-dimensional examination," *The Hague, LEI*, 2009. Report 2009-086. 4, 5, 10

[22] A. Smith, P. Watkiss, *et al.*, "The validity of food miles as an indicator of sustainable development," *AEA Technology Environment Report ED50254*. 4, 8

[23] W. Zittel and J. Schindler, "Crude oil: The supply outlook.," *Energy Watch Group*, 2007. EWG-Series No 3/2007. 4

[24] K. Aleklett, M. Höök, K. Jakobsson, M. Lardelli, S. Snowden, and B. Sderbergh, "The peak of the oil age.," *Energy Policy*, vol. 38, pp. 1398–1414, 2009. 4

[25] N. A. Owen, O. R. Inderwildi, and D. A. King, "The status of conventional world oil reserves hype or cause for concern?," *Energy Policy*, vol. 38, pp. 4743–4749, 2010. 4

[26] C. Lagerberg and M. T. Brown, "Improving agricultural sustainability: the case of swedish greenhouse tomatoes," *Journal of Cleaner Production*, vol. 7, no. 6, pp. 421–434, 1999. 5

[27] C. von Zabeltitz, "Effective use of renewable energies for greenhouse heating," *Renewable Energy*, vol. 5, no. 1-4, pp. 479–485, 1994. 5

[28] F. H. J. Bunte and Y. Dijkxhoorn, "Co_2 emission trading in 2020; significance for dutch greenhouse horticulture," *The Hague, LEI*, 2009. Report 2009-055. 5, 8

[29] J. K. Nienhuis, A. van der Knijff, and R. van der Meer, "Sustainable energy monitoring programme for greenhouse horticulture 2003," *The Hague, LEI*, 2005. Report 3.05.02. 6, 9, 10

[30] P. Diederen, F. van Tongeren, and H. van der Veen, "Returns on investments in energy-saving technologies under energy price uncertainty in dutch greenhouse horticulture," *Environmental and Resource Economics*, vol. 24, no. 4, pp. 379–394, 2003. 8, 11

[31] "United kingdom frequency allocation table," *Cabinet Official Committee on UK Spectrum Strategy*, no. 15, pp. 192–193, 2008. 22, 23, 69, 70

[32] M. S. Venkatesh and G. S. V. Raghavan, "An overview of dielectric properties measuring techniques," *Canadian Biosystems Engineering*, vol. 47, pp. 715–730, 2005. 23, 37, 48, 49, 50, 51, 85

[33] A. C. Metaxas, "Microwave heating," *Power Engineering Journal*, vol. 5, pp. 237–247, 1991. 23, 34, 37, 63

[34] A. C. Metaxas and R. Meredith, *Industrial microwave heating*. I.E.E. Power Engineering, London: Peter Peregrinus, 1983. 24, 26, 27

[35] D. Pozar, *Microwave engineering*. New York: John Wiley and Sons, 2nd ed., 1998. 26, 216

[36] B. Jecko and F. Torres, "Complete fdtd analysis of microwave heating process in frequency-dependent and temperature-dependent media," *IEEE Transactions on Microwave Theory and Techniques*, vol. 45, no. 1, p. 10, 1997. 27, 28, 41, 42

[37] G. P. Sharma and S. Prasad, "Dielectric properties of garlic (allium sativum l.) at 2450 mhz as function of temperature and moisture content," *Journal of Food Engineering*, vol. 52, no. 4, pp. 343–348, 2002. 27, 28, 37, 45, 49

[38] S. Wang, G. Tiwari, S. Jiao, J. A. Johnson, and J. Tang, "Developing postharvest disinfestation treatments for legumes using radio frequency energy," *Biosystems Engineering*, vol. 105, no. 3, pp. 341–349, 2010. 28

[39] A. Heredia, C. Barrera, and A. Andrs, "Drying of cherry tomato by a combination of different dehydration techniques. comparison of kinetics and other related properties," *Journal of Food Engineering*, vol. 80, no. 1, pp. 111–118, 2007. 28, 30, 37, 46, 51, 64

[40] M. E. Sosa-Morales, L. Valerio-Junco, A. López-Malo, and H. S. Garca, "Dielectric properties of foods: Reported data in the 21st century and their potential applications," *LWT - Food Science and Technology*. In Press, Accepted Manuscript. 29, 30, 32, 35, 37, 39, 40, 48, 49, 64

[41] O. O. Fasina, B. E. Farkas, and H. P. Fleming, "Thermal and dielectric properties of sweetpotato puree," *International Journal of Food Properties*, vol. 6, no. 3, pp. 461–472, 2003. 29, 45

[42] A. Technologies, "Basics of measuring the dielectric properties of materials," tech. rep., 2006. 30, 31, 34, 35, 36, 41, 43, 49, 50

[43] I. H. Boyaci, G. Sumnu, and O. Sakiyan, "Estimation of dielectric properties of cakes based on porosity, moisture content, and formulations using statistical methods and artificial neural networks," *Food and Bioprocess Technology*, vol. 2, no. 4, pp. 353–360, 2009. 30

[44] W. Guo, X. Zhu, Y. Liu, and H. Zhuang, "Sugar and water contents of honey with dielectric property sensing," *Journal of Food Engineering*, vol. 97, no. 2, pp. 275–281, 2010. 32, 39, 44

[45] Y. H. Liu, J. M. Tang, and Z. H. Mao, "Analysis of bread loss factor using modified debye equations," *Journal of Food Engineering*, vol. 93, no. 4, pp. 453–459, 2009. 34, 37, 40

[46] T. Ohlsson and N. E. Bengtsson, "Microwave heating in the food industry," *Proceedings of the IEEE*, vol. 62, no. 1, pp. 44–55, 1974. 34, 37, 63

[47] C. Kittel, *Introduction to solid state physics*. New York: John Wiley and Sons, 7th ed., 1996. 36

[48] N. W. Ashcroft and N. D. Mermin, *Solid state physics.* Fort Worth: Harcourt College Publishing, 1976. 36

[49] L. D. Landau, L. P. Pitaevskii, and E. M. Lifshitz, *Electrodynamics of continuous media*, vol. 8. Oxford: Pergamon Press, 2nd ed., 1984. 36

[50] E. Kreyszig, *Advanced engineering mathematics.* New York: John Wiley and Sons, 9th ed., 2006. 36

[51] J. Ahmed, H. S. Ramaswamy, and G. S. V. Raghavan, "Dielectric properties of butter in the mw frequency range as affected by salt and temperature," *Journal of Food Engineering*, vol. 82, no. 3, pp. 351–358, 2007. 37, 40, 64

[52] W. Guo, G. Tiwari, J. Tang, and S. Wang, "Frequency, moisture and temperature-dependent dielectric properties of chickpea flour," *Biosystems Engineering*, vol. 101, no. 2, pp. 217–224, 2008. 37, 47, 49, 50, 57

[53] Y. Liu, J. Tang, and Z. Mao, "Analysis of bread dielectric properties using mixture equations," *Journal of Food Engineering*, vol. 93, no. 1, pp. 72–79, 2009. 37, 47, 48, 49, 64

[54] F. Henry, M. Gaudillat, L. C. Costa, and F. Lakkis, "Free and/or bound water by dielectric measurements," *Food Chemistry*, vol. 82, no. 1, pp. 29–34, 2003. 38, 40

[55] J. B. Hasted, *Aqueous dielectrics.* London: Chapman and Hall, 1973. 38

[56] S. Wang, J. Tang, J. A. Johnson, E. Mitcham, J. D. Hansen, G. Hallman, S. R. Drake, and Y. Wang, "Dielectric properties of fruits and insect pests as related to radio frequency and microwave treatments," *Biosystems Engineering*, vol. 85, no. 2, pp. 201–212, 2003. 39, 46

[57] U. Kaatze, "Complex permittivity of water as a function of frequency and temperature," *Journal of Chemical and Engineering Data*, vol. 34, no. 4, pp. 371–374, 1989. 40, 41, 55

[58] P. Debye, *Polar molecules.* New York: Chemical Catalog Co., 1929. 40

[59] N. Agmon, "Tetrahedral displacement: The molecular mechanism behind the debye relaxation in water," *Journal of Physical Chemistry*, vol. 100, no. 3, pp. 1072–1080, 1996. 40, 41

[60] H. Fröhlich, *Theory of dielectrics: Dielectrics constant and dielectric loss.* Oxford: Clarendon Press, 2nd ed., 1958. 42

[61] R. H. Cole and K. S. Cole, "Dispersion and absorption in dielectrics - i alternating current characteristics," vol. 9, pp. 341–352, 1941. 43

[62] D. V. Blackham and R. D. Pollard, "An improved technique for permittivity measurements using a coaxial probe," *Instrumentation and Measurement, IEEE Transactions on*, vol. 46, no. 5, pp. 1093–1099, 1997. 43, 49, 50

[63] S. L. Birla, S. Wang, J. Tang, and G. Tiwari, "Characterization of radio frequency heating of fresh fruits influenced by dielectric properties," *Journal of Food Engineering*, vol. 89, no. 4, pp. 390–398, 2008. 45, 46, 85, 101

[64] X. Hu and P. Mallikarjunan, "Thermal and dielectric properties of shucked oysters," *LWT - Food Science and Technology*, vol. 38, no. 5, pp. 489–494, 2005. 45

[65] H. Feng, J. Tang, and R. P. Cavalieri, "Dielectric properties of dehydrated apples as affected by moisture and temperature," *Transactions of the Asae*, vol. 45, no. 1, pp. 129–135, 2002. 45

[66] M. E. Sosa-Morales, G. Tiwari, S. Wang, J. Tang, H. S. Garcia, and A. López-Malo, "Dielectric heating as a potential post-harvest treatment of disinfesting mangoes, part i: Relation between dielectric properties and ripening," *Biosystems Engineering*, vol. 103, no. 3, pp. 297–303, 2009. 45

[67] S. Wang, J. Tang, R. P. Cavalieri, and D. C. Davies, "Differential heating of insects in dried nuts and fruits associated with radio frequency and microwave treatments," *Transactions of the Asae*, vol. 46, no. 4, pp. 1175–1182, 2003. 46, 81

[68] S. R. S. Dev, G. S. V. Raghavan, and Y. Gariepy, "Dielectric properties of egg components and microwave heating for in-shell pasteurization of eggs," *Journal of Food Engineering*, vol. 86, no. 2, pp. 207–214, 2008. 46

[69] J. Ahmed, H. S. Ramaswamy, and G. S. V. Raghavan, "Dielectric properties of indian basmati rice flour slurry," *Journal of Food Engineering*, vol. 80, no. 4, pp. 1125–1133, 2007. 46

[70] H. S. Chua, G. Parkinson, A. D. Haigh, and A. A. P. Gibson, "A method of determining the moisture content of bulk wheat grain," *Journal of Food Engineering*, vol. 78, no. 4, pp. 1155 - 1158, 2007. 46

[71] S. K. Ng, P. Ainsworth, A. Plunkett, A. D. Haigh, A. A. P. Gibson, G. Parkinson, A. Stojceska, and G. Jacobs, "The characterisation of extruded brewer's spent grain and resistant starch using a microwave transmission line technique," *Journal of Food Engineering*, vol. 83, no. 4, pp. 614 - 620, 2007. 46

[72] M. K. Ndife, G. Sumnu, and L. Bayindirli, "Dielectric properties of six different species of starch at 2450 mhz," *Food Research International*, vol. 31, no. 1, pp. 43–52, 1998. 47

[73] S. Sokhansanj and S. O. Nelson, "Dependence of dielectric properties of whole-grain wheat on bulk density," *Journal of Agricultural Engineering Research*, vol. 39, no. 3, pp. 173–179, 1988. 47

[74] D. W. Sheriff, "An apparatus for the measurement of leaf dielectric properties in the high frequency region," *Journal of Experimental Botany*, vol. 27, no. 99, pp. 645–650, 1976. 48

[75] A. Technologies, "Microwave dielectric spectroscopy workshop," 2004. 49, 50

[76] A. A. P. Gibson, S. K. Ng, B. B. M. Noha, H. S. Chua, A. D. Haigh, G. Parkinson, P. Ainsworth, and A. Plunkett, "An overview of microwave techniques for the efficient measurement of food materials," *Food Manufacturing Efficiency*, vol. 2, no. 1, pp. 1–8, 2008. 49

[77] A. von Hippel, "The dielectric relaxation spectra of water, ice, and aqueous solutions, and their interpret at ion," *IEEE transactions on Electrical Insulation*, vol. 23, no. 5, pp. 801–816, 1988. 55

[78] P. Pissis, A. Anagnostopoulou-Konsta, and L. Apekis, "Binding modes of water in plant leaves: A dielectric study," *EPL (Europhysics Letters)*, no. 1, p. 119, 1987. 55

[79] S. Wang, J. Yue, J. Tang, and B. Chen, "Mathematical modelling of heating uniformity for in-shell walnuts subjected to radio frequency treatments with intermittent stirrings," *Postharvest Biology and Technology*, vol. 35, no. 1, pp. 97–107, 2005. 81, 85, 86, 90

[80] R. B. Pandit and S. Prasad, "Finite element analysis of microwave heating of potato–transient temperature profiles," *Journal of Food Engineering*, vol. 60, no. 2, pp. 193–202, 2003. 81, 82

[81] S. L. Birla, S. Wang, J. Tang, and G. Hallman, "Improving heating uniformity of fresh fruit in radio frequency treatments for pest control," *Postharvest Biology and Technology*, vol. 33, no. 2, pp. 205–217, 2004. 81, 82, 85, 98

[82] F. Marra, M. V. De Bonis, and G. Ruocco, "Combined microwaves and convection heating: A conjugate approach," *Journal of Food Engineering*, vol. 97, no. 1, pp. 31–39, 2010. 81, 87

[83] S. V. Egorov *et al.*, "Edge effect in microwave heating of conductive plates," *Journal of Physics D: Applied Physics*, vol. 39, no. 14, p. 3036, 2006. 82

[84] H. Chen, J. Tang, and F. Liu, "Simulation model for moving food packages in microwave heating processes using conformal fdtd method," *Journal of Food Engineering*, vol. 88, no. 3, pp. 294–305, 2008. 82, 86

[85] G. J. Fleischman, "Predicting temperature range in food slabs undergoing long term/low power microwave heating," *Journal of Food Engineering*, vol. 27, no. 4, pp. 337–351, 1996. 82, 100, 101

[86] K. G. Ayappa, H. T. Davis, G. Crapiste, E. A. Davis, and J. Gordon, "Microwave heating: an evaluation of power formulations," *Chemical Engineering Science*, vol. 46, no. 4, pp. 1005–1016, 1991. 83

[87] T. Basak and K. G. Ayappa, "Role of length scales on microwave thawing dynamics in 2d cylinders," *International Journal of Heat and Mass Transfer*, vol. 45, no. 23, pp. 4543–4559, 2002. 83

[88] J. N. Ikediala, J. D. Hansen, J. Tang, S. R. Drake, and S. Wang, "Development of a saline water immersion technique with rf energy as a postharvest treatment against codling moth in cherries," *Postharvest Biology and Technology*, vol. 24, pp. 209–221, 2002. 85

[89] S. L. Birla, S. Wang, and J. Tang, "Computer simulation of radio frequency heating of model fruit immersed in water," *Journal of Food Engineering*, vol. 84, no. 2, pp. 270–280, 2008. 85

[90] S. S. R. Geedipalli, V. Rakesh, and A. K. Datta, "Modeling the heating uniformity contributed by a rotating turntable in microwave ovens," *Journal of Food Engineering*, vol. 82, no. 3, pp. 359–368, 2007. 86, 89, 90

[91] S. Gunasekaran and H.-W. Yang, "Effect of experimental parameters on temperature distribution during continuous and pulsed microwave heating," *Journal of Food Engineering*, vol. 78, no. 4, pp. 1452–1456, 2007. 87

[92] S. Gunasekaran and H.-W. Yang, "Optimization of pulsed microwave heating," *Journal of Food Engineering*, vol. 78, no. 4, pp. 1457–1462, 2007. 87

[93] H.-W. Yang and S. Gunasekaran, "Comparison of temperature distribution in model food cylinders based on maxwell's equations and lambert's law during pulsed microwave heating," *Journal of Food Engineering*, vol. 64, no. 4, pp. 445–453, 2004. 87, 98

[94] Y. V. V. Rao, *Heat transfer*, p. 293. Universities Press (India) Limited, 3rd ed., 2001. 88

[95] C. T. M. Choi and A. Konrad, "Finite-element modeling of the rf heating process.," *IEEE Transactions on Magnetics*, vol. 27, p. 42274230, 1991. 98

[96] N. Sakai, W. Mao, Y. Koshima, and M. Watanabe, "A method for developing model food system in microwave heating studies," *Journal of Food Engineering*, vol. 66, no. 4, pp. 525–531, 2005. 100

[97] *The Met Office book of the British weather.* David & Charles, 2010. 189

[98] D. Betounes, *Partial differential equations for computational science*, ch. 2, pp. 23–28. New York: Springer-Verlag, 1998. 192, 194

[99] C. A. Balanis, *Antenna theory analysis and design*, pp. 283–371. Wiley, New Jersey, 3rd ed., 2005. 215, 216, 220

[100] R. Garg, P. Bhartia, I. Bahl, and A. Ittipiboon, *Microstrip antenna design handbook*, pp. 496–497. Norwood MA: Artech House, 2001. 215

[101] R. J. Mailloux, *Phased array antenna handbook.* Artech House, 2nd ed., 2005. 216, 220